

SUSTAINABLE CATALYTIC PRODUCTION OF BIO-BASED HETEROATOM-CONTAINING COMPOUNDS

EDITED BY: Hu Li, Song Yang and Yaqiong Su
PUBLISHED IN: Frontiers in Chemistry





frontiers

Frontiers eBook Copyright Statement

The copyright in the text of individual articles in this eBook is the property of their respective authors or their respective institutions or funders. The copyright in graphics and images within each article may be subject to copyright of other parties. In both cases this is subject to a license granted to Frontiers.

The compilation of articles constituting this eBook is the property of Frontiers.

Each article within this eBook, and the eBook itself, are published under the most recent version of the Creative Commons CC-BY licence.

The version current at the date of publication of this eBook is CC-BY 4.0. If the CC-BY licence is updated, the licence granted by Frontiers is automatically updated to the new version.

When exercising any right under the CC-BY licence, Frontiers must be attributed as the original publisher of the article or eBook, as applicable.

Authors have the responsibility of ensuring that any graphics or other materials which are the property of others may be included in the CC-BY licence, but this should be checked before relying on the CC-BY licence to reproduce those materials. Any copyright notices relating to those materials must be complied with.

Copyright and source acknowledgement notices may not be removed and must be displayed in any copy, derivative work or partial copy which includes the elements in question.

All copyright, and all rights therein, are protected by national and international copyright laws. The above represents a summary only. For further information please read Frontiers' Conditions for Website Use and Copyright Statement, and the applicable CC-BY licence.

ISSN 1664-8714

ISBN 978-2-88966-439-9

DOI 10.3389/978-2-88966-439-9

About Frontiers

Frontiers is more than just an open-access publisher of scholarly articles: it is a pioneering approach to the world of academia, radically improving the way scholarly research is managed. The grand vision of Frontiers is a world where all people have an equal opportunity to seek, share and generate knowledge. Frontiers provides immediate and permanent online open access to all its publications, but this alone is not enough to realize our grand goals.

Frontiers Journal Series

The Frontiers Journal Series is a multi-tier and interdisciplinary set of open-access, online journals, promising a paradigm shift from the current review, selection and dissemination processes in academic publishing. All Frontiers journals are driven by researchers for researchers; therefore, they constitute a service to the scholarly community. At the same time, the Frontiers Journal Series operates on a revolutionary invention, the tiered publishing system, initially addressing specific communities of scholars, and gradually climbing up to broader public understanding, thus serving the interests of the lay society, too.

Dedication to Quality

Each Frontiers article is a landmark of the highest quality, thanks to genuinely collaborative interactions between authors and review editors, who include some of the world's best academicians. Research must be certified by peers before entering a stream of knowledge that may eventually reach the public - and shape society; therefore, Frontiers only applies the most rigorous and unbiased reviews.

Frontiers revolutionizes research publishing by freely delivering the most outstanding research, evaluated with no bias from both the academic and social point of view. By applying the most advanced information technologies, Frontiers is catapulting scholarly publishing into a new generation.

What are Frontiers Research Topics?

Frontiers Research Topics are very popular trademarks of the Frontiers Journals Series: they are collections of at least ten articles, all centered on a particular subject. With their unique mix of varied contributions from Original Research to Review Articles, Frontiers Research Topics unify the most influential researchers, the latest key findings and historical advances in a hot research area! Find out more on how to host your own Frontiers Research Topic or contribute to one as an author by contacting the Frontiers Editorial Office: frontiersin.org/about/contact

SUSTAINABLE CATALYTIC PRODUCTION OF BIO-BASED HETEROATOM-CONTAINING COMPOUNDS

Topic Editors:

Hu Li, Guizhou University, China

Song Yang, Guizhou University, China

Yaqiong Su, Eindhoven University of Technology, Netherlands

Citation: Li, H., Yang, S., Su, Y., eds. (2021). Sustainable Catalytic Production of Bio-Based Heteroatom-Containing Compounds. Lausanne: Frontiers Media SA. doi: 10.3389/978-2-88966-439-9

Table of Contents

- 04 Editorial: Sustainable Catalytic Production of Bio-Based Heteroatom-Containing Compounds**
Hu Li, Song Yang and Yaqiong Su
- 06 Green and Facile Synthesis of Metal-Organic Framework Cu-BTC-Supported Sn (II)-Substituted Keggin Heteropoly Composites as an Esterification Nanocatalyst for Biodiesel Production**
Qiuyun Zhang, Dan Ling, Dandan Lei, Jialu Wang, Xiaofang Liu, Yutao Zhang and Peihua Ma
- 16 A Synthetic View on Haedoxans and Related Neolignans From Phryma leptostachya**
Yang Chen, Shu Xiao, Jian Huang, Wei Xue and Shuzhong He
- 22 Green and Facile Synthesis of Spirocyclopentanes Through NaOH-Promoted Chemo- and Diastereo-Selective (3 + 2) Cycloaddition Reactions of Activated Cyclopropanes and Enamides**
Xun Zhu, Dingwu Pan, Chengli Mou, Bo Zhou, Lutai Pan and Zhichao Jin
- 29 Synthesis and Bioactivities Study of Novel Pyridylpyrazol Amide Derivatives Containing Pyrimidine Motifs**
Wenneng Wu, Meihang Chen, Qiang Fei, Yonghui Ge, Yingying Zhu, Haijiang Chen, Maofa Yang and Guiping Ouyang
- 37 Evaluation of General Synthesis Procedures for Bioflavonoid–Metal Complexes in Air-Saturated Alkaline Solutions**
Yuanyong Yao, Meng Zhang, Laibing He, Yunyang Wang and Shixue Chen
- 48 Corrigendum: Evaluation of General Synthesis Procedures for Bioflavonoid–Metal Complexes in Air-Saturated Alkaline Solutions**
Yuanyong Yao, Meng Zhang, Laibing He, Yunyang Wang and Shixue Chen
- 49 Heteropoly Acid-Based Catalysts for Hydrolytic Depolymerization of Cellulosic Biomass**
Xiaoxiang Luo, Hongguo Wu, Chuanhui Li, Zhengyi Li, Hu Li, Heng Zhang, Yan Li, Yaqiong Su and Song Yang
- 78 The Effect of Ni-ZSM-5 Catalysts on Catalytic Pyrolysis and Hydro-Pyrolysis of Biomass**
Ya-Long Ding, Hua-Qin Wang, Mei Xiang, Pei Yu, Rong-Qiang Li and Qing-Ping Ke
- 89 Sustainably Adjusting the Up-Conversion White-Emitting Luminescence Properties of $GdAlO_3: Er^{3+}/Yb^{3+}/Tm^{3+}$ Phosphors**
Taoli Deng, Xianbang Jiang and Qiuyun Zhang
- 96 Current Approaches to Alkyl Levulinates via Efficient Valorization of Biomass Derivatives**
Xiaofang Liu, Wenjia Yang, Qiuyun Zhang, Can Li and Hongguo Wu



Editorial: Sustainable Catalytic Production of Bio-Based Heteroatom-Containing Compounds

Hu Li^{1*}, Song Yang^{1*} and Yaqiong Su²

¹ State Key Laboratory Breeding Base of Green Pesticide and Agricultural Bioengineering, Key Laboratory of Green Pesticide and Agricultural Bioengineering, Ministry of Education, State-Local Joint Laboratory for Comprehensive Utilization of Biomass, Center for R and D of Fine Chemicals, Guizhou University, Guiyang, China, ² Laboratory of Inorganic Materials and Catalysis, Schuit Institute of Catalysis, Eindhoven University of Technology, Eindhoven, Netherlands

Keywords: sustainable chemistry, biomass conversion, catalytic mechanism, biorefinery, biofuels

Editorial on the Research Topic

Sustainable Catalytic Production of Bio-Based Heteroatom-Containing Compounds

Organic synthesis is a versatile tool in the design and creation of desirable scaffolding molecules. These processes typically involve toxic and non-renewable starting materials as well as the formation of waste or byproducts. Biomass, on the other hand, is deemed as the most abundant organic carbon resource, and the development of sustainable approaches to producing valuable organic molecules from waste and biomass feedstocks is of great significance for alleviating environmental pollution, deterioration, and the greenhouse effect.

One of the prominent features of biomass is that it is rich in oxygen, the compounds it yields are typically functionalized with oxygen-containing species such as hydroxy, ether, carbonyl, carboxyl, and ester groups, which significantly enrich the product variety. Derived from these oxygen-rich bio-products, the catalytic functionalization of biomass derivatives with heteroatoms such as nitrogen, sulfur, phosphorus, and silicon can also be realized via specific reaction routes or pathways. These functionalized compounds are crucial core scaffolds or key intermediates in a wide range of pharmaceutical molecules, fiber dyes, and printing ink, which can also be directly used as solvents, surfactants, and so on.

This Research Topic presents a collection of original research and review articles on bio-based heteroatom-containing compounds, including green and facile production of biodiesel (Zhang et al.; Zhu et al.), chemical synthesis, structure, and the evaluation of the bioactivities of naturally occurring haedoxan-like molecules (Chen et al.), pyridylpyrazolamide derivatives containing pyrimidine motifs (Wu et al.), and bioflavonoid-metal complexes (Yao et al.). The Research Topic provides insights into the effect of Ni-ZSM-5 catalysts on biomass pyrolysis (Ding et al.), and into the catalytic strategies developed for depolymerization of cellulosic biomass to value-added products (Luo et al.; Liu et al.). The Research Topic also depicts the process of doping heteroatom in phosphor to improve the resulting luminescent properties of the material (Deng et al.).

An original research paper by Zhang et al. reports a simple and low-cost impregnation method for the facile preparation of metal-organic framework Cu-BTC-supported Sn (II)-substituted Keggin heteropoly nanocomposites (Sn1.5PW/Cu-BTC). The obtained Sn1.5PW/Cu-BTC nanocatalyst show high activity in the production of biodiesel from oleic acid through esterification, with relatively low apparent activation energy (E_a) of 38.3 kJ mol⁻¹, and can be reused seven times with no significant loss of activity. Zhu et al. disclose that Donor-Acceptor (D-A) cyclopropanes can react with α,β -unsaturated enamide substrates via chemo- and diastereoselective

OPEN ACCESS

Edited and reviewed by:

Valeria Conte,
University of Rome Tor Vergata, Italy

*Correspondence:

Hu Li
hli13@gzu.edu.cn
Song Yang
jhzx.msm@gmail.com

Specialty section:

This article was submitted to
Green and Sustainable Chemistry,
a section of the journal
Frontiers in Chemistry

Received: 13 November 2020

Accepted: 25 November 2020

Published: 11 December 2020

Citation:

Li H, Yang S and Su Y (2020) Editorial:
Sustainable Catalytic Production of
Bio-Based Heteroatom-Containing
Compounds. *Front. Chem.* 8:628859.
doi: 10.3389/fchem.2020.628859

(3 + 2) cycloaddition reaction under basic conditions for efficient access to spiro (cyclopentane-1,3'-indoline) derivatives, in which green, inexpensive, and readily available NaOH were used as the sole catalyst to promote this transformation. The authors expand a broad range of D-A cyclopropanes as the C-3 synthons to react with oxindole-derived α,β -unsaturated enamides, furnishing structurally sophisticated spiro(cyclopentane-1,3'-indoline) derivatives with up to 3 adjacent chiral centers in excellent yields as single diastereomers.

The work of Wu et al. reveals the antifungal and insecticidal activities of pyridylpyrazol amide derivatives containing a pyrimidine moiety, synthesized via six-step reactions, including hydrazidation, cyclization, bromination or chlorination, oxidation, hydrolyzation, and condensation. The antifungal properties of some title compounds against *Sclerotinia sclerotiorum*, *Phytophthora infestans*, *Thanatephorus cucumeris*, *Gibberella zeae*, *Fusarium oxysporum*, *Cytospora mandshurica*, *Botryosphaeria dothidea*, and *Phomopsis* sp. are similar to those of Kresoxim-methyl or Pyrimethanil at 50 $\mu\text{g/mL}$. These synthesized compounds show a certain insecticidal activity against *Spodoptera litura*, *Mythimna separata*, *Pyrausta nubilalis*, *Tetranychus urticae*, *Rhopalosiphum maidis*, and *Nilaparvata lugens* at 200 $\mu\text{g/mL}$. Yao et al. evaluate the general synthetic procedures for bioflavonoid-metal complexes that are unstable in air-saturated alkaline solutions. All examined bioflavonoid-metal complex ligands (e.g., dihydromyricetin, myricetin, quercetin, daidzein, genistein, chrysin, baicalein, rutin hydrate, and kaempferol) dissolved in air-saturated alkaline solutions can generate O_2^- at different capacities, as demonstrated by electron paramagnetic resonance (EPR) analysis, indicating that the general procedures for the synthesis of bioflavonoid-metal complexes using a transition metal ion and an air-saturated alkaline solution may require improvement. Deng et al. uncover that doping GdAlO_3 phosphors with $\text{Er}^{3+}/\text{Yb}^{3+}/\text{Tm}^{3+}$, which were prepared by the co-precipitation method, can effectively adjust the up-conversion light performance, especially the white-emitting luminescence properties.

This Research Topic features several review articles with distinct scopes (Ding et al.; Luo et al.; Liu et al.; Chen et al.). Ding et al. mainly review the research progress of ZSM-5 zeolite supported Ni (Ni-ZSM-5) catalysts in pyrolysis and hydro-pyrolysis of biomass, including (i) the single metal Ni-ZSM-5-enabled catalytic conversion of biomass in the absence of hydrogen, (ii) Ni-ZSM-5-promoted biomass catalytic conversion in a hydrogen atmosphere, and (iii) biomass valorization using ZSM-5 supported bimetal catalysts composed of Ni and other metals. The authors focus on the recent investigation of Ni-modified microporous ZSM-5 materials used in catalytic pyrolysis of lignin and cellulose, covering applications of metal-modified hierarchical ZSM-5. Luo et al. provide a comprehensive view on state-of-the-art heteropoly acid (HPA)-based catalysts for the hydrolytic depolymerization of cellulosic biomass. With unique properties such as good solubility, high thermal stability, and strong acidity, HPA-based catalysts are revealed to be efficient for depolymerization and conversion of cellulose into valuable chemicals and biofuels, which is one of the most

remarkable processes in chemistry for sustainability. The authors summarize the characteristics, advantages, and applications of HPAs in different categories for cellulose degradation and discuss the mechanisms of HPAs catalysts in the effective degradation of cellulosic biomass, which provides more avenues for the further development of renewed and robust HPAs utilized for cellulose degradation. Liu et al. illustrate the effects of biomass pretreatment method, catalyst texture/acidity, involved catalytic mechanisms, and different possible intermediates (e.g., diethyl ether, 4,5,5-triethoxypentan-2-one, ethoxymethylfuran, ethyl-D-fructofuranoside, and ethyl-D-glucopyranoside) on the catalytic transformation of biomass saccharides into alkyl levulinates (ALs), which have widespread applications like fuel additives, flavorings, plasticizing agents, and synthetic precursors to various building blocks. The authors disclose several typical conversion processes or routes for the synthesis of ALs from renewable resources, mainly including (i) direct esterification of levulinic acid with alkyl alcohols and (ii) alcoholysis of relevant biomass feedstocks, such as furfuryl alcohol, chloromethyl furfural, and saccharide. Chen et al. briefly introduce the chemical structures of naturally occurring haedoxan-like molecules that exhibit promising insecticidal, antifungal, antibacterial, and anticancer activities. The authors detail the synthetic efforts toward haedoxans and phrymarolins in the past three decades.

This Research Topic intends to enlighten researchers about more eco-friendly and sustainable synthetic procedures, shedding light on renewed catalytic strategies and routes developed for the production of bio-based heteroatom-containing compounds, indicating the enthusiasm and commitment of researchers working in this area.

AUTHOR CONTRIBUTIONS

All authors made a substantial, direct, intellectual contribution to the work, and approved it for publication.

ACKNOWLEDGMENTS

HL acknowledges the financial support from the National Natural Science Foundation of China (Nos. 21908033 and 21666008), the Fok Ying-Tong Education Foundation (161030), Guizhou Science and Technology Foundation ([2018]1037), and the Program of Introducing Talents of Discipline to Universities of China (111 Program, D20023). Special thanks to the editorial teams at Frontiers, particularly those of Green and Sustainable Chemistry, Organic Chemistry, and Catalysis and Photocatalysis, for support and assisting the Guest Editors in organizing this Research Topic.

Conflict of Interest: The authors declare that the research was conducted in the absence of any commercial or financial relationships that could be construed as a potential conflict of interest.

Copyright © 2020 Li, Yang and Su. This is an open-access article distributed under the terms of the Creative Commons Attribution License (CC BY). The use, distribution or reproduction in other forums is permitted, provided the original author(s) and the copyright owner(s) are credited and that the original publication in this journal is cited, in accordance with accepted academic practice. No use, distribution or reproduction is permitted which does not comply with these terms.



Green and Facile Synthesis of Metal-Organic Framework Cu-BTC-Supported Sn (II)-Substituted Keggin Heteropoly Composites as an Esterification Nanocatalyst for Biodiesel Production

Qiuyun Zhang^{1,2*}, Dan Ling¹, Dandan Lei¹, Jialu Wang^{3*}, Xiaofang Liu⁴, Yutao Zhang^{2,3} and Peihua Ma^{5*}

OPEN ACCESS

Edited by:

Yaqiong Su,
Eindhoven University of
Technology, Netherlands

Reviewed by:

Yeh-Yung Lin,
Dalian University of Technology, China
Ya-Long Ding,
Huanghuai University, China

*Correspondence:

Qiuyun Zhang
qyzhang.asu@gmail.com
Jialu Wang
lu226@163.com
Peihua Ma
phma@gzu.edu.cn

Specialty section:

This article was submitted to
Green and Sustainable Chemistry,
a section of the journal
Frontiers in Chemistry

Received: 08 January 2020

Accepted: 12 February 2020

Published: 18 March 2020

Citation:

Zhang Q, Ling D, Lei D, Wang J, Liu X,
Zhang Y and Ma P (2020) Green and
Facile Synthesis of Metal-Organic
Framework Cu-BTC-Supported Sn
(II)-Substituted Keggin Heteropoly
Composites as an Esterification
Nanocatalyst for Biodiesel Production.
Front. Chem. 8:129.
doi: 10.3389/fchem.2020.00129

¹ School of Chemistry and Chemical Engineering, Anshun University, Anshun, China, ² Engineering Technology Center of Control and Remediation of Soil Contamination of Provincial Science & Technology Bureau, Anshun University, Anshun, China, ³ School of Resource and Environmental Engineering, Anshun University, Anshun, China, ⁴ Food and Pharmaceutical Engineering Institute, Guiyang University, Guiyang, China, ⁵ School of Chemistry and Chemical Engineering, Guizhou University, Guiyang, China

In the present study, metal-organic framework Cu-BTC-supported Sn (II)-substituted Keggin heteropoly nanocomposite (Sn_{1.5}PW/Cu-BTC) was successfully prepared by a simple impregnation method and applied as a novel nanocatalyst for producing biodiesel from oleic acid (OA) through esterification. The nanocatalyst was characterized by Fourier transform infrared spectrometry (FTIR), wide-angle X-ray diffraction (XRD), scanning electron microscopy (SEM), transmission electron microscopy (TEM), nitrogen adsorption-desorption, thermogravimetrics (TG), and NH₃-temperature-programmed desorption (NH₃-TPD). Accordingly, the synthesized nanocatalyst with a Sn_{1.5}PW/Cu-BTC weight ratio of 1 exhibited a relatively large specific surface area, appropriate pore size, and high acidity. Moreover, an OA conversion of 87.7% was achieved under optimum reaction conditions. The nanocatalyst was reused seven times, and the OA conversion remained at more than 80% after three uses. Kinetic study showed that the esterification reaction followed first-order kinetics, and the activation energy (E_a) was calculated to be 38.3 kJ/mol.

Keywords: heteropolys, Cu-BTC, nanocomposites, esterification, biodiesel

INTRODUCTION

Nowadays, fossil fuel resource demand is expanding progressively due to industrial growth and constant population rise. Meanwhile, the utilization of fossil fuels along with environmental pollution and global warming has led to the consideration of alternative energy sources like biofuels (Bhanja and Bhaumik, 2016; Long et al., 2019; Negm et al., 2019; Xu et al., 2019; Li et al., 2020). Among the various biofuels, biodiesel is considered to be the most promising renewable

fuel, possibly due to its biodegradable, non-toxic, and environmentally friendly features (Al-Saadi et al., 2018; Li H. et al., 2019). Further, the typical way of producing biodiesel is the catalytic esterification of free fatty acids or transesterification of triglyceride with an alcohol in the presence of a homogeneous/heterogeneous catalyst (Mahmoud, 2019). A homogeneous acid catalyst, such as HCl, H₂SO₄, or H₃PO₄, can catalyze esterification with high activity; however, the major drawbacks of homogeneous acid catalysts are the generation of a huge amount of chemical wastewater and the high cost for catalyst separation and non-reusability (Zhang et al., 2019a). Therefore, heterogeneous solid catalysts have been widely applied to catalyze the esterification reaction for biodiesel synthesis.

One option is to use hetopolyacids as strong Brønsted acid catalysts for catalytic esterification and transesterification reactions to produce biodiesel with high conversions (Talebian-Kiakalaieh et al., 2013; Sun et al., 2015; Xie and Wan, 2019a). Unfortunately, hetopolyacids have certain disadvantages, such as good solubility in polar media and a low surface area (Parida and Mallick, 2007; Ekinici and Oktar, 2019). Therefore, supporting hetopolyacids on porous supports is an interesting approach to produce heterogeneous catalysts, since it can provide high surface area and insolubility in the polar solvent.

Various types of supported hetopolyacid catalysts have been utilized. Montmorillonite K10 (Nandiwale and Bokade, 2014), Nb₂O₅ (da Conceição et al., 2017), and carbon (Ghubayra et al., 2019) can be used as supports, but they were more or less subject to the disadvantages of weak interaction between object and host, low stability, high-cost synthesis, etc. By contrast, metal-organic frameworks (MOFs) provide excellent support, having the features of stability, adjustable tunnels, ultra-high specific surface area, and high catalytic efficiency (Kang et al., 2019; Li D. D. et al., 2019). Examples are PTA@MIL-53 (Fe) (Nikseresht et al., 2017), AILs/HPW/Uio-66-2COOH (Xie and Wan, 2019b), and ZnFe₂O₄/MIL-100(Fe) (Hu et al., 2019). Meanwhile, our previous studies showed the esterification of oleic acid or lauric acid with methanol over silicotungstic acid and nickel salts of Keggin-type hetopolyacids encapsulated into metal-organic framework (Uio-66) hybrid nanocatalysts that had excellent activity and reusability (Zhang et al., 2019b, 2020).

To date, there have been no reports on carrying out esterification reaction for biodiesel production using metal-organic framework Cu-BTC-supported Sn (II)-substituted Keggin hetopolyacids as nanocatalysts. Thus, in this work, we successfully synthesized a series of nanocatalysts consisting of Sn (II)-substituted 12-tungstophosphoric acid on a Cu-BTC matrix (Sn_{1.5}PW/Cu-BTC-x) at different ratios and used those nanocatalysts for producing biodiesel from OA with methanol. The characterization of synthesized nanocomposites was done using FTIR, XRD, SEM, TEM, nitrogen adsorption-desorption, TG, and NH₃-TPD. Further, the effect of different reaction parameters such as the molar ratio of methanol to OA, amount of catalyst, and reaction time and temperature were investigated to optimize the esterification conditions. Kinetic studies of the OA esterification reaction over the Sn_{1.5}PW/Cu-BTC nanocatalyst were studied. Finally, the reusability of those composites was also studied for seven successive runs.

EXPERIMENTAL SECTION

Materials and Synthesis

All chemicals were obtained from commercial sources and used without further purification. Copper (II) acetate monohydrate (Cu(CO₂CH₃)₂·H₂O, AR), 1,3,5-benzenetricarboxylic acid (H₃-BTC) (AR), tin chloride dehydrate (SnCl₂·2H₂O, AR), and 12-tungstophosphoric acid (H₃PW₁₂O₄₀, HPW, AR) were purchased from Shanghai Aladdin Industrial Inc. Oleic acid (OA, AR), N,N-dimethylformamide (DMF, AR), acetic acid (AR), absolute ethanol (AR), and anhydrous methanol (AR) were purchased from Sinopharm Chemical Reagent Co., Ltd.

Firstly, Sn_{1.5}PW₁₂O₄₀ (Sn_{1.5}PW) salts were prepared by stirring an aqueous solution containing the HPW and SnCl₂ at room temperature for 3 h; then, the obtained mixture was dried overnight at 120°C, according to our previous reports (Zhang et al., 2019a). Second, Cu-BTC was prepared from 0.06 g of copper (II) acetate monohydrate and 0.6 g of acetic acid dissolved in 6 mL distilled water, and 0.16 g of H₃-BTC dissolved in 6 mL of DMF was added dropwise from above the mixture solution. The resulting solution continued to be stirred for 3 h at room temperature. Then, the precipitate was collected by centrifugation and washed with 50 mL of hot ethanol two times and hot water once, and the blue powder was dried at 120°C for 12 h, according to the literature (Na et al., 2012). Finally, Cu-BTC-supported Sn (II)-substitute phosphotungstic acid catalysts were prepared by an impregnation method. Sn_{1.5}PW (0.25, 0.50, and 0.75 g) and the framework of Cu-BTC (0.50 g) at certain weight ratios were mixed in water. The obtained mixture was treated by ultrasonication for 10 min and was stirred continuously for 8 h at room temperature, followed by centrifugation and washing with distilled water three times. The resulting material was dried overnight in an oven (120°C). The synthesized Sn_{1.5}PW/Cu-BTC-x hybrids with different Sn_{1.5}PW to Cu-BTC weight ratios of 0.5, 1, and 1.5 were identified as Sn_{1.5}PW/Cu-BTC-0.5, Sn_{1.5}PW/Cu-BTC-1, and Sn_{1.5}PW/Cu-BTC-1.5, respectively.

Instrumentation

Fourier-transformed infrared spectroscopy (FTIR) spectra of the synthesized catalysts were obtained for powdered samples on KBr pellets using a PerkinElmer Spectrum 100 in the range of 400–4,000 cm⁻¹. Wide-angle X-ray diffraction (XRD) patterns were recorded on a D8 ADVANCE (Germany) using CuK α (1.5406 Å) radiation to get insight into the composition of the catalysts. The morphology of the catalysts was obtained on a scanning electron microscope (SEM) at 2.0 kV (Hitachi S4800) and a transmission electron microscope (TEM) at 200 kV (FEI Tecnai G2 20). The BET surface area and pore size were determined based on nitrogen adsorption-desorption isotherms with a Quantachrome instrument (Quantachrome Instruments, Boynton Beach, USA). Thermogravimetric (TG) analysis was carried out in a NETZSCH/STA 409 PC Luxx simultaneous thermal analyzer; the samples were heated up from room temperature to 600°C at a heating rate of 5°C/min. The acidic properties of the Sn_{1.5}PW/Cu-BTC-1

hybrid catalysts were characterized by temperature-programmed desorption (NH_3 -TPD) (Micromeritics AutoChem II 2920).

Catalytic Evaluation

Using a typical approach, the esterification of OA and methanol was performed in a 50-ml stainless-steel high-pressure autoclave reactor, and an appropriate amount of catalyst was charged into the autoclave reactor. Then, the reactor was preheated in an oil bath with a magnetic stirrer at an appropriate temperature for a specific time. After completion of the reaction period, all catalysts were recovered by centrifugation at 8,000 rpm for 5–7 min and washed by anhydrous methanol. In order to calculate the OA conversion, the reactants were purified in a rotary evaporator to remove water and residual methanol. The conversion of methyl oleate was estimated by measuring the acid value of feedstock and product, and the acid value was determined according to the method described in the ISO 660-2009 standard (Animal and vegetable fats and oils—determination of acid value and acidity).

RESULTS AND DISCUSSION

Catalyst Characterization

The $\text{Sn}_{1.5}\text{PW}$, Cu-BTC, and $\text{Sn}_{1.5}\text{PW}/\text{Cu-BTC-x}$ hybrids were firstly characterized by wide-angle XRD (Figure 1). For the $\text{Sn}_{1.5}\text{PW}$ sample, the peaks at 10.5° , 14.8° , 18.2° , 20.8° , 23.3° , 25.7° , 29.7° , 35.4° , and 38.0° can be related to the Keggin unit of HPW (Pasha et al., 2019), indicating the intact Keggin ion in the Sn-exchanged HPW catalysts. According to the literature (Yang et al., 2015), the wide-angle XRD spectrum of the synthesized Cu-BTC was in perfect agreement with the spectrum of simulated Cu-BTC. After supporting Sn (II)-substituted Keggin HPW, all $\text{Sn}_{1.5}\text{PW}/\text{Cu-BTC-x}$ hybrids showed a decrease in the peak intensities of the Cu-BTC characteristic phase, and the XRD spectrum of $\text{Sn}_{1.5}\text{PW}$ could not be distinguished from the XRD spectra of $\text{Sn}_{1.5}\text{PW}/\text{Cu-BTC}$ hybrids, suggesting that the $\text{Sn}_{1.5}\text{PW}$ salts were relatively uniformly distributed on the surface of Cu-BTC cages. Interestingly, the peak intensities of $\text{Sn}_{1.5}\text{PW}/\text{Cu-BTC-1}$ were much stronger than those of $\text{Sn}_{1.5}\text{PW}/\text{Cu-BTC-0.5}$ and $\text{Sn}_{1.5}\text{PW}/\text{Cu-BTC-1.5}$, which is probably due to the existence of interaction between the uniformly dispersed $\text{Sn}_{1.5}\text{PW}$ molecules and Cu-BTC matrix. These results showed that $\text{Sn}_{1.5}\text{PW}$ molecules were loaded on the surface of Cu-BTC nanocages through strong interaction.

The FTIR spectra of the HPW and $\text{Sn}_{1.5}\text{PW}$ samples were given in Figure S1. The FTIR spectra of HPW and Sn (II)-substituted HPW salts presented four characteristic peaks at 1,080, 982, 889, and 801 cm^{-1} , which was correlated with the Keggin unit of HPW, in agreement with the literature (Zhang et al., 2016). Moreover, as can be seen in Figure 2, the FTIR spectra of all $\text{Sn}_{1.5}\text{PW}/\text{Cu-BTC-x}$ hybrids showed the peaks corresponding to Cu-BTC, the coordinated acac ligand showed peaks at 1,450 and $1,373\text{ cm}^{-1}$, and some characteristic peaks at 1,645 and $1,586\text{ cm}^{-1}$ were shifted to 1,621 and $1,571\text{ cm}^{-1}$, respectively, indicating strong interaction between $\text{Sn}_{1.5}\text{PW}$ and Cu-BTC nanoparticles. Surprisingly, the various $\text{Sn}_{1.5}\text{PW}$ concentrations for $\text{Sn}_{1.5}\text{PW}/\text{Cu-BTC}$ showed four peaks at 1,080,

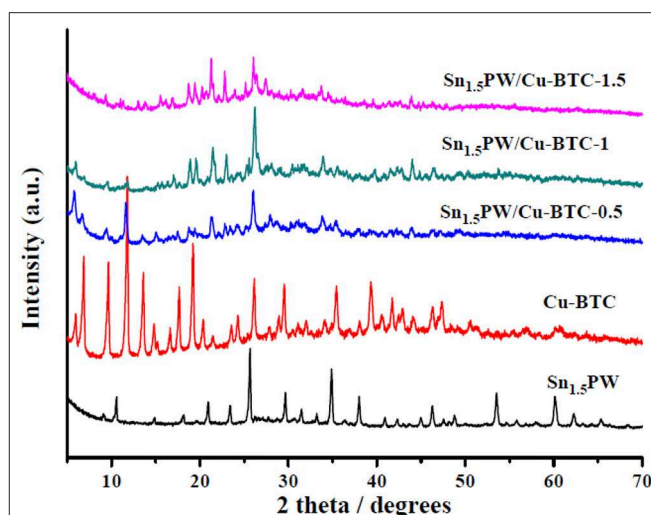


FIGURE 1 | Wide-angle XRD patterns of the $\text{Sn}_{1.5}\text{PW}$, Cu-BTC, and $\text{Sn}_{1.5}\text{PW}/\text{Cu-BTC-x}$ hybrids.

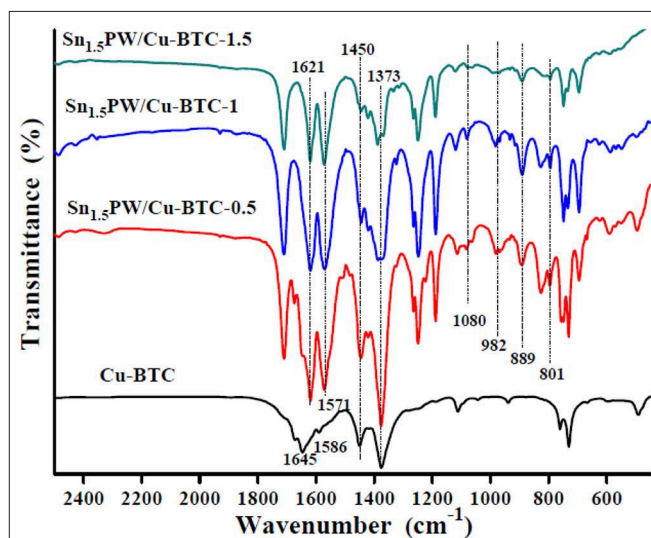


FIGURE 2 | FTIR spectra of the Cu-BTC and $\text{Sn}_{1.5}\text{PW}/\text{Cu-BTC-x}$ hybrids.

982, 889, and 801 cm^{-1} , respectively, further indicating that $\text{Sn}_{1.5}\text{PW}$ molecules were embedded around the surface of the Cu-BTC matrix. This also probably confirmed its stability and that it would suffer less leaching during the esterification reaction.

Figure 3 shows the SEM images of the pure HPW, $\text{Sn}_{1.5}\text{PW}$, Cu-BTC, and $\text{Sn}_{1.5}\text{PW}/\text{Cu-BTC-x}$ hybrids. The image of the pure HPW shows a large-blocked aggregate morphology. After Sn had been doped with HPW, the $\text{Sn}_{1.5}\text{PW}$ sample showed large nanoparticles of irregular shape and with a rough surface, indicating the successful exchange of protons by Sn ions, which was similar to our previously reported results (Cai et al., 2019). Moreover, Figure 3c shows a 100–200-nm size for the synthesized Cu-BTC nanoparticles, which are irregular octahedral crystals with low crystallinity and a

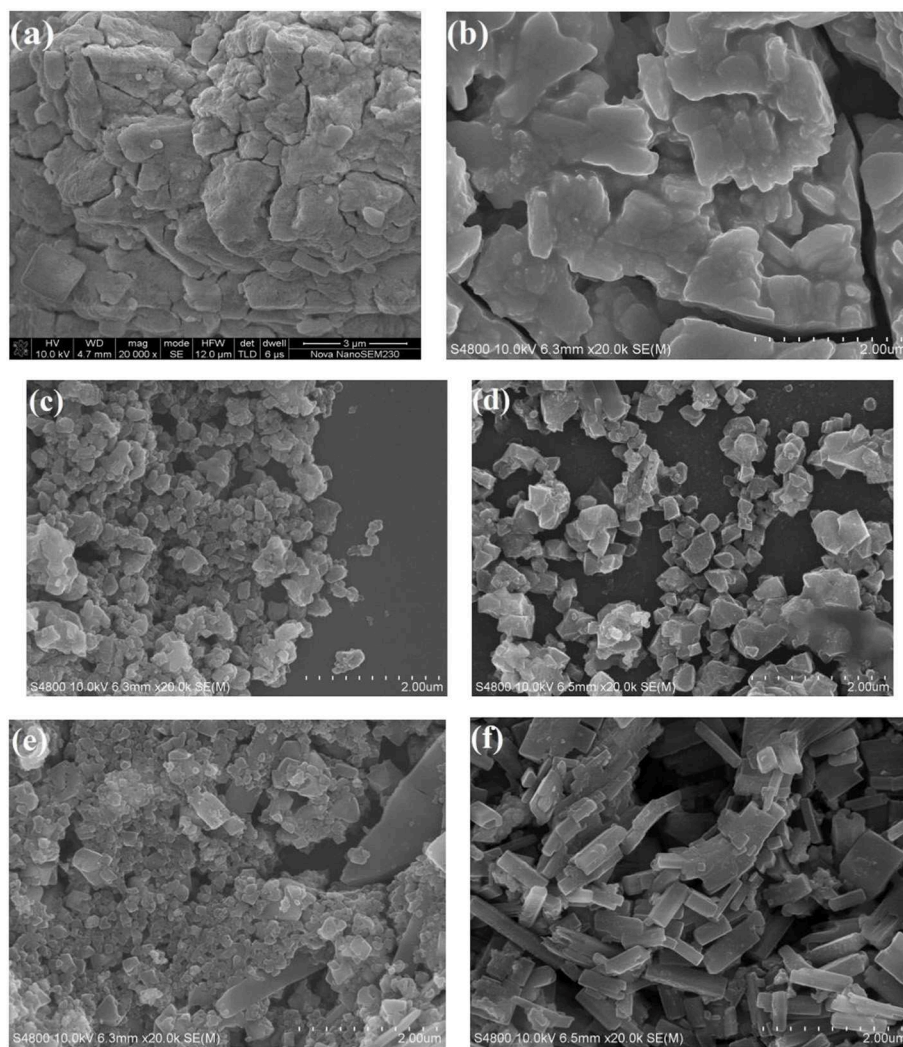


FIGURE 3 | SEM images of (a) pure HPW, (b) $\text{Sn}_{1.5}\text{PW}$, (c) Cu-BTC, (d) $\text{Sn}_{1.5}\text{PW}/\text{Cu-BTC-0.5}$, (e) $\text{Sn}_{1.5}\text{PW}/\text{Cu-BTC-1}$, and (f) $\text{Sn}_{1.5}\text{PW}/\text{Cu-BTC-1.5}$.

similar morphology as observed by Na et al. (2012). When $\text{Sn}_{1.5}\text{PW}$ was supported on Cu-BTC nanoparticles, the octahedral morphologies were markedly improved, suggesting that the addition of $\text{Sn}_{1.5}\text{PW}$ can be a modulator. Of note, the images (Figures 3d–f) showed a gradual increase in the $\text{Sn}_{1.5}\text{PW}$ coating on the surface of Cu-BTC nanoparticles, and, at 0.5 g $\text{Sn}_{1.5}\text{PW}$ loading, the surface morphology of $\text{Sn}_{1.5}\text{PW}/\text{Cu-BTC-1}$ was smooth, with no $\text{Sn}_{1.5}\text{PW}$ agglomeration. This observation might be due to the Cu-BTC matrix being completely coated. Meanwhile, compared to $\text{Sn}_{1.5}\text{PW}/\text{Cu-BTC-0.5}$ and $\text{Sn}_{1.5}\text{PW}/\text{Cu-BTC-1.5}$, the particle size of $\text{Sn}_{1.5}\text{PW}/\text{Cu-BTC-1}$ hybrids, which was in a range of 100–250 nm, was lower; thus, the $\text{Sn}_{1.5}\text{PW}/\text{Cu-BTC-1}$ hybrids possessed a high specific surface. Based on the above analyses, $\text{Sn}_{1.5}\text{PW}/\text{Cu-BTC-1}$ was selected for further characterization.

To visualize $\text{Sn}_{1.5}\text{PW}$ supported on Cu-BTC, TEM images of the $\text{Sn}_{1.5}\text{PW}/\text{Cu-BTC-1}$ were acquired; these are shown in

Figure 4. From **Figure 4a**, it can be seen that the $\text{Sn}_{1.5}\text{PW}/\text{Cu-BTC-1}$ presented an octahedral shape, confirming that the framework of Cu-BTC was properly retained. As highlighted in **Figures 4b,c**, the edges became noticeably roughened, and this reveals that many small $\text{Sn}_{1.5}\text{PW}$ particles were relatively uniformly distributed on the edges, which is consistent with the XRD and SEM results.

The N_2 adsorption-desorption isotherms and BJH pore size distributions of Cu-BTC and $\text{Sn}_{1.5}\text{PW}/\text{Cu-BTC-1}$ samples are shown in **Figure 5**. All samples show a type I isotherm, which revealed their microporous nature. Of note, the pore size distribution (**Figure 5B**) proved that the pores had an average diameter of 2–10 nm and a narrow size distribution. Moreover, the surface area decreased from 578.2 to 29.7 m^2/g , and the average pore size increased from 2.38 to 7.11 nm for Cu-BTC and $\text{Sn}_{1.5}\text{PW}/\text{Cu-BTC-1}$, respectively. The decrease in the BET surface area may be attributed to the presence

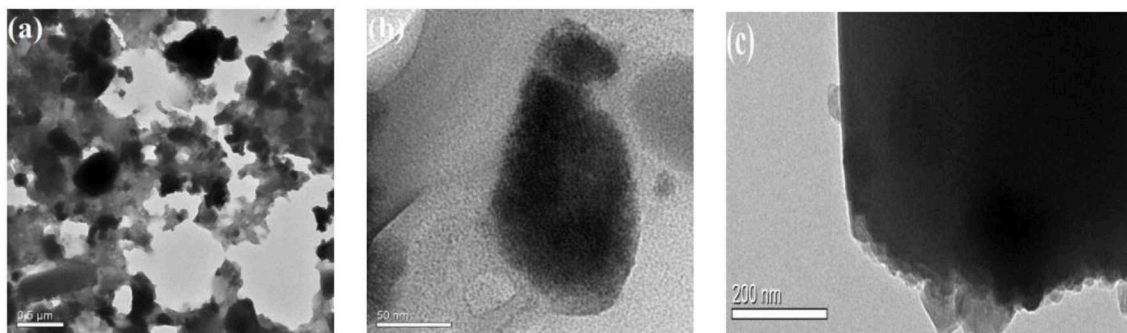


FIGURE 4 | (a–c) Typical TEM images of the $\text{Sn}_{1.5}\text{PW/Cu-BTC-1}$ hybrids.

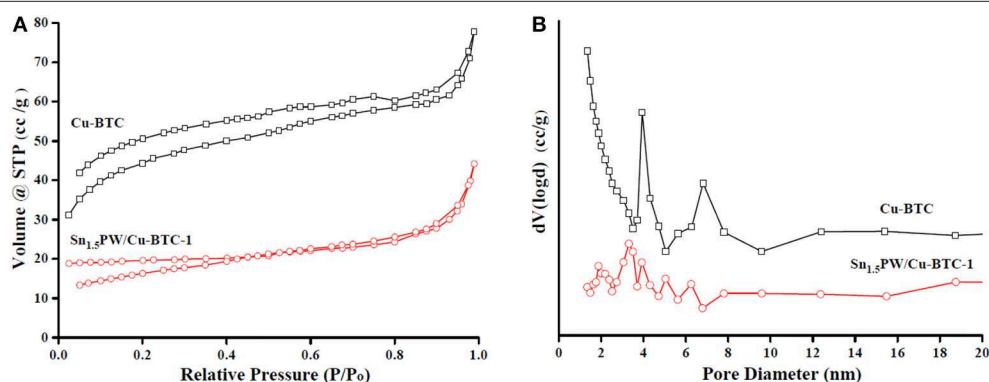


FIGURE 5 | (A) N_2 adsorption-desorption isotherm plots and **(B)** pore size distributions of Cu-BTC and $\text{Sn}_{1.5}\text{PW/Cu-BTC-1}$ samples.

of $\text{Sn}_{1.5}\text{PW}$ inside the Cu-BTC nanocages. The increase in the average pore size was probably due to a collapsed microporous structure, which was similar to previously reported results (Jeona et al., 2019). Meanwhile, the open cavities and relatively high specific surface area of $\text{Sn}_{1.5}\text{PW/Cu-BTC-1}$ nanocomposites were retained, which made for the free diffusion of the reactants or products, consistent with SEM results.

The thermal stabilities of the $\text{Sn}_{1.5}\text{PW}$, Cu-BTC, and $\text{Sn}_{1.5}\text{PW/Cu-BTC-1}$ samples were established with TG analysis (Figure 6). The $\text{Sn}_{1.5}\text{PW}$ sample showed no significant decomposition, and only 6% mass loss was observed up to 600°C . For the Cu-BTC and $\text{Sn}_{1.5}\text{PW/Cu-BTC-1}$ samples, the TG curve exhibited two stages of mass-loss, namely $40\text{--}250$ and $250\text{--}400^\circ\text{C}$; these intervals can be associated with the release of physically adsorbed water on the surface of sample and bonded water from the crystal hydrates (Azmoon et al., 2019) and the decomposition of the Cu-BTC frameworks (Xie and Wan, 2018), respectively. Above 400°C , almost no obvious mass loss was observed in the TG curve. The results indicated that the prepared catalysts had better stability and could be employed as heterogeneous catalysts for the esterification reaction.

Figure 7 displays the NH_3 -TPD profiles of $\text{Sn}_{1.5}\text{PW/Cu-BTC-1}$ nanocomposites. The minimum and maximum desorption

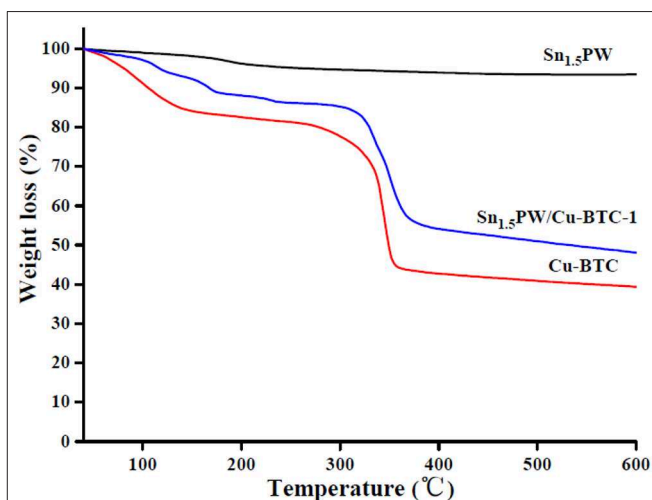


FIGURE 6 | TG curves of $\text{Sn}_{1.5}\text{PW}$, Cu-BTC, and $\text{Sn}_{1.5}\text{PW/Cu-BTC-1}$ samples.

temperatures of NH_3 are 225 and 319°C . The acidity present is attributed to the surface acidity of $\text{Sn}_{1.5}\text{PW}$. Based on these results, the nanocomposites possessed 24.6 mmol/g of total acidity. The results of NH_3 -TPD also show that the catalyst

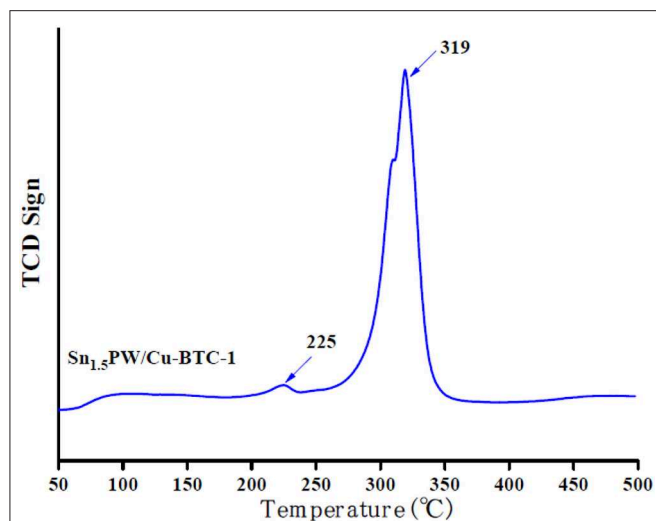


FIGURE 7 | NH_3 -TPD patterns of $\text{Sn}_{1.5}\text{PW}/\text{Cu-BTC-1}$ nanocomposite.

performance can be correlated with low and medium acidity strength. Therefore, the $\text{Sn}_{1.5}\text{PW}/\text{Cu-BTC-1}$ nanocomposites exhibit higher catalytic activity in the OA esterification.

Catalytic Performance of Different Catalysts

The influence of the molar ratio of $\text{Sn}_{1.5}\text{PW}/\text{Cu-BTC}$ on the esterification of OA was studied at 160°C by using 0.2 g catalyst and a 1:20 OA to methanol molar ratio within 4 h of reaction time. The results in Figure 8 reveal that the OA conversion was enhanced with the increase of the $\text{Sn}_{1.5}\text{PW}/\text{Cu-BTC}$ ratio up to 1. The highest OA conversion was obtained by utilizing $\text{Sn}_{1.5}\text{PW}/\text{Cu-BTC-1}$ and $\text{Sn}_{1.5}\text{PW}/\text{Cu-BTC-1.5}$ at 5 h. Most probably, this increase in the catalytic activity can be attributed to its relatively large specific surface area and appropriate particle size. In order to save raw material and avoid $\text{Sn}_{1.5}\text{PW}$ agglomeration on the support surface, we used this $\text{Sn}_{1.5}\text{PW}/\text{Cu-BTC-1}$ as the catalyst for further research.

Effect of Esterification Conditions

Biodiesel was produced by esterification, which is a reversible reaction that converts the OA into methyl oleate (biodiesel) and water in the presence of a nanocatalyst such as the $\text{Sn}_{1.5}\text{PW}/\text{Cu-BTC-1}$. The reaction temperature is one of the key parameters of the esterification reaction. Thus, the effect of temperature in the range 120 – 160°C on the esterification reaction of OA with methanol with $\text{Sn}_{1.5}\text{PW}/\text{Cu-BTC-1}$ nanocatalyst was examined, and the results are presented in Figure 9. The results indicated that the OA conversion was improved with an increase in the temperature, which indicates that high temperature would improve the $\text{Sn}_{1.5}\text{PW}/\text{Cu-BTC-1}$ catalytic activity due to the endothermic nature of the esterification reaction. When the temperature rose to 160°C , the OA conversion increased to 87.7% at 4 h. Moreover, the OA conversion was increased as the reaction time was increased from 1 to 4 h, but no significant increase

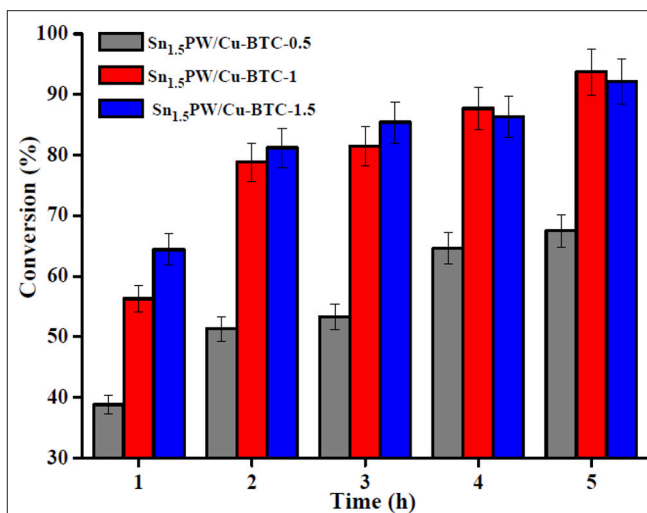


FIGURE 8 | Effects of various nanocatalysts for esterification of OA.

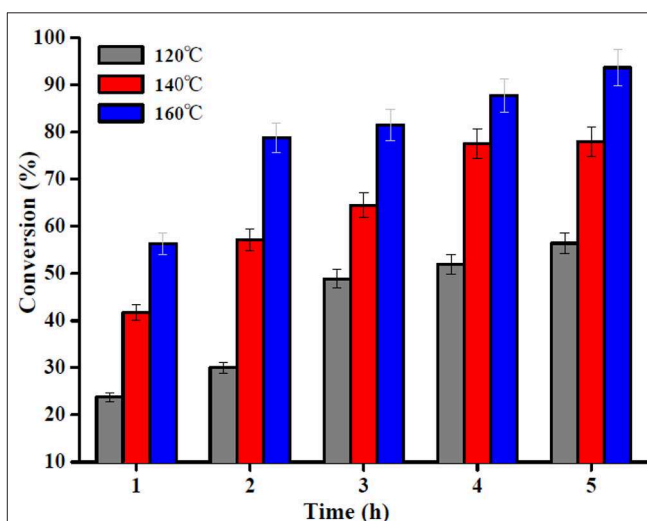


FIGURE 9 | Effect of reaction time and temperature. Reaction conditions: OA/methanol molar ratio 1:20, catalyst amount 0.2 g.

in OA conversion was observed beyond 4 h until 5 h. Thus, the selected temperature and time for further studies were 160°C and 4 h, respectively.

The OA to methanol molar ratio is one of the most important factors affecting the OA conversion and the cost of biodiesel production. Therefore, the effect of the OA to methanol molar ratio on OA esterification to biodiesel is shown in Figure 10A. Since esterification is a reversible reaction, high OA conversion could be achieved by using excess methanol in the reaction. It is evident that with the increase in the molar ratio of OA to methanol from 1:10 to 1:20, the OA conversion increased somewhat; however, no important change occurred as the molar ratio increased up to 1:30, and a large amount of methanol probably affected the OA conversion adversely, as the reactant was diluted and reduced the OA concentration (Nandiwale et al.,

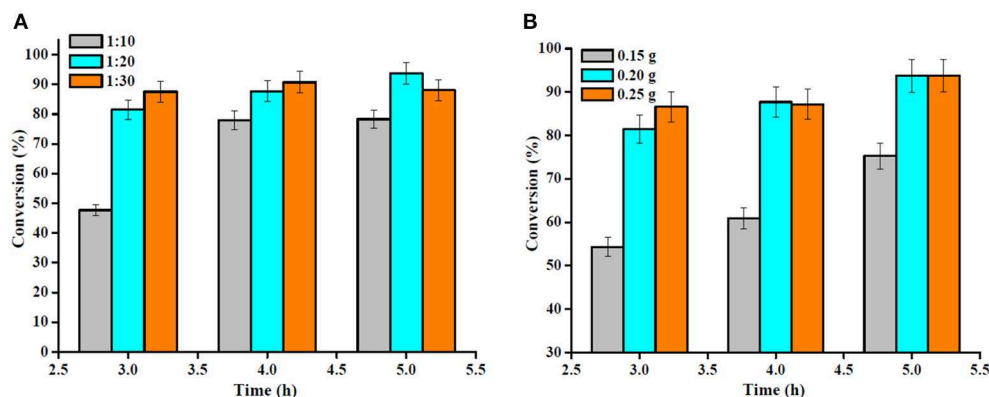


FIGURE 10 | (A) Effect of the molar ratio of OA to methanol (reaction conditions: temperature 160°C, catalyst amount 0.2 g) and **(B)** catalyst amount (reaction conditions: temperature 160°C, OA/methanol molar ratio 1:20).

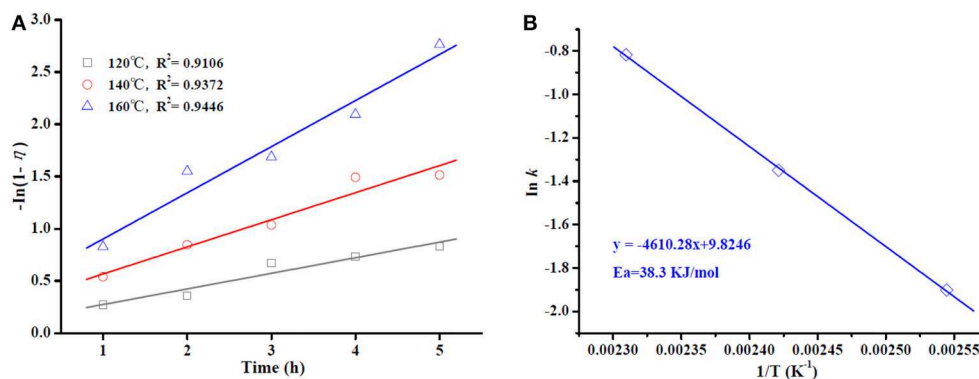


FIGURE 11 | Plot of $-\ln(1-\eta)$ vs. reaction time at different temperatures (A). Arrhenius plot of $\ln k$ vs. $1/T$ (B).

2013). Hence, the OA to methanol molar ratio was restricted to 1:20.

The study was further extended to the investigation of the effect of catalyst amount on the OA esterification reaction (Figure 10B). Under similar operating conditions, the OA conversion reached after 4 h of reaction was 60.9 and 87.7% using a $\text{Sn}_{1.5}\text{PW/Cu-BTC-1}$ nanocatalyst amount of 0.15 and 0.20 g, respectively. This is attributed to the acceleration of the reaction rate by there being a larger number of active sites in the reaction mixture. However, when a catalyst amount of 0.25 g was used, an OA conversion of 87.2% was reached, remaining practically constant in comparison with a catalyst amount of 0.20 g. Thus, it is suggested that 0.2 g of $\text{Sn}_{1.5}\text{PW/Cu-BTC-1}$ was the optimum amount, and this was used in the subsequent reactions.

Kinetic Studies of Biodiesel Production Using $\text{Sn}_{1.5}\text{PW/Cu-BTC-1}$ Nanocatalyst

Kinetic study for the OA esterification process was conducted under optimal conditions for $\text{Sn}_{1.5}\text{PW/Cu-BTC-1}$ at three different temperatures (120, 140, and 160°C). Because an excess

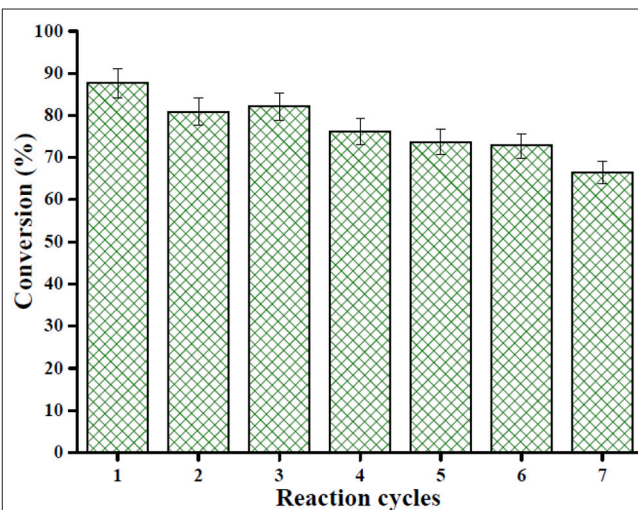


FIGURE 12 | Reusability of the nanocatalyst $\text{Sn}_{1.5}\text{PW/Cu-BTC-1}$ for seven cycles under optimum esterification conditions: temperature 160°C, catalyst amount 0.2 g, reaction time 4 h, and OA-methanol molar ratio 1:20.

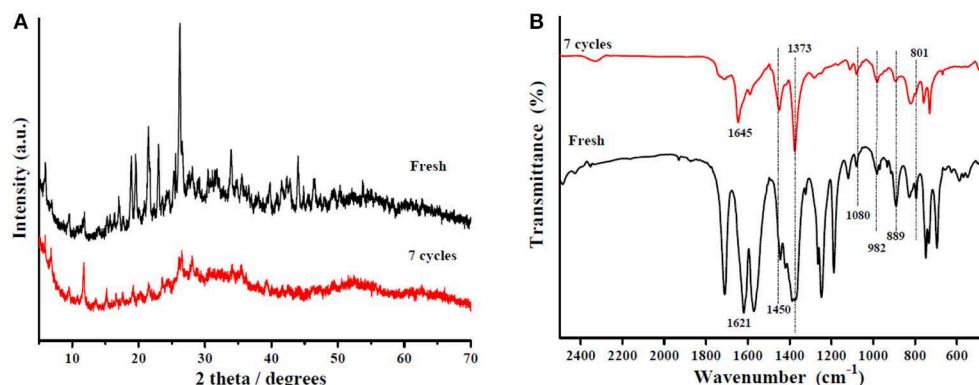


FIGURE 13 | (A) XRD patterns of the $\text{Sn}_{1.5}\text{PW/Cu-BTC-1}$ nanocatalyst and the nanocatalyst after seven cycles. **(B)** FT-IR spectra of the $\text{Sn}_{1.5}\text{PW/Cu-BTC-1}$ nanocatalyst and the nanocatalyst after seven cycles.

amount of methanol was used, the reverse reaction can be ignored, and the esterification reaction can also be assumed to follow the pseudo-first-order kinetic model (Kaur and Ali, 2015; Shalini and Chandra, 2018). Thus, the reaction rate constant is fitted in Equation (1), and the activation energy (E_a) required for the esterification process is calculated according to the Arrhenius, Equation (2).

$$k = -\ln \frac{1-\eta}{t} \quad (1)$$

$$\ln k = \ln A - \frac{E_a}{RT} \quad (2)$$

where k is the reaction rate constant; η is the conversion of OA at time t ; A is the Arrhenius constant or frequency factor; R is the universal gas constant; T is a reaction temperature.

A graph of $\ln(1-\eta)$ vs. time is given in **Figure 11A**. The plots display decent linearity with high regression coefficients ($R^2 = 0.9106, 0.9372$, and 0.9446 for 120, 140, and 160°C, respectively), indicating that the model is appropriate in terms of pseudo-first-order kinetics. The plot of $\ln k$ vs. $1/T$ in **Figure 11B** is found to be linear, with a high regression coefficient ($R^2 = 0.9994$). The value of E_a was determined to be 38.3 kJ/mol, which is much lower than the values determined in the works of Lieu et al. (2016) and Mazubert et al. (2014) for similar systems. More importantly, a value of $E_a > 15$ kJ/mol further supports that the OA esterification process in this work is controlled chemically (Patel and Brahmkhatri, 2013).

Reusability of Catalyst

Reusability is considered the most important characteristic of heterogeneous solid acid catalysts. In this work, the $\text{Sn}_{1.5}\text{PW/Cu-BTC-1}$ nanocatalyst was separated by centrifugation after the completion of the reaction, washed with anhydrous methanol, and then used directly after each cycle. Under the same optimum conditions, the esterification of OA was performed seven times, and **Figure 12** displays the results obtained. It was detected that the activity of the catalyst can still keep the conversion above 80% after three-time reuse. Nevertheless, it was found that, after seven times, the conversion was more than 60%.

Furthermore, XRD and FT-IR tests were performed to determine the stability of the synthesized nanocatalyst; the results are presented in **Figures 13A,B**. According to **Figure 13A**, the XRD pattern of the recycled catalyst was almost consistent with that of the fresh one, and only the peak intensity decreased. As exhibited in **Figure 13B**, the featured peaks of the Keggin structure and the characteristic peaks of Cu-BTC were found in the FT-IR spectrum of the recycled catalyst, indicating that the $\text{Sn}_{1.5}\text{PW/Cu-BTC-1}$ nanocatalyst had a durable structure. Based on the above discussion, the catalytic activity loss might be due to the composites in the reaction mixture losing few $\text{Sn}_{1.5}\text{PW}$ active sites. Thus, in comparison with earlier reported solid acid catalysts, the synthesized $\text{Sn}_{1.5}\text{PW/Cu-BTC-1}$ nanocatalyst showed better stability in biodiesel synthesis.

CONCLUSION

In summary, an efficient solid acid nanocatalyst, $\text{Sn}_{1.5}\text{PW/Cu-BTC-1}$, was prepared through the immobilization of $\text{Sn}_{1.5}\text{PW}$ salts on Cu-BTC. The prepared nanocomposites were then implemented for the production of biodiesel from OA and methanol. A high conversion of 87.7% was obtained under the optimized conditions of 160°C for 4 h with a molar ratio of OA to methanol of 1:20, and the addition of 0.2 g of catalyst. In addition, this nanocomposite catalyst showed good stability, and even after seven cycles of reuse, a considerable OA conversion could still be achieved. Moreover, a pseudo-first-order kinetic model was found to represent the data more appropriately, with the E_a of the reaction being 38.3 kJ/mol. The remarkable point in this study was the use of a facile, simple, and cheap method for the synthesis of $\text{Sn}_{1.5}\text{PW/Cu-BTC}$ nanocomposites in the large-scale production of biodiesel.

DATA AVAILABILITY STATEMENT

The raw data supporting the conclusions of this article will be made available by the authors, without undue reservation, to any qualified researcher.

AUTHOR CONTRIBUTIONS

QZ was in charge of designing the experiments and writing the manuscript. DLi and DLe performed experiments. XL, JW, YZ, and PM were in charge of revising the manuscript.

FUNDING

This work was financially supported by the Guizhou Science and Technology Foundation ([2020]1Y054), the Technical Talent Support Program of Guizhou Education Department (KY [2018]069), the Academician Workstation of Guizhou

Science and Technology Plan (S&T Cooperation Platform Talents [2016]5602), the Guizhou Science and Technology Cooperation Project (LH[2017]7059), the Key Support Discipline in Agricultural Resources and Environment of Anshun University, and the Creative Research Groups Support Program of Guizhou Education Department (KY [2017]049).

SUPPLEMENTARY MATERIAL

The Supplementary Material for this article can be found online at: <https://www.frontiersin.org/articles/10.3389/fchem.2020.00129/full#supplementary-material>

REFERENCES

- Al-Saadi, L. S., Eze, V. C., and Harvey, A. P. (2018). Experimental determination of optimal conditions for reactive coupling of biodiesel production with in situ glycerol carbonate formation in a triglyceride transesterification process. *Front. Chem.* 6:625. doi: 10.3389/fchem.2018.00625
- Azmoon, A. H., Ahmadvpour, A., Nayebezhadeh, H., Saghatoleslami, N., and Heydari, A. (2019). Fabrication of nanosized $\text{SO}_4^{2-}/\text{Co-Al}$ mixed oxide via solution combustion method used in esterification reaction: effect of urea-nitrate ratio on the properties and performance. *J. Nanostruct. Chem.* 9, 247–258. doi: 10.1007/s40097-019-00315-y
- Bhanja, P., and Bhaumik, A. (2016). Porous nanomaterials as green catalyst for the conversion of biomass to bioenergy. *Fuel* 185, 432–441. doi: 10.1016/j.fuel.2016.08.004
- Cai, J., Yang, T. T., Yue, C. Y., Pu, Q. L., Wang, R. Y., and Zhang, Q. Y. (2019). Preparation of silver-exchanged heteropolyacid catalyst and its application for biodiesel production. *Energ. Source. Part A* 1–11. doi: 10.1080/15567036.2019.1623945
- da Conceição, L. R. V., Carneiro, L. M., Giordani, D. S., and de Castro, H. F. (2017). Synthesis of biodiesel from macaw palm oil using mesoporous solid catalyst comprising 12-molybdophosphoric acid and niobia. *Renew. Energ.* 113, 119–128. doi: 10.1016/j.renene.2017.05.080
- Ekinici, E. K., and Oktar, N. (2019). Production of value-added chemicals from esterification of waste glycerol over MCM-41 supported catalysts. *Green Process. Synth.* 8, 128–134. doi: 10.1515/gps-2018-0034
- Ghubayra, R., Nuttall, C., Hodgkiss, S., Craven, M., Kozhevnikov, E. F., and Kozhevnikov, I. V. (2019). Oxidative desulfurization of model diesel fuel catalyzed by carbon-supported heteropoly acids. *Appl. Catal. B Environ.* 253, 309–316. doi: 10.1016/j.apcatb.2019.04.063
- Hu, P. F., Chen, C. C., Wang, Y. F., Pan, L., and Lu, C. H. (2019). Room-temperature self-assembled preparation of porous $\text{ZnFe}_2\text{O}_4/\text{MIL-100}(\text{Fe})$ nanocomposites and their visible-light derived photocatalytic properties. *Chem. Select* 4, 9703–9709. doi: 10.1002/slct.201902246
- Jeona, Y., Chia, W. S., Hwang, J., Kim, D. H., Kim, J. H., and Shul, Y. G. (2019). Core-shell nanostructured heteropoly acid-functionalized metal-organic frameworks: bifunctional heterogeneous catalyst for efficient biodiesel production. *Appl. Catal. B Environ.* 242, 51–59. doi: 10.1016/j.apcatb.2018.09.071
- Kang, Y. S., Lu, Y., Chen, K., Zhao, Y., Wang, P., and Sun, W. Y. (2019). Metal-organic frameworks with catalytic centers: from synthesis to catalytic application. *Coordin. Chem. Rev.* 378, 262–280. doi: 10.1016/j.ccr.2018.02.009
- Kaur, N., and Ali, A. (2015). Preparation and application of $\text{Ce}/\text{ZrO}_2\text{-TiO}_2/\text{SO}_4^{2-}$ as solid catalyst for the esterification of fatty acids. *Renew. Energ.* 81, 421–431. doi: 10.1016/j.renene.2015.03.051
- Li, D. D., Xu, H. O., Jiao, L., and Jiang, H. L. (2019). Metal-organic frameworks for catalysis: State of the art, challenges, and opportunities. *EnergyChem* 1:100005. doi: 10.1016/j.enchem.2019.100005
- Li, H., Liu, F. S., Ma, X. L., Wu, Z. J., Li, Y., Zhang, L. H., et al. (2019). Catalytic performance of strontium oxide supported by MIL-100(Fe) derivate as transesterification catalyst for biodiesel production. *Energ. Convers. Manage.* 180, 401–410. doi: 10.1016/j.enconman.2018.11.012
- Li, H., Wang, C. H., Xu, Y. F., Yu, Z. Z., Saravanamurugan, S., Wu, Z. L., et al. (2020). Heterogeneous (de) chlorination-enabled control of reactivity in the liquid-phase synthesis of furanic biofuel from cellulosic feedstock. *Green Chem.* 22, 637–645. doi: 10.1039/C9GC04092G
- Lieu, T., Yusup, S., and Moniruzzaman, M. (2016). Kinetic study on microwave-assisted esterification of free fatty acids derived from Ceiba pentandra seed oil. *Bioresour. Technol.* 211, 248–256. doi: 10.1016/j.biortech.2016.03.105
- Long, J., Xu, Y., Zhao, W., Li, H., and Yang, S. (2019). Heterogeneous catalytic upgrading of biofuranic aldehydes to alcohols. *Front. Chem.* 7:529. doi: 10.3389/fchem.2019.00529
- Mahmoud, H. R. (2019). Bismuth silicate ($\text{Bi}_4\text{Si}_3\text{O}_{12}$ and Bi_2SiO_5) prepared by ultrasonic-assisted hydrothermal method as novel catalysts for biodiesel production via oleic acid esterification with methanol. *Fuel* 256:115979. doi: 10.1016/j.fuel.2019.115979
- Mazubert, A., Taylor, C., Aubin, J., and Poux, M. (2014). Key role of temperature monitoring in interpretation of microwave effect on transesterification and esterification reactions for biodiesel production. *Bioresour. Technol.* 161, 270–279. doi: 10.1016/j.biortech.2014.03.011
- Na, L. Y., Hua, R. N., Ning, G. L., and Ou, X. X. (2012). Nano/micro HKUST-1 fabricated by coordination modulation method at room temperature. *Chem. Res. Chin. Univ.* 28, 555–558.
- Nandiwale, K. Y., and Bokade, V. V. (2014). Process optimization by response surface methodology and kinetic modeling for synthesis of methyl oleate biodiesel over $\text{H}_3\text{PW}_{12}\text{O}_{40}$ anchored montmorillonite K10. *Ind. Eng. Chem. Res.* 53, 18690–18698. doi: 10.1021/ie500672v
- Nandiwale, K. Y., Sonar, S. K., Niphadkar, P. S., Joshi, P. N., Deshpande, S. S., Patil, V. S., et al. (2013). Catalytic upgrading of renewable levulinic acid to ethyl levulinate biodiesel using dodecatungstophosphoric acid supported on desilicated H-ZSM-5 as catalyst. *Appl. Catal. A Gen.* 460–461, 90–98. doi: 10.1016/j.apcata.2013.04.024
- Negm, N. A., Betiha, M. A., Alhumaimess, M. S., Hassan, H. M. A., and Rabie, A. M. (2019). Clean transesterification process for biodiesel production using heterogeneous polymer-heteropoly acid nanocatalyst. *J. Clean. Prod.* 238:117854. doi: 10.1016/j.jclepro.2019.117854
- Nikseresht, A., Daniyal, A., Ali-Mohammadi, M., Afzalnia, A., and Mirzaie, A. (2017). Ultrasound-assisted biodiesel production by a novel composite of Fe (III)-based MOF and phosphotungstic acid as efficient and reusable catalyst. *Ultrason. Sonochem.* 37, 203–207. doi: 10.1016/j.ultsonch.2017.01.011
- Parida, K. M., and Mallick, S. (2007). Silicotungstic acid supported zirconia: an effective catalyst for esterification reaction. *J. Mol. Catal. A Chem.* 275, 77–83. doi: 10.1016/j.molcata.2007.05.022
- Pasha, N., Lingaiah, N., and Shiva, R. (2019). Zirconium exchanged phosphotungstic acid catalysts for esterification of levulinic acid to ethyl levulinate. *Catal. Lett.* 149, 2500–2507. doi: 10.1007/s10562-019-02862-z
- Patel, A., and Brahmakhat, V. (2013). Kinetic study of oleic acid esterification over 12-tungstophosphoric acid catalyst anchored to different mesoporous silica supports. *Fuel Process. Technol.* 113, 141–149. doi: 10.1016/j.fuproc.2013.03.022

- Shalini, S., and Chandra, S. Y. (2018). Economically viable production of biodiesel using a novel heterogeneous catalyst: kinetic and thermodynamic investigations. *Energ. Convers. Manage.* 171, 969–983. doi: 10.1016/j.enconman.2018.06.059
- Sun, Z., Duan, X. X., Zhao, J., Wang, X. H., and Jiang, Z. J. (2015). Homogeneous borotungstic acid and heterogeneous micellar borotungstic acid catalysts for biodiesel production by esterification of free fatty acid. *Biomass Bioenerg.* 76, 31–42. doi: 10.1016/j.biombioe.2015.03.002
- Talebian-Kiakalaieh, A., Amin, N. A. S., Zarei, A., and Noshadi, I. (2013). Transesterification of waste cooking oil by heteropoly acid (hpa) catalyst: optimization and kinetic model. *Appl. Energ.* 102, 283–292. doi: 10.1016/j.apenergy.2012.07.018
- Xie, W. L., and Wan, F. (2018). Basic ionic liquid functionalized magnetically responsive $\text{Fe}_3\text{O}_4/\text{HKUST-1}$ composites used for biodiesel production. *Fuel* 220, 248–256. doi: 10.1016/j.fuel.2018.02.014
- Xie, W. L., and Wan, F. (2019a). Biodiesel production from acidic oils using polyoxometalate-based sulfonated ionic liquids functionalized metal-organic frameworks. *Catal. Lett.* 149, 2916–2929. doi: 10.1007/s10562-019-02800-z
- Xie, W. L., and Wan, F. (2019b). Immobilization of polyoxometalate-based sulfonated ionic liquids on UiO-66-2COOH metal-organic frameworks for biodiesel production via one-pot transesterification-esterification of acidic vegetable oils. *Chem. Eng. J.* 365, 40–50. doi: 10.1016/j.cej.2019.02.016
- Xu, Y. F., Long, J. X., Zhao, W. F., Li, H., and Yang, S. (2019). Efficient transfer hydrogenation of nitro compounds to amines enabled by mesoporous N-stabilized Co-Zn/C. *Front. Chem.* 7:590. doi: 10.3389/fchem.2019.00590
- Yang, X. L., Qiao, L., and Dai, W. (2015). One-pot synthesis of a hierarchical microporous-mesoporous phosphotungstic acid-HKUST-1 catalyst and its application in the selective oxidation of cyclopentene to glutaraldehyde. *Chin. J. Catal.* 36, 1875–1885. doi: 10.1016/S1872-2067(15)60972-X
- Zhang, D. Y., Duan, M. H., Yao, X. H., Fu, Y. J., and Zu, Y. G. (2016). Preparation of a novel cellulose-based immobilized heteropoly acid system and its application on the biodiesel production. *Fuel* 172, 293–300. doi: 10.1016/j.fuel.2015.12.020
- Zhang, Q. Y., Ling, D., Lei, D. D., Deng, T. L., Zhang, Y. T., and Ma, P. H. (2020). Synthesis and catalytic properties of nickel salts of kegglin-type heteropolyacids embedded metal-organic framework hybrid nanocatalyst. *Green Process. Synth.* 9, 131–138. doi: 10.1515/gps-2020-0014
- Zhang, Q. Y., Yang, T. T., Liu, X. F., Yue, C. Y., Ao, L. F., Deng, T. L., et al. (2019b). Heteropoly acid-encapsulated metal-organic framework as a stable and highly efficient nanocatalyst for esterification reaction. *RSC Adv.* 9, 16357–16365. doi: 10.1039/C9RA03209F
- Zhang, Q. Y., Yue, C. Y., Pu, Q. L., Yang, T. T., Wu, Z. F., and Zhang, Y. T. (2019a). Facile synthesis of ferric-modified phosphomolybdic acid composite catalysts for biodiesel production with response surface optimization. *ACS Omega* 4, 9041–9048. doi: 10.1021/acsomega.9b01037

Conflict of Interest: The authors declare that the research was conducted in the absence of any commercial or financial relationships that could be construed as a potential conflict of interest.

Copyright © 2020 Zhang, Ling, Lei, Wang, Liu, Zhang and Ma. This is an open-access article distributed under the terms of the Creative Commons Attribution License (CC BY). The use, distribution or reproduction in other forums is permitted, provided the original author(s) and the copyright owner(s) are credited and that the original publication in this journal is cited, in accordance with accepted academic practice. No use, distribution or reproduction is permitted which does not comply with these terms.



A Synthetic View on Haedoxans and Related Neolignans From *Phryma leptostachya*

Yang Chen^{1*}, Shu Xiao¹, Jian Huang¹, Wei Xue¹ and Shuzhong He^{2*}

¹ Laboratory Breeding Base of Green Pesticide and Agricultural Bioengineering, Key Laboratory of Green Pesticide and Agricultural Bioengineering Ministry of Education, Guizhou University, Guiyang, China, ² Guizhou Engineering Laboratory for Synthetic Drugs, School of Pharmaceutical Sciences, Guizhou University, Guiyang, China

OPEN ACCESS

Edited by:

Yaqiong Su,
Eindhoven University of
Technology, Netherlands

Reviewed by:

Min Zhang,
Chongqing University, China
Yang Hua,
Zhengzhou University, China
Pei Tang,
Sichuan University, China

*Correspondence:

Yang Chen
ychen1@gzu.edu.cn
Shuzhong He
szhe@gzu.edu.cn

Specialty section:

This article was submitted to
Organic Chemistry,
a section of the journal
Frontiers in Chemistry

Received: 27 March 2020

Accepted: 04 May 2020

Published: 17 June 2020

Citation:

Chen Y, Xiao S, Huang J, Xue W and
He S (2020) A Synthetic View on
Haedoxans and Related Neolignans
From *Phryma leptostachya*.
Front. Chem. 8:460.
doi: 10.3389/fchem.2020.00460

Keywords: haedoxans, neolignans, *Phryma leptostachya*, insecticidal activity, natural products

INTRODUCTION

Phryma leptostachya is a perennial herb that is widespread in nature (Lee et al., 2002; Park et al., 2005; Endo and Miyauchi, 2006; Li et al., 2019a,b; Xu et al., 2019). In Chinese culture, the plant has been used as a traditional Chinese medicine to treat inflammatory diseases, such as itching, allergic dermatitis, and gout (Jung et al., 2013). In East Asia, *P. leptostachya* has also been traditionally used as a natural insecticide (Taniguchi and Oshima, 1972a,b; Ishibashi and Taniguchi, 1998; Xiao et al., 2012a; Jung et al., 2013), for instance being used to repel mosquitos and flies in the southwest district of China (Chen et al., 2012). As a result, the secondary metabolites isolated from *P. leptostachya* have drawn much attention.

Previous phytochemical investigations showed that this plant is rich in lignans. Among them, (+)-haedoxan A (**1**, see **Figure 1A**), isolated in 1989 by Taniguchi, represents the major insecticidal ingredient (Taniguchi et al., 1989; Yamaguchi and Taniguchi, 1992a; Seo and Park, 2012). Structurally, this natural product is a sesquilignan, that is, a trimer of C₆C₃ units (*n*-propyl benzene). The skeleton features a furofuran core and a dioxane core with six stereogenic centers. Haedoxan D (**2**) and E (**3**) are from the same natural product family, which structurally differs from haedoxan A (**1**) at one of the aromatic rings. (+)-Phrymarolin I (**4**) and II (**5**) are also important ingredients of *P. leptostachya* extracts. As neolignans, these two compounds are phenylpropianoid dimers that share the same furofuran core with haedoxans.

Haedoxans exhibit excellent insecticidal activity against several insects, such as *Musca domestica* [*Culex pipiens pallens* (Xiao et al., 2012b)] and *Mythimna separata* (Xiao et al., 2012a). It is noteworthy that the insecticidal activity of Haedoxan A (**1**) is comparable to that of the commercial synthetic pyrethroids (Taniguchi et al., 1989; Hu et al., 2016). (+)-Phrymarolins I (**4**) and II (**5**) also show considerable synergistic activities with pyrethrin and carbamate pesticides (Park et al., 2005). Accordingly, haedoxans and phrymarolins could be used as the main insecticidal ingredients in new botanical pesticides. In addition, the potential utilities of these natural products as lead compounds in pesticide discovery are also attractive.

To date, Haedoxan A (**1**) has only been found in the root of *P. leptostachya* at very low concentration (from 0.004 to 0.009%). Although two total syntheses of haedoxan A (**1**) have been reported by Taniguchi and Ishibashi, over 20 synthetic steps are needed to achieve a natural product with moderate selectivities (Ishibashi and Taniguchi, 1989, 1998). As a result, the availability of haedoxan A (**1**) is the main obstacle in its commercialization process. To address this problem, new synthetic routes for haedoxans with high efficiencies and stereoselectivities are needed.

SYNTHETIC STUDIES TOWARD HAEDOXAN-LIKE MOLECULES

In this review, we focus on the chemical synthesis of haedoxans and some closely related natural products such as phrymarolin I (**4**) and II (**5**). While a number of synthetic studies on the lignan family have been reported, there have been limited reports on the synthesis of haedoxans. Since a phenylpropanoid trimer bears six stereogenic centers, haedoxans are the most structurally complex members in this family. It is noteworthy that besides the four contiguous stereocenters, the two chiral carbons that are remote from the furofuran core might also be a significant synthetic challenge due to stereocorrelation problems in the fragment coupling process. As a result, it would be extremely difficult to control stereoselectivities in the total synthesis of haedoxans.

In 1986, Ishibashi and Taniguchi reported the synthesis of (±)-phrymarolin II (**5**), which represents a pioneering study on the chemical synthesis of haedoxan-like natural products (Ishibashi and Taniguchi, 1986). As shown in **Figure 1B**, the authors started their synthesis with an aldol reaction between lactone **6** and benzaldehyde **7** to build the left fragment of phrymarolin II (**5**). The adduct **8** was protected with a TBS group, and the lactone was then reduced with LiAlH₄ to afford diol **9**. After Upjohn dihydroxylation and oxidative cleavage with NaIO₄, diol **9** was converted to semiacetal **10**, which possesses one of the two tetrahydrofurans in the central fragment of the natural product. The semiacetal was then oxidized to corresponding lactone (**11**) with a quantitative yield. Once the lactone was established, a two-step reaction sequence was carried out to realize a β-elimination process. The resulting α, β-unsaturated lactone **12** was then oxidized with Upjohn dihydroxylation to give diol **13** at 97% yield. After deprotection of the TBS group with TBAF, the second tetrahydrofuran ring and the C6 stereocenter were established through an acid-promoted etherification reaction. The product **14** was treated with DIBAL-H to reduce the lactone moiety, and the newly formed diol was differentiated within four steps to afford chloride **16**. Finally, a CdCO₃ catalyzed substitution successfully introduced the right fragment to give (±)-phrymarolin II (**5**) with its stereoisomer **17** in a ratio of 1:3 (55% total yield).

In 1988, Ishibashi and Taniguchi improved the previous synthetic route and reported the total synthesis of (+)-phrymarolin I [**4**, (Ishibashi and Taniguchi, 1988)]. This asymmetric synthesis commenced with the preparation of the

optically pure (+)-**4**. As shown in **Figure 1C**, aminolysis of (±)-**6** with (S)-1-phenylethanamine gave two diastereoisomers that could be separated through chromatography. Then, hydrolysis of **18** followed by lactonization afforded (+)-**6** at 58% yield. This chiral starting material was subjected to the above synthetic route to give **14** in an asymmetric fashion. Different from the previous synthesis, **14** was first protected by the TBS group and then reduced to lactol **20**, which was then fluorinated to set the stage for the subsequent fragment coupling. In the next event, phenol **22** was introduced in the presence of SnCl₂ and trityl perchlorate to provide the coupling product **23** with a diastereomeric ratio of 1:2, favoring the undesired diastereomer. The mixed products were desilylated and separated by preparative TLC to afford **24** in 11% yield over two steps. Finally, acylation of **24** provided the desired natural product (+)-phrymarolin I (**4**).

One year later, Ishibashi and Taniguchi applied their developed synthetic route to the total synthesis of (±)-haedoxan A (**1**), D (**2**), and E [**3**, (Ishibashi and Taniguchi, 1989)]. As shown in **Figure 1D**, the preparation of the benzodioxane fragment **33** is not trivial. Their synthesis commenced with selective methylation and MOM protection of the benzaldehyde **25**. After Dakin oxidation and hydrolysis, the resultant phenol **27** was etherified with bromide **28** to give **29** as the coupling product. Global reduction with NaBH₄ was followed with acid promoted deprotection to generate **30** at 74% yield. A PPA-mediated cyclization was then introduced to build the dioxane ring. Finally, methylation and selective formylation provided the desired aromatic fragment (±)-**33**.

With the above fragment in hand, the authors followed their previous synthesis to carry out an aldol reaction between lactone **6** and aldehyde **33**, as shown in **Figure 2A**. However, although the reaction worked well, product **34** was obtained as a mixture of diastereomers due to stereochemical correlation issues. The adduct was protected with the TBS group and then purified by chromatography to afford an inseparable mixture of **35** and **36** at 55% total yield. The mixture was then submitted to the known synthetic route to give fluoride **38** within 11 steps. With this key intermediate, haedoxin A (**1**), D (**2**), E (**3**) were synthesized in diastereoselective fashion.

In the following decade, Taniguchi and coworkers applied their strategy to synthesizing a series of lignan analogs to explore potential insecticidal compounds (Yamaguchi and Taniguchi, 1991, 1992a,b,c; Yamaguchi et al., 1992a,b). A significant improvement of the synthetic strategy was published by Okazaki et al. (1997). In this report, the authors developed a concise synthetic route toward (+)-phrymarolin I (**4**). As shown in **Figure 2B**, the synthesis commenced with an aldol reaction using chiral lactone **40** as the nucleophile, which could be easily prepared from (R)-malate. After reductive opening of the lactone ring, the tetraol intermediate was treated with HCl solution to close the tetrahydrofuran ring and give **42**. Then, a three-step reaction sequence, including alcohol protection, Swern oxidation, and Tebbe olefination, was used to prepare alkene **43**. Diastereoselective dihydroxylation followed by Pfizner-Moffatt oxidation and desilylation provided chiral lactol **15** at a good yield. The key intermediate that had been used in the authors' synthesis of phrymarolin II (**5**), **15**, was subjected directly to an

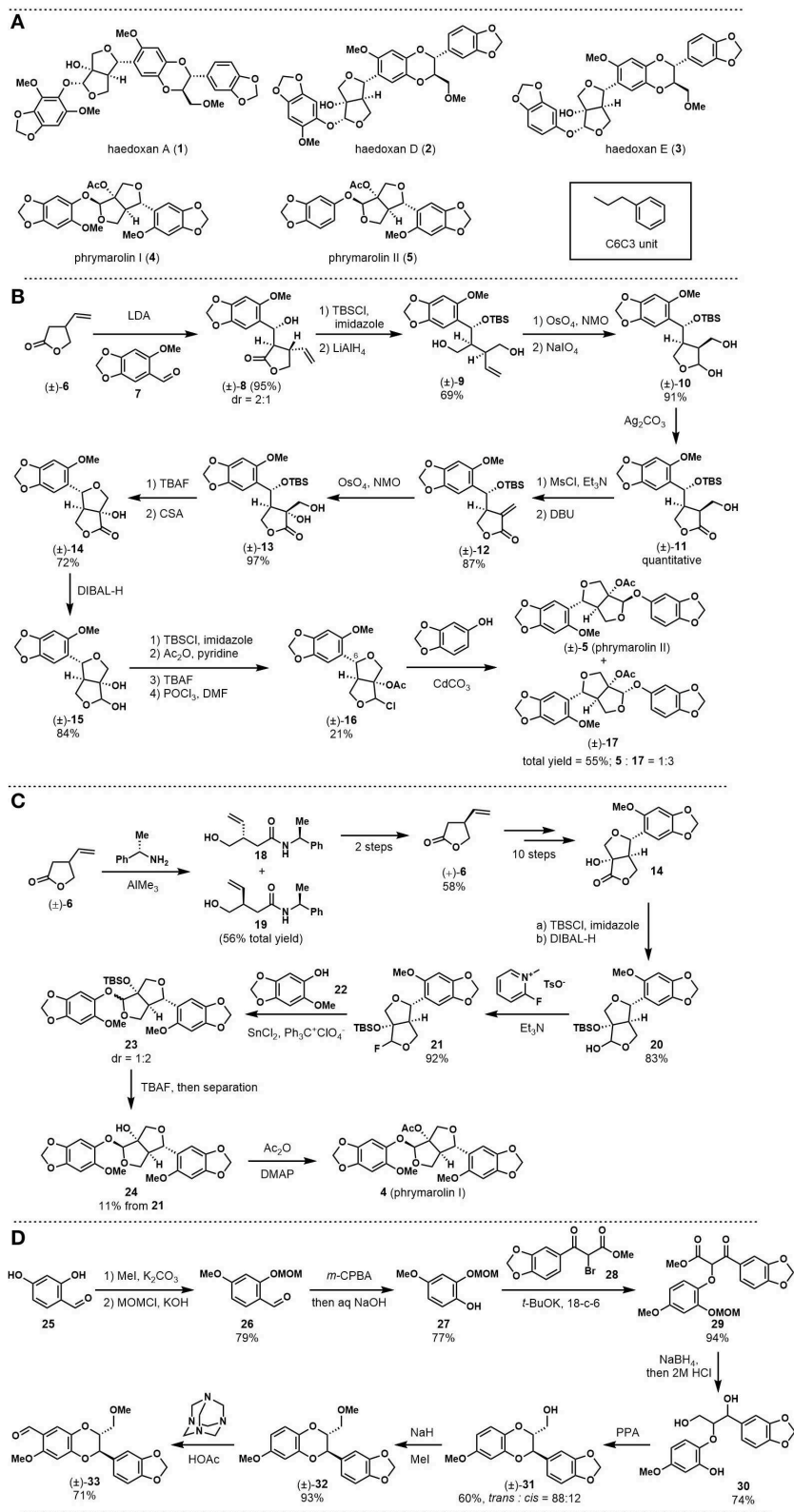
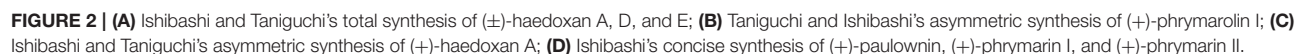


FIGURE 1 | (A) Structures of haedoxans and phymarolins; **(B)** Taniguchi's first total synthesis of (±)-phymarolin II; **(C)** Taniguchi's total synthesis of (+)-phymarolin I; **(D)** Taniguchi's synthesis toward (±)-haedoxan A, D, and E: fragment preparation.



acid-promoted replacement reaction with phenol **22** to afford the coupling product with desired stereochemistry at 15% yield. Then, a simple acylation reaction of the above product completed the asymmetric total synthesis of (+)-phrymarolin I (**4**).

In 1998, Ishibashi and Taniguchi reported their asymmetric synthesis of (+)-haedoxin A (**1**, Ishibashi and Taniguchi, 1998). While the core strategy followed the concept of Taniguchi's previous synthesis, this new synthesis featured the use of chiral synthons to avoid stereochemical correlation problems. As shown in **Figure 2C**, chiral compound **33** was first prepared *via* an optical resolution strategy from (\pm)-**31**. This synthon was coupled with another chiral building block (*S*)-**6** to give **34** as the adduct. Key intermediate **47** was then prepared through the known reaction sequence to set the stage for the last coupling. Instead of halogenation, the authors used the same key reaction in their synthesis of (+)-phrymarolin I (**4**) to install the phenol fragment directly on the lactol. This reaction provided the desired natural product, (+)-haedoxan A (**1**), at 21% yield.

In 2001, Ishibashi published a synthesis of (+)-paulownin, (+)-phrymarin I, and (+)-phrymarin II (Ishibashi et al., 2001). The report featured an elegant photochemical reaction that was developed by Kraus in 1990 (Kraus and Chen, 1990). As shown in **Figure 2D**, tetrahydrofuran intermediate **42** was synthesized through the procedures reported in Ishibashi's (+)-phrymarolin I (**4**) synthesis (**Figure 2B**). A coupling reaction between alcohol **42** and benzyl trichloroacetimidate **48**, followed by a Swern oxidation, provided the key intermediate **50** at 98% yield. Ketone **50** was then submitted to the photochemical condition developed by Kraus and Chen. In this event, a new C-C bond was formed between the irradiated benzylic position and the furan carbonyl in a diastereoselective manner to give furofuran **51** and **24** at 40% total yield. Finally, **51** was transformed into the desired natural product (+)-phrymarin I through a simple acylation reaction. With this concise synthetic route, the authors also completed the synthesis of (+)-paulownin and (+)-phrymarin II. It is noteworthy that compound **24** could serve as a key intermediate in the synthesis of (+)-phrymarolin I.

However, the diastereoselectivity of the key reaction did not favor this intermediate.

SUMMARY AND FURTHER PROSPECTS

Haedoxans and related neolignans are a family of natural insecticidal products with prominent potential applications. The main problem with the insecticide research process is the availability of sufficient samples. This review detailed the synthetic efforts toward haedoxans and phrymarolins in the past three decades. While these syntheses represent pioneering investigations on this topic, we are expecting new syntheses of haedoxans with higher efficiency, higher stereoselectivities, better step economy and redox economy, and more environmentally friendly procedures. This review may shed some light to guide future synthetic efforts on haedoxans.

AUTHOR CONTRIBUTIONS

YC collected and organized all articles in the literature regarding haedoxans and related neolignans from *Phryma leptostachya*, reviewing the abstract, introduction, details of haedoxan syntheses, and summary and further prospects of each. SX helped check all of the figures and references. JH and WX reviewed all articles in the literature and participated in significant discussions. SH reviewed the synthetic efforts toward haedoxans and phrymarolins in the past three decades and summed them up in reaction figures.

ACKNOWLEDGMENTS

We acknowledge financial support from the National Key R & D Program of China (2018YFD0200702, 2018YFD0200802, and 2018YFD0200106), the National Natural Science Foundation of China (21861010 and 21562011), the Science and Technology Foundation of Guizhou Province [2018]5781 and [2020]1Y108, and Guizhou University [2017]32.

REFERENCES

- Chen, C., Zhu, H., Zhao, D., and Deng, J. (2012). Lignans from *Phryma leptostachya* L. *Helvetica Chimica Acta* 95, 333–338. doi: 10.1002/hlca.201100311
- Endo, Y., and Miyauchi, T. (2006). Thermonasty of young main stems of *Phryma leptostachya* (Phrymaceae). *J. Plant Res.* 119, 449–457. doi: 10.1007/s10265-006-0007-6
- Hu, Z., Du, Y., Xiao, X., Dong, K., and Wu, W. (2016). Insight into the mode of action of Haedoxan A from *Phryma leptostachya*. *Toxins* 8, 53/51–53/12. doi: 10.3390/toxins8020053
- Ishibashi, F., Hayashita, M., Okazaki, M., and Shuto, Y. (2001). Improved procedure for the enantiometric synthesis of 1-Hydroxy/acetoxo-2,6-diaryl-3,7-dioxabicyclo[3.3.0]octane Lignans: Total Syntheses of (+)-Paulownin, (+)-Phrymarin I and (+)-Phrymarin II. *Biosci. Biotech. Biochem.* 65, 29–34. doi: 10.1271/bbb.65.29
- Ishibashi, F., and Taniguchi, E. (1986). Synthesis of (\pm)-Phrymarolin II and Its Stereoisomers. *Agric. Biol. Chem.* 50, 3119–3125. doi: 10.1080/00021369.1986.10867871
- Ishibashi, F., and Taniguchi, E. (1988). Synthesis and absolute configuration of the acetalic lignan (+)-Phrymarolin I. *Bull. Chem. Soc. Jpn.* 61, 4361–4366. doi: 10.1246/bcsj.61.4361
- Ishibashi, F., and Taniguchi, E. (1989). Synthesis of (\pm)-Haedoxan A, D, E and their stereoisomers. *Agric. Biol. Chem.* 53, 1565–1573. doi: 10.1271/bbb1961.53.1565
- Ishibashi, F., and Taniguchi, E. (1998). Synthesis and absolute configuration of the insecticidal sesquigignan (+)-Haedoxan A. *Phytochemistry* 49, 613–622. doi: 10.1016/S0031-9422(98)00270-2
- Jung, H., Cho, Y., Lim, H., Choi, H., Ji, D., and Lim, C. (2013). Anti-inflammatory, antioxidant, anti-angiogenic and skin whitening activities of *Phryma leptostachya* var. *asiatica* Hara extract. *Biomol. Ther.* 21, 72–78. doi: 10.4062/biomolther.2012.059
- Kraus, G. A., and Chen, L. (1990). A total synthesis of racemic paulownin using a type II photocyclization reaction. *J. Am. Chem. Soc.* 112, 3464–3466. doi: 10.1021/ja00165a033
- Lee, S., Min, B., and Kho, Y. (2002). Brine shrimp lethality of the compounds from *Phryma leptostachya* L. *Arch. Pharm. Res.* 25, 652–654. doi: 10.1007/BF02976939

- Li, Y., Wang, S., Aioub, A. A. A., Qie, X., Wu, W., and Hu, Z. (2019b). Identification and analysis of full-length transcripts involved in the biosynthesis of insecticidal lignan (+)-haedoxan A in *Phryma leptostachya*. *Ind. Crops Prod.* 142:111868. doi: 10.1016/j.indcrop.2019.111868
- Li, Y., Wei, J., Fang, J., Lv, W., Ji, Y., Aioub, A. A. A., Zhang, J., and Hu, Z. (2019a). Insecticidal activity of four lignans isolated from *Phryma leptostachya*. *Molecules* 24:1976. doi: 10.3390/molecules24101976
- Okazaki, M., Ishibashi, F., Shuto, Y., and Taniguchi, E. (1997). Total synthesis of (+)-Phrymarolin I from (+)-malic acid. *Biosci. Biotech. Biochem.* 61, 660–663. doi: 10.1271/bbb.61.660
- Park, I. I., Shin, S., Kim, C., Lee, H., Choi, W., and Ahn, Y. (2005). Larvicidal activity of lignans identified in *Phryma leptostachya* Var. asiatica roots against three mosquito species. *J. Agric. Food Chem.* 53, 969–972. doi: 10.1021/jf048208h
- Seo, S., and Park, I. I. (2012). Larvicidal activity of medicinal plant extracts and lignan identified in *Phryma leptostachya* var. asiatica roots against housefly (*Musca domestica* L.). *Parasitol. Res.* 110, 1849–1853. doi: 10.1007/s00436-011-2709-5
- Taniguchi, E., Imamura, K., Ishibashi, F., Matsui, T., and Nishio, A. (1989). Structure of the novel insecticidal sesquiligand, haedoxan A. *Agric. Biol. Chem.* 53, 631–643. doi: 10.1080/00021369.1989.10869338
- Taniguchi, E., and Oshima, Y. (1972a). Phrymarolin-I, a Novel Lignan from *Phryma leptostachya* L. *Agric. Biol. Chem.* 36, 1013–1025. doi: 10.1271/bbb1961.36.1013
- Taniguchi, E., and Oshima, Y. (1972b). Structure of Phrymarolin-II. *Agric. Biol. Chem.* 36, 1489–1496. doi: 10.1080/00021369.1972.10860431
- Xiao, X., Hu, Z., Ji, Z., Shi, J., Zhang, J., Wei, S., et al. (2012a). Isolation, structure identification and bioactivity of active ingredients from *Phryma leptostachya*. *Chin. J. Pestic. Sci.* 14, 583–586. doi: 10.3969/j.issn.1008-7303.2012.05.19
- Xiao, X., Hu, Z., Shi, B., Wei, S., and Wu, W. (2012b). Larvicidal activity of lignans from *Phryma leptostachya* L. against *Culex pipiens pallens*. *Parasitol. Res.* 110, 1079–1084. doi: 10.1007/s00436-011-2591-1
- Xu, W., Zhao, P., Wang, M., and Liang, Q. (2019). Naturally occurring furofuran lignans: structural diversity and biological activities. *Nat. Prod. Res.* 33, 1357–1373. doi: 10.1080/14786419.2018.1474467
- Yamaguchi, S., Ishibashi, F., and Taniguchi, E. (1992b). Insecticidal Activity of Sesquiligand with a 3-Aryl-6-methoxy-2-methoxymethyl-1,4-benzodioxanyl Group. *Biosci. Biotech. Biochem.* 56, 1760–1768. doi: 10.1271/bbb.56.1760
- Yamaguchi, S., Nagata, S., and Taniguchi, E. (1992a). Effect on insecticidal activity of substituents at the 1,4-benzodioxanyl moiety of haedoxan. *Biosci. Biotech. Biochem.* 56, 1193–1197. doi: 10.1271/bbb.56.1193
- Yamaguchi, S., and Taniguchi, E. (1991). Synthesis and insecticidal activity of lignan analogs (I). *Agric. Biol. Chem.* 55, 3075–3084. doi: 10.1080/00021369.1991.10867924
- Yamaguchi, S., and Taniguchi, E. (1992a). Synthesis and insecticidal activity of lignan analogs (III). *Biosci. Biotech. Biochem.* 56, 418–422. doi: 10.1271/bbb.56.418
- Yamaguchi, S., and Taniguchi, E. (1992b). Synthesis and insecticidal activity of lignan analogs (II). *Biosci. Biotech. Biochem.* 56, 412–417. doi: 10.1271/bbb.56.412
- Yamaguchi, S., and Taniguchi, E. (1992c). Influence on insecticidal activity of the 3-(3,4-Methylenedioxyphenyl) group in the 1,4-Benzodioxanyl Moiety of Haedoxan. *Biosci. Biotech. Biochem.* 56, 1744–1750. doi: 10.1271/bbb.56.1744

Conflict of Interest: The authors declare that the research was conducted in the absence of any commercial or financial relationships that could be construed as a potential conflict of interest.

Copyright © 2020 Chen, Xiao, Huang, Xue and He. This is an open-access article distributed under the terms of the Creative Commons Attribution License (CC BY). The use, distribution or reproduction in other forums is permitted, provided the original author(s) and the copyright owner(s) are credited and that the original publication in this journal is cited, in accordance with accepted academic practice. No use, distribution or reproduction is permitted which does not comply with these terms.



Green and Facile Synthesis of Spirocyclopentanes Through NaOH-Promoted Chemo- and Diastereo-Selective (3 + 2) Cycloaddition Reactions of Activated Cyclopropanes and Enamides

OPEN ACCESS

Edited by:

Yaqiong Su,
Eindhoven University of
Technology, Netherlands

Reviewed by:

Huanzhen Ni,
Georgia Institute of Technology,
United States
Wai Lun Chan,
Hong Kong Baptist University,
Hong Kong

*Correspondence:

Chengli Mou
mouchengli_h@163.com
Zhichao Jin
zjcin@gzu.edu.cn

[†]These authors have contributed
equally to this work

Specialty section:

This article was submitted to
Green and Sustainable Chemistry,
a section of the journal
Frontiers in Chemistry

Received: 07 April 2020

Accepted: 26 May 2020

Published: 26 June 2020

Citation:

Zhu X, Pan D, Mou C, Zhou B, Pan L
and Jin Z (2020) Green and Facile
Synthesis of Spirocyclopentanes
Through NaOH-Promoted Chemo-
and Diastereo-Selective (3 + 2)
Cycloaddition Reactions of Activated
Cyclopropanes and Enamides.
Front. Chem. 8:542.
doi: 10.3389/fchem.2020.00542

Xun Zhu^{1†}, Dingwu Pan^{1†}, Chengli Mou^{2*}, Bo Zhou³, Lutai Pan² and Zhichao Jin^{1*}

¹ Laboratory Breeding Base of Green Pesticide and Agricultural Bioengineering, Key Laboratory of Green Pesticide and Agricultural Bioengineering Ministry of Education, Guizhou University, Guiyang, China, ² School of Pharmacy, Guizhou University of Traditional Chinese Medicine, Guiyang, China, ³ R&D Center, Shenzhen AmTech Bioengineering Ltd., Inc., Shenzhen, China

A chemo- and diastereo-selective (3 + 2) cycloaddition reaction between Donor-Acceptor (D-A) cyclopropanes and α,β -unsaturated enamides is developed for efficient access to spiro(cyclopentane-1,3'-indoline) derivatives. Simple, inexpensive and readily available NaOH is used as the sole catalyst for this process. A broad range of D-A cyclopropanes could be used as the C-3 synthons to react with oxindole-derived α,β -unsaturated enamides. The structurally sophisticated spiro(cyclopentane-1,3'-indoline) derivatives bearing up to 3 adjacent chiral centers are afforded in excellent yields as single diastereomers.

Keywords: green, NaOH, donor-acceptor cyclopropane, (3 + 2) cycloaddition, spirocyclopentane, indole derivative

INTRODUCTION

Spirocyclopentanes are interesting structural units with broad applications in organic synthesis and medicinal chemistry. They have existed as core structures in various bioactive molecules (Boeyens et al., 1979; Tsuda et al., 2004; Mugishima et al., 2005; Zhang et al., 2019). Specifically, spiro(cyclopentane-1,3'-indoline) derivatives are frequently found in natural products with proven biological activities (Figure 1). For example, Citrinadin A and B are active molecules against murine leukemia L1210 and human epidermoid carcinoma KB cells, which have been isolated from a culture broth of *Penicillium citrinum*. Cyclopiamines A and B are extracts from a toxinogenic strain of *Penicillium cyclopium*. The Notoamides A and B are key members of paraherquamide family which belongs to prenylated indole alkaloids that exhibit various bioactivities including antitumor, antibacterial, and insecticidal properties. Therefore, the development of efficient methods for the preparation of

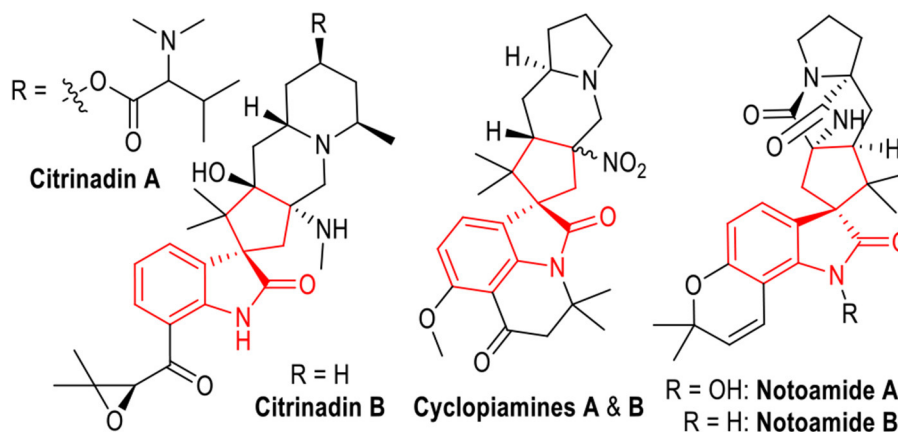


FIGURE 1 | Bioactive Natural Products Containing Spiro(cyclopentane-1,3'-indoline) Units.

spiro(cyclopentane-1,3'-indoline) derivatives has attracted much interest. Success within this field has been achieved through both organocatalysis (Chen et al., 2009; Antonchick et al., 2010; Tan et al., 2011; Tian and Melchiorre, 2013; Zhang et al., 2016; Chaudhari et al., 2017) and transition metal catalysis (Trost et al., 2007; Brazeau et al., 2012; Ball-Jones et al., 2014; Deiana et al., 2014; Afewerki et al., 2015; Frost et al., 2015; Qiu et al., 2019). Despite of the great achievement obtained in the synthesis of spiro(cyclopentane-1,3'-indoline) molecules, the development of green and economical methods for efficient and stereoselective synthesis of them is still of great interest.

Cyclopropanes are important building blocks in organic synthesis (Sohn and Bode, 2006; Bode and Sohn, 2007; Li et al., 2009; Lv et al., 2011; Sparr and Gilmour, 2011; Halskov et al., 2015; Sanchez-Diez et al., 2016; Blom et al., 2017; Apel et al., 2019). Especially, the cyclopropanes bearing both an electron-donating and an electron-withdrawing group on their cyclic structures, which are commonly named as Donor-Acceptor (D-A) cyclopropanes (Danishefsky, 1979; Wenkert, 1980; Reissig and Zimmer, 2003; Carson and Kerr, 2009; Cavitt et al., 2014; Nanteuil et al., 2014; Schneider et al., 2014; Grover et al., 2015; Talukdar et al., 2016; Wang and Tang, 2016; Werz and Biju, 2019), have been extensively studied in the construction of various functional molecules. D-A Cyclopropanes are conventionally activated by transition metal catalysts (Nanteuil et al., 2014), Lewis acids (Reissig and Zimmer, 2003; Carson and Kerr, 2009; Cavitt et al., 2014; Schneider et al., 2014; Grover et al., 2015; Talukdar et al., 2016; Wang and Tang, 2016; Werz and Biju, 2019) or amine-based organic catalysts (Halskov et al., 2015; Sanchez-Diez et al., 2016; Blom et al., 2017) (Figure 2a). Efficient activation of D-A cyclopropanes by simple, inexpensive and readily available bases has been much less developed.

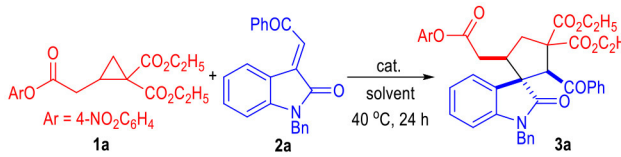
Very recently, we have disclosed that the D-A cyclopropanes could be activated by simple NaOH and reacted with α,β -unsaturated imines to give a variety of bioactive

cyclopenta(c)pyridine derivatives in generally excellent yields and moderate diastereoselectivities (Pan et al., 2019) (Figure 2b). This approach has provided us with a green and facile method for the construction of structurally complex molecules from D-A cyclopropanes with simple and inexpensive reaction catalysts. Therefore, it is interesting and important to extend the border of this strategy to a wide range of substrates in order to get access to a broad scope of complex functional molecules in a green, facile, and economic fashion.

Herein, we disclose that the D-A cyclopropanes **1** can react with α,β -unsaturated enamide substrates **2** under basic conditions in chemoselective fashion (Figure 2c). Heavily substituted spiro(cyclopentane-1,3'-indoline) derivatives could be afforded in good to excellent yields. NaOH was used as the sole reaction catalyst. All the spirocyclic products bearing up to 3 adjacent chiral centers were afforded as single diastereomers. It is worth noting that both an enone and an enamide motif exist in the electrophilic substrate **2**. After deprotonation of the D-A cyclopropane substrate **1**, the afforded ring-opening intermediate **I** could selectively react with the electrophile **2** through an enamide 1,4-addition process and gave intermediate **II** bearing a highly reactive nucleophilic carbon center. The enamide 1,4-addition reaction was believed to go faster than the enone 1,4-addition reaction because that there were less steric hindrance around the enamide β -carbon. After an intramolecular Michael addition process, the spiral cyclopentane products **3** or **4** were afforded in excellent diastereoselectivities. Interestingly, an additional β -elimination could happen during this catalytic transformation when using the D-A cyclopropyl ketone bearing *gem*-dicyano groups as the reaction substrate. Spiral cyclopentenones **5** were afforded as the final products in this case. Product **6** that might be formed from the enone 1,4-addition intermediate **III** were not observed. The less nucleophilicity of the enol moiety of the intermediate **III** might be another reason for the difficult formation of the enone 1,4-addition products.



June 2020 | Volume 8 | Article 542

TABLE 1 | Optimization of Reaction Conditions^a.


Entry	Cat.	Solvent	Yield (%) ^b	dr ^c
1	NaOH	THF	82	>20:1
2	NaOCH ₃	THF	80	>20:1
3	K ₂ CO ₃	THF	74	>20:1
4	DBU	THF	< 5	
5	Et ₃ N	THF	< 5	
6	NaOH	EtOAc	72	>20:1
7	NaOH	CH ₃ CN	25	>20:1
8	NaOH	CH ₂ Cl ₂	<5	
9	NaOH	PhCH ₃	<5	
10 ^d	NaOH	THF	83	>20:1
11 ^e	NaOH	THF	90	>20:1
12 ^e	NaOH	2-Me THF	72	>20:1
13 ^e	NaOH	Anisole	<5	
14 ^e	NaOH	H ₂ O	<5	
15 ^e	NaOH	EtOH	75	>20:1
16 ^f	NaOH	EtOH	74	>20:1

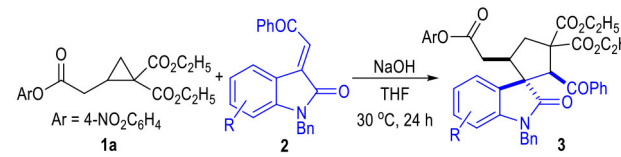
^aGeneral conditions (unless otherwise specified): **1a** (0.075 mmol), **2a** (0.05 mmol), cat. (0.01 mmol), THF (1.0 mL), 40 °C, 24 h. ^bIsolated yield of **3a**. ^cDr was determined via ¹H NMR on the crude product. ^dThe reaction was carried out at 30 °C for 24 h. ^e**1a** (0.1 mmol), **2a** (0.05 mmol), NaOH. (0.01 mmol), solvent (1.0 mL), 30 °C, 24 h. ^f**1a** (1.0 mmol), **2a** (0.5 mmol), NaOH. (0.1 mmol), EtOH (10.0 mL), 30 °C, 24 h.

be slightly decreased to 30 °C without erosion of the product yield (entry 10). Finally, the yield of the spiro(cyclopentane-1,3'-indoline) product **3a** could be increased to 90% with a larger excess amount of **1a** used under the catalysis of NaOH in THF at 30 °C (entry 11). Note that, all the products afforded in these reactions were obtained as single diastereomers.

We were also very interested in developing a green and efficient method for the construction of the spiro(cyclopentane-1,3'-indoline) product **3a**. Therefore, several green solvents were further examined after obtaining the optimized reaction condition (Table 1, entries 12 to 15). 2-Methyl-substituted THF could give the desired product in a good yield (entry 12). Anisole or water could not be used as the solvents for this transformation (entries 13 to 14). To our delight, the inexpensive and non-toxic ethanol could be used as a suitable medium for the construction of the spiro(cyclopentane-1,3'-indoline) products through this protocol (entry 15). Therefore, we carried out a large-scale reaction of the substrate **1a** and **2a** in ethanol, with the desired product **3a** afforded in a 74% yield as a single diastereomer (entry 16).

Reaction Scope Investigation and Synthetic Application

With the optimized reaction conditions at hand (Table 1, entry 11), we then examined the substrate scope of this (3 + 2)

TABLE 2 | Scope of α,β Unsaturated Enamides **2**^a.


3a , 90%, > 20:1 dr	3b , 89%, > 20:1 dr	3c , 65%, > 20:1 dr
3d , X = Cl, 74%, > 20:1 dr	3h , X = Cl, > 99%, 4:1 dr	3j , X = F, 88%, > 20:1 dr
3e , X = Br, 89%, > 20:1 dr	3i , X = Br, > 99%, 7:1 dr	3k , X = Br, 72%, > 20:1 dr
3f , X = I, 90%, > 20:1 dr	3g , X = F, 77%, > 20:1 dr	
3l , 76%, > 20:1 dr	3m , 79%, > 20:1 dr	3n , 89%, > 20:1 dr

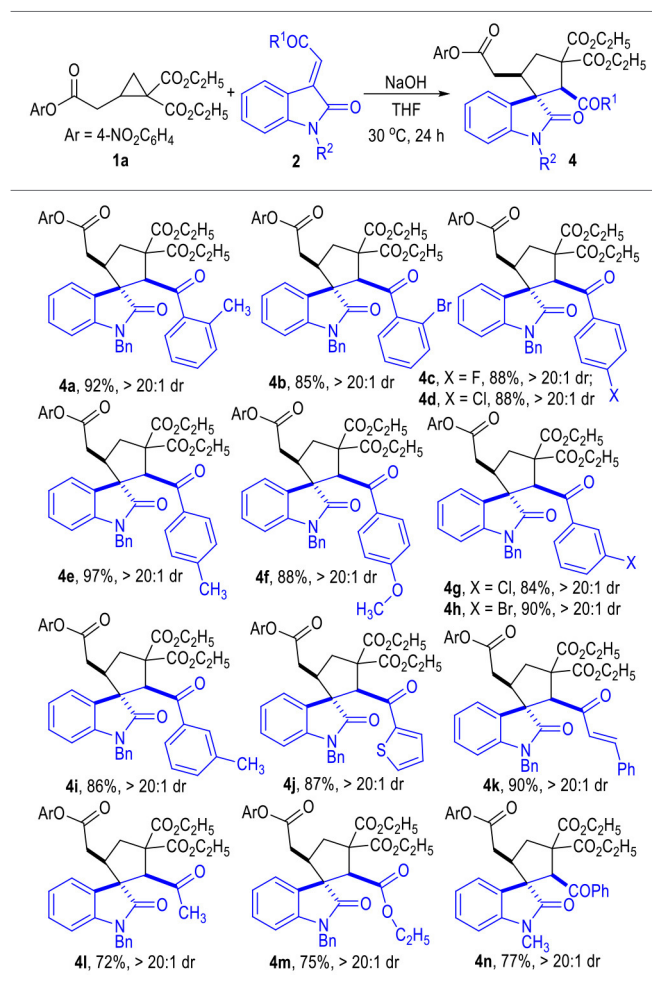
^aReaction conditions as stated in Table 1, entry 11. Isolated yields are reported after purification via SiO₂ column chromatography. Dr was determined via ¹H NMR on the crude product.

cycloaddition reaction with respect to both D-A cyclopropyl acetates **1** and α,β -unsaturated enamides **2** (Tables 2–4).

The R substituent on the phenyl group of the indoline motif of the α,β -unsaturated enamides **2** could be either electron-donating groups (Table 2, **3b** and **3c**) or electron-withdrawing groups (**3d** to **3n**), with most of the spirocyclic products being afforded in good to excellent yields and diastereo-selectivities.

The R¹ group of ketone moieties could be phenyl rings of different substitution patterns, with the corresponding products being afforded in excellent yields as single diastereomers (Table 3, **4a** to **4i**). Moreover, the R¹ group could also be switched to a heteroaromatic group or a vinylogous phenyl group without erosion on the product yields or diastereoselectivities (**4j** to **4k**). Interestingly, the R¹ group of the ketones **2** could even be replaced with a simple methyl or ethoxyl group, and the corresponding products **4l** and **4m** could be afforded in good yields as single diastereomers. The N-protecting benzyl group of indoline motif could be replaced with an N-methyl group, and the desired product **4n** could also be afforded in a good yield as a single diastereomer. Unprotected isatin-derived enamide substrates were not effective in this transformation.

The scope of the D-A cyclopropyl acetates **1** was also examined (Table 4). The electron deficient 4-nitrophenol group

TABLE 3 | Scope of α,β -Unsaturated Enamides **2**^a.

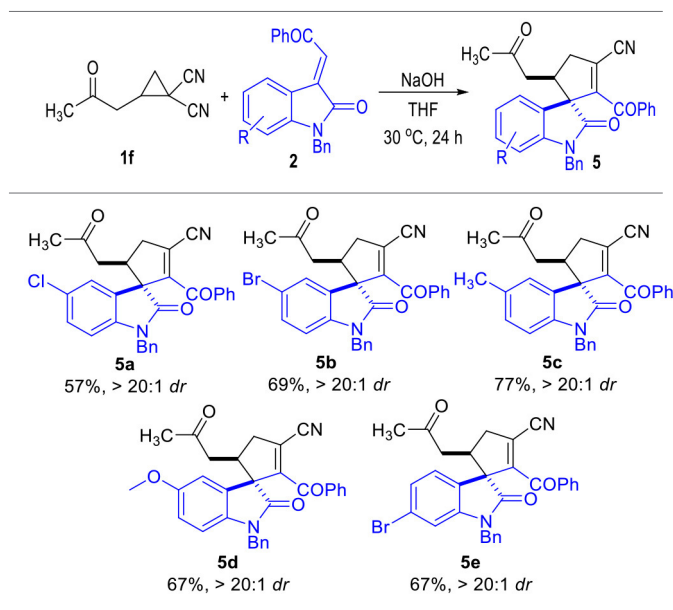
^aReaction conditions as stated in **Table 1**, entry 11. Isolated yields are reported after purification via SiO_2 column chromatography. Dr was determined via ^1H NMR on the crude product.

TABLE 4 | Scope of the D-A Cyclopropanes **1**^a.

Entry	R	R'	4	Yield (%)	dr
1	4- $\text{CH}_3\text{OC}_6\text{H}_4$	CH_3CH_2	4o	86	> 20:1
2	4- $\text{NO}_2\text{C}_6\text{H}_4$	$(\text{CH}_3)_2\text{CH}$	4p	79	> 20:1
3	CH_3	CH_3CH_2	-	0	-
4	H	CH_3CH_2	-	0	-

^aReaction conditions as stated in **Table 1**, entry 11. Isolated yields are reported after purification via SiO_2 column chromatography. Dr was determined via ^1H NMR on the crude product.

on **1a** could be switched to an electron rich aromatic group (**1b**) without erosion on the reaction diastereoselectivity, although the yield of the product was slightly decreased to 86%. Replacing

TABLE 5 | Scope of α,β -Unsaturated Enamides **2**^a.

^aReaction conditions as stated in **Table 1**, entry 11. Isolated yields are reported after purification via SiO_2 column chromatography. Dr was determined via ^1H NMR on the crude product.

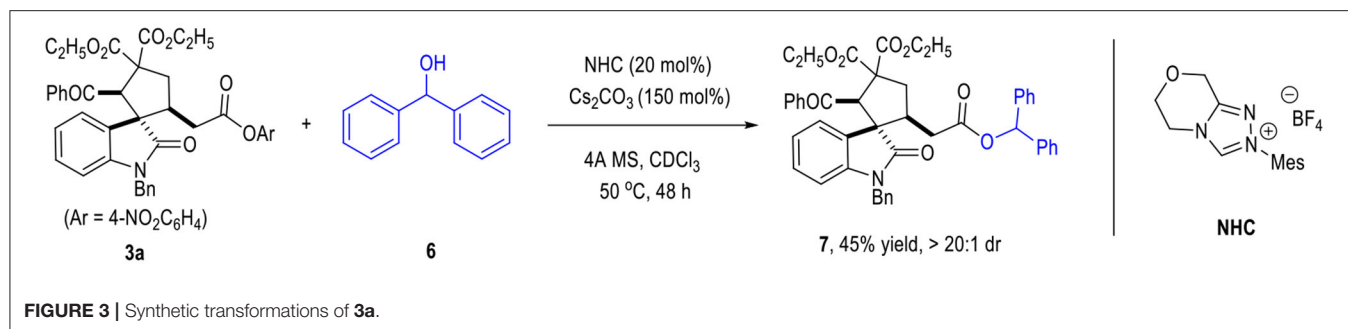
the R group on ester substrate **1** with a simple methyl group (**1c**) led to only trace formation of the target product. The sterically bulkier isopropyl ester (**1d**) also worked well in this transformation and afforded the desired product in a good yield as a single diastereomer. It is worth noting that the cyclopropyl aldehyde **1e** was not a suitable substrate for this (3 + 2) cycloaddition reaction.

To our great delight, the D-A cyclopropyl acetone **1f** bearing two cyano groups also worked well in the (3 + 2) cycloaddition reaction with the oxindole-derived α,β -unsaturated enamide **2** under the current catalytic conditions (**Table 5**). The spirocyclopentenes **5** were afforded as the final products with the elimination of one equiv. of HCN. Both electron-donating and electron-withdrawing groups could be installed on the indoline moieties of the α,β -unsaturated enamides **2**, with the corresponding products being afforded in moderate yields as single diastereomers.

The afforded spiro(cyclopentane-1,3'-indoline) product **3a** could be used as the reaction material for further transformations (**Figure 3**). For example, a trans-esterification reaction of **3a** could give other ester products (e.g., **7**) in moderate yields without erosion of the diastereomeric ratio.

CONCLUSION

In conclusion, we have developed a chemo- and diastereo-selective (3 + 2) cycloaddition between D-A cyclopropanes and α,β -unsaturated enones. Green, inexpensive, and readily available NaOH was used as the sole catalyst to promote this transformation. Structurally sophisticated spiro(cyclopentane-1,3'-indoline) derivatives bearing up to 3 adjacent chiral centers



were afforded as the final products in generally good to excellent yields as single diastereomers. This study could provide us with a green, facile and economic approach in preparing complex functional molecules through simple operations. Further investigations on the development of efficient methods for the construction of complex molecules are in progress in our laboratory.

DATA AVAILABILITY STATEMENT

The raw data supporting the conclusions of this article will be made available by the authors, without undue reservation.

AUTHOR CONTRIBUTIONS

XZ and DP conducted most of the experiments. CM, LP, and ZJ conceptualized and directed the whole project. ZJ drafted the manuscript. BZ participated in some experimental work and

manuscript writing. All of the authors contributed in scientific discussions. All authors contributed to the article and approved the submitted version.

FUNDING

We acknowledge financial support from the National Natural Science Foundation of China (Nos. 21801051 and 21961006), Department of Science and Technology of Guizhou Province (Nos. (2019)1020 and (2009)700122), Undergraduate Innovation and Pioneer Training Program, Guizhou University of Traditional Chinese Medicine (Nos. (2018)31 and (2017)37) and Guizhou University (Nos. GZU(2017)34 and KY(2017)376).

SUPPLEMENTARY MATERIAL

The Supplementary Material for this article can be found online at: <https://www.frontiersin.org/articles/10.3389/fchem.2020.00542/full#supplementary-material>

REFERENCES

- Afewerki, S., Ma, G., Ibrahim, I., Liu, L., Sun, J., and Córdova, A. (2015). Highly enantioselective control of dynamic cascade transformations by dual catalysis: asymmetric synthesis of polysubstituted spirocyclic oxindoles. *ACS Catal.* 5, 1266–1272. doi: 10.1021/cs501975u
- Antonchick, A. P., Gerding-Reimers, C., Catarinella, M., Schürmann, M., Preut, H., Ziegler, S., et al. (2010). Highly enantioselective synthesis and cellular evaluation of spirooxindoles inspired by natural products. *Nat. Chem.* 2, 735–740. doi: 10.1038/nchem.730
- Apel, C., Hartmann, S. S., Lentz, D., and Christmann, M. (2019). Dienamine-induced divinylcyclopropane-cycloheptadienerearrangements. *Angew. Chem. Int. Ed.* 58, 5075–5133. doi: 10.1002/anie.201813880
- Ball-Jones, N. R., Badillo, J. J., Tran, N. T., and Franz, A. K. (2014). Catalytic enantioselective carboannulation with allylsilanes. *Angew. Chem. Int. Ed.* 53, 9462–9465. doi: 10.1002/anie.201403607
- Blom, J., Vidal-Albalat, A., Jørgensen, J., Barløse, C. L., Jessen, K. S., Iversen, M. V., et al. (2017). Directing the activation of donor-acceptor cyclopropanes towards stereoselective 1,3-dipolar cycloaddition reactions by brønsted base catalysis. *Angew. Chem. Int. Ed.* 56, 11831–11835. doi: 10.1002/anie.201706150
- Bode, J. W., and Sohn, S. S. (2007). *N*-Heterocyclic carbene-catalyzed redox amidations of α -functionalized aldehydes with amines. *J. Am. Chem. Soc.* 129, 13798–13799. doi: 10.1021/ja0768136
- Boeyens, J. C. A., Holzapfel, C. W., and Steyn, P. S. (1979). Cyclopiamines A and B, novel oxindole metabolites of penicillium cyclopium westling. *J. Chem. Soc. Perkin 1*, 1751–1761. doi: 10.1039/p19790001751
- Brazeau, J.-F., Zhang, S., Colomer, I., Corkey, B. K., and Toste, F. D. (2012). Enantioselective cyclizations of silyloxyenynes catalyzed by cationic metal phosphine complexes. *J. Am. Chem. Soc.* 134, 2742–2749. doi: 10.1021/ja210388g
- Carson, C. A., and Kerr, M. A. (2009). Heterocycles from cyclopropanes: applications in natural product synthesis. *Chem. Soc. Rev.* 38, 3051–3060. doi: 10.1039/b901245c
- Cavitt, M. A., Phun, L. H., and France, S. (2014). Intramolecular donor-acceptor cyclopropane ring-opening cyclizations. *Chem. Soc. Rev.* 43, 804–818. doi: 10.1039/C3CS60238A
- Chaudhari, P. D., Hong, B.-C., and Lee, G.-H. (2017). Organocatalytic enantioselective michael–michael–michael–aldol condensation reactions: control of six stereocenters in a quadruple-cascade asymmetric synthesis of polysubstituted spirocyclic oxindoles. *Org. Lett.* 19, 6112–6115. doi: 10.1021/acs.orglett.7b02962
- Chen, X.-H., Wei, Q., Luo, S.-W., Xiao, H., and Gong, L.-Z. (2009). Organocatalytic synthesis of spiro (pyrrolidin-3,3'-oxindoles) with high enantiopurity and structural diversity. *J. Am. Chem. Soc.* 131, 13819–13825. doi: 10.1021/ja905302f
- Danishefsky, S. (1979). Electrophilic cyclopropanes in organic synthesis. *Acc. Chem. Res.* 12, 66–72. doi: 10.1021/ar50134a004
- Deiana, L., Jiang, Y., Palo-Nieto, C., Afewerki, S., Incerti-Pradillos, C. A., Verho, O., et al. (2014). Combined heterogeneous metal/chiral amine: multiple relay catalysis for versatile eco-friendly synthesis. *Angew. Chem. Int. Ed.* 53, 3447–3451. doi: 10.1002/anie.201310216

- Frost, J. R., Huber, S. M., Breitenlechner, S., Bannwarth, C., and Bach, T. (2015). Enantiotopos-selective C-H oxygenation catalyzed by a supramolecular ruthenium complex *angew. Chem. Int. Ed.* 54, 691–695. doi: 10.1002/anie.201409224
- Grover, H. K., Emmett, M. R., and Kerr, M. A. (2015). Carbocycles from donor-acceptor cyclopropanes. *Org. Biomol. Chem.* 13, 655–671. doi: 10.1039/C4OB02117G
- Halskov, K. S., Kniep, F., Lauridsen, V. H., Iversen, E. H., Donslund, B. S., and Jørgensen, K. A. (2015). Organocatalytic enamine-activation of cyclopropanes for highly stereoselective formation of cyclobutanes. *J. Am. Chem. Soc.* 137, 1685–1691. doi: 10.1021/ja512573q
- Li, G.-Q., Dai, L.-X., and You, S.-L. (2009). *N*-Heterocyclic carbene catalyzed ring expansion of formylcyclopropanes: synthesis of 3,4-dihydro- α -pyrone derivatives. *Org. Lett.* 11, 1623–1625. doi: 10.1021/ol9002898
- Lv, H., Mo, J., Fang, X., and Chi, Y. R. (2011). Formal diels-alder reactions of chalcones and formylcyclopropanes catalyzed by chiral *N*-heterocyclic carbenes. *Org. Lett.* 13, 5366–5369. doi: 10.1021/ol202250s
- Mugishima, T., Tsuda, M., Kasai, Y., Ishiyama, H., Fukushi, E., Kawabata, J., et al. (2005). Absolute stereochemistry of citrinadins A and B from marine-derived fungus. *J. Org. Chem.* 70, 9430–9435. doi: 10.1021/jo051499o
- Nanteuil, F., De Simone, F., Frei, R., Benfatti, F., Serrano, E., and Waser, J. (2014). Cyclization and annulation reactions of nitrogen-substituted cyclopropanes and cyclobutanes. *Chem. Commun.* 50, 10912–10928. doi: 10.1039/C4CC03194F
- Pan, D., Mou, C., Zan, N., Lv, Y., Song, B.-A., Chi, R. C., et al. (2019). NaOH-promoted chemoselective cascade cyclization of cyclopropyl esters with unsaturated imines: access to bioactive cyclopenta(c)pyridine derivatives. *Org. Lett.* 21, 6624–6627. doi: 10.1021/acs.orglett.9b02088
- Qiu, B., Xu, D., Sun, Q., Lin, J., and Sun, W. (2019). Manganese-catalyzed asymmetric oxidation of methylene C–H of spirocyclic oxindoles and dihydroquinolinones with hydrogen peroxide. *Org. Lett.* 21, 618–622. doi: 10.1021/acs.orglett.8b03652
- Reissig, H.-U., and Zimmer, R. (2003). Donor-acceptor-substituted cyclopropane derivatives and their application in organic synthesis. *Chem. Rev.* 103, 1151–1196. doi: 10.1021/cr010016n
- Sanchez-Diez, E., Vesga, D. L., Reyes, E., Uria, U., Carrillo, L., and Vicario, J. L. (2016). Organocatalytically Generated Donor-Acceptor Cyclopropanes in Domino Reactions. One-Step Enantioselective synthesis of pyrrolo(1,2-a)quinolines. *Org. Lett.* 18, 1270–1273. doi: 10.1021/acs.orglett.6b00173
- Schneider, T. F., Kaschel, J., and Werz, D. B. (2014). A new golden age for donor-acceptor cyclopropanes. *Angew. Chem. Int. Ed.* 53, 5504–5523. doi: 10.1002/anie.201309886
- Sohn, S. S., and Bode, J. W. (2006). *N*-Heterocyclic carbene catalyzed C-C bond cleavage in redox esterifications of chiral formylcyclopropanes. *Angew. Chem. Int. Ed.* 45, 6021–6024. doi: 10.1002/anie.200601919
- Sparr, C., and Gilmour, R. (2011). Cyclopropyl iminium activation: reactivity umpolung in enantioselective organocatalytic reaction design. *Angew. Chem. Int. Ed.* 50, 8391–8395. doi: 10.1002/anie.201103360
- Talukdar, R., Saha, A., and Ghorai, M. K. (2016). Domino-ring opening-cyclization (DROC) of donor-acceptor (DA) cyclopropanes. *Isr. J. Chem.* 56, 445–453. doi: 10.1002/ijch.201500092
- Tan, B., Candeias, N. R., and Barbas, C. F. III. (2011). Core-structure-motivated design of a phosphine-catalyzed (3+2) cycloaddition reaction: enantioselective syntheses of spirocyclopenteneoxindoles. *J. Am. Chem. Soc.* 133, 4672–4675. doi: 10.1021/ja110147w
- Tian, X., and Melchiorre, P. (2013). Control of remote stereochemistry in the synthesis of spirocyclic oxindoles: vinylogous organocascade catalysis. *Angew. Chem. Int. Ed.* 52, 5360–5363. doi: 10.1002/anie.201301017
- Trost, B. M., Cramer, N., and Silverman, S. M. (2007). Enantioselective construction of spirocyclic oxindolic cyclopentanes by palladium-catalyzed trimethylenemethane - (3+2) - cycloaddition. *J. Am. Chem. Soc.* 129, 12396–12397. doi: 10.1021/ja075335w
- Tsuda, M., Kasai, Y., Komatsu, K., Sone, T., Tanaka, M., Mikami, Y., et al. (2004). A novel pentacyclic alkaloid from marine-derived fungus *penicillium citrinum*. *Org. Lett.* 6, 3087–3089. doi: 10.1002/ol.200452182
- Wang, L., and Tang, Y. (2016). Asymmetric ring-opening reactions of donor-acceptor cyclopropanes and cyclobutanes. *Isr. J. Chem.* 56, 463–475. doi: 10.1002/ijch.201500094
- Wenkert, E. (1980). Oxycyclopropanes in organochemical synthesis. *Acc. Chem. Res.* 13, 27–31. doi: 10.1021/ar50145a005
- Werz, D. B., and Biju, A. T. (2019). Uncovering the neglected similarities of arynes and donor-acceptor cyclopropanes. *Angew. Chem. Int. Ed.* 59, 3385–3398. doi: 10.1002/anie.201909213
- Zhang, J., Cao, D., Wang, H., Zheng, C., Zhao, G., and Shang, Y. (2016). Enantioselective construction of spirocyclic oxindoles via tandem michael/michael reactions catalyzed by multifunctional quaternary phosphonium salt. *J. Org. Chem.* 81, 10558–10568. doi: 10.1021/acs.joc.6b01553
- Zhang, P., Yuan, X.-L., Du, Y.-M., Zhang, H.-B., Shen, G.-M., Zhang, Z.-F., et al. (2019). Angularly Prenylated Indole Alkaloids with Antimicrobial and Insecticidal Activities from an Endophytic fungus *fusarium sambucinum* TE-6L. *J. Agric. Food Chem.* 67, 11994–12001. doi: 10.1021/acs.jafc.9b05827

Conflict of Interest: BZ was employed by the company Shenzhen AmTech Bioengineering Ltd.

The remaining authors declare that the research was conducted in the absence of any commercial or financial relationships that could be construed as a potential conflict of interest.

Copyright © 2020 Zhu, Pan, Mou, Zhou, Pan and Jin. This is an open-access article distributed under the terms of the Creative Commons Attribution License (CC BY). The use, distribution or reproduction in other forums is permitted, provided the original author(s) and the copyright owner(s) are credited and that the original publication in this journal is cited, in accordance with accepted academic practice. No use, distribution or reproduction is permitted which does not comply with these terms.



Synthesis and Bioactivities Study of Novel Pyridylpyrazol Amide Derivatives Containing Pyrimidine Motifs

Wenneng Wu^{1,2}, Meihang Chen³, Qiang Fei¹, Yonghui Ge¹, Yingying Zhu⁴, Haijiang Chen¹, Maofa Yang^{2*} and Guiping Ouyang^{2*}

¹ Food and Pharmaceutical Engineering Institute, Guiyang University, Guiyang, China, ² Center for Research and Development of Fine Chemicals, School of Pharmaceutical Sciences, Entomology of Institute, Guizhou University, Guiyang, China, ³ Material and Chemistry Engineering Institute, Tongren College, Tongren, China, ⁴ School of Chemical Engineering, Guizhou Institute of Technology, Guiyang, China

OPEN ACCESS

Edited by:

Hu Li,
Guizhou University, China

Reviewed by:

Pei Li,
Kailli University, China
Guo Ping Zhang,
Huaibei Normal University, China
Tianrui Ren,
Shanghai Normal University, China

*Correspondence:

Maofa Yang
gdgdly@126.com
Guiping Ouyang
oygp710@163.com

Specialty section:

This article was submitted to
Organic Chemistry,
a section of the journal
Frontiers in Chemistry

Received: 01 May 2020

Accepted: 21 May 2020

Published: 31 July 2020

Citation:

Wu W, Chen M, Fei Q, Ge Y, Zhu Y, Chen H, Yang M and Ouyang G (2020) Synthesis and Bioactivities Study of Novel Pyridylpyrazol Amide Derivatives Containing Pyrimidine Motifs. *Front. Chem.* 8:522. doi: 10.3389/fchem.2020.00522

In this study, thirteen new pyridylpyrazolamide derivatives containing pyrimidine motifs were synthesized via six-step reactions. Bioassay results showed that some of the synthesized compounds revealed good antifungal properties against *Sclerotinia sclerotiorum*, *Phytophthora infestans*, *Thanatephorus cucumeris*, *Gibberella zeae*, *Fusarium oxysporum*, *Cytospora mandshurica*, *Botryosphaeria dothidea*, and *Phomopsis* sp. at 50 μ g/mL, which were similar to those of Kresoxim-methyl or Pyrimethanil. Meanwhile, bioassay results indicated that the synthesized compounds showed a certain insecticidal activity against *Spodoptera litura*, *Mythimna separata*, *Pyrausta nubilalis*, *Tetranychus urticae*, *Rhopalosiphum maidis*, and *Nilaparvata lugens* at 200 μ g/mL, which was lower than that of Chlorantraniliprole. To the best of our knowledge, this study is the first report on the antifungal and insecticidal activities of pyridylpyrazol amide derivatives containing a pyrimidine moiety.

Keywords: pyridylpyrazol, amide, pyrimidine, antifungal activity, insecticidal activity

INTRODUCTION

Plant fungal and insect diseases have posed serious threats to crops in the world and caused a severe loss throughout the world (Strange and Scott, 2005; Yang et al., 2015). Nowadays, some of the available traditional fungicides and insecticides, such as Kresoxim-methyl, Pyrimethanil, Chlorantraniliprole, etc., are widely used to prevent plant harmful fungal and insect diseases. However, prolonged use of traditional pesticides can not only lead to drug resistance, but also have a harmful influence on the safety of the plants and the environment. Therefore, the development of novel and promising fungicides and insecticides is still an urgent task.

Pyrimidine derivatives, which play an important role in synthesis of various active molecules, have versatile properties in modern life, such as antifungal (Chen et al., 2008; Zhang et al., 2016), antibacterial (Triloknadh et al., 2018; Fang et al., 2019), insecticidal (Liu et al., 2017; Shen et al., 2018), herbicidal (Chen et al., 2015; Li et al., 2018), and antiviral (Xu et al., 2015; Wang Y. Y. et al., 2018) activities. In the previous work, some of the pyrimidine derivatives (for example, Mepanipyrim, Pyrimethanil, Diflufenorim, Azoxystrobin, and so on), which were known for their abilities to control severe fungal diseases, have been marketed as commercial pesticides worldwide. Meanwhile, in our preliminary work, several series of pyrimidine derivatives containing 1,3,4-oxadiazole

(Figures 1A,E), 1,3,4-thiadiazole (Figures 1B,E), 1,2,4-triazole (Figure 1C) or amide (Figure 1D) moiety, as shown in Figure 1, were reported and revealed better antiviral, antifungal, and antibacterial activities (Wu et al., 2015, 2016a,b, 2019a,b).

In recent years, pyridylpyrazole amide derivatives have attracted more and more considerable attention owing to their broad class of biological activities in pesticide chemistry, such as antifungal (Yan et al., 2012; Wang B. L. et al., 2018) and insecticidal (Wang et al., 2013, 2019; Shi et al., 2017; Wang B. L. et al., 2018) activity. In the past few years, some representative examples of pyridylpyrazole amide derivatives (for example, chlorantraniliprole and cyantraniliprole) were commercialized as pesticides, as shown in Figure 2.

To develop effective pesticide agents, we aim to introduce the pyrimidine ring to the pyridylpyrazol amide skeleton to design a series of novel pyridylpyrazol amide derivatives containing a pyrimidine moiety (Figure 3). As far as we know, it is the first report on the antifungal and insecticidal activities of pyridylpyrazol amide derivatives containing a pyrimidine moiety.

EXPERIMENTAL AND METHODS

General Information

JEOL-ECX 500 NMR spectrometer (JEOL, Tokyo, Japan) was used to analyse the NMR spectral (^1H NMR and ^{13}C NMR) at room temperature using TMS as an internal standard and DMSO- d_6 as the solvent. Elemental analysis was performed on the Elementar Vario-III CHN analyser (Elementar, Hanau, Germany). Mass spectral were conducted on the Agilent 5973 organic mass spectrometer (Agilent Technologies, Palo Alto, CA, USA). Melting points were determined on the XT-4 binocular microscope (Beijing Tech Instrument Co., China). All commercial reagents and solvents were used as they did not require any purification before use.

Synthesis

Preparation Procedure of the Key Intermediate 5

The synthetic procedure for the key intermediate 5 is shown in Scheme 1. To a mixture of 2,3-dichloropyridine (0.1 mol) dissolved in anhydrous ethanol (120 mL), 80% hydrazine hydrate (80 mL) was added dropwise and reacted under reflux. Upon completion of the reaction, the reaction solution was cooled to room temperature and the solvent was removed under reduced pressure. The residue was washed with water and recrystallized with ethanol to gain intermediate 1. Intermediate 1 (90 mmol) and diethyl maleate (90 mmol) were added to the mixture of sodium ethoxide (90 mmol) and ethanol (100 mL), then a moderate amount of glacial acetic acid was added when the temperature was below 60°C. Upon completion of the reaction, the reaction solution was poured into 100 mL distilled water to precipitate the solid, then the solid was recrystallized with ethanol to obtain intermediate 2. Then, a mixture of intermediate 2 (45 mmol), phosphorus oxychloride (POCl_3 , 50 mmol) or phosphorus oxybromide (POBr_3 , 50 mmol), and acetonitrile (CH_3CN , 50 mL) was reacted under reflux. After ending the reaction, the reaction mixture was poured into

30 mL distilled water, extracted with dichloromethane (CH_2Cl_2), and dried with anhydrous sodium sulfate (Na_2SO_4) to give intermediate 3 (Wang B. L. et al., 2018). After that, a mixture of intermediate 3 (40 mmol), potassium persulfate ($\text{K}_2\text{S}_2\text{O}_8$, 44 mmol), and CH_3CN (50 mL) reacted under reflux. Upon completion of the reaction, the reaction mixture was poured into 100 mL of distilled water. The residue was washed with water and recrystallized with ethanol to obtain intermediate 4 (Wang B. L. et al., 2018). Finally, sodium hydroxide (NaOH , 30 mmol) dissolved in 10 mL of water was added to the mixture of intermediate 4 and methanol (20 mL) and reacted under reflux. When the reaction was completed, the reaction mixture was poured into 100 mL of distilled water and acidified the mixture to pH 5–6 using concentrated hydrochloric acid. The key intermediate 5 was attained after recrystallization with ethanol. ^1H NMR spectral data for intermediates 1–5 are reported in the Supplementary Data.

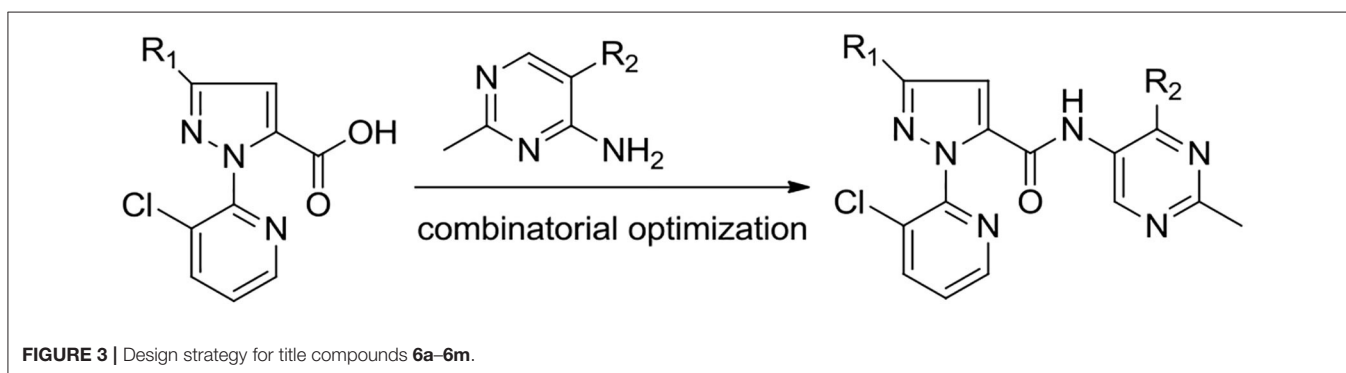
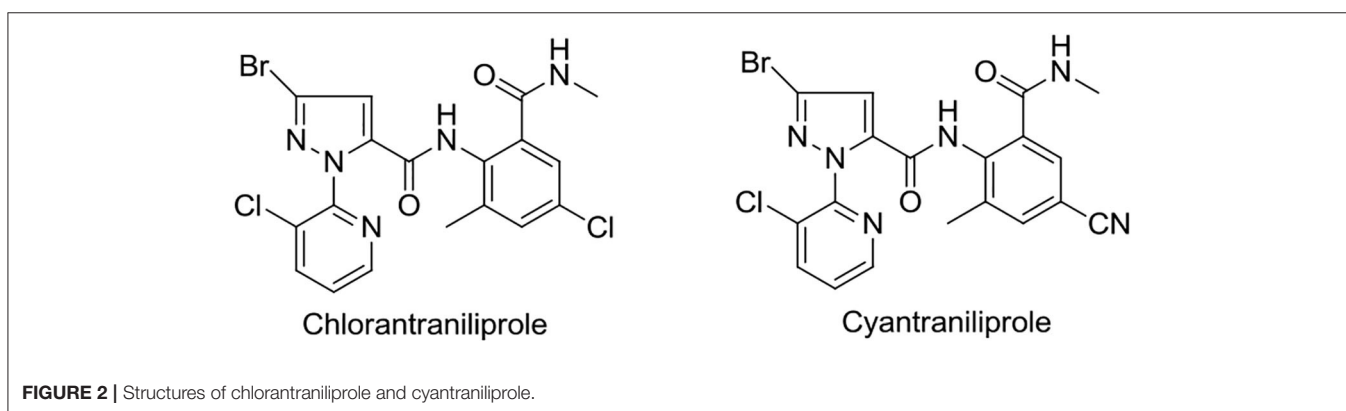
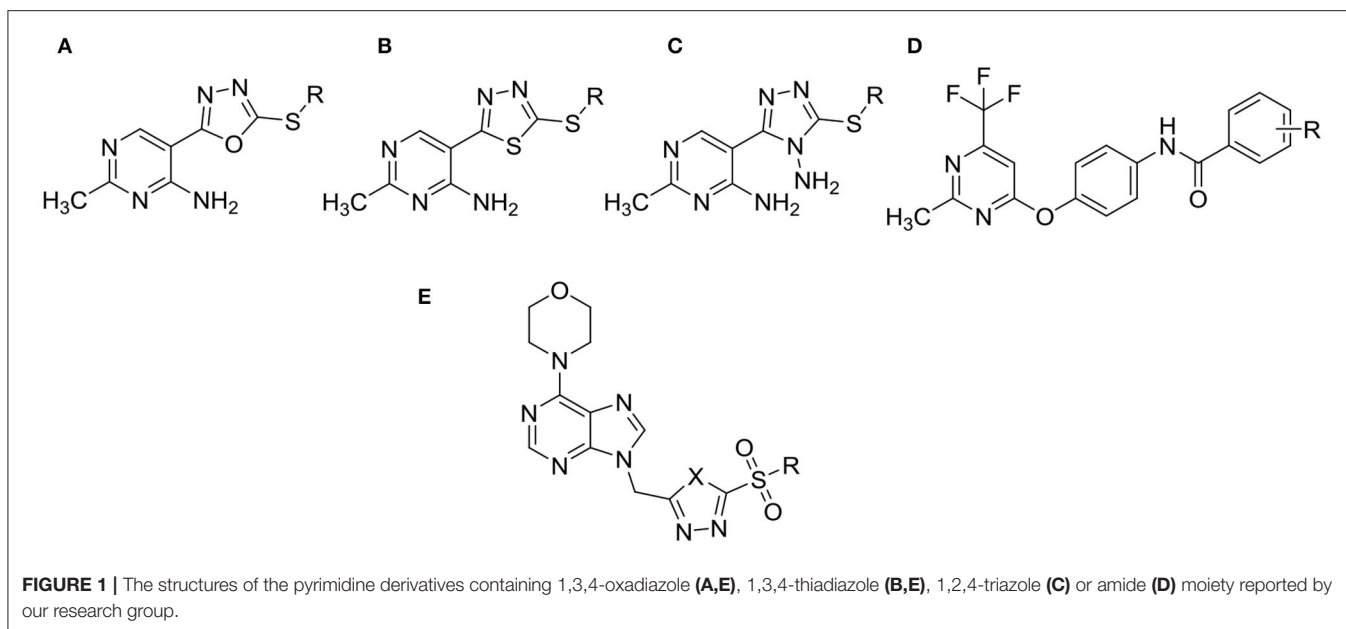
General Procedure for the Preparation of the Target Compounds 6a–6m

As shown in Scheme 1, oxalyl chloride (2 mL) and 4 drops of *N,N*-dimethylformamide (DMF) were added to a mixture of intermediate 5 dissolved in 10 mL CH_2Cl_2 , and reacted at room temperature. When the reaction was completed, the CH_2Cl_2 and excess oxalyl chloride were removed under reduced pressure. Then, 5-substituted-4-amino-2-methylpyrimidine was added to the residue dissolved in 5 mL tetrahydrofuran (THF) and reacted under reflux. At the end of the reaction, the reaction mixture was poured into 20 mL of water, extracted with ethyl acetate, and recrystallized with ethanol to obtain the title compounds 6a–6m.

Methyl-4-(3-bromo-1-(3-chloropyridin-2-yl)-1H-pyrazole-5-carboxamido)-2-methyl-pyrimidine-5-carboxylate (6a). White solid; yield 45.1%; m.p. 220–222°C; ^1H NMR (DMSO- d_6 , 500 MHz) δ : 11.85 (s, 1H, CONH), 8.84 (s, 1H, Pyrimidine-H), 8.52 (d, 1H, $J = 4.6$ Hz, Pyridine-H), 8.23 (d, 1H, $J = 6.9$ Hz, pyridine-H), 7.67 (dd, 1H, $J_1 = 4.55$ Hz, $J_2 = 8.0$ Hz, pyridine-H), 7.58 (s, 1H, Pyrazole-H), 3.61 (s, 3H), 2.62 (s, 3H); ^{13}C NMR (DMSO- d_6 , 125 MHz) δ : 170.51, 165.33, 159.38, 156.62, 154.98, 148.73, 147.82, 140.40, 140.06, 138.27, 128.50, 127.55, 115.07, 109.32, 52.83, 26.00; MS (ESI) m/z : 451.1 ($[\text{M}+\text{H}]^+$); Anal. Calcd. for $\text{C}_{16}\text{H}_{12}\text{BrClN}_6\text{O}_3$: C 42.55, H 2.68, N 18.61; found: C 42.60, H 2.70, N 18.66.

Ethyl-4-(3-bromo-1-(3-chloropyridin-2-yl)-1H-pyrazole-5-carboxamido)-2-methyl-pyrimidine-5-carboxylate (6b). White crystals; yield 50.4%; m.p. 176–177°C; ^1H NMR (DMSO- d_6 , 500 MHz) δ : 11.88 (s, 1H, CONH), 8.84 (s, 1H, Pyrimidine-H), 8.51 (d, 1H, $J = 4.0$ Hz, Pyridine-H), 8.24 (d, 1H, $J = 8.0$ Hz, pyridine-H), 7.66 (dd, 1H, $J_1 = 4.55$ Hz, $J_2 = 8.0$ Hz, pyridine-H), 7.59 (s, 1H, Pyrazole-H), 4.09 (q, 2H, $J = 6.9$ Hz), 2.64 (s, 3H), 1.08 (t, 3H, $J = 7.45$ Hz); ^{13}C NMR (DMSO- d_6 , 125 MHz) δ : 170.51, 164.80, 159.38, 156.64, 148.73, 147.80, 140.33, 140.07, 138.27, 128.46, 127.52, 115.38, 109.34, 61.68, 25.97, 14.32; MS (ESI) m/z : 465.1 ($[\text{M}+\text{H}]^+$); Anal. Calcd. for $\text{C}_{17}\text{H}_{14}\text{BrClN}_6\text{O}_3$: C 43.85, H 3.03, N 18.05; found: C 43.90, H 3.00, N 18.06.

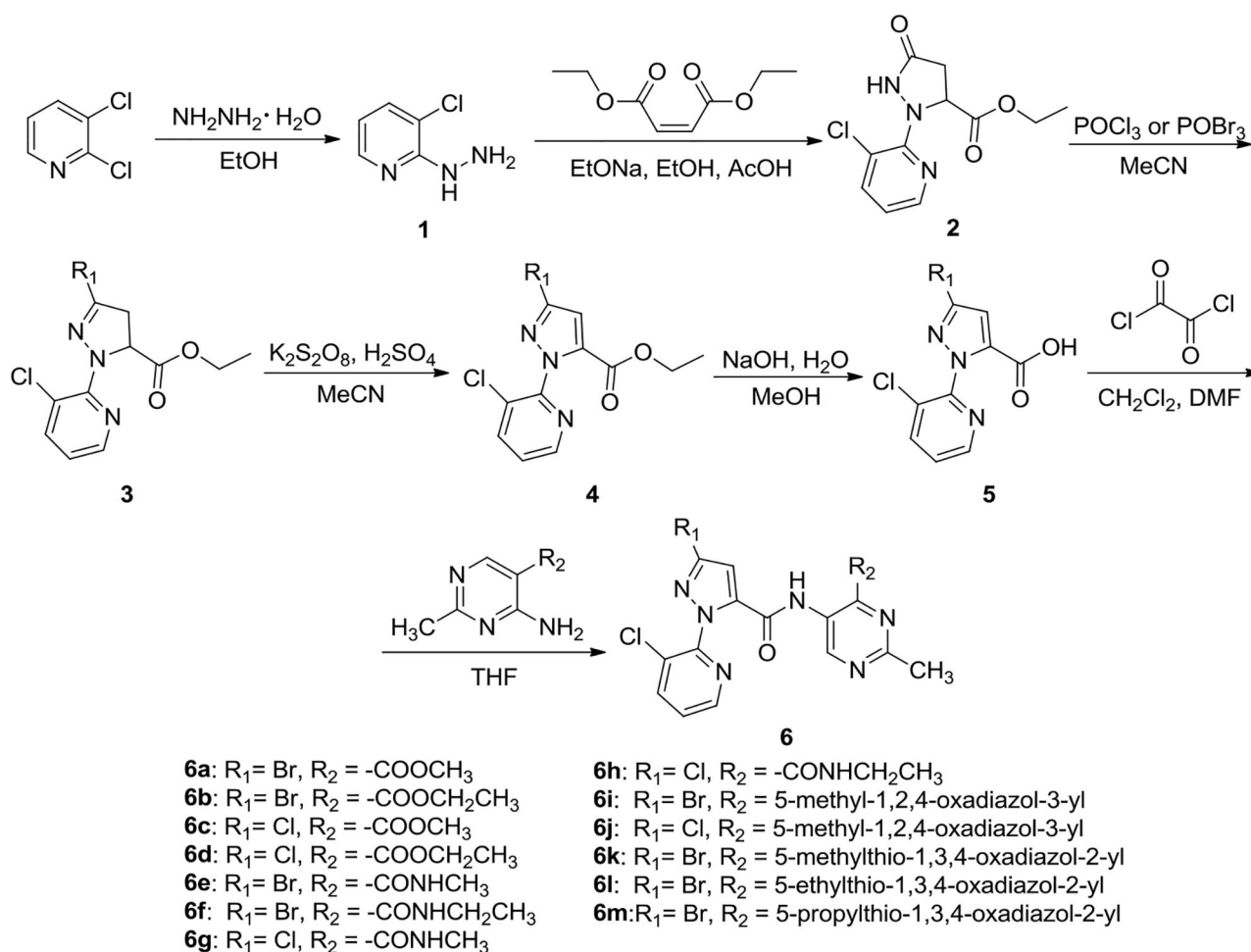
Methyl-4-(3-chloro-1-(3-chloropyridin-2-yl)-1H-pyrazole-5-carboxamido)-2-methyl-pyrimidine-5-carboxylate (6c). White



solid; yield 48.2%; m.p. 213–215°C; ^1H NMR (DMSO- d_6 , 500 MHz) δ : 11.87 (s, 1H, CONH), 8.85 (s, 1H, Pyrimidine-H), 8.53 (d, 1H, $J = 2.85$ Hz, Pyridine-H), 8.25 (d, 1H, $J = 7.65$ Hz, pyridine-H), 7.68 (dd, 1H, $J_1 = 2.85$ Hz, $J_2 = 8.0$ Hz, pyridine-H), 7.55 (s, 1H, Pyrazole-H), 3.62 (s, 3H), 2.64 (s, 3H); ^{13}C NMR (DMSO- d_6 , 125 MHz) δ : 170.54, 165.32, 159.41, 156.62, 155.01,

148.71, 147.85, 140.48, 140.01, 138.30, 128.51, 127.54, 115.05, 109.30, 52.82, 26.01; MS (ESI) m/z : 407.1 ($[\text{M}+\text{H}]^+$); Anal. Calcd. for $\text{C}_{16}\text{H}_{12}\text{Cl}_2\text{N}_6\text{O}_3$: C 47.19, H 2.97, N 20.64; found: C 47.20, H 3.00, N 20.62.

Ethyl4-(3-chloro-1-(3-chloropyridin-2-yl)-1H-pyrazole-5-carboxamido)-2-methyl-pyrimidine-5-carboxylate (**6d**). Yellow



SCHEME 1 | Synthetic route of the title compounds **6a–6m**.

crystals; yield 38.5%; m.p. 191–192°C; ^1H NMR (DMSO- d_6 , 500 MHz) δ : 11.88 (s, 1H, CONH), 8.84 (s, 1H, Pyrimidine-H), 8.51 (d, 1H, $J = 2.85\text{ Hz}$, Pyridine-H), 8.23 (d, 1H, $J = 7.65\text{ Hz}$, pyridine-H), 7.66 (dd, 1H, $J_1 = 2.85\text{ Hz}$, $J_2 = 8.00\text{ Hz}$, pyridine-H), 7.53 (s, 1H, Pyrazole-H), 4.06 (q, 2H, $J = 6.90\text{ Hz}$), 2.64 (s, 3H), 1.08 (t, 3H, $J = 6.85\text{ Hz}$); ^{13}C NMR (DMSO- d_6 , 125 MHz) δ : 170.52, 164.80, 159.38, 156.64, 148.73, 147.80, 140.33, 140.07, 138.27, 128.46, 127.52, 115.38, 109.34, 61.68, 25.97, 14.32; MS (ESI) m/z : 422.1 ($[\text{M}+\text{H}]^+$); Anal. Calcd. for $\text{C}_{17}\text{H}_{14}\text{Cl}_2\text{N}_6\text{O}_3$: C 48.47, H 3.35, N 19.95; found: C 48.50, H 3.40, N 20.02.

4-(3-Bromo-1-(3-chloropyridin-2-yl)-1H-pyrazole-5-carboxamido)-N-2-dimethylpyrimidine-5-carboxamide (**6e**). White solid; yield 52.6%; m.p. 228–233°C; ^1H NMR (DMSO- d_6 , 500 MHz) δ : 12.33 (s, 1H, CONH), 8.78 (s, 1H, Pyrimidine-H), 8.74 (d, 1H, $J = 4.55\text{ Hz}$, CONH), 8.48 (d, 1H, $J = 4.00\text{ Hz}$, Pyridine-H), 8.19 (d, 1H, $J = 8.05\text{ Hz}$, Pyridine-H), 7.62 (dd, 1H, $J_1 = 4.60\text{ Hz}$, $J_2 = 8.00\text{ Hz}$, Pyridine-H), 7.32 (s, 1H, Pyrazole-H), 2.67 (d, 3H, $J = 4.6\text{ Hz}$), 2.45 (s, 3H); ^{13}C NMR (DMSO- d_6 , 125 MHz) δ : 169.38, 165.98, 157.28, 156.02, 154.80, 148.58, 147.82, 140.09, 139.38, 128.40, 127.68, 127.48, 114.27, 111.72, 26.67, 26.07; MS (ESI) m/z : 450.1 ($[\text{M}+\text{H}]^+$); Anal. Calcd. for

$\text{C}_{16}\text{H}_{13}\text{BrClN}_7\text{O}_2$: C 42.64, H 2.91, N 21.76; found: C 42.66, H 2.90, N 21.77.

4-(3-Bromo-1-(3-chloropyridin-2-yl)-1H-pyrazole-5-carboxamido)-N-ethyl-2-methylpyrimidine-5-carboxamide (**6f**). White solid; yield 60.1%; m.p. 236–237°C; ^1H NMR (DMSO- d_6 , 500 MHz) δ : 12.33 (s, 1H, CONH), 8.78 (s, 1H, Pyrimidine-H), 8.72 (s, 1H, CONH), 8.48 (d, 1H, $J = 4.00\text{ Hz}$, Pyridine-H), 8.19 (d, 1H, $J = 8.05\text{ Hz}$, Pyridine-H), 7.62 (dd, 1H, $J_1 = 4.60\text{ Hz}$, $J_2 = 8.00\text{ Hz}$, Pyridine-H), 7.32 (s, 1H, Pyrazole-H), 2.84 (q, 2H, $J = 6.85\text{ Hz}$), 2.45 (s, 3H), 1.04 (t, 3H, $J = 6.25\text{ Hz}$); ^{13}C NMR (DMSO- d_6 , 125 MHz) δ : 169.35, 166.00, 157.31, 156.04, 154.78, 148.60, 147.81, 140.11, 139.35, 128.42, 127.65, 127.49, 114.27, 111.76, 26.66, 26.03, 15.32; MS (ESI) m/z : 464.1 ($[\text{M}+\text{H}]^+$); Anal. Calcd. for $\text{C}_{17}\text{H}_{15}\text{BrClN}_7\text{O}_2$: C 42.64, H 2.91, N 21.76; found: C 42.66, H 2.90, N 21.77.

4-(3-Chloro-1-(3-chloropyridin-2-yl)-1H-pyrazole-5-carboxamido)-N-2-dimethylpyrimidine-5-carboxamide (**6g**). White solid; yield 45.9%; m.p. 213–215°C; ^1H NMR (DMSO- d_6 , 500 MHz) δ : 11.87 (s, 1H, CONH), 8.85 (s, 1H, Pyrimidine-H), 8.71 (s, 1H, CONH), 8.53 (d, 1H, $J = 2.85\text{ Hz}$, Pyridine-H), 8.25 (d, 1H, $J = 7.65\text{ Hz}$, Pyridine-H), 7.68 (dd, 1H, $J_1 = 2.85\text{ Hz}$, J_2

TABLE 1 | The *in vitro* antifungal activity of the title compounds 6a–6m at 50 µg/mL.

Compds.	Inhibition rate (%)							
	<i>S. sclerotiorum</i>	<i>P. infestans</i>	<i>T. cucumeris</i>	<i>G. zeae</i>	<i>F. oxysporum</i>	<i>C. mandshurica</i>	<i>B. dothidea</i>	<i>Phomopsis sp.</i>
6a	27.5 ± 1.1	20.7 ± 1.0	6.8 ± 1.9	0	16.9 ± 0.9	10.7 ± 1.1	31.6 ± 2.1	36.2 ± 1.4
6b	37.8 ± 1.6	29.6 ± 1.3	19.7 ± 1.4	8.7 ± 1.1	36.0 ± 1.3	40.2 ± 1.7	36.5 ± 1.6	42.1 ± 1.0
6c	35.0 ± 1.4	16.8 ± 1.3	14.2 ± 0.9	34.2 ± 1.3	12.1 ± 0.9	22.2 ± 1.0	45.9 ± 3.3	53.5 ± 1.2
6d	34.0 ± 1.3	8.7 ± 0.8	8.1 ± 1.2	0	2.6 ± 1.1	11.7 ± 0.9	50.8 ± 3.1	57.5 ± 2.1
6e	6.5 ± 0.9	10.0 ± 0.9	3.2 ± 1.0	9.9 ± 0.9	0	12.8 ± 3.0	30.1 ± 1.9	40.3 ± 2.7
6f	11.8 ± 3.8	15.1 ± 1.2	9.4 ± 1.2	7.8 ± 2.2	16.2 ± 1.7	21.2 ± 0.9	37.5 ± 3.0	46.2 ± 1.4
6g	41.5 ± 1.0	32.9 ± 1.0	35.2 ± 1.3	15.1 ± 1.5	32.1 ± 0.9	14.8 ± 0.9	38.4 ± 1.2	41.8 ± 3.3
6h	37.4 ± 1.2	27.0 ± 0.9	37.5 ± 1.0	21.6 ± 1.5	25.3 ± 1.9	20.7 ± 1.0	44.9 ± 3.0	46.3 ± 2.2
6i	47.9 ± 1.6	48.6 ± 1.4	49.2 ± 1.8	48.8 ± 1.6	66.3 ± 1.0	41.5 ± 1.4	85.9 ± 1.1	81.2 ± 2.4
6j	54.1 ± 1.1	42.5 ± 1.2	54.7 ± 2.3	54.9 ± 1.5	53.8 ± 1.3	49.4 ± 1.2	83.6 ± 2.1	78.8 ± 1.2
6k	39.9 ± 3.1	30.1 ± 0.9	47.9 ± 1.2	41.2 ± 1.1	45.6 ± 1.1	47.7 ± 1.3	55.6 ± 2.8	57.0 ± 1.9
6l	30.6 ± 2.3	24.1 ± 1.7	40.3 ± 2.6	33.7 ± 2.8	38.5 ± 2.3	40.2 ± 1.8	59.5 ± 3.0	62.2 ± 3.5
6m	24.8 ± 1.2	16.3 ± 1.4	34.6 ± 0.9	24.9 ± 1.7	32.2 ± 1.6	32.5 ± 1.6	46.2 ± 2.7	51.4 ± 2.0
Kresoxim-methyl	52.3 ± 1.1	49.8 ± 1.0	64.1 ± 1.2	56.9 ± 1.0	70.6 ± 1.2	51.1 ± 1.3	/	/
Pyrimethanil	/	/	/	/	/	/	84.4 ± 2.1	85.1 ± 1.4

= 8.0 Hz, Pyridine-H), 7.55 (s, 1H, Pyrazole-H), 2.85 (s, 3H), 2.64 (s, 3H); ¹³C NMR (DMSO-*d*₆, 125 MHz) δ: 170.51, 165.33, 159.38, 156.62, 154.98, 148.73, 147.82, 140.40, 140.06, 138.27, 128.50, 127.55, 115.07, 109.32, 52.83, 26.62, 26.04; MS (ESI) *m/z*: 406.1 ([M+H]⁺); Anal. Calcd. for C₁₆H₁₃Cl₂N₇O₂: C 47.31, H 3.23, N 24.14; found: C 47.32, H 3.20, N 24.12.

4-(3-Chloro-1-(3-chloropyridin-2-yl)-1H-pyrazole-5-carboxamido)-N-ethyl-2-methylpyrimidine-5-carboxamide (**6h**). Yellow crystals; yield 47.8%; m.p. 191–192°C; ¹H NMR (DMSO-*d*₆, 500 MHz) δ: 11.88 (s, 1H, CONH), 8.84 (s, 1H, Pyrimidine-H), 8.71 (s, 1H, CONH), 8.51 (d, 1H, *J* = 2.85 Hz, Pyridine-H), 8.23 (d, 1H, *J* = 7.65 Hz, pyridine-H), 7.66 (dd, 1H, *J*₁ = 2.85 Hz, *J*₂ = 8.00 Hz, pyridine-H), 7.53 (s, 1H, Pyrazole-H), 4.06 (q, 2H, *J* = 6.90 Hz), 2.64 (s, 3H), 1.08 (t, 3H, *J* = 6.85 Hz); ¹³C NMR (DMSO-*d*₆, 125 MHz) δ: 170.52, 164.89, 159.38, 156.64, 148.73, 147.80, 140.33, 140.07, 138.27, 128.46, 127.52, 115.38, 109.34, 61.68, 25.97, 15.32; MS (ESI) *m/z*: 420.1 ([M+H]⁺); Anal. Calcd. for C₁₇H₁₅Cl₂N₇O₂: C 48.59, H 3.60, N 23.33; found: C 48.61, H 3.62, N 23.30.

3-Bromo-1-(3-chloropyridin-2-yl)-N-(2-methyl-5-(5-methyl-1,2,4-oxadiazol-3-yl)pyrimidin-4-yl)-1H-pyrazole-5-carboxamide (**6i**). Yellow crystals; yield 36.5%; m.p. 180–181°C; ¹H NMR (DMSO-*d*₆, 500 MHz) δ: 11.64 (s, 1H, CONH), 8.99 (s, 1H, Pyrimidine-H), 8.49 (d, 1H, *J* = 4.55 Hz, Pyridine-H), 8.18 (d, 1H, *J* = 8.05 Hz, Pyridine-H), 7.63 (dd, 1H, *J*₁ = 4.60 Hz, *J*₂ = 8.0 Hz, Pyridine-H), 7.54 (s, 1H, Pyrazole-H), 2.67 (s, 3H), 2.61 (s, 3H); ¹³C NMR (DMSO-*d*₆, 125 MHz) δ: 177.49, 169.89, 164.89, 158.92, 155.80, 155.08, 148.68, 147.69, 139.94, 138.68, 128.48, 127.52, 127.41, 112.34, 111.50, 25.96, 12.43; MS (ESI) *m/z*: 475.1 ([M+H]⁺); Anal. Calcd. for C₁₇H₁₂BrClN₈O₂: C 42.92, H 2.54, N 23.56; found: C 42.91, H 2.50, N 23.60.

3-Chloro-1-(3-chloropyridin-2-yl)-N-(2-methyl-5-(5-methyl-1,2,4-oxadiazol-3-yl)pyrimidin-4-yl)-1H-pyrazole-5-carboxamide (**6j**). Yellow crystals; yield 41.3%; m.p. 151–152°C; ¹H NMR

TABLE 2 | The EC₅₀ values of compounds 6i and 6j against *B. dothidea*.

Compounds	Toxic regression equation	<i>r</i>	EC ₅₀ (µg/mL)
6i	y = 1.21x + 3.56	0.99	56.4 ± 1.2
6j	y = 0.85x + 4.15	0.99	65.3 ± 1.1
Pyrimethanil	y = 1.01x + 6.25	0.99	57.6 ± 1.8

(DMSO-*d*₆, 500 MHz) δ: 11.64 (s, 1H, CONH), 8.99 (s, 1H, Pyrimidine-H), 8.49 (d, 1H, *J* = 4.55 Hz, Pyridine-H), 8.18 (d, 1H, *J* = 8.05 Hz, Pyridine-H), 7.63 (dd, 1H, *J*₁ = 4.60 Hz, *J*₂ = 8.0 Hz, Pyridine-H), 7.54 (s, 1H, Pyrazole-H), 2.67 (s, 3H), 2.61 (s, 3H); ¹³C NMR (DMSO-*d*₆, 125 MHz) δ: 177.52, 169.87, 164.92, 158.94, 155.85, 155.11, 148.65, 147.72, 139.99, 138.71, 128.50, 127.53, 127.45, 112.36, 111.32, 26.02, 12.45; MS (ESI) *m/z*: 431.1 ([M+H]⁺); Anal. Calcd. for C₁₇H₁₂BrClN₈O₂: C 47.35, H 2.80, N 25.98; found: 47.37, H 2.77, N 25.99.

3-Bromo-1-(3-chloropyridin-2-yl)-N-(2-methyl-5-(5-methylthio)-1,3,4-oxadiazol-2-yl)pyrimidin-4-yl)-1H-pyrazole-5-carboxamide (**6k**). Yellow crystals; yield 46.8%; m.p. 166–168°C; ¹H NMR (DMSO-*d*₆, 500 MHz) δ: 11.84 (s, 1H, CONH), 9.04 (s, 1H, Pyrimidine-H), 8.46 (d, 1H, *J* = 5.15 Hz, Pyridine-H), 8.18 (d, 1H, *J* = 8.0 Hz, Pyridine-H), 7.62 (dd, 1H, *J*₁ = 4.55 Hz, *J*₂ = 7.7 Hz, Pyridine-H), 7.58 (s, 1H, Pyrazole-H), 2.72 (s, 3H), 2.66 (s, 3H); ¹³C NMR (DMSO-*d*₆, 125 MHz) δ: 170.30, 164.72, 162.00, 158.79, 156.05, 148.51, 148.10, 147.81, 140.01, 138.54, 128.35, 127.60, 127.42, 112.61, 108.46, 26.10, 15.62; MS (ESI) *m/z*: 507.1 ([M+H]⁺); Anal. Calcd. for C₁₇H₁₂BrClN₈O₂S: C 40.21, H 2.38, N 22.07; found: C 40.24, H 2.40, N 22.05.

3-Bromo-1-(3-chloropyridin-2-yl)-N-(5-(5-(ethylthio)-1,3,4-oxadiazol-2-yl)-2-methylpyrimidin-4-yl)-1H-pyrazole-5-carboxamide (**6l**). Yellow crystals; yield 42.5%; m.p. 176–177°C; ¹H

TABLE 3 | The insecticidal activities of the title compounds 6a–6m at 200 µg/mL.

Compds.	Mortality rate (%)					
	<i>S. litura</i>	<i>M. separata</i>	<i>P. nubilalis</i>	<i>T. urticae</i>	<i>R. maidis</i>	<i>N. lugens</i>
6a	21.8 ± 1.2	12.0 ± 2.5	25.6 ± 2.0	49.8 ± 0.9	20.0 ± 1.8	64.1 ± 2.6
6b	10.0 ± 1.0	48.5 ± 3.2	31.6 ± 1.5	59.6 ± 2.2	30.0 ± 2.2	74.6 ± 3.0
6c	11.8 ± 1.5	56.8 ± 2.8	28.1 ± 1.2	43.0 ± 2.6	88.9 ± 2.0	67.3 ± 2.8
6d	18.6 ± 2.0	16.7 ± 2.2	0	57.2 ± 2.5	22.4 ± 1.1	63.5 ± 2.5
6e	43.3 ± 2.5	66.3 ± 2.0	42.7 ± 2.3	51.6 ± 2.0	26.7 ± 1.5	50.3 ± 1.5
6f	70.2 ± 2.8	75.4 ± 2.8	61.3 ± 4.5	80.9 ± 4.5	65.5 ± 3.0	78.6 ± 3.3
6g	45.2 ± 2.0	19.6 ± 1.0	38.3 ± 1.1	57.2 ± 3.5	40.9 ± 2.0	41.6 ± 2.5
6h	37.5 ± 2.2	24.8 ± 1.5	46.9 ± 3.2	61.4 ± 2.8	36.5 ± 1.5	50.5 ± 3.1
6i	30.0 ± 1.8	26.6 ± 2.0	10.0 ± 2.2	52.7 ± 2.5	37.8 ± 1.2	28.4 ± 1.8
6j	35.3 ± 1.5	31.2 ± 2.8	26.1 ± 1.8	61.7 ± 3.0	43.2 ± 1.8	24.1 ± 1.5
6k	40.2 ± 1.4	32.0 ± 2.1	18.4 ± 1.5	72.6 ± 2.6	40.2 ± 1.5	32.5 ± 2.8
6l	32.4 ± 1.0	27.5 ± 1.5	23.5 ± 1.5	64.5 ± 2.2	33.8 ± 1.0	23.8 ± 1.9
6m	26.1 ± 0.8	23.4 ± 1.2	28.2 ± 1.0	57.8 ± 2.0	26.6 ± 0.8	11.0 ± 2.5
Chlorantraniliprole	100.0	100.0	100.0	100.0	100.0	100.0

NMR (DMSO-*d*₆, 500 MHz) δ : 11.84 (s, 1H, CONH), 9.04 (s, 1H, Pyrimidine-H), 8.46 (d, 1H, *J* = 5.15 Hz, Pyridine-H), 8.18 (d, 1H, *J* = 8.0 Hz, Pyridine-H), 7.62 (dd, 1H, *J*₁ = 4.55 Hz, *J*₂ = 7.7 Hz, Pyridine-H), 7.58 (s, 1H, Pyrazole-H), 3.12 (q, 2H, *J* = 6.9 Hz), 2.66 (s, 3H), 1.35 (t, 3H, *J* = 7.45 Hz); ¹³C NMR (DMSO-*d*₆, 125 MHz) δ : 170.25, 164.74, 161.95, 158.75, 156.08, 148.25, 148.12, 147.69, 140.07, 138.55, 128.27, 127.60, 127.44, 112.63, 108.56, 27.86, 26.10, 14.23; MS (ESI) *m/z*: 521.1 ([M+H]⁺); Anal. Calcd. for C₁₈H₁₄BrClN₈O₂S: C 41.43, H 2.70, N 21.48; found: C 41.45, H 2.74, N 21.49.

3-Bromo-1-(3-chloropyridin-2-yl)-N-(2-methyl-5-(5-(propylthio)-1,3,4-oxadiazol-2-yl)pyrimidin-4-yl)-1*H*-pyrazole-5-carboxamide (**6m**). Yellow crystals; yield 39.8%; m.p. 197–199°C; ¹H NMR (DMSO-*d*₆, 500 MHz) δ : 11.84 (s, 1H, CONH), 9.04 (s, 1H, Pyrimidine-H), 8.46 (d, 1H, *J* = 5.15 Hz, Pyridine-H), 8.18 (d, 1H, *J* = 8.0 Hz, Pyridine-H), 7.62 (dd, 1H, *J*₁ = 4.55 Hz, *J*₂ = 7.7 Hz, Pyridine-H), 7.58 (s, 1H, Pyrazole-H), 3.15 (t, 2H, *J* = 6.9 Hz), 2.66 (s, 3H), 1.68 (m, 2H), 0.95 (t, 3H, *J* = 7.45 Hz); ¹³C NMR (DMSO-*d*₆, 125 MHz) δ : 170.31, 164.70, 162.03, 158.75, 156.02, 148.48, 148.07, 147.77, 140.04, 138.50, 128.32, 127.60, 127.44, 112.67, 108.49, 34.43, 26.10, 22.92, 13.33; MS (ESI) *m/z*: 535.1 ([M+H]⁺); Anal. Calcd. for C₁₉H₁₆BrClN₈O₂S: C 42.59, H 3.01, N 20.91; found: C 42.53, H 3.00, N 20.92.

Antifungal Biological Assay

The antifungal activities of the title compounds **6a–6m** against *Sclerotinia sclerotiorum* (*S. sclerotiorum*), *Phytophthora infestans* (*P. infestans*), *Thanatephorus cucumeris* (*T. cucumeris*), *Gibberella zeae* (*G. zeae*), *Fusarium oxysporum* (*F. oxysporum*), *Cytospora mandshurica* (*C. mandshurica*), *Botryosphaeria dothidea* (*B. dothidea*), and *Phomopsis* sp. were evaluated at the concentration of 50 µg/mL (Min et al., 2016; Wu et al., 2019a,b). The target compounds **6a–6m** (5 mg) were dissolved in dimethyl sulfoxide (1 mL) and sterile water (9 mL) before mixing with 90 mL potato dextrose agar (PDA) to generate a

final concentration of 50 µg/mL. Then, 4 mm diameter of the mycelia dishes were cut from a culture medium of pathogenic fungi, then inoculated in the middle of PDA and cultivated at 27 ± 1°C for 4–5 days. DMSO in sterile distilled water served as a negative control, while Kresoxim-methyl and Pyrimethanil acted as positive controls. For each treatment, three replicates were conducted. The radial growth of the fungal colonies was measured and the data were statistically analyzed. The inhibition rate *I* (%) of the test compounds against eight pathogenic fungi were calculated by the following formula, where *C* represents the diameter of fungi growth on untreated PDA, and *T* represents the diameter of fungi on treated PDA.

$$I(\%) = [(C - T)/(C - 0.4)] \times 100 \quad (1)$$

Insecticidal Biological Assay

The insecticidal activities of all synthesized compounds **6a–6m** against *Spodoptera litura* (*S. litura*), *Mythimna separata* (*M. separata*), *Pyrausta nubilalis* (*P. nubilalis*), *Tetranychus urticae* (*T. urticae*), *Rhopalosiphum maidis* (*R. maidis*), and *Nilaparvata lugens* (*N. lugens*) were performed according to the reported method (Wang B. L. et al., 2018; Wang et al., 2019). The target compounds **6a–6m** were dissolved in NP-10 (0.1 mg/L) solution to generate a final concentration of 200 µg/mL. Then, 15 maize leaves (approximately 5 cm in length) and 5 sweet potato leaves (diameter 3 cm) were dipped in the test compounds solutions for 10 s, dried and placed into a tumbler. After that, 30 larvae of second-instar *S. litura*, *M. separata*, *P. nubilalis*, *T. urticae*, *R. maidis*, and *N. lugens* were transferred to the petri dish. Chlorantraniliprole was used as a control. All bioassays were performed in the laboratory at 27 ± 1°C for 48 h. Three replicates were performed for each treatment. The percentage of mortalities for the target compounds were determined using Abbott's formula.

RESULTS AND DISCUSSION

In this study, using 2,3-dichloropyridine as the starting material, the title compounds **6a–6m** were synthesized in six steps, including hydrazidation, cyclization, bromination or chlorination, oxidation, hydrolyzation, and condensation. The target compounds structures were confirmed by ^1H NMR, ^{13}C NMR, MS, and elemental analysis. In the ^1H NMR spectra of compound **6a**, a singlet at 2.45 ppm assigned to CH_3 protons of pyrimidine- CH_3 , the doublet signal at 2.67 ppm indicated the presence of CH_3 proton in CONH-CH_3 , meanwhile, a singlet at 8.78 and 7.32 ppm indicated the presence of pyrimidine and pyrazole ring. Two proton signals of two $-\text{CONH-}$ in amide moiety was observed at 12.33 and 8.74 ppm. The structure of **6b** was also confirmed by its mass spectral data. In its mass spectrum, the molecular ion peak was noticed m/z at 450.1 ($[\text{M}+\text{H}]^+$) corresponding to its molecular weight.

The *in vitro* antifungal activities at 50 $\mu\text{g/mL}$ of the target compounds against eight plant fungi are listed in **Table 1**. **Table 1** showed that, at 50 $\mu\text{g/mL}$, compounds **6a–6m** indicated certain antifungal activities against *S. sclerotiorum*, *P. infestans*, *T. cucumeris*, *G. zeae*, *F. oxysporum*, *C. mandshurica*, *B. dothidea*, and *Phomopsis* sp. with the inhibition rates of 6.5–54.1%, 8.7–48.6%, 3.2–54.7%, 0–54.9%, 0–66.3%, 10.7–49.4%, 30.1–85.9%, and 36.2–81.2%, respectively. Among the title compounds, compound **6i** revealed good *in vitro* antifungal activities against *P. infestans* and *B. dothidea*, with the inhibition rates of 48.6% and 85.9%, respectively, which were equally to those of Kresoxim-methyl or Pyrimethanil. Meanwhile, compound **6j** revealed good *in vitro* antifungal activities against *S. sclerotiorum*, *G. zeae*, *C. mandshurica*, and *B. dothidea*, with the inhibition rates of 54.1, 54.9, 49.4, and 85.9%, respectively, which were similar with those of Kresoxim-methyl or Pyrimethanil.

Based on the preliminary antifungal bioassays, the EC_{50} values of compounds **6i** and **6j** were also tested and presented in **Table 2**. **Table 2** showed that compounds **6i** and **6j** showed good activities against *B. dothidea*, with EC_{50} values of 56.4 and 65.3 $\mu\text{g/mL}$, respectively, which were similar to that of Pyrimethanil (57.6 $\mu\text{g/mL}$).

The *in vitro* insecticidal properties of title compounds against *S. litura*, *M. separata*, *P. nubilalis*, *T. urticae*, *R. maidis*, and *N. lugens* were evaluated and the insecticidal bioassay results are listed in **Table 3**. **Table 3** showed that the target compounds **6a–6m** indicated certain insecticidal activities against *S. litura*, *M. separata*, *P. nubilalis*, *T. urticae*, *R. maidis*, and *N. lugens* at 200 $\mu\text{g/mL}$, with the mortality rates of 10.0–70.2%, 12.0–75.4%, 0–61.3%, 43.0–80.9%, 20.0–88.9%, and 11.0–78.6%, respectively, which were lower than those of Chlorantraniliprole. Especially, compound **6f** revealed good insecticidal activities

against *S. litura*, *M. separata*, *P. nubilalis*, *T. urticae*, and *N. lugens* with mortality rates of 70.2, 75.4, 61.3, 80.9, and 78.6%, respectively. Meanwhile, compound **6c** had a good mortality rate of 88.9% against *R. maidis*.

CONCLUSIONS

In summary, thirteen novel pyridylpyrazolamide derivatives containing pyrimidine motifs were synthesized, and their structures confirmed by ^1H NMR, ^{13}C NMR, MS and elemental analysis. Bioassay results showed that some of title compounds revealed good antifungal and insecticidal properties. The results provided strategy for leading the synthesis of novel pyridylpyrazolamide derivatives containing pyrimidine motifs.

DATA AVAILABILITY STATEMENT

The original contributions presented in the study are included in the article/**Supplementary Material**, further inquiries can be directed to the corresponding author/s.

AUTHOR CONTRIBUTIONS

WW and QF contributed to the synthesis, purification, characterization of all compounds, and prepared the original manuscript. YZ and YG performed the activity research. MC and HC perfected the language and assisted with the structure elucidation and manuscript revision. GO and MY designed and supervised the research and revised the manuscript. All authors discussed, edited, and approved the final version.

FUNDING

This research was financially supported by China Postdoctoral Science Foundation (No. 2017M623070), the National Natural Science Foundation of China (No. 31701821 and 21762037), the Opening Foundation of the Key Laboratory of Green Pesticide and Agricultural Bioengineering, Ministry of Education, Guizhou University (No. 2018GDGP0102), the Guizhou Province Biological and Pharmaceutical engineering Research Center and (No. QJHKY[2019]051), and the special Funding of Guiyang Science and Technology Bureau and Guiyang University [GYU-KYZ(2019~2020)PT10-06].

SUPPLEMENTARY MATERIAL

The Supplementary Material for this article can be found online at: <https://www.frontiersin.org/articles/10.3389/fchem.2020.00522/full#supplementary-material>

REFERENCES

- Chen, Q., Zhu, X. L., Jiang, L. L., Liu, Z. M., and Yang, G. F. (2008). Synthesis, antifungal activity and CoMFA analysis of novel 1,2,4-triazolo[1,5-a]pyrimidine derivatives. *Eur. J. Med. Chem.* 43, 595–603. doi: 10.1016/j.ejmech.2007.04.021
- Chen, X. M., Wang, S. H., and Cui, D. L. (2015). The synthesis and herbicidal activity of 5-(substituted-phenyl)-4,6-dioxo-4,5,6,7-tetrahydropyrazolo(3,4-d)pyrimidines. *J. Heterocyclic Chem.* 52, 607–610. doi: 10.1002/jhet.2047
- Fang, Z., Zheng, S., Chan, K. F., Yuan, W., Guo, Q., Wu, W. Y., et al. (2019). Design, synthesis and antibacterial evaluation of 2, 4-disubstituted-6-thiophenyl-pyrimidines.

- Eur. J. Med. Chem.* 161, 141–153. doi: 10.1016/j.ejmech.2018.10.039
- Li, K. J., Qu, R. Y., Liu, Y. C., Yang, J. F., Devendar, P., Chen, Q., et al. (2018). Design, synthesis, and herbicidal activity of pyrimidine-biphenyl hybrids as novel acetohydroxyacid synthase inhibitors. *J. Agric. Food Chem.* 66, 3773–3782. doi: 10.1021/acs.jafc.8b00665
- Liu, X. H., Wang, Q., Sun, Z. H., Wedge, D. P. E., Estep, J. J., Tan, C. X., et al. (2017). Synthesis and insecticidal activity of novel pyrimidine derivatives containing urea pharmacophore against *aedes aegypti*. *Pest Manag. Sci.* 73, 953–959. doi: 10.1002/ps.4370
- Min, L. J., Shi, Y. X., Wu, H. K., Sun, Z. H., Liu, X. H., Li, B. J., et al. (2016). Microwave-assisted synthesis and antifungal activity of some novel thioethers containing 1,2,4-triazole moiety. *Appl. Sci.* 5, 1211–1220. doi: 10.3390/app5041211
- Shen, Z. H., Sun, Z. H., Becnel, J. J., Estep, A., David, D. E., Tan, C. X., et al. (2018). Synthesis and mosquitocidal activity of novel hydrazone containing pyrimidine derivatives against *aedes aegypti*. *Lett. Drug Des. Discov.* 15, 951–956. doi: 10.2174/1570180815666180102141640
- Shi, J. J., Ren, G. H., Wu, N. J., Weng, J. Q., Xu, T. M., Liu, X. H., et al. (2017). Design, synthesis and insecticidal activities of novel anthranilic diamides containing polyfluoroalkyl pyrazole moiety. *Chinese Chem. Lett.* 28, 1727–1730. doi: 10.1016/j.cclet.2017.05.015
- Strange, R. N., and Scott, P. R. (2005). Plant disease: a threat to global food security. *Annu. Rev. Phytopathol.* 43, 83–116. doi: 10.1146/annurev.phyto.43.113004.133839
- Triloknadh, S., Rao, C. V., Nagaraju, K., Krishna, N. H., Ramaiahb, C. V., Rajendra, W., et al. (2018). Design, synthesis, neuroprotective, antibacterial activities and docking studies of novel thieno[2,3-d]pyrimidine-alkyne Mannich base and oxadiazole hybrids. *Bioorg. Med. Chem. Lett.* 28, 1663–1669. doi: 10.1016/j.bmcl.2018.03.030
- Wang, B., Zhu, H., Li, Z., Zhang, X., Yu, S., Ma, Y., et al. (2019). One-pot synthesis, structure and structure-activity relationship of novel bioactive diphenyl/diethyl (3-bromo-1-(3-chloropyridin-2-yl)-1 H-pyrazol-5-yl)(arylamino)methylphosphonates. *Pest Manag. Sci.* 75, 3273–3281. doi: 10.1002/ps.5449
- Wang, B. L., Zhu, H. W., Li, Z. M., Wang, L. Z., Zhang, X., Xiong, L. X., et al. (2018). Synthesis, biological evaluation and SAR analysis of novel poly-heterocyclic compounds containing pyridylpyrazole group. *Pest Manag. Sci.* 74, 726–736. doi: 10.1002/ps.4770
- Wang, B. L., Zhu, H. W., Ma, Y., Xiong, L. X., Li, Y. Q., Zhao, Y., et al. (2013). Synthesis, insecticidal activities, and SAR studies of novel pyridylpyrazole acid derivatives based on amide bridge modification of anthranilic diamide insecticides. *J. Agric. Food Chem.* 61, 5483–5493. doi: 10.1021/jf4012467
- Wang, Y. Y., Xu, F. Z., Zhu, Y. Y., Song, B. A., Liu, D. X., Yu, G., et al. (2018). Pyrazolo[3,4-d]pyrimidine derivatives containing a schiff base moiety as potential antiviral agents. *Bioorg. Med. Chem. Lett.* 28, 2979–2984. doi: 10.1016/j.bmcl.2018.06.049
- Wu, W. N., Chen, M. H., Wang, R., Tu, H. T., Yang, M. F., and Ouyang, G. P. (2019a). Novel pyrimidine derivatives containing an amide moiety: design, synthesis, and antifungal activity. *Chem. Pap.* 73, 719–729. doi: 10.1007/s11696-018-0583-7
- Wu, W. N., Chen, Q., Tai, A. Q., Jiang, G. Q., and Ouyang, G. P. (2015). Synthesis and antiviral activity of 2-substituted methythio-5-(4-amino-2-methylpyrimidin-5-yl)-1,3,4-oxadiazole derivatives. *Bioorg. Med. Chem. Lett.* 25, 2243–2246. doi: 10.1016/j.bmcl.2015.02.069
- Wu, W. N., Gao, M. N., Tu, H., and Ouyang, G. P. (2016a). Synthesis and antibacterial of novel Substituted purine derivatives. *J. Heterocyclic Chem.* 53, 2042–2048. doi: 10.1002/jhet.2527
- Wu, W. N., Jiang, Y. M., Fei, Q., and Du, H. T. (2019b). Synthesis and fungicidal activity of novel 1,2,4-triazole derivatives containing a pyrimidine moiety. *Phosphorus Sulfur* 194, 1171–1175. doi: 10.1080/10426507.2019.1633321
- Wu, W. N., Tai, A. Q., Chen, Q., and Ouyang, G. P. (2016b). Synthesis and antiviral bioactivity of novel 2-substituted methythio-5-(4-amino-2-methylpyrimidin-5-yl)-1,3,4-thiadiazole derivatives. *J. Heterocyclic Chem.* 53, 626–632. doi: 10.1002/jhet.2435
- Xu, X. J., Wang, J., and Yao, Q. Z. (2015). Synthesis and quantitative structure-activity relationship(QSAR) analysis of some novel oxadiazolo[3,4-d]pyrimidine nucleosides derivatives as antiviral agents. *Bioorg. Med. Chem. Lett.* 25, 241–244. doi: 10.1016/j.bmcl.2014.11.065
- Yan, T., Yu, S., Liu, P., Liu, Z., Wang, B., Xiong, L., et al. (2012). Design, synthesis and biological activities of novel benzoyl hydrazines containing pyrazole. *Chin. J. Chem.* 30, 919–923. doi: 10.1002/cjoc.201100347
- Yang, R., Gao, Z. F., Zhao, J. Y., Li, W. B., Zhou, L., and Miao, F. (2015). New class of 2-aryl-6-chloro-3,4-dihydro-isoquinolinium salts as potential antifungal agents for plant protection: synthesis, bioactivity and structure-activity relationships. *J. Agric. Food Chem.* 63, 1906–1914. doi: 10.1021/jf505609z
- Zhang, J., Peng, J. F., Bai, Y. B., Wang, P., Wang, T., Gao, J. M., et al. (2016). Synthesis of pyrazolo[1,5-a]pyrimidine derivatives and their antifungal activities against phytopathogenic fungi *in vitro*. *Mol. Divers.* 20, 887–896. doi: 10.1007/s11030-016-9690-y

Conflict of Interest: The authors declare that the research was conducted in the absence of any commercial or financial relationships that could be construed as a potential conflict of interest.

The handling editor declared a shared affiliation, though no other collaboration, with the authors YZ, MY, and GO.

Copyright © 2020 Wu, Chen, Fei, Ge, Zhu, Chen, Yang and Ouyang. This is an open-access article distributed under the terms of the Creative Commons Attribution License (CC BY). The use, distribution or reproduction in other forums is permitted, provided the original author(s) and the copyright owner(s) are credited and that the original publication in this journal is cited, in accordance with accepted academic practice. No use, distribution or reproduction is permitted which does not comply with these terms.



Evaluation of General Synthesis Procedures for Bioflavonoid–Metal Complexes in Air-Saturated Alkaline Solutions

Yuanyong Yao*, Meng Zhang, Laibing He, Yunyang Wang and Shixue Chen*

Tongren Key Laboratory for Modernization Research, Development and Utilization of Traditional Chinese Medicine and National Medicine, School of Material and Chemical Engineering, Tongren University, Tongren, China

OPEN ACCESS

Edited by:

Hu Li,
Guizhou University, China

Reviewed by:

Zhichao Jin,
Guizhou University, China

Ping Zhu,
Technical University of
Denmark, Denmark

Hu Pan,
Jiaxing University, China

*Correspondence:

Yuanyong Yao
chyuyy@gztrc.edu.cn
Shixue Chen
tongrencsx01@126.com

Specialty section:

This article was submitted to
Organic Chemistry,
a section of the journal
Frontiers in Chemistry

Received: 15 April 2020

Accepted: 08 June 2020

Published: 05 August 2020

Citation:

Yao Y, Zhang M, He L, Wang Y and
Chen S (2020) Evaluation of General
Synthesis Procedures for
Bioflavonoid–Metal Complexes in
Air-Saturated Alkaline Solutions.
Front. Chem. 8:589.
doi: 10.3389/fchem.2020.00589

The general synthesis methods of bioflavonoid–metal complexes are considered to be unreliable due to the instability of flavonoids in air-saturated alkaline solutions. In this study, dihydromyricetin (DHM), as a representative bioflavonoid, was selected for complexation with various transition metal ions in an air-saturated alkaline solution to form DHM–metal(II) complexes, following the general synthetic procedure. After characterization, the metal complexes were hydrolyzed to observe the stability of DHM under acidic conditions via HPLC. The effects of synthetic conditions (metal ion, alkalinity, and reflux time) on DHM stability were then investigated by UV-vis spectroscopy and HPLC. Finally, using electron paramagnetic resonance, DHM and its analogs were observed with DMPO (5,5-dimethyl-1-pyrroline-N-oxide) to form a relatively stable free radical adduct. Multiple peaks corresponding to unknown compounds appeared in the LC spectra of the DHM–metal(II) complexes after hydrolysis, indicating that some DHM reacted during synthesis. Subsequently, the transition metal ion and solution alkalinity were found to have notable effects on the stability of free DHM. Furthermore, DHM and several of its analogs generated the superoxide-anion radical in air-saturated alkaline solutions. Their capacities for generating the superoxide anion seemed to correspond to the number and/or location of hydroxyl groups or their configurations. Interestingly, DHM can react with the superoxide anion to transform into myricetin, which involves the abstraction of a C3–H atom from DHM by O_2^- . Therefore, the general synthetic procedure for bioflavonoid–metal complexes in air-saturated alkaline solutions should be improved.

Keywords: dihydromyricetin, flavonoids, bioflavonoid–metal complexes, alkaline conditions, superoxide anion, HPLC, UV-visible spectrophotometer, transition metal ions

INTRODUCTION

Bioflavonoids are naturally occurring phenolic substances that can be isolated from a wide range of vascular plants, with more than 8,000 individual compounds currently identified. They have been widely used as potent bioactive agents in biological and pharmaceutical fields (Raffa et al., 2017; Spagnuolo et al., 2018; Dai et al., 2019). Recently, numerous studies have revealed that bioflavonoids with novel inherent molecular skeletons [e.g., dihydromyricetin, dihydroquercetin, myricetin, quercetin, kaempferol, and so on (Figure 1)] show valuable biological activities, including anticancer (Raffa et al., 2017; Madunić et al., 2018; Imran et al., 2019), antiviral (Lani et al., 2016; Dai et al., 2019; Lalani and Poh, 2020), anti-inflammatory (Zhang and Tsao, 2016;

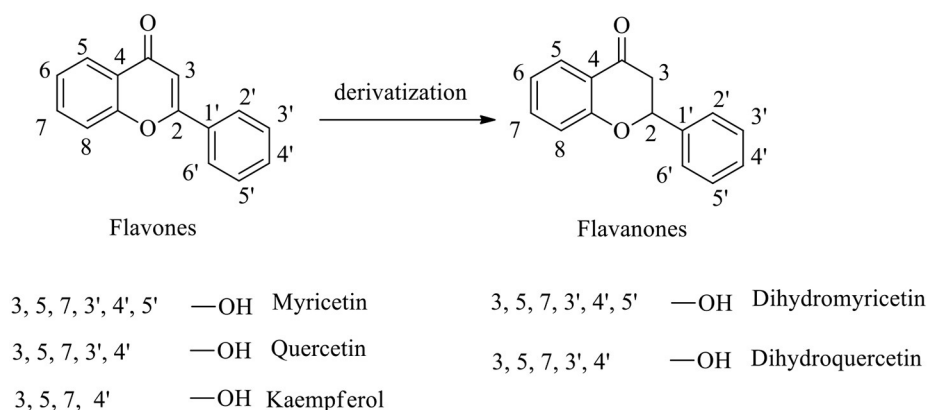


FIGURE 1 | Molecular structures of flavones, flavanones, and their derivatives.

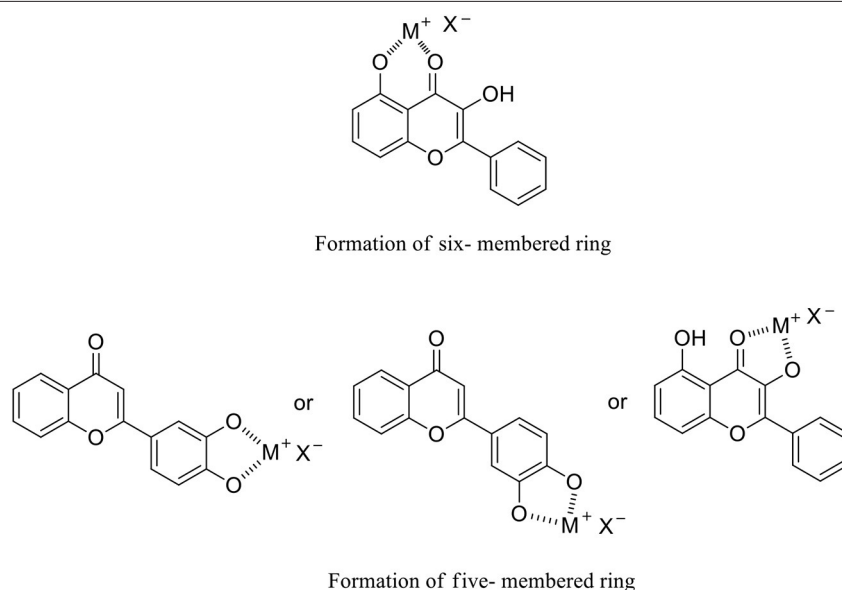


FIGURE 2 | Flavanone-metal complexes via the formation of five- and/or six-membered rings.

Chen et al., 2017; Spagnuolo et al., 2018), and other effects (Amirhossein and Shadboorestan, 2016; Liang et al., 2019).

To further improve bioflavonoids in terms of their bioactivities, metal complexes with bioflavonoids as ligands to chelate transition metal ions have gained significant scientific interest (Thangavel et al., 2018; Gençkal et al., 2020; Silva et al., 2020; Wu et al., 2020). These complexes form five- and/or six-membered rings through the interaction of the metal ion with the hydroxyl moiety and/or single carbonyl group on the bioflavonoid skeleton (Figure 2). Therefore, approaches to synthesizing bioflavonoid-metal complexes with novel structures are highly desirable.

For instance, metal(II) complexes with quercetin (Gençkal et al., 2020; Silva et al., 2020), hesperitin (Tamayo et al., 2016), kaempferol (Tu et al., 2016; Thangavel et al., 2018), myricetin (Uivarosi et al., 2019), and dihydromyricetin (Li

et al., 2016; Wu et al., 2020) as representative examples have been synthesized by following a general synthetic procedure for bioflavonoid-metal complexes (Tu et al., 2016; Maitera et al., 2018; Thangavel et al., 2018; Khater et al., 2019; Gençkal et al., 2020). The general procedure involves the deprotonation of the phenolic hydroxyl group(s) of the bioflavonoid into the corresponding phenolate, which then chelates the metal ion in an air-saturated alkaline solution. These metal complexes have been characterized by FT-IR and UV-vis spectroscopy, elemental analysis, X-ray analyses, and so on. Furthermore, their potential bioactivities have been observed as somewhat higher than that of the corresponding original bioflavonoids in terms of antioxidant capacity (Samsonowicz et al., 2017; Khater et al., 2019), anticancer effects (Qian et al., 2015; Khater et al., 2019), and superoxide anion/hydroxyl free radical scavenging (Jabeen et al., 2017).

In our previous work on bioflavonoid stabilization, we found via UV-vis spectroscopy that most bioflavonoids are unstable in air-saturated alkaline solutions, which prompted us to reevaluate the general synthetic procedure for bioflavonoid-metal complexes. To address this, in this study, dihydromyricetin (DHM) was selected as a representative bioflavonoid to prepare DHM-M(II) complexes using the general procedure. Subsequently, the metal complexes were identified by FT-IR and UV-vis spectroscopy, elemental analysis, and evaluation of antioxidant capacity. Finally, the DHM-M(II) complexes were hydrolyzed to observe any changes in their molecular structures under acidic conditions by means of high-performance liquid chromatography (HPLC). The results indicated that the air-saturated alkaline solution used in the general synthetic procedure is not suitable for the synthesis of bioflavonoid-metal complexes. Moreover, to determine the probable causes of the observed issue with the general synthetic procedure, the synthetic conditions (e.g., metal ion, alkalinity, and reflux time) affecting DHM stabilization were discussed.

EXPERIMENTAL SECTION

Materials and Synthesis

All of the reagents are analytical grade or chromatographically pure, and were purchased from commercial sources. All solutions were prepared using double-distilled water. Dihydromyricetin (DHM) was extracted by our laboratory from tender stems and leaves of *Ampelopsis grossedentata* with more than 95% purity. Standard DHM was purchased from Aladdin Reagent, Shanghai (China). Metal ion reagents (copper, zinc, iron, nickel, and cobalt acetates) were also bought from Aladdin Reagent, Shanghai (China). Organic solvents were obtained from Kemiou reagent, Tianjin (China).

General DHM-M(II) Synthetic Procedure

According to the literature (Tu et al., 2016; Maitera et al., 2018; Thangavel et al., 2018; Khater et al., 2019; Gençkal et al., 2020), the general synthetic procedure for DHM-M(II) complexes is as follows: solid DHM (0.5820 g, 1.82 mmol) was dissolved completely in ethanol (5 mL, 95%, W/W). Then, the mixture was transferred to 50 mL of an alkaline solution (sodium acetate dissolved in a water-ethanol solution (50%, v/v) at pH = 8.2) under stirring for 5 min. Afterward, metal ion reagents (2 mmol) (copper, zinc, iron, nickel, and cobalt acetates) were separately dissolved in ethanol (5 mL, 95%, W/W) and added to the above mixture under reflux for 120 min. The reaction mixture was cooled to room temperature, precipitated, and filtered, and the resulting solid was washed three times with EtOH and double-distilled water in turn. Subsequently, after re-crystallization in acetone, the solid product was dried under vacuum for 48 h at -20°C to afford the DHM-M(II) complexes.

INSTRUMENTATION

EPR spectra were recorded at room temperature, utilizing a Bruker A300 spectrometer for detection of superoxide anion using a center magnetic field at 3500.00 G, sweep width at

150.00 G, microwave power at 3.99 mW, modulation amplitude at 1.000 G, with scanning field and switching time operating for 30 s and 40 ms, respectively. The UV-vis spectra were measured on a UV-759S UV-visible spectrophotometer (Jingke, China). The IR spectroscopies were recorded as KBr pellets on an IR Affinity-1S infrared spectrometer in the frequency range $400\text{--}4,000\text{ cm}^{-1}$. The HPLC was recorded on a LC-20AT spectrometer, equipped with a DAD detector (Shimadzu, Japan). The NMR spectra were recorded on a JEOL-ECX 500 instrument (500 MHz for ^1H , 125 MHz for ^{13}C) using DMSO- d_6 as the solvent. Tetramethylsilane ($\delta = 0$) and DMSO- d_6 ($\delta = 40.1$) served as internal standards for ^1H NMR and ^{13}C NMR spectral experiments, respectively. The mass spectral analysis was performed on Waters XevoTQ-XS Ms Apparatus. The element analysis (Flash Smart, Thermo Fisher, Germany) was used to identify compound composition.

Evaluation of Antioxidant Activity by Pyrogallol Autoxidation

Control Group

Na_2EDTA (1 mM) was added to a Tris-HCl buffer (0.05 M, pH = 8.2, 2.90 mL) solution, followed by the addition of 100 μL of a pyrogallol solution (6 mg in 1 mM HCl). After shaking vigorously for 30 min at room temperature, the resulting mixture was measured by UV-vis spectrophotometer from 200 to 800 nm. The resulting spectra were regarded as the control group.

Testing Group

Samples of the DHM-M(II) complexes were prepared at 0.01 mg/mL in DMSO, and free DHM as a positive control was prepared at 0.01 mg/mL in ethanol. Then, 100 μL of each sample was transferred to the above control group sample and shaken vigorously for 1 min. The reaction mixture was then prepared and measured according to the same procedure as for the control group.

$$\frac{\frac{\Delta A_{325\text{nm},\text{control}}}{T} - \frac{\Delta A_{325\text{nm},\text{sample}}}{T}}{\frac{\Delta A_{325\text{nm},\text{control}}}{T}} \times 100\%$$

$\Delta A_{325\text{nm},\text{control}}$: absorbance of control group at 325 nm

$\Delta A_{325\text{nm},\text{sample}}$: absorbance of testing group at 325 nm

T: 25°C .

Hydrolyzing DHM-M(II) Complexes Under Acidic Conditions for HPLC Analysis

The DHM-M(II) complexes (0.9050 g) were each added to an acidic solution (20 mL, 1 mL HCl in 100 mL of ethanol, pH = 2) and stirred for 3 h at 50°C under a nitrogen atmosphere. Afterward, the reaction mixtures were moderated to pH = 5–6 by 0.1% aqueous NaOH. After filtering and evaporation, the residues were dissolved in chromatographic methanol and subjected to HPLC analysis.

Chromatographic Conditions

Hypersil BDS C18 (4.6*200 mm, 5 μ m), Elute: (Acetonitrile / Water (0.1 % phosphoric acid) = 24 / 76), Flow rate = 1 ml/min, UV = 254 nm.

Assessment of Conditions Affecting the Stability of Free DHM

Reflux Time

Solid DHM was dissolved in a water–ethanol solution (50%, v/v) at a concentration of 0.05 mg/mL, and 10 mL was refluxed for different periods. After cooling to room temperature, all samples were subjected to UV-vis analysis.

Metal Ion (Ni^{2+} , Zn^{2+} , Cu^{2+} , Co^{2+} , Fe^{2+})

A solution (10 mL) of 0.05 mg/mL DHM in water–ethanol (50%, v/v) was combined with each of the metal ion reagents (0.0016 mmol, 0.5 mL in water–ethanol solution) under stirring for 120 min at 25°C. The reaction mixtures were then measured by UV-vis spectroscopy.

Alkalinity

A 1.0 mg/mL solution of DHM (0.5 mL) was added to 10 mL of a sodium acetate solution (pH = 8.2) under stirring for 1, 3, 5, 10, 20, and 30 min at room temperature. Afterward, the reaction mixtures were subjected to UV-vis analysis.

Alkalinity Investigated Quantitatively by HPLC

Solutions at pH = 7.4, 8.2, and 9.4 were prepared by dissolving sodium acetate/acetic acid in water–ethanol (50%, v/v). Of a 0.8 mg/mL DHM solution, 1 mL was added to 10 mL of each alkaline solution with stirring for several minutes at room temperature. The resulting mixtures were moderated to weak acidity (approximately pH = 6) with 0.1% HCl. The control group was prepared in the same manner without the alkaline solution. After evaporating the solvent under vacuum, the test and control groups were dissolved in 1 mL of methanol and filtered (0.45 μ m). Finally, the samples were subjected to HPLC for quantitative analysis.

Chromatographic conditions: Hypersil BDS C18 (4.6*200 mm, 5 μ m), Elute: (Acetonitrile / Water (0.1 % phosphoric acid) = 24 / 76), Flow rate = 1 ml/min, UV = 254 nm.

Separation and Purification of Myricetin (MYR) as an Oxidized Product of DHM in Air-Saturated Alkaline Solution (pH = 8.2)

A 100 mg/mL DHM solution was prepared, to which 3–20 mL of an alkaline solution (pH = 8.2) was added, and the reaction mixture was stirred continuously. After 2 h, the mixture was quenched with 0.1% HCl to pH = 5–6. After evaporating the solvent under vacuum, the residue was dissolved in ethanol and dried over MgSO_4 . Subsequently, after filtering and evaporation of the solvent under vacuum, the solution was evaporated to dryness. The residue was separated and purified by column chromatography on silica gel (EtOAc /petroleum ether from 1/25 to 1/3) to afford product **A** (50.2 mg) as a yellow solid. ^1H -NMR (500 MHz, $\text{DMSO}-d_6$, 25°C, TMS): δ (ppm) 12.51 (s, 1H), 10.82 (s, 1H), 9.36 (s, 1H), 9.25 (s, 2H), 8.83 (s, 1H), 7.25 (s, 2H), 6.38 (s,

1H), 6.19 (s, 1H); ^{13}C -NMR (125 MHz, $\text{DMSO}-d_6$, 25°C, TMS): δ (ppm) 176.21, 164.31, 161.17, 156.52, 147.27, 146.16, 136.31, 121.23, 107.60, 103.42, 98.61, 93.66. Anal. Calcd for $\text{C}_{15}\text{H}_{10}\text{O}_8$: C, 56.61; H, 3.17; O, 40.22; Found: C, 56.45; H, 3.24. ESI-MS m/z (CH_3OH): 318.04; Found: 358 $[\text{M}+\text{H}+\text{K}]^+$.

A solution of product **A** at 1.0 mg/mL was prepared and subjected to HPLC analysis. **Chromatographic conditions:** Hypersil BDS C18 (4.6*200 mm, 5 μ m), Elute: (Acetonitrile / Water (0.1% phosphoric acid) = 24 / 76), Flow rate = 1 ml/min, UV = 254 nm.

Superoxide Anion From DHM in Air-Saturated Alkaline Solution

Using an air supplier, air, nitrogen, and oxygen were continuously forced into separate alkaline solutions (pH = 8.2) for 10 min. DHM was dissolved in methanol to 0.20 mg/mL, and 100 μL was added to 1 mL of each of the air-, oxygen-, and nitrogen-saturated alkaline solutions with continuous stirring for 1 min. To 100 μL of those solutions, 5,5-dimethyl-1-pyrroline-N-oxide (DMPO) (100 mg/L in methanol, 10 μL) was added, and the resulting mixtures were transferred into silica tubes and subjected to EPR analysis.

Superoxide Anions Generated by the DMSO System

Dry DMSO (1 mL) was transferred to a test tube (5 mL), and oxygen was introduced to the system for 10 min at room temperature using an air supplier. Sodium phenolate (100 mmol/L, 100 μL) was immediately added to the system and stirred slowly for 30 min at 37°C under an oxygen atmosphere. DMPO (100 mg/L in methanol, 10 μL) was added to 100 μL of this solution, and the resulting mixture was transferred into a silica tube and subjected to EPR analysis.

Transformation of DHM Into MYR by Superoxide-Anion Radicals

To the above described DMSO system, a DHM solution (1.0 mg/mL in dry DMSO) was added with shaking for ~5 min. When the solution changed from colorless to yellow, it was quenched with saturated aqueous NH_4Cl . After filtering (0.45 μm), the solution was subjected to HPLC analysis using the above chromatographic conditions.

DHM Analogs Autoxidized in Air-Saturated Alkaline Solution and Observed by EPR

Following the above conditions for the DHM generation of superoxide anions, DHM analogs (MYR, quercetin, daidzein, genistein, chrysin, baicalein, rutin hydrate, and kaempferol) were each prepared at the same concentration (2.0 mg/mL). The solutions were transferred to an air-saturated alkaline solution (1 mL, pH = 8.2) with continuous stirring for 1 min. To 100 μL of these solutions DMPO (100 mg/L in methanol, 10 μL) was added. The resulting mixtures were transferred to silica tubes and subjected to EPR analysis.

RESULTS AND DISCUSSION

Antioxidant Activity of DHM-M(II) Complexes

By following the reported general synthetic procedure (Tu et al., 2016; Maitera et al., 2018; Thangavel et al., 2018; Khater et al., 2019; Gençkal et al., 2020), the DHM-M(II) complexes DHM-Co(II), DHM-Cu(II), DHM-Fe(II), DHM-Zn(II), and DHM-Ni(II) were obtained. The metal complexes were characterized by FT-IR, elemental analysis, UV-vis, and antioxidant capacity. The IR absorption frequency of the functional groups attached to the DHM-M(II) complexes were red-shifted compared with those of free DHM, indicating the complexation of DHM with metal ions (Supplementary Figure 1 and Supplementary Table 1). Elemental analysis demonstrated that the DHM-metal(II) complexes had the expected compositions (Supplementary Table 2). The UV-vis spectra showed red-shifts and changes in intensity of the absorption of the complexes, further evidencing the complexation of DHM with the metal ions under the selected experimental conditions (Supplementary Figure 2). Finally, the antioxidant activities of the DHM-M(II) complexes were confirmed as higher than that of DHM at the same concentration (Supplementary Figure 3 and Supplementary Table 3). Therefore, it is reasonable to assume that the prepared DHM-M(II) complexes are consistent with those in previous studies.

Hydrolysis of DHM-M(II) Complexes

To further understand whether DHM changes during complexation, DHM and its metal complexes were hydrolyzed under the same acidic conditions. After stirring for 3 h at 50°C, the resulting mixtures were subjected to HPLC with a monitoring wavelength of 254 nm. In the LC spectra, we found that free DHM stirred in an acidic solution was stable, without any impurity peaks. However, in the spectra of the DHM-M(II) complexes, many unknown absorption peaks with different intensities appeared (Supplementary Figure 4). This caused us

to question the general synthetic procedure for bioflavonoid-metal complexes. Subsequently, to address this, the synthetic conditions of the metal ion, alkalinity, and reflux time were investigated by UV-vis or HPLC to observe their influence on the stability of free DHM.

Effect of Synthesis Conditions on Stability of Free DHM

Reflux time was first investigated by refluxing free DHM for different times in a water-ethanol solution (v/v, 50%) followed by observation by UV-vis spectroscopy. In the resulting spectra, no notable shift in the DHM absorption peak at 325 nm was observed after refluxing for several minutes compared with free DHM without any workup (Figure 3). This indicated that reflux time does not significantly affect the stability of free DHM in an aqueous solution in the absence of alkalinity or metal ions. Therefore, we did not consider reflux time to be a crucial factor affecting the synthesis of the DHM-metal complexes.

To the best of our knowledge, bioflavonoids are generally weakly acidic in ethanol or aqueous solutions, relying on their phenolic hydroxyl moieties to ionize in the liquid phase. In the general synthetic procedure for bioflavonoid-metal complexes, alkalinity promotes the deprotonation of the bioflavonoid phenolic hydroxyl groups to form the corresponding phenolate. Since phenolates can easily donate a pair of electrons, they are better ligands to chelate with metal ions. Thus, alkalinity seems to be a dominant factor in synthesizing DHM-M(II) complexes. A pH of 8.2 for the reaction solution was selected to investigate the influence of alkalinity on free DHM by UV-vis spectroscopy. With longer stirring times at room temperature, the absorbance at 290 nm shifted to 325 nm and increased in intensity (Figure 4), implying that dissolving DHM in an air-saturated alkaline solution decreased the amount of DHM over time. Therefore, the effect of alkalinity on DHM stabilization required further investigation.

HPLC as a quantitative and qualitative analysis method was first utilized to investigate the effect of alkalinity on

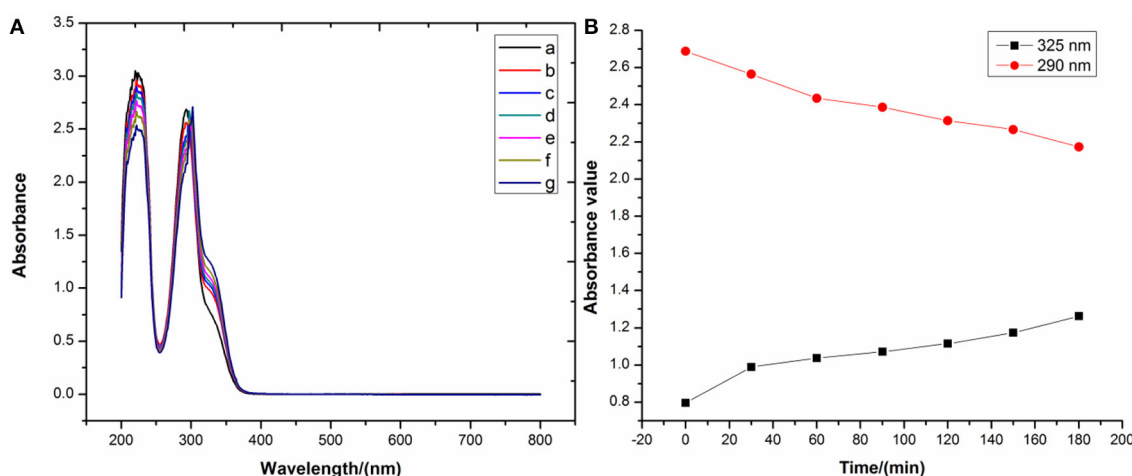
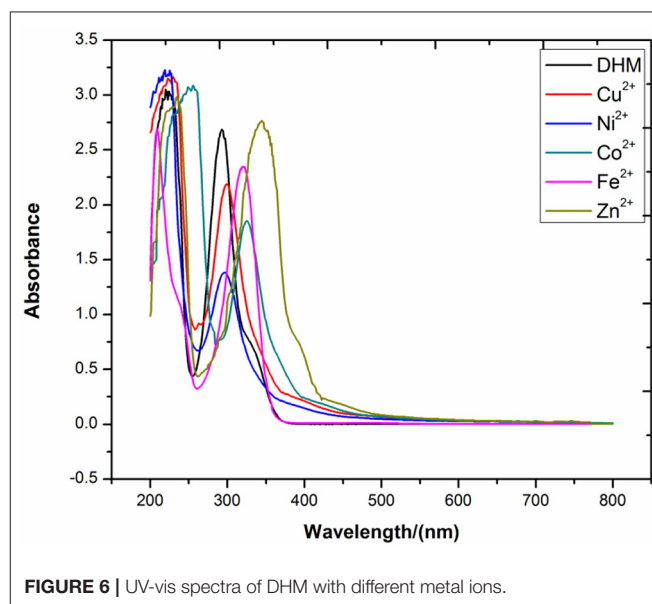
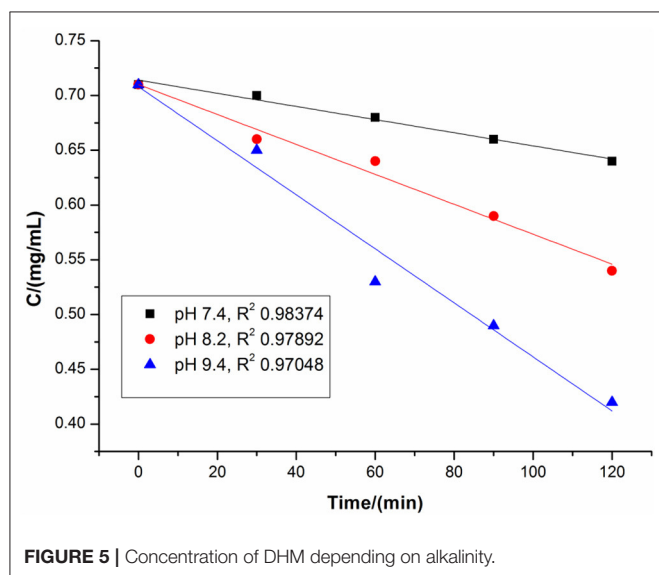
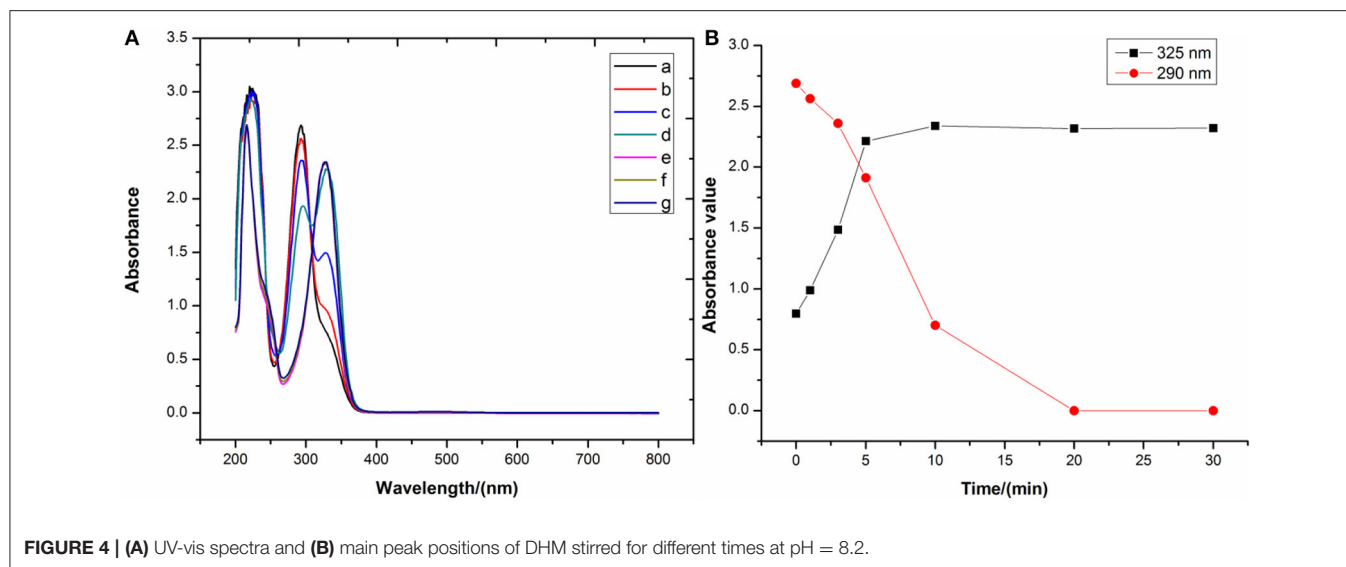


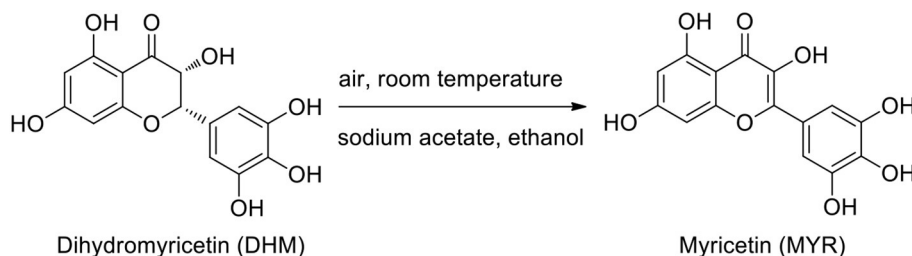
FIGURE 3 | (A) UV-vis spectra and (B) main peak positions of DHM refluxed for different times.



free DHM stabilization (Supplementary Figures 5–8 and Supplementary Tables 4–6). As shown in Figure 5, the air-saturated alkaline solution was adjusted to a pH of 7.4 by sodium acetate/acetic acid, and free DHM was stirred for different times in the solution at room temperature. The resulting mixtures were quenched with 0.1% HCl to approximately pH = 6 and subjected to HPLC. We found that the concentration of DHM decreased from 0.71 to 0.64 mg/mL after stirring for 120 min. When the solution pH was moderated to 8.2, the DHM concentration decreased more than at pH = 7.4; similarly, the concentration decrease was the most severe for pH = 9.4. This confirmed the alkalinity as a significant factor in the synthesis of the DHM–M(II) complexes.

The metal ion is an important participant in the synthesis of the DHM–M(II) complexes as it supplies empty orbitals

for complexation with the ligand. Importantly, most transition metal ions in an electron-loss state are electronegative and are thus generally considered to be oxidants. In addition, bioflavonoids are electron-rich and thus easily lose electrons after deprotonation of their phenolic hydroxyl moieties. The presence of electronegative metal ions with the phenolates derived from deprotonated bioflavonoids can initiate a redox reaction. Therefore, the effect of metal ions with different electronegativities on DHM stabilization deserves further consideration. DHM was stirred for 2 h in the presence of the different metal ions without alkalinity at room temperature, and the resulting mixtures were subjected to UV-vis analysis. As shown in Figure 6, the intensity and position of the DHM absorption peak were affected by the metal ion. With Zn²⁺,



SCHEME 1 | Transformation of DHM into MYR in an alkaline solution.

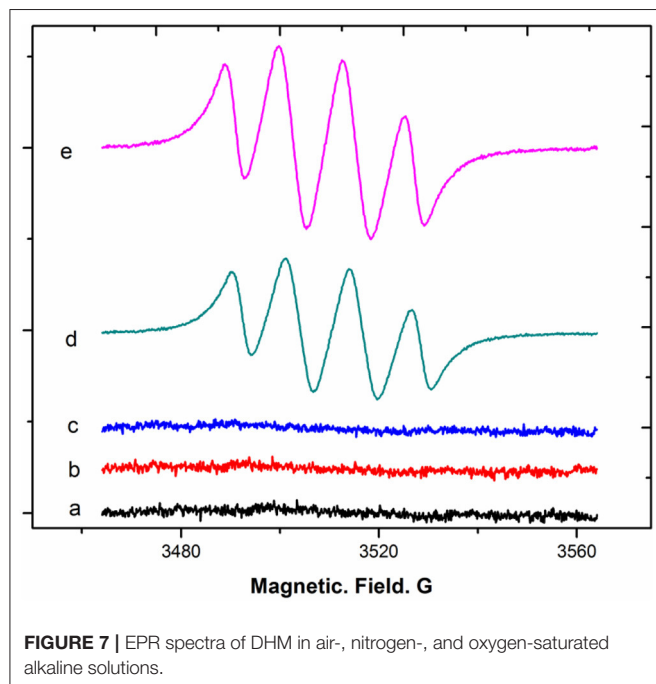


FIGURE 7 | EPR spectra of DHM in air-, nitrogen-, and oxygen-saturated alkaline solutions.

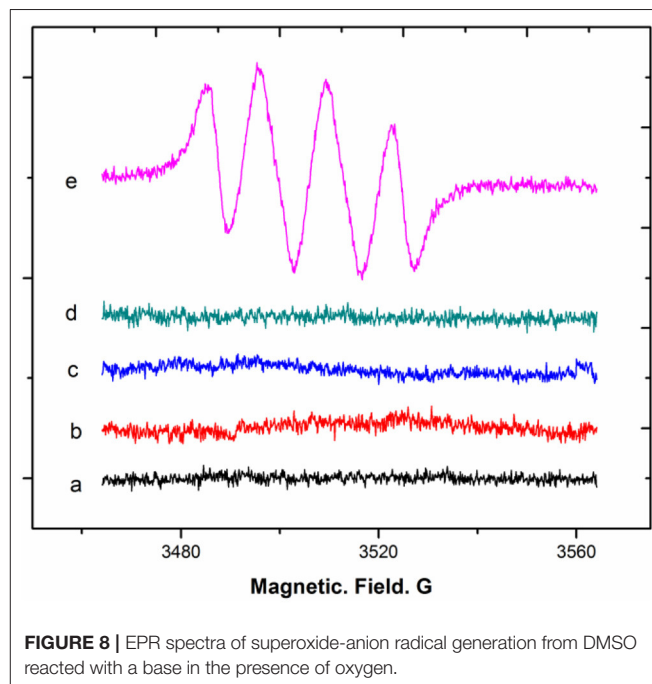


FIGURE 8 | EPR spectra of superoxide-anion radical generation from DMSO reacted with a base in the presence of oxygen.

the DHM peak red-shifted from 290 to 345 nm, indicating the effective complexation of Zn^{2+} with free DHM. In contrast, Ni^{2+} , Cu^{2+} , Co^{2+} , and Fe^{2+} not only red-shifted the peak at 290 nm to different extents but also changed the intensity, suggesting that the redox of free DHM also occurred. These results showed that the metal ions affect the DHM stability according to their electronegativity in the order of $\text{Ni}^{2+} > \text{Co}^{2+} > \text{Cu}^{2+} > \text{Fe}^{2+} > \text{Zn}^{2+}$. Therefore, the metal ion is a dominant factor affecting the stability of DHM in DHM-M(II) complexes.

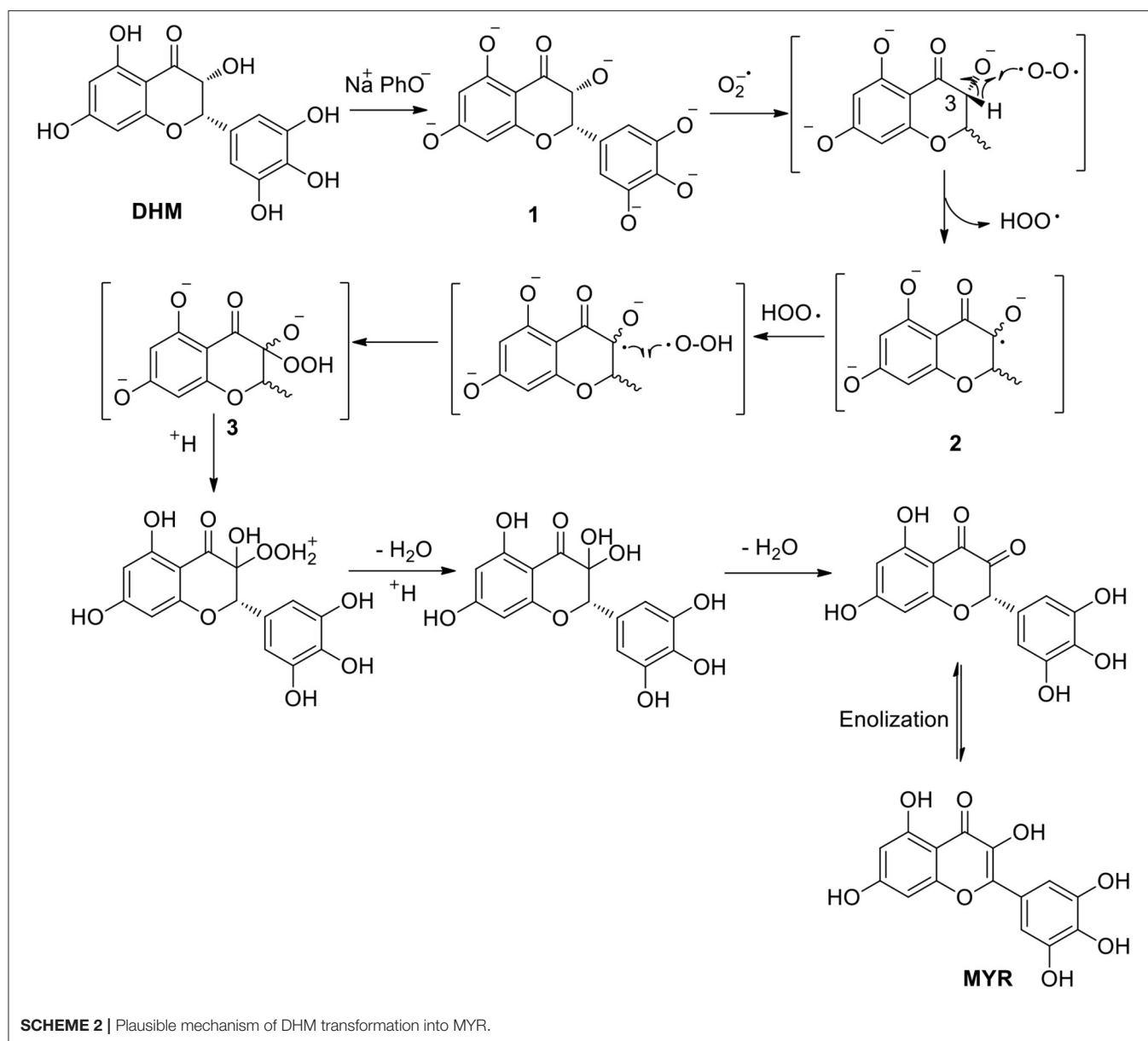
In summary, synthesizing bioflavonoid-metal complexes in air-saturated alkaline solutions is rational in theory. However, in reality, both the alkalinity and metal ions as important participants in the synthesis of DHM-M(II) complexes were shown to be probable reasons for the lack of stability.

Transformation of DHM Into MYR in the Presence of Superoxide-Anion Radical

Based on the above results regarding the synthetic factors affecting DHM stabilization, it was notable that alkalinity is likely

the main factor for the general synthesis of bioflavonoid-metal complexes. In the general synthetic procedure, free DHM was first stirred for different times in an air-saturated alkaline solution ($\text{pH} = 8.2$) for deprotonation into the corresponding phenolate, and the resulting solution was subjected to HPLC. The intensity of the absorption peak ($t = 15.7$ min) at 254 nm increased with stirring time (**Supplementary Figure 7**). Subsequently, the absorption peak was separated by column chromatography with an eluent of P/E (from 25/1 to 3/1) and identified by ^1H - and ^{13}C -NMR, ESI-MS, elemental analysis, and HPLC (**Supplementary Figures 9, 10**). Interestingly, the component was found to be MYR. As far as we know, MYR is the oxidized product of DHM. Thus, the transformation of DHM into MYR in an air-oxidized alkaline solution required further consideration (**Scheme 1**).

For the transformation of DHM into MYR, DHM after deprotonation by a base forms its electron-rich phenolate, which undergoes a redox reaction upon exposure to an oxidant. We noted that oxygen molecules from the air can dissolve into the

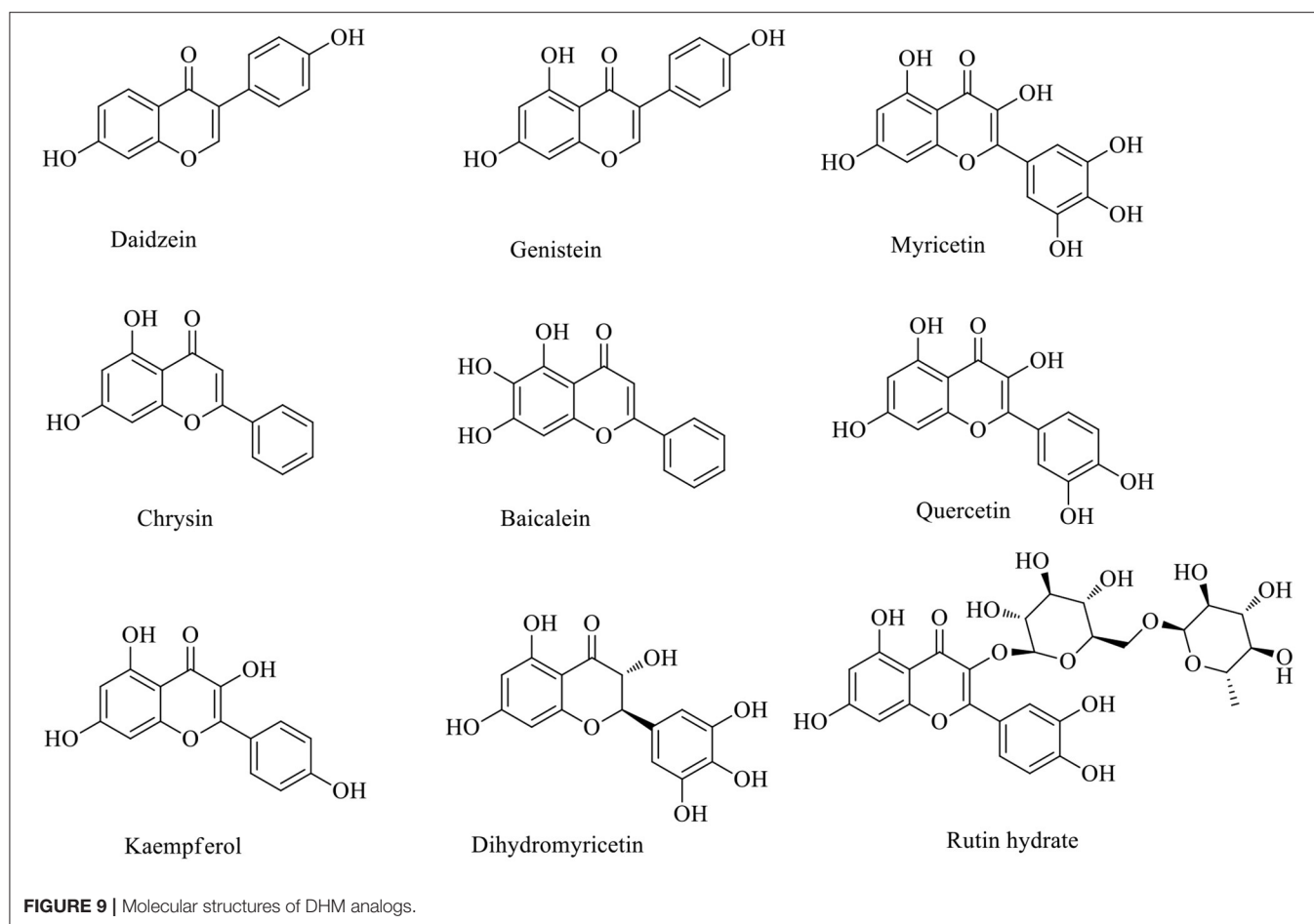


alkaline solution. The collision of diatomic oxygen with the phenolate can promote the univalent reduction (single electron transfer) of diatomic oxygen, resulting in one filled and one half-filled antibonding π^*2p molecular orbitals. This ultimately forms a radical. To validate our proposition, electron paramagnetic resonance (EPR) was applied to observe the radicals generated from DHM dissolved in an air-saturated alkaline (pH = 8.2) solution with DMPO as a spin-trapping electron reagent. DHM dissolved in oxygen- and nitrogen-saturated alkaline solutions at the same pH was also observed for comparison. The EPR results demonstrated that the intensity of the typical signals of the superoxide anion adduct (DMPO-OO $^-$) of DHM in an air-saturated alkaline solution was less than that of the oxygen-saturated alkaline solution, with an overlapping “doublet of a doublet” arising from hyperfine interactions with ^{14}N (Liu et al.,

1996). When DHM was dissolved in a nitrogen-saturated alkaline solution, no typical adduct signals were observed (**Figure 7**). Thus, DHM dissolved in an alkaline solution in the presence of oxygen molecules generates superoxide-anion radicals (O_2^-) via univalent reduction.

Next, whether the transformation of DHM into MYR in an air-saturated alkaline solution is associated with O_2^- generation was considered. A system of dry DMSO reacted with sodium phenolate in the presence of oxygen molecules to generate O_2^- was selected according to a previous report (Branchini et al., 2015). The DMSO system was analyzed by EPR with the aid of DMPO. The typical signals of the DMPO-OO $^-$ adduct derived from the DMSO system are shown below (**Figure 8**).

Subsequently, DHM was added to this system of generated superoxide anions with full shaking. Within a few minutes,



the color of the resulting solution gradually changed from colorless to yellow. After quenching with a 0.1% HCl solution, the resulting mixture was subjected to HPLC with MYR as a standard for comparison (**Supplementary Figure 11**). As a result, the compound in the reaction mixture was identified as MYR from the reaction of DHM with superoxide-anion radicals ($O_2^{\cdot -}$). Therefore, we proposed a pathway of DHM transformation into MYR that involves the abstraction of a C3-H atom of phenolate **1** abstracted by $O_2^{\cdot -}$ to form the potent radical **2**. Phenolate **1** was obtained by the deprotonation of the phenolic hydroxyl moieties of DHM. Subsequently, peroxide **3** was generated from the combination of radical **2** with peroxy radical HOO^{\cdot} . Then, under acidic conditions, terminal product MYR was formed by successive acidification, dehydration, and enolization (Branchini et al., 2015) (**Scheme 2**).

Generation of Superoxide-Anion Radical by Other Bioflavonoids as Ligands for Metal Complexes

Since DHM generates $O_2^{\cdot -}$ in an oxygenated alkaline solution, its analogs MYR, quercetin, daidzein, genistein, chrysin, baicalein, rutin hydrate, and kaempferol were also considered as potential

ligands for metal complexes based on the multi-hydroxyl moieties attached to their molecular backbones (**Figure 9**). Thus, their behaviors in an air-saturated alkaline solution were investigated by EPR. All of these bioflavonoids originate from natural products and were tested at the same concentration in an air-saturated alkaline solution, then observed by EPR with DMPO (**Figure 10**). We found that the intensities of the DMPO-OO-adduct signal could be correlated to the location and/or number of phenolic hydroxyl groups or their configurations.

As shown in **Table 1**, the more phenolic hydroxyl groups are attached to the molecular skeleton, the higher the signal strength of the DMPO-OO-adduct in general. Comparing DHM with MYR, which have the same number of hydroxyl groups, the adduct signal was stronger for MYR under the same conditions. This indicated that molecular configuration contributes to the capacity for generating superoxide anions, potentially because of the transformation of DHM into MYR in the presence of $O_2^{\cdot -}$. For the flavonoids with three hydroxyl moieties, baicalein showed a higher adduct signal than genistein. At the same time, chrysin with two hydroxyl groups at the 5,7-positions of the molecular skeleton exhibited a higher DMPO-OO-adduct signal than daidzein. This indicated that molecular skeletons rich with electrons can promote the capacity for superoxide anion generation because of the +C effect from the hydroxyl

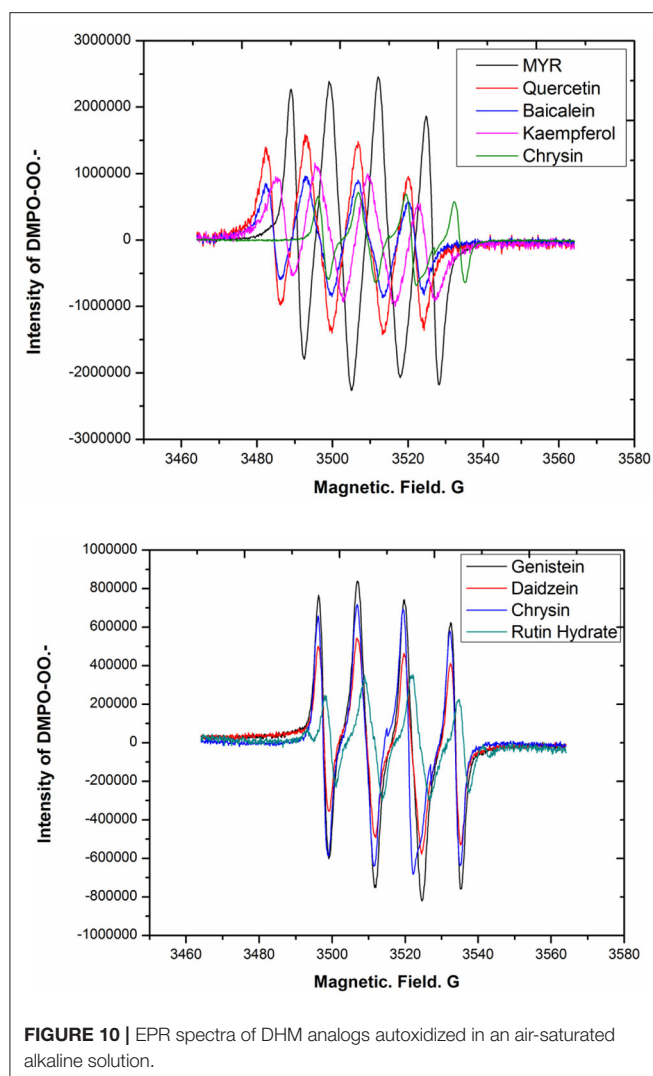


FIGURE 10 | EPR spectra of DHM analogs autoxidized in an air-saturated alkaline solution.

functional groups. Rutin hydrate, composed of quercetin with rutinose, was a particular example, as the adduct signal was markedly weaker than that of quercetin. These experimental results confirmed that the synthesis of bioflavonoid-metal complexes should exclude molecular oxygen from the reaction solution and employ fewer electronegative metal ions. Further investigations on work related to this issue is ongoing in our laboratory.

CONCLUSION

The general synthesis of bioflavonoid-metal complexes involves dissolving bioflavonoids in an air-saturated alkaline solution to undergo the deprotonation of phenolic hydroxyl groups and chelation with metals. However, because most bioflavonoids are unstable in air-saturated alkaline solutions, the general synthetic procedure may be inadequate. In this study, DHM as a representative bioflavonoid was selected as a potent ligand to synthesize DHM-M(II) complexes following the general

TABLE 1 | Intensity of DMPO-OO-adduct EPR signal related to the characterization of bioflavonoids.

Entry	Bioflavonoids	Characterization	Intensity of DMPO-OO-adduct ^a
1	Dihydromyricetin	3, 5, 7, 3', 4', 5' -OH	1827117.71
2	Myricetin	3, 5, 7, 3', 4', 5' -OH	2383714.06
3	Quercetin	3, 5, 7, 3', 4' -OH	1576987.37
4	Kaempferol	3, 5, 7, 4' -OH	1148836.33
5	Chrysin	5, 7 -OH	717476.37
6	Baicalein	5, 6, 7 -OH	952788.229
7	Daidzein	7, 4' -OH	544170.9081
8	Genistein	5, 7, 4' -OH	838478.55
9	Rutin hydrate	5, 7, 3', 4' -OH	349361.2188

^aTypical signals of DMPO-OO⁻ adduct performed to be maximum in value.

procedure. The metal complexes were shown to be consistent with previous examples through spectroscopic analyses and evaluation of antioxidant capacity. Furthermore, the complexes were hydrolyzed to observe the stability of DHM via HPLC under acidic conditions. Surprisingly, many unknown absorption peaks with different intensities were observed at 254 nm in the LC spectra, indicating that the molecular structure of DHM was damaged during the synthesis of the DHM-M(II) complexes. This caused us to question the employed general synthetic procedure. To address this, the synthetic conditions and their effects on the DHM stability were investigated by UV-vis spectroscopy and HPLC. More electronegative metal ions and the solution alkalinity were shown to affect the DHM stability in an air-saturated solution and were thus regarded as probable causes of the observed damage to DHM using the general procedure. Furthermore, considering the content of MYR in the air-saturated alkaline solution of DHM, a pathway for the transformation of DHM into MYR via interaction with O₂⁻ was proposed, involving a C3-H atom of DHM abstracted by O₂⁻. The DHM analogs MYR, quercetin, daidzein, genistein, chrysin, baicalein, rutin hydrate, and kaempferol as potential bioflavonoid-metal complex ligands were also dissolved in air-saturated alkaline solutions and observed by EPR to generate O₂⁻ at different capacities. These differences are possibly associated with the number and location of the multi-hydroxyl moieties attached to their molecular skeleton or their configurations. Therefore, the general synthetic procedure for bioflavonoid-metal complexes using a transition metal ion and air-saturated alkaline solution was shown to require improvement.

DATA AVAILABILITY STATEMENT

The raw data supporting the conclusions of this article will be made available by the authors, without undue reservation.

AUTHOR CONTRIBUTIONS

YY and SC were in charge of designing the experiments and writing the manuscript. YY, LH, YW, and MZ performed

experiments. All authors contributed to the article and approved the submitted version.

FUNDING

We are grateful for the financial support received from the Natural Science Foundations of the Education Ministry of Guizhou Province (Grant No. KY[2018]033); Tongren

Science and Technology Bureau (Grant No. TSKY2019-3); Guizhou Science and Technology Department (Grant No. QKHPTRC[2020]5009).

SUPPLEMENTARY MATERIAL

The Supplementary Material for this article can be found online at: <https://www.frontiersin.org/articles/10.3389/fchem.2020.00589/full#supplementary-material>

REFERENCES

- Amirhossein, A., and Shadboorestan, A. (2016). Oxidative stress and cancer; the role of hesperidin, a citrus natural bioflavonoid, as a cancer chemoprotective agent. *Nutr. Cancer* 68, 29–39. doi: 10.1080/01635581.2015.1078822
- Branchini, B. R., Behney, C. E., Southworth, T. L., Fontaine, D. M., Gulick, A. M., Vinyard, D. J., et al. (2015). Experimental support for a single electron-transfer oxidation mechanism in firefly bioluminescence. *J. Am. Chem. Soc.* 137, 7592–7595. doi: 10.1021/jacs.5b03820
- Chen, X. M., Tait, A. R., and Kitts, D. D. (2017). Flavonoid composition of orange peel and its association with antioxidant and anti-inflammatory activities. *Food Chem.* 218, 15–21. doi: 10.1016/j.foodchem.2016.09.016
- Dai, W., Bi, J., Li, F., Wang, S., Huang, X., Meng, X., et al. (2019). Antiviral efficacy of flavonoids against enterovirus 71 infection *in vitro* and in newborn mice. *Viruses* 11:625. doi: 10.3390/v11070625
- Gençkal, H. M., Erkisa, M., Alper, P., Sahin, S., Ulukaya, E., and Ari, F. (2020). Mixed ligand complexes of Co (II), Ni (II) and Cu (II) with quercetin and diimine ligands: synthesis, characterization, anti-cancer and anti-oxidant activity. *J. Biol. Inorg. Chem.* 25, 161–177. doi: 10.1007/s00775-019-01749-z
- Imran, M., Rauf, A., Abu-Izneid, T., Nadeem, M., Shariati, M. A., Khan, I. A., et al. (2019). Luteolin, a flavonoid, as an anticancer agent: a review. *Biomed. Pharmacother.* 112:108612. doi: 10.1016/j.biopha.2019.108612
- Jabeen, E., Janjua, N. K., Ahmed, S., Murtaza, I., Ali, T., and Hameed, S. (2017). Radical scavenging propensity of Cu²⁺, Fe³⁺ complexes of flavonoids and *in vivo* radical scavenging by Fe³⁺-primuletin. *Spectrochim. Acta Part A Mol. Biomol. Spectrosc.* 171, 432–438. doi: 10.1016/j.saa.2016.08.035
- Khater, M., Ravishankar, D., Greco, F., and Osborn, H. M. (2019). Metal complexes of flavonoids: their synthesis, characterization and enhanced antioxidant and anticancer activities. *Future Med. Chem.* 11, 2845–2867. doi: 10.1155/fmc-2019-0237
- Lalani, S., and Poh, C. L. (2020). Flavonoids as antiviral agents for Enterovirus A71 (EV-A71). *Viruses* 12:184. doi: 10.3390/v12020184
- Lani, R., Hassandarvish, P., Shu, M. H., Phoon, W. H., Chu, J. J. H., Higgs, S., et al. (2016). Antiviral activity of selected flavonoids against Chikungunya virus. *Antiviral. Res.* 133, 50–61. doi: 10.1016/j.antiviral.2016.07.009
- Li, X., Liu, J., Lin, J., Wang, T., Huang, J., Lin, Y., et al. (2016). Protective effects of dihydromyricetin against •OH-induced mesenchymal stem cells damage and mechanistic chemistry. *Molecules* 21:604. doi: 10.3390/molecules21050604
- Liang, J., Wu, J., Wang, F., Zhang, P. F., and Zhang, X. M. (2019). Semaphoring 4D is required for the induction of antioxidant stress and anti-inflammatory effects of dihydromyricetin in colon cancer. *Int. Immunopharmac.* 67, 220–230. doi: 10.1016/j.intimp.2018.12.025
- Liu, K. J., Jiang, J. J., Ji, L. L., Shi, X., L., and Swartz, H. M. (1996). An HPLC and EPR investigation on the stability of DMPO and DMPO spin adducts *in vivo*. *Res. Chem. Intermediat.* 22, 499–509. doi: 10.1163/156856796X00700
- Madunić, J., Madunić, I. V., Gajski, G., Popić, J., and Garaj-Vrhovac, V. (2018). Apigenin: a dietary flavonoid with diverse anticancer properties. *Cancer Lett.* 413, 11–22. doi: 10.1016/j.canlet.2017.10.041
- Maitera, O. N., Louis, H., Barminas, J. T., Akakuru, O. U., and Boro, G. (2018). Synthesis and characterization of some metal complexes using herbal flavonoids. *Nat. Prod. Chem. Res.* 6:314. doi: 10.4172/2329-6836.1000314
- Qian, J. Z., Wang, B. C., Fan, Y., Tan, J., and Yang, X. (2015). QSAR study of flavonoid-metal complexes and their anticancer activities. *J. Struct. Chem.* 56, 338–345. doi: 10.1134/S0022476615020195
- Raffa, D., Maggio, B., Raimondi, M. V., Plescia, F., and Daidone, G. (2017). Recent discoveries of anticancer flavonoids. *Eur. J. Med. Chem.* 142, 213–228. doi: 10.1016/j.ejmech.2017.07.034
- Samsonowicz, M., Regulska, E., and Kalinowska, M. (2017). Hydroxyflavone metal complexes-molecular structure, antioxidant activity and biological effects. *Chem. Biol. Interact.* 273, 245–256. doi: 10.1016/j.cbi.2017.06.016
- Silva, W. M. B., Oliveira Pinheiro, S., Alves, D. R., Menezes, J. E. S. A., Magalhães, F. E. A., Silva, F. C. O., et al. (2020). Synthesis of Quercetin-metal complexes, *in vitro* and *in silico* anticholinesterase and antioxidant evaluation, and *in vivo* toxicological and anxiolytic activities. *Neurotox. Res.* 37, 893–903. doi: 10.1007/s12640-019-00142-7
- Spagnuolo, C., Moccia, S. G., and Russo, L. (2018). Anti-inflammatory effects of flavonoids in neurodegenerative disorders. *Eur. J. Med. Chem.* 153, 105–115. doi: 10.1016/j.ejmech.2017.09.001
- Tamayo, L. V., Gouvea, L. R., Sousa, A. C., Albuquerque, R. M., Teixeira, S. F., and de Azevedo, R. A. (2016). Copper (II) complexes with naringenin and hesperetin: cytotoxic activity against A 549 human lung adenocarcinoma cells and investigation on the mode of action. *Bio. Metals* 29, 39–52. doi: 10.1007/s10534-015-9894-0
- Thangavel, P., Viswanath, B., and Kim, S. (2018). Synthesis and characterization of kaempferol-based ruthenium (II) complex: a facile approach for superior anticancer application. *Mater. Sci. Eng.* 89, 87–94. doi: 10.1016/j.msec.2018.03.020
- Tu, L. Y., Pi, J., Jin, H., Cai, J. Y., and Deng, S. P. (2016). Synthesis, characterization and anticancer activity of kaempferol-zinc(II) complex. *Bioorg. Med. Chem. Lett.* 26, 2730–2734. doi: 10.1016/j.bmcl.2016.03.091
- Uivarosi, V., Munteanu, A. C., Sharma, A., and Singh Tuli, H. (2019). “Metal complexation and patent studies of flavonoid,” in *Current Aspects of Flavonoids: Their Role in Cancer Treatment*, H. Singh Tuli (Singapore: Springer), 39–77.
- Wu, Y., Xiao, Y., Yue, Y., Zhong, K., Zhao, Y., and Gao, H. (2020). A deep insight into mechanism for inclusion of 2R, 3R-dihydromyricetin with cyclodextrins and the effect of complexation on antioxidant and lipid-lowering activities. *Food Hydrocolloid* 103:105718. doi: 10.1016/j.foodhyd.2020.105718
- Zhang, H., and Tsao, R. (2016). Dietary polyphenols, oxidative stress and antioxidant and anti-inflammatory effects. *Curr. Opin. Food Sci.* 8, 33–42. doi: 10.1016/j.cofs.2016.02.002

Conflict of Interest: The authors declare that the research was conducted in the absence of any commercial or financial relationships that could be construed as a potential conflict of interest.

Copyright © 2020 Yao, Zhang, He, Wang and Chen. This is an open-access article distributed under the terms of the Creative Commons Attribution License (CC BY). The use, distribution or reproduction in other forums is permitted, provided the original author(s) and the copyright owner(s) are credited and that the original publication in this journal is cited, in accordance with accepted academic practice. No use, distribution or reproduction is permitted which does not comply with these terms.



Corrigendum: Evaluation of General Synthesis Procedures for Bioflavonoid–Metal Complexes in Air-Saturated Alkaline Solutions

Yuanrong Yao*, Meng Zhang, Laibing He, Yunyang Wang and Shixue Chen*

Tongren Key Laboratory for Modernization Research, Development and Utilization of Traditional Chinese Medicine and National Medicine, School of Material and Chemical Engineering, Tongren University, Tongren, China

Keywords: dihydromyricetin, flavonoids, bioflavonoid–metal complexes, alkaline conditions, superoxide anion, HPLC, UV-visible spectrophotometer, transition metal ions

OPEN ACCESS

Edited by:

Hu Li,
Guizhou University, China

Reviewed by:

Zhichao Jin,
Guizhou University, China

*Correspondence:

Yuanrong Yao
chyzyy@gztrc.edu.cn
Shixue Chen
tongrencsx01@126.com

Specialty section:

This article was submitted to
Organic Chemistry,
a section of the journal
Frontiers in Chemistry

Received: 13 August 2020

Accepted: 24 August 2020

Published: 11 November 2020

Citation:

Yao Y, Zhang M, He L, Wang Y and
Chen S (2020) Corrigendum:
Evaluation of General Synthesis
Procedures for Bioflavonoid–Metal
Complexes in Air-Saturated Alkaline
Solutions. *Front. Chem.* 8:594058.
doi: 10.3389/fchem.2020.594058

A Corrigendum on

Evaluation of General Synthesis Procedures for Bioflavonoid–Metal Complexes in Air-Saturated Alkaline Solutions

by Yao, Y., Zhang, M., He, L., Wang, Y., and Chen, S. (2020). *Front. Chem.* 8:589.
doi: 10.3389/fchem.2020.00589

In the original article, there was a mistake in the legends for **Figures 3, 4, 7, and 8** as published. In these Figures, marks such as a, b, c, d, e, f, and g have not been explained. The updated legends appear below.

Figure 3. (A) UV-vis spectra and **(B)** main peak positions of DHM refluxed for different times. (a) DHM; (b–g) DHM refluxing for 30, 60, 90, 120, 150, and 180 min.

Figure 4. (A) UV-vis spectra and **(B)** main peak positions of DHM stirred for different times at pH = 8.2. (a) DHM; (b–g) DHM stirring for 1, 3, 5, 10, 20, and 30 min in pH 8.2.

Figure 7. EPR spectra of DHM in air-, nitrogen-, and oxygen-saturated alkaline solutions. (a) DHM only; (b) DHM + DMPO; (c–e) DHM + DMPO, in nitrogen-, air-, oxygen-saturated alkaline solution.

Figure 8. EPR spectra of superoxide-anion radical generation from DMSO reacted with a base in the presence of oxygen. (a) DMSO + DMPO + O₂; (b) Na⁺PhO[−] + DMPO + O₂; (c) Na⁺PhO[−] + O₂; (d) DMSO + Na⁺PhO[−] + O₂; (e) DMSO + Na⁺PhO[−] + DMPO + O₂.

The authors apologize for this error and state that this does not change the scientific conclusions of the article in any way. The original article has been updated.

Copyright © 2020 Yao, Zhang, He, Wang and Chen. This is an open-access article distributed under the terms of the Creative Commons Attribution License (CC BY). The use, distribution or reproduction in other forums is permitted, provided the original author(s) and the copyright owner(s) are credited and that the original publication in this journal is cited, in accordance with accepted academic practice. No use, distribution or reproduction is permitted which does not comply with these terms.



Heteropoly Acid-Based Catalysts for Hydrolytic Depolymerization of Cellulosic Biomass

Xiaoxiang Luo¹, Hongguo Wu¹, Chuanhui Li¹, Zhengyi Li¹, Hu Li^{1*}, Heng Zhang¹, Yan Li¹, Yaqiong Su² and Song Yang^{1*}

¹ State Key Laboratory Breeding Base of Green Pesticide and Agricultural Bioengineering, Key Laboratory of Green Pesticide and Agricultural Bioengineering, Ministry of Education, State-Local Joint Laboratory for Comprehensive Utilization of Biomass, Center for Research and Development of Fine Chemicals, Guizhou University, Guiyang, China, ² Laboratory of Inorganic Materials and Catalysis, Schuit Institute of Catalysis, Department of Chemical Engineering and Chemistry, Eindhoven University of Technology, Eindhoven, Netherlands

OPEN ACCESS

Edited by:

Svetlana Ivanova,
University of Seville, Spain

Reviewed by:

Sara Navarro-Jaén,
Université de Lille, France

Fabien Drault,
Centrale Lille, France

*Correspondence:

Song Yang
jhzx.msm@gmail.com
Hu Li
hli13@gzu.edu.cn

Specialty section:

This article was submitted to
Green and Sustainable Chemistry,
a section of the journal
Frontiers in Chemistry

Received: 04 July 2020

Accepted: 17 August 2020

Published: 25 September 2020

Citation:

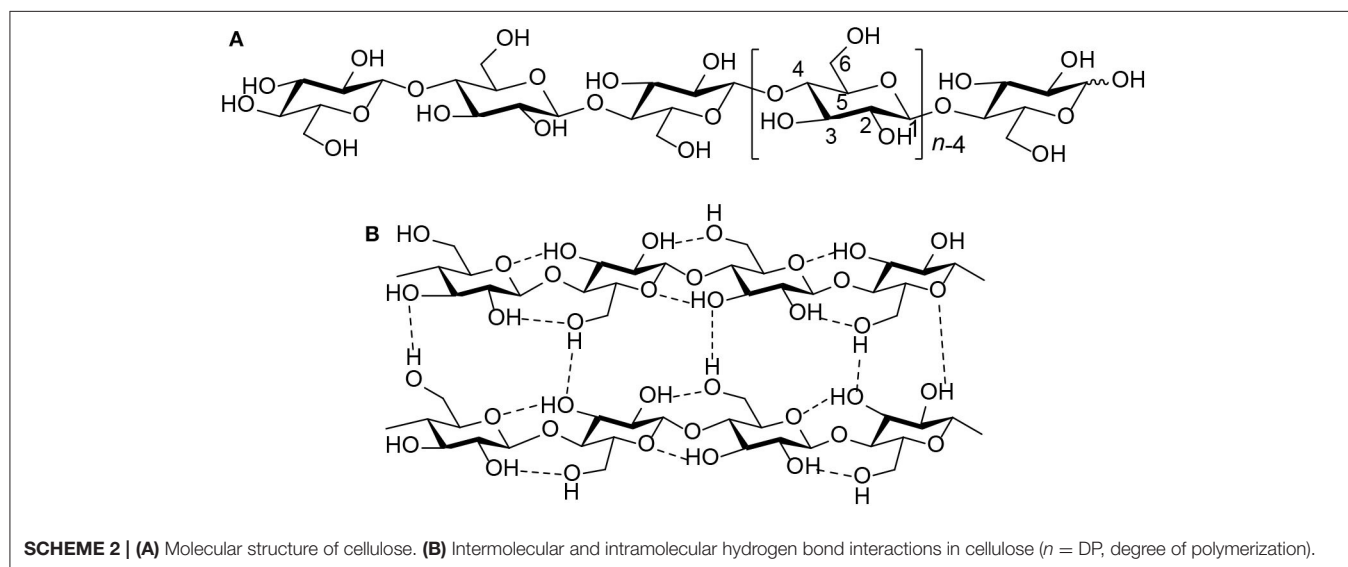
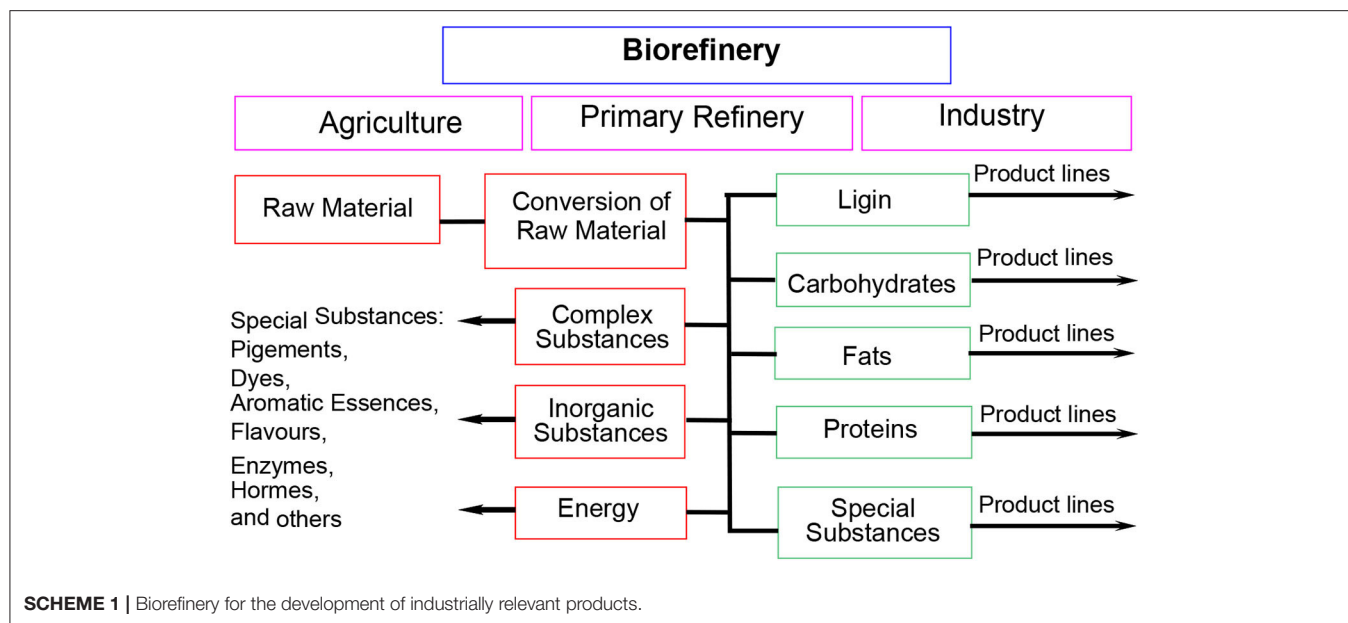
Luo X, Wu H, Li C, Li Z, Li H, Zhang H,
Li Y, Su Y and Yang S (2020)
Heteropoly Acid-Based Catalysts for
Hydrolytic Depolymerization of
Cellulosic Biomass.
Front. Chem. 8:580146.
doi: 10.3389/fchem.2020.580146

Cellulose is the most abundant source of biomass, which can be converted into monosaccharide or other chemical platform molecules for the sustainable production of chemicals and fuels. Acid catalysts can promote hydrolytic degradation of cellulose into valuable platform molecules, which is of great significance in the development of chemicals and biofuels. However, there are still some shortcomings and limitations of the catalysts for the hydrolytic degradation of cellulosic biomass. Heteropoly acid (HPA), as a green catalyst, seems to be more conducive to the degradation of cellulosic biomass due to its extreme acidity. HPAs can be designed in homogeneous and heterogeneous systems. Moreover, they can be easily separated from the products in both systems by a simple extraction process. According to the unique properties of HPAs (e.g., good solubility, high thermal stability, and strong acidity), using heteropoly acid-based catalysts to depolymerize and convert cellulose into value-added chemicals and biofuels has become one of the most remarkable processes in chemistry for sustainability. In this review, the characteristics, advantages, and applications of HPAs in different categories for cellulose degradation, especially hydrolysis hydrolytic degradation, are summarized. Moreover, the mechanisms of HPAs catalysts in the effective degradation of cellulosic biomass are discussed. This review provides more avenues for the development of renewed and robust HPAs for cellulose degradation in the future.

Keywords: cellulose hydrolysis, heteropoly acid, biomass conversion, green chemistry, sustainable catalysis

INTRODUCTION

With the continuous exploitation of human beings, the amount of fossil energy that is the most main energy consumed in the world is decreasing gradually. Therefore, developing a sustainable renewable energy source that can provide valuable chemicals and biofuels is of great importance (Zhang et al., 2015). To furnish the desired bioproducts, some resources are needed which can provide us with basic elements such as C, H, and O in luxuriant amounts (Dhepe and Fukuoka, 2008). Compared with other energy sources (e.g., coal, oil, and natural gas), biomass energy has incomparable advantages as a renewable energy source with little pollution. Moreover, biomass

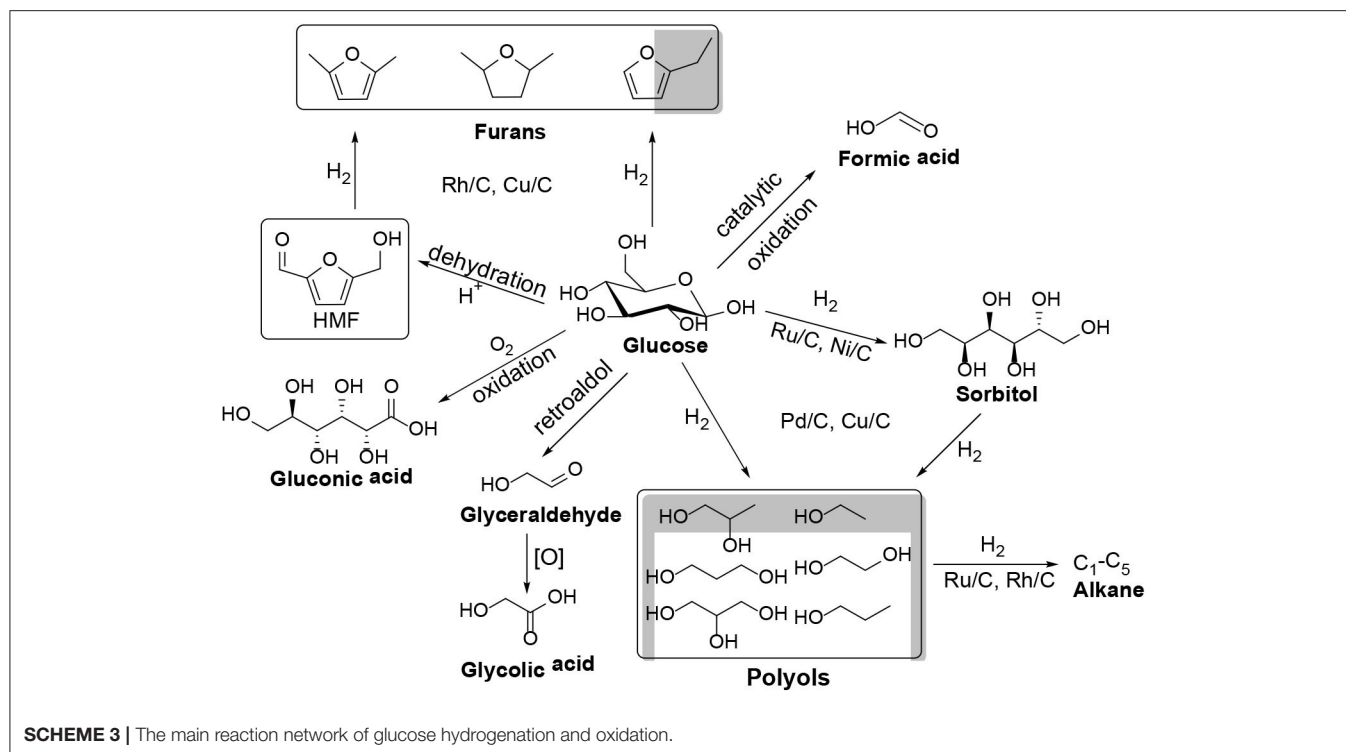


has become the focus of development because of its universality, abundance, and low pollution. In some biorefinery typically using biomass instead of oil, biomass can be converted into energy and relevant bioproducts through multifarious platforms (Chang et al., 2013; Hu et al., 2015; Li et al., 2016; Liu et al., 2016). Especially, biorefinery combines the key technologies of transforming biological raw materials into industrial intermediates and final products (Scheme 1; Kamm and Kamm, 2004; Dhepe and Fukuoka, 2008; Li et al., 2015; Liu and Zhang, 2015; Zhang et al., 2018). Therefore, the utilization of biomass is a wonderful choice to develop sustainable and renewable energy.

As the most abundant source of biomass and one of the most widely distributed and abundant polysaccharides in nature, cellulose provides more possibilities for sustainable chemicals

and fuels in the future (Huber et al., 2006; Climent et al., 2014; Sheldon, 2014; To et al., 2015). Hence, the conversion of cellulose could become a significant part of biomass utilization, which plays an important role in the development of chemicals and fuels in the future. However, cellulose is a homopolymer of D-glucose made up of β -1,4 glycosidic bonds (Scheme 2A). Its intramolecular and intermolecular hydrogen bonds are formed (Scheme 2B), resulting in its water insolubility (Geboers et al., 2011; Wang et al., 2012; Harada et al., 2014; Yabushita et al., 2014). Therefore, the processes of cellulose conversion are complicated because this biopolymer is insoluble in water, and most organic solvents (Klemm et al., 2005; Albert et al., 2014).

Many homogeneous and heterogeneous acid catalysts were found to be capable of converting cellulose into glucose, a monosaccharide which is an important component for

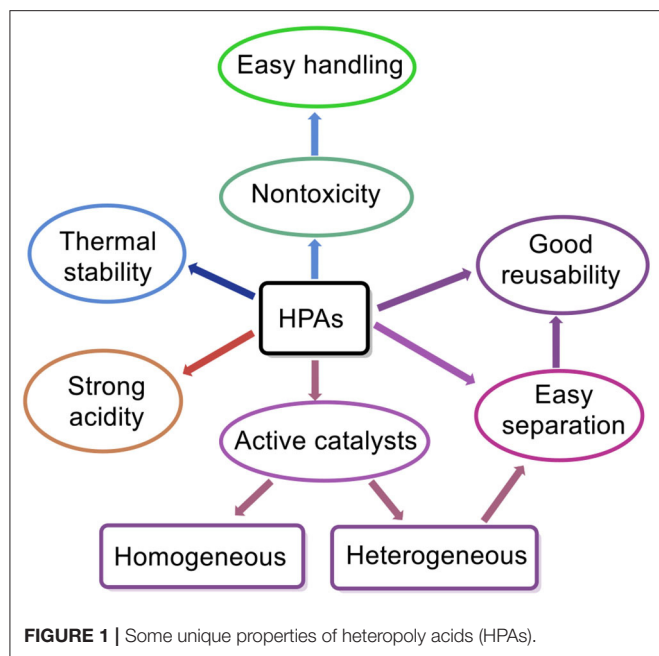
**TABLE 1** | Cellulose hydrolysis over different solid acid catalysts.

Catalyst	Solvents	Temp (°C)	Time (h)	Glucose/TRS yield	TRS yield/%	References
Amberlyst-15	[BMIm]Cl/H ₂ O	100	5	11.0		Rinaldi et al., 2010
PCPs-SO ₃ H	H ₂ O	120	3	5.30		Akiyama et al., 2011
BC-SO ₃ H	H ₂ O	90	1	19.8		Wu et al., 2010
CMK-3-SO ₃ H	H ₂ O	150	24	74.5		Pang et al., 2010
Zn-Ca-Fe	H ₂ O	160	20	29		Zhang et al., 2011
CsH ₂ PW ₁₂ O ₄₀	H ₂ O	160	6	27.0		Tian et al., 2011
Ru/CMK-3	H ₂ O	230	24	34.2		Kobayashi et al., 2010
Fe ₃ O ₄ -SBA-SO ₃ H	H ₂ O	150	3	26.0		Lai et al., 2011
CaFe ₂ O ₄	H ₂ O	150	24	36.0		Komanoya et al., 2011
H ₃ PW ₁₂ O ₄₀	H ₂ O	180	2	50.5		Tian et al., 2010
H ₅ BW ₁₂ O ₄₀	H ₂ O	60	6	77.0		Ogasawara et al., 2011
H ₅ AlW ₁₂ O ₄₀	H ₂ O	60	24	68.0		Ogasawara et al., 2011
H ₅ GaW ₁₂ O ₄₀	H ₂ O	60	24	62.0		Ogasawara et al., 2011
H ₆ CoW ₁₂ O ₄₀	H ₂ O	60	24	59.0		Ogasawara et al., 2011

synthesizing different kinds of chemicals and fuels (**Scheme 3**), such as furans (Li et al., 2014), ethanol (Chheda et al., 2007), polyhydric alcohol (Geboers et al., 2010; de Op Beeck et al., 2013; Xie et al., 2014; He et al., 2018), furfural (Yu et al., 2009b; Feng et al., 2011; Li et al., 2013; Pan et al., 2013), organic acid (Yan et al., 2014; Zhang et al., 2014; Ren et al., 2015), and so on. Several excellent review literature on the conversion of cellulose have been reported, with focus on the discussion of different solid acid catalysts (e.g., Amberlyst-15, PCPs-SO₃H, BC-SO₃H, CMK-3-SO₃H, Zn-Ca-Fe, CsH₂PW₁₂O₄₀, Ru/CMK-3, Fe₃O₄-SBA-SO₃H, CaFe₂O₄, H₃PW₁₂O₄₀, H₅BW₁₂O₄₀, H₅AlW₁₂O₄₀, H₅GaW₁₂O₄₀, and H₆CoW₁₂O₄₀) for hydrolysis

of cellulose (**Table 1**; Kobayashi et al., 2010; Pang et al., 2010; Rinaldi et al., 2010; Tian et al., 2010, 2011; Wu et al., 2010; Akiyama et al., 2011; Komanoya et al., 2011; Lai et al., 2011; Ogasawara et al., 2011; Zhang et al., 2011).

Compared with other solid acids, HPA catalysts are more favorable for hydrolysis of cellulose, considering that they have some unique properties such as stronger acidity compared to other mineral acids (e.g., H₂SO₄, HCl), high redox properties, good thermal stability, easy separation, good reusability, fewer side products, less waste generation, non-toxicity, and easy handling, as illustrated in **Figure 1** (Kozhevnikov, 1987, 1998; Mizuno and Misono, 1994; Kaur and Kozhevnikov, 2002; Yu



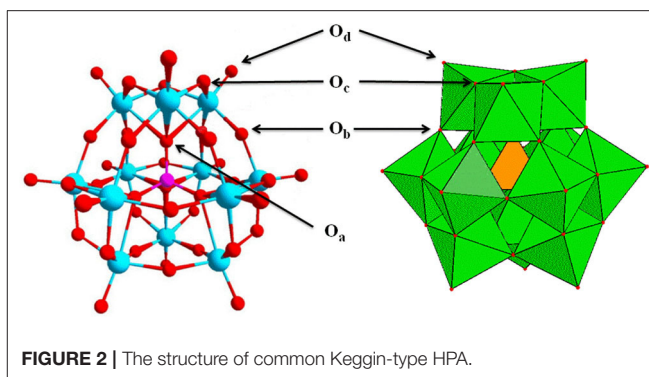
et al., 2009a; Yang et al., 2011; Deng et al., 2012; Reddy et al., 2012; de Op Beeck et al., 2013). Furthermore, HPA catalysts can be used in both homogeneous and heterogeneous systems. The most significant advantage of the heterogeneous system is that the HPA catalysts can be easily separated from the reaction products, thus improving the catalyst reusability. The most common HPAs are Keggin-type HPAs, which have the anions of $[XM_{12}O_{40}]^{n-}$, where X is a heteroatom (e.g., P, Si) and M is a metal ion (e.g., W^{6+} , Mo^{6+}). Among them, $H_3PW_{12}O_{40}$ is the most common Keggin-type HPA. Moreover, $H_3PW_{12}O_{40}$ with strong acidity is highly soluble in water and can completely dissociate protons, which facilitates contact with the heterogeneous substrates, thus endowing enhanced reaction rates (Tian et al., 2010). Besides, the basic structural units of Keggin-type HPAs are oxygen-containing tetrahedron and octahedron anions in good symmetry and low charge density (Figure 2).

Given the unique features and rapid development of HPAs-based catalysts in the preliminary degradation of cellulosic biomass with high efficiency, this review mainly reports the design and structural characterization of different types of HPAs employed for hydrolytic depolymerization of cellulosic biomass. In addition, the properties and preparation methods of HPAs as well as their advantages in the hydrolysis of cellulose are discussed. Also, possible research trends of HPAs in the future are forecasted.

HPAs-BASED CATALYSTS

HPA Properties and Classification

HPA catalysts have attracted people's attention, and are known as effective, environmentally friendly and economically viable acid catalysts (Kozhevnikov, 1998), which can be used in either homogeneous or heterogeneous state (Izumi et al., 1983;

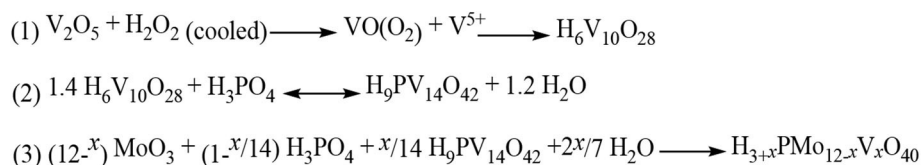


Nowinska et al., 1996; Song and Lee, 2004; Bennardi et al., 2010; Zhao et al., 2013). Compared with a homogeneous system, the heterogeneous system has the advantage that the catalyst is easy to separate from the reaction products. Due to these special features, HPA catalysts are more beneficial to the degradation of cellulosic biomass than other catalysts.

HPA catalysts can be classified into the following categories: (1) Keggin-type HPAs, the most common HPAs with the anions of $[XM_{12}O_{40}]^{n-}$, where X is a heteroatom (e.g., P, Si) and M is a metal ion (e.g., W^{6+} , Mo^{6+}). (2) Substituted HPAs, the H^+ ions on conventional HPAs are substituted by monovalent cations, such as Cs^+ ions. (3) Supported HPAs, the heteropoly compounds are supported on suitable supporters, such as silica. (4) Assembled HPAs, the new catalysts with higher activity are synthesized by self-assembly of HPAs with other substances, such as ionic liquids. (5) Other types, new types of heterogeneous catalysts formed by an effective combination of HPAs with other substances.

Catalyst Preparation Methods

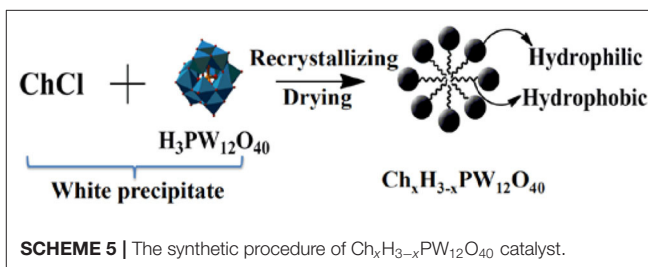
Up to the present, many patents and literature on the preparation of HPAs were published, including e.g., traditional acidification method incorporated with an ether extraction, ion exchange method, impregnation method, and sol-gel method (Bechtold and Square, 1950; Laferty and John, 1966; Chiola and Lawrence, 1969; Chiola et al., 1969; Izumi et al., 1995; Vázquez et al., 2000; Mrowiec-Białoń et al., 2002; Cardoso et al., 2004; Yang et al., 2005; Ahmed et al., 2011). The traditional synthesis method of conventional HPAs is an acidification process coupled with an ether extraction, which is commonly used for the synthesis of phosphotungstate HPA catalysts. In this method, the HPA is prepared by mixing heteroatom oxygen-containing acid and ligand oxide in a certain proportion, heating, refluxing, and then acidifying to obtain HPA. The HPA is dissolved in ether, and the solid HPA is obtained after ether volatilization (Chiola and Lawrence, 1969; Chiola et al., 1969). However, the acidification procedure coupled with an ether extraction has the disadvantages of low safety due to the use of toxic substances and low yield of some HPAs. In connection with this, the ion-exchange method has been developed, which first obtains the corresponding ammonium salt, and then obtains HPA through hydrogen ion-exchange resin. This method avoids the use of ether and improves process safety, but the production cycle is



SCHEME 4 | The overall scheme for the synthesis of Mo-V-P HPA catalysts.

relatively long (Bechtold and Square, 1950; Laferty and John, 1966). For some supported HPAs, the impregnation method is commonly used. The method is to add the carrier into the solution of HPA with a certain concentration, stir for a long time at a certain temperature, stand still, and then remove the excess solvent to obtain the catalyst. The method is simple and safe, but there are some problems such as the loss of catalyst activity and limited recycling ability. Therefore, the support should be screened and optimized (Vázquez et al., 2000; Cardoso et al., 2004; Liu et al., 2004). The sol-gel method is to add raw materials to the HPA colloid and obtain the HPA catalyst through a series of specific processes, such as drying and heat treatment. This method can be used to prepare catalysts at a low temperature or mild condition, which is widely used in manufacturing nanomaterials catalysts. Likewise, this method has the disadvantages of low security and long cycle (Izumi et al., 1995; Mrowiec-Białoń et al., 2002; Yang et al., 2005). Some examples of catalysts for the preparation of HPAs are as follows:

1. Keggin-type Mo-V-P heteropoly acid catalysts (**Scheme 4**; Zhizhina and Odyakov, 2008; Odyakov and Zhizhina, 2009): Firstly, V_2O_5 was dissolved in cold diluted H_2O_2 solution to form peroxy complexes, which was gradually decomposed with oxygen to give $\text{H}_6\text{O}_{10}\text{V}_{28}$. Then, by adding excess H_3PO_4 , $\text{H}_6\text{O}_{10}\text{V}_{28}$ acid produced was immediately stabilized to give $\text{H}_9\text{PV}_{14}\text{O}_{42}$, following by addition into the boiling suspension of MoO_3 and H_3PO_4 to form the catalyst.
2. Substituted heteropoly tungstic acid catalyst $\text{Cs}_x\text{H}_{3-x}\text{PW}_{12}\text{O}_{40}$ ($x = 1-3$): It is usually prepared by titration method (Okuhara et al., 1992, 1996, 2000; Tian et al., 2011). At room temperature, dropping 0.10 mol dm^{-3} Cs_2CO_3 aqueous solution into 0.8 mol dm^{-3} of $\text{H}_3\text{PW}_{12}\text{O}_{40}$ aqueous solution at a constant rate was stirred continuously. Then the resulting solution was aged overnight at room temperature and heated at 50°C to obtain the catalyst.
3. The synthesis of catalyst $(\text{HOCH}_2\text{CH}_2\text{N}(\text{CH}_3)_3)_x\text{H}_{3-x}\text{PW}_{12}\text{O}_{40}$ (abbreviated as $\text{Ch}_x\text{H}_{3-x}\text{PW}_{12}\text{O}_{40}$) is shown in **Scheme 5** (Duan et al., 2013; Zhang et al., 2016): choline chloride (ChCl , $\text{HOCH}_2\text{CH}_2\text{N}(\text{CH}_3)_3\text{Cl}$) (3.34 mmol) was added to $\text{H}_3\text{PW}_{12}\text{O}_{40}$ (3.34 mmol) solution and the white precipitate was formed after stirring in 20 mL distilled water for 8 h at room temperature. Then the white precipitate was washed with distilled water, followed by recrystallization twice with CH_3CN , drying at 60°C , and finally getting the white product $\text{ChH}_2\text{PW}_{12}\text{O}_{40}$ ($\text{HOCH}_2\text{CH}_2\text{N}(\text{CH}_3)_3\text{H}_2\text{PW}_{12}\text{O}_{40}$).
4. The self-assembled HPA ionic liquid catalyst $[\text{C}_4\text{H}_6\text{N}_2(\text{CH}_2)_3\text{SO}_3\text{H}]\text{PW}_{12}\text{O}_{40}$ (**Scheme 6**; Leng et al.,



2010): 0.11 mol methyl imidazole and 0.10 mol 1,3-propane sulfone were dissolved in 20 mL toluene under nitrogen and stirred for 24 h at 50°C . The resulting white precipitate is filtered and washed three times with ether and then dried in a vacuum. Then it was added to the aqueous solution of $\text{H}_3\text{PW}_{12}\text{O}_{40}$ (0.02 mol) and stirred for 24 h at room temperature. Then water was removed in vacuum to obtain solid products, washed with water and ethanol, and dried at 100°C for 3 h .

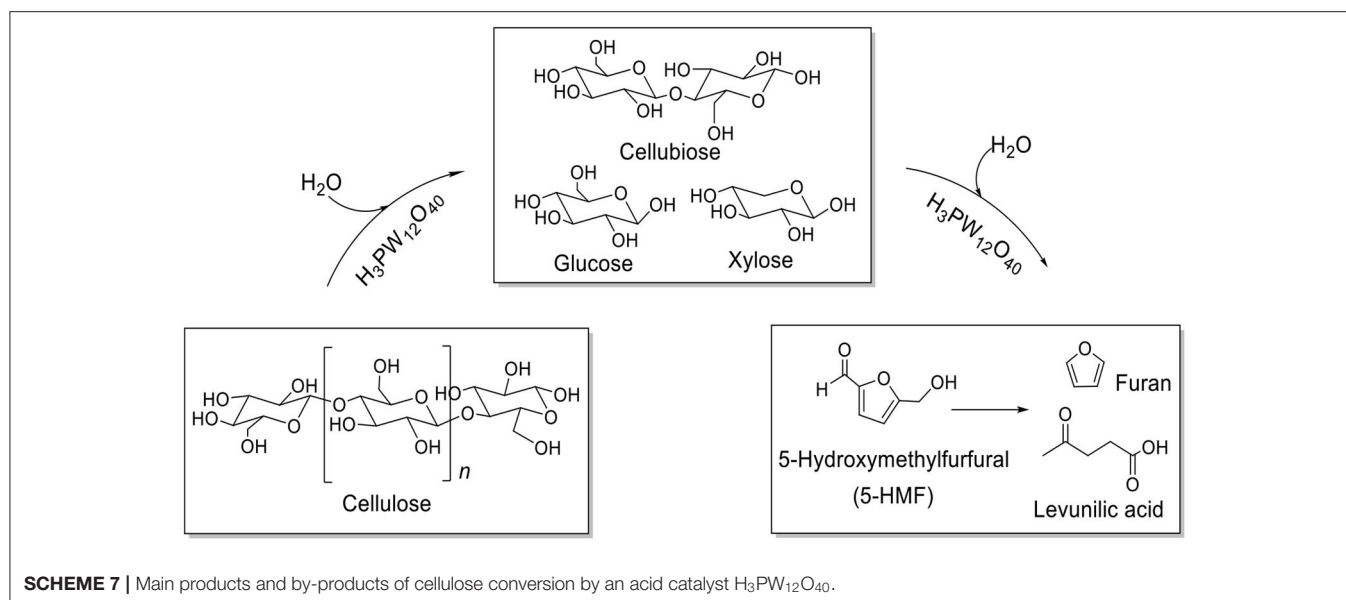
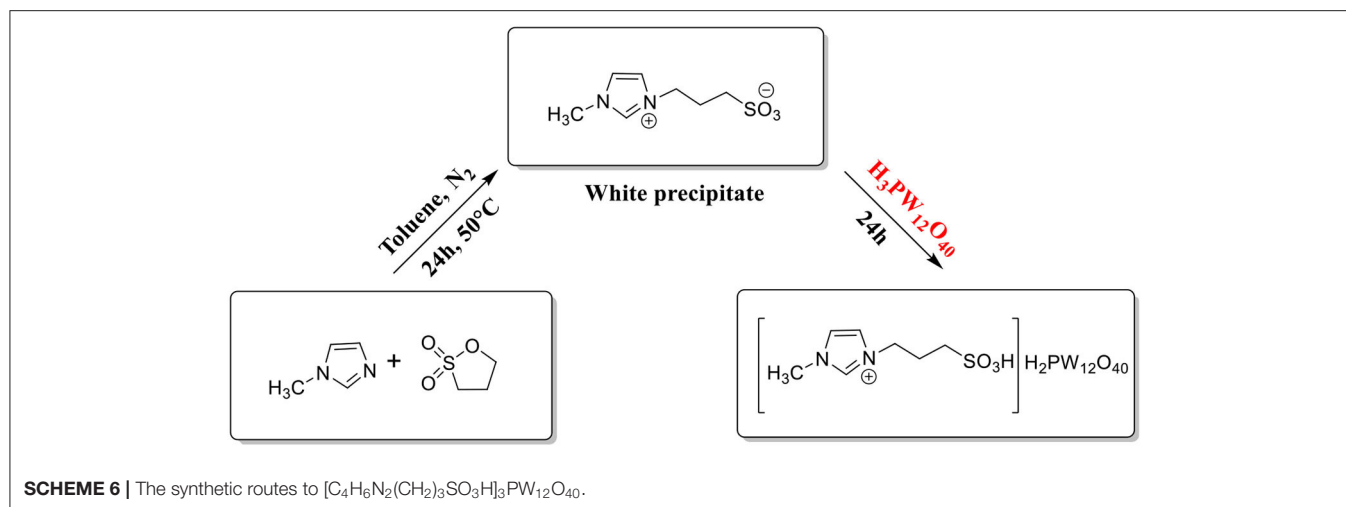
HYDROLYTIC DEPOLYMERIZATION OF BIOMASS WITH HPAS-BASED CATALYSTS

Keggin-Type HPAs

Keggin-type HPAs are the most common HPA catalysts, which have great application prospects for biomass degradation. The potential of HPAs for catalyzing the hydrolysis of cellulose to glucose has been explored.

Cellulose Conversion to Glucose

Tian et al. developed the heteropoly acid $\text{H}_3\text{PW}_{12}\text{O}_{40}$ for selective conversion of cellulose (**Scheme 7**). The heteropoly acid catalyst can promote cellulose hydrolysis, achieving the glucose selectivity and yield of 92.3 and 50.5% , respectively at 180°C for 2 h with 0.10 g cellulose amount. The authors also studied and optimized reaction parameters influencing the hydrolysis of cellulose and determined the most optimizing reaction conditions. Compared with HCl , $\text{H}_3\text{PW}_{12}\text{O}_{40}$ had greater catalytic activity and glucose selectivity under identical reaction conditions with the same acid concentration (**Table 2**: 0.2 mmol HCl is equivalent to $0.06 \text{ mmol H}_3\text{PW}_{12}\text{O}_{40}$, and $0.06 \text{ mmol H}_3\text{PW}_{12}\text{O}_{40}$ had higher catalytic activity). After testing the catalytic activity of $\text{H}_3\text{PW}_{12}\text{O}_{40}$ in six consecutive reaction cycles, the total loss of $\text{H}_3\text{PW}_{12}\text{O}_{40}$ was 8.8% of its initial loss (**Figure 3**; Tian et al., 2010). It was found that the acid catalyst $\text{H}_3\text{PW}_{12}\text{O}_{40}$ was generally stable and could be recycled



by extraction using diethyl ether. However, there was still a little loss of catalyst activity, which led to a slight decrease in the yield of TRS and glucose.

In 2009, Shimizu et al. studied the effects of Brønsted and Lewis acidities on the activity and selectivity of HPA catalysts for hydrolysis of cellulose (Furukawa et al., 2009). The authors also reported that HPAs (i.e., $H_3PW_{12}O_{40}$ and $H_4SiW_{12}O_{40}$) could catalyze the hydrolysis of cellulose with high selectivity to glucose. It was concluded that for Brønsted acid catalysts, the activity increases with the decrease in the deprotonation enthalpies (DPE, for the description of the acid strength of HPAs) (Macht et al., 2008; Shimizu and Satsuma, 2011), indicating that stronger Brønsted acidity is more beneficial to the hydrolysis of cellulose (The effect of DPE on catalysts activity shown in **Figure 4**). In other words, stronger Brønsted acid is more beneficial to the hydrolysis of β -1,4 glucosidic bonds of cellulose. More interestingly, the obtained catalyst

rates are higher for moderate Lewis acidity, while the catalysts with moderate Lewis acidity have higher TOFs for glucose production than $H_3PW_{12}O_{40}$ (**Figure 5**). Therefore, the Brønsted and Lewis acidities of HPA catalysts can influence the hydrolysis of cellulose. Moreover, with the increase of the catalyst dosage, the yield of glucose increased, which is due to the increase in the number of catalytic active sites. As shown in **Figure 4**, the lower DPE corresponds to stronger acidity of the catalysts, which is responsible for higher catalytic activity, with the TRS yield in the order of $H_4SiW_{12}O_{40} > H_3PW_{12}O_{40} > HClO_4 > H_2SO_4 > H_3PO_4$.

Ogasawara et al. found that the highly negatively charged HPAs (e.g., $H_5BW_{12}O_{40}$, $H_5AlW_{12}O_{40}$, and $H_5GaW_{12}O_{40}$) could efficiently promote the hydrolysis of crystalline cellulose into glucose in concentrated aqueous solutions (Ogasawara et al., 2011). In particular, $H_5BW_{12}O_{40}$ showed a superior yield of glucose (77%) for 48 h in 0.7 mol/L cellulose solution at a

TABLE 2 | Hydrolysis of cellulose with different acid catalysts (Tian et al., 2010).

Catalyst (mmol)	Conversion (%)	TRS yield (%)	Glucose yield (%)	Selectivity (%)
None	0	0	0	0
HCl (0.20 mmol)	25.6	25.3	13.8	53.9
H ₃ PW ₁₂ O ₄₀ (0.01 mmol)	10.4	10.4	8.2	78.8
H ₃ PW ₁₂ O ₄₀ (0.02 mmol)	17.1	16.7	13.8	80.7
H ₃ PW ₁₂ O ₄₀ (0.03 mmol)	23.0	22.1	20.9	90.7
H ₃ PW ₁₂ O ₄₀ (0.05 mmol)	29.7	28.4	26.5	89.2
H ₃ PW ₁₂ O ₄₀ (0.05 mmol)	33.2	32.8	30.7	92.5
H ₃ PW ₁₂ O ₄₀ (0.06 mmol)	38.5	38.5	36.6	95.1
H ₃ PW ₁₂ O ₄₀ (0.07 mmol)	44.0	43.8	41.8	95.0
H ₃ PW ₁₂ O ₄₀ (0.08 mmol)	54.7	54	50.5	92.3
H ₃ PW ₁₂ O ₄₀ (0.09 mmol)	57.4	56.3	51.9	90.4

TRS, total reducing sugars. Reaction conditions: 0.1 g cellulose, 5 mL water, at 180°C for 2 h.

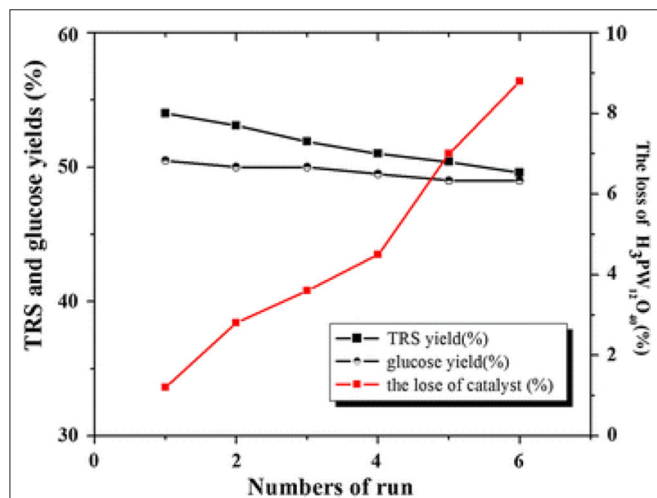


FIGURE 3 | The recyclability of H₃PW₁₂O₄₀ in six consecutive reaction cycles. Reaction conditions: 0.1 g cellulose, 0.08 mmol catalyst, 5 mL water at 180°C for 2 h. Reproduced with permission from Tian et al. (2010).

lower reaction temperature (60°C), which avoided the formation of undesirable byproducts such as humic substances and dehydration products. And its performance is much better than the commonly utilized mineral acids and HPAs, such as H₂SO₄, HCl, H₃PW₁₂O₄₀, and H₄SiW₁₂O₄₀ (Table 3). Procedures for saccharification contains two important points: turning the acidity of catalysts and decreasing the crystallinity of cellulose by breaking intermolecular hydrogen bonding that can be achieved by concentrated H₅BW₁₂O₄₀ aqueous solutions (0.70 mol/L). Besides crystalline cellulose, the present system was suitable for the selective transformation of cellobiose and starch into glucose with a good yield of 82 and 85%, respectively (Scheme 8). Also, H₅BW₁₂O₄₀ and saccharide can be completely separated from aqueous reaction solutions by extraction using alcoholic solvents due to their different solubility. And the retrieved highly negatively charged HPA H₅BW₁₂O₄₀ can be used repeatedly at

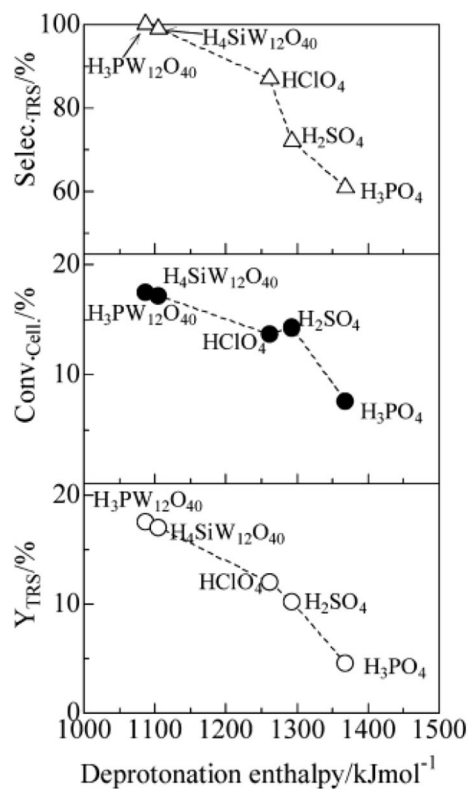


FIGURE 4 | The effect of deprotonation enthalpy (DPE) of acid catalysts on catalysts activity (○, TRS yield; ●, cellulose conversion; △, TRS selectivity of cellulose hydrolysis). Reaction conditions: 0.58 mmol cellulose, 6 mL H₂O, 6 mol catalyst (M_{n/3}PW₁₂O₄₀) at 150°C for 2 h. Reproduced with permission from Macht et al. (2008) and Shimizu and Satsuma (2011).

least ten times without significant performance loss (Figure 6; Ogasawara et al., 2011).

For the conversion pathways, the HPAs can initially hydrolyze cellulose into glucose that can be further converted into other substance in the assistance of their bifunctional properties (i.e., acidity and redox property), such as catalytic oxidation of cellulose to formic acid (Wölfel et al., 2011; Albert et al., 2012, 2014; Gromov et al., 2016; Lu et al., 2016), direct conversion of cellulose to glycolic acid (Zhang et al., 2012), and cellulose transformation into methyl glucosides (Scheme 9; Zheng et al., 2018).

Cellulose Conversion to Formic Acid

Conversion of cellulose to formic acid using HPAs as catalysts is an efficient and environmentally friendly catalytic system (Lu et al., 2016). This conversion system involves two stages (Scheme 10): (1) acid-catalyzed the hydrolysis of cellulose into glucose, and (2) oxidation of glucose to formic acid with an oxidizer (C-C bond in glucose is oxidized and cracked by HPA catalysts) (Albert et al., 2014; Gromov et al., 2016).

In 2014, different Keggin-type HPAs H_{3+n}[PV_nMo_{12-n}O₄₀] (*n* = 0–6) were synthesized, and the optimized HPA catalyst

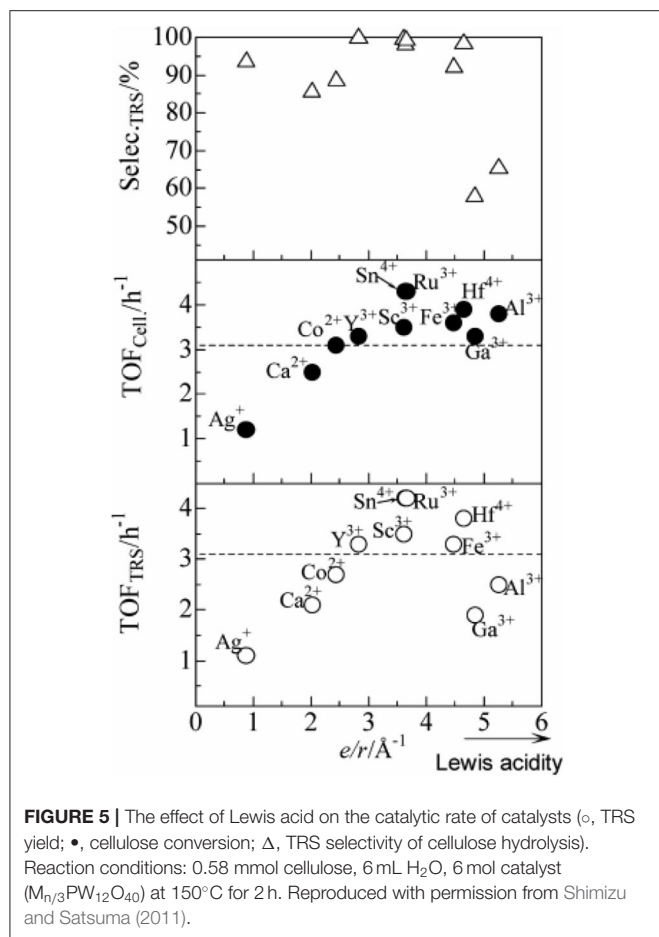


FIGURE 5 | The effect of Lewis acid on the catalytic rate of catalysts (○, TRS yield; ●, cellulose conversion; △, TRS selectivity of cellulose hydrolysis). Reaction conditions: 0.58 mmol cellulose, 6 mL H₂O, 6 mol catalyst (M_{n/3}PW₁₂O₄₀) at 150°C for 2 h. Reproduced with permission from Shimizu and Satsuma (2011).

system H₈[PV₅Mo₇O₄₀] could selectively oxidize biomass to formic acid (Albert et al., 2014). The whole reaction mechanism was divided into three steps: acid-assisted hydrolysis of the insoluble substrate, oxidative cleavage of C–C bonds in the substrate, and re-oxidation of the *in situ* reduced HPA catalyst by molecular oxygen. The acid catalyst redox cycle is shown in **Scheme 11**. Albert et al. also confirmed that the HPA catalysts screened with glucose as substrate had general reactivity, and the higher V-substituted catalysts ($n = 2-6$) showed better activities than the lower V-substituted catalysts ($n = 0-1$) (Albert et al., 2014). The comparison of the yields of glucose to formic acid under different HPA catalysts is shown in **Table 4**. Moreover, when H₅PV₂Mo₁₀O₄₀ and *p*-toluenesulfonic acid (TSA) are used as a catalyst and an additive, respectively, the conversion of cellulose was explained as a two-stage process that acid-catalyzed both cellulose hydrolysis and glucose oxidation to formic acid (Wölfel et al., 2011; Albert et al., 2014). In the system, TSA was used for the hydrolysis of cellulose, while H₅PV₂Mo₁₀O₄₀ was used for the oxidant of glucose. It is worth noting that H₈[PV₅Mo₇O₄₀] catalyst has pronounced activity for the conversion of cellulose to formic acid, but with the disadvantage of low selectivity toward formic acid.

TABLE 3 | Hydrolysis of cellulose using different concentrations of aqueous acidic solutions (Ogasawara et al., 2011).

No.	Acid catalysts	Concentration		Glucose yield (%)
		Anion (mol/L)	Proton (mol/L)	
1	H ₃ PW ₁₂ O ₄₀	0.70	2.1	8
2 ^a	H ₃ PW ₁₂ O ₄₀	0.60 ^b	3.5	18
3	H ₄ SiW ₁₂ O ₄₀	0.70	2.8	37
4 ^a	H ₄ SiW ₁₂ O ₄₀	0.70	3.5	61
5	H ₅ BW ₁₂ O ₄₀	0.70	3.5	77
6	H ₅ BW ₁₂ O ₄₀	0.40	2.0	4
7	H ₅ AlW ₁₂ O ₄₀	0.70	3.5	68
8	H ₅ GaW ₁₂ O ₄₀	0.70	3.5	62
9	H ₆ CoW ₁₂ O ₄₀	0.70	4.2	59
10	H ₂ SO ₄	1.75	3.5	<1
11	H ₂ SO ₄	4.5 ^c	9.0	5
12	HCl	3.5	3.5	4
13	HCl	6.0 ^c	6.0	9

^aThe proton concentration was adjusted using H₂SO₄.

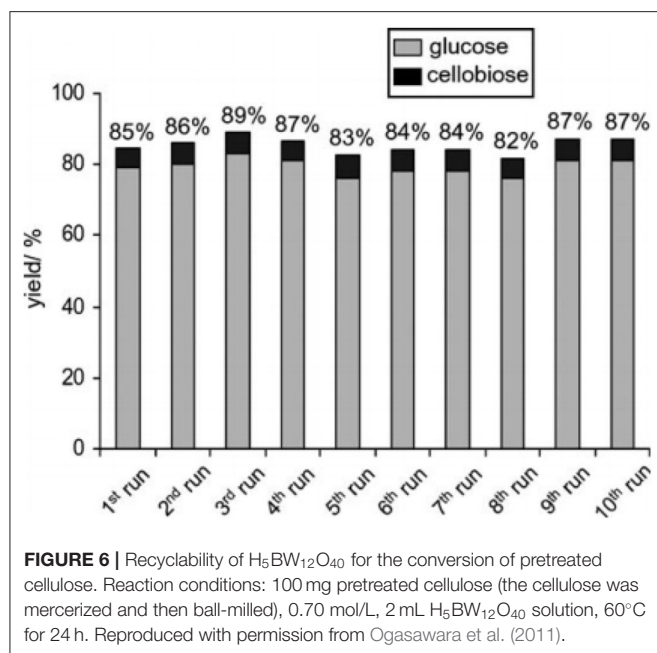
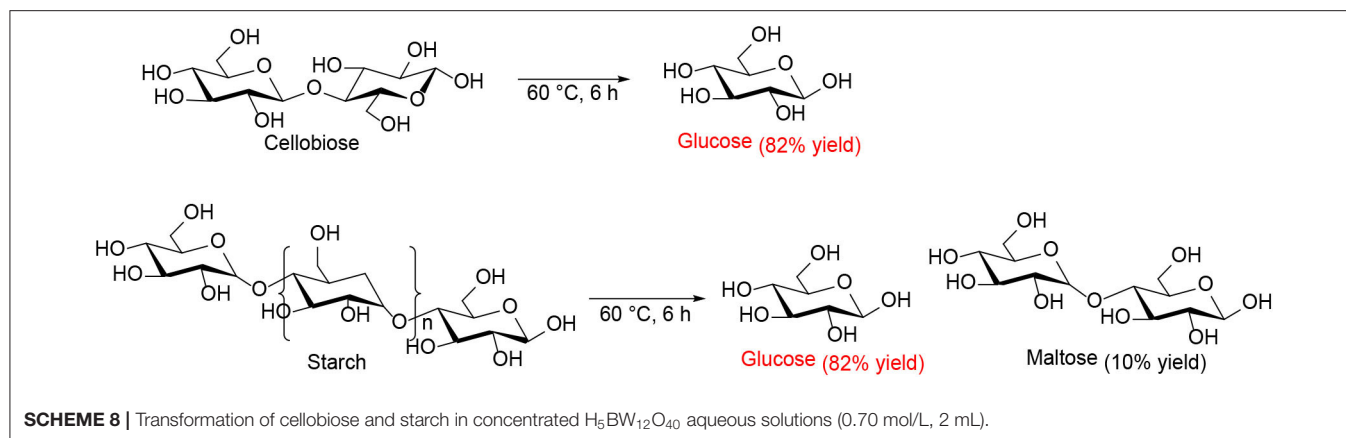
^bSaturated concentration.

^cThe same as that of the H₅BW₁₂O₄₀ solution (0.7 mol/L).

Reaction conditions: crystalline cellulose (100 mg), aqueous acidic solution (2 mL), 60°C for 48 h.

In 2016, Lu et al. found that a Keggin-type heteropoly acid catalyst H₅PV₂Mo₁₀O₄₀ with H₂SO₄ was efficient for catalytic oxidation of cellulose to formic acid with oxygen as an oxidant (Lu et al., 2016). The authors discussed the effects of the pH on the catalyst and reaction pathway by adding H₂SO₄ with variable amounts (**Table 5**). It was shown in **Figure 7** that when 1.6 wt% H₂SO₄ was added (equivalent to a significant reduction in pH), the conversion of cellulose increased from 60 to 100%, and the yield of formic acid increased from 28 to 61% in a reaction time of 5 min. It can be concluded that adding H₂SO₄ to the solution promotes the protonation of H₅PV₂Mo₁₀O₄₀. Decreasing the pH from 1.87 to 0.56 is beneficial for the catalyst protonation and can increase the oxidation potential. In summary, the H₅PV₂Mo₁₀O₄₀ + H₂SO₄ system shows a stronger catalytic impact by reducing pH than the direct use of H₅PV₂Mo₁₀O₄₀ (Lu et al., 2016).

Likewise, Gromov et al. reported the one-pot catalytic process which was applied to hydrolytic oxidation of cellulose to formic acid (Gromov et al., 2016). In their work, Mo-V-P heteropoly acid catalysts were found to be beneficial for hydrolytic oxidation of cellulose to formic acid because of their bifunctional (i.e., oxidizing and acidic) catalytic properties. The oxidizing and acidic catalytic properties correspond to the conversion process of cellulose to formic acid which involves two stages: Step 1: hydrolysis of cellulose to glucose via acidic HPA sites; Step 2: The oxidation of glucose to formic acid taking place at the oxidation sites of Mo-V-P HPA (V⁵⁺) (**Scheme 12**). Therefore, cellulose was hydrolyzed and then oxidized to formic acid using the low-cost Mo-V-P HPA catalysts. Cascade hydrolysis and oxidation of cellulose to formic acid with high yields (65–66 mol%) were achieved by the single-step



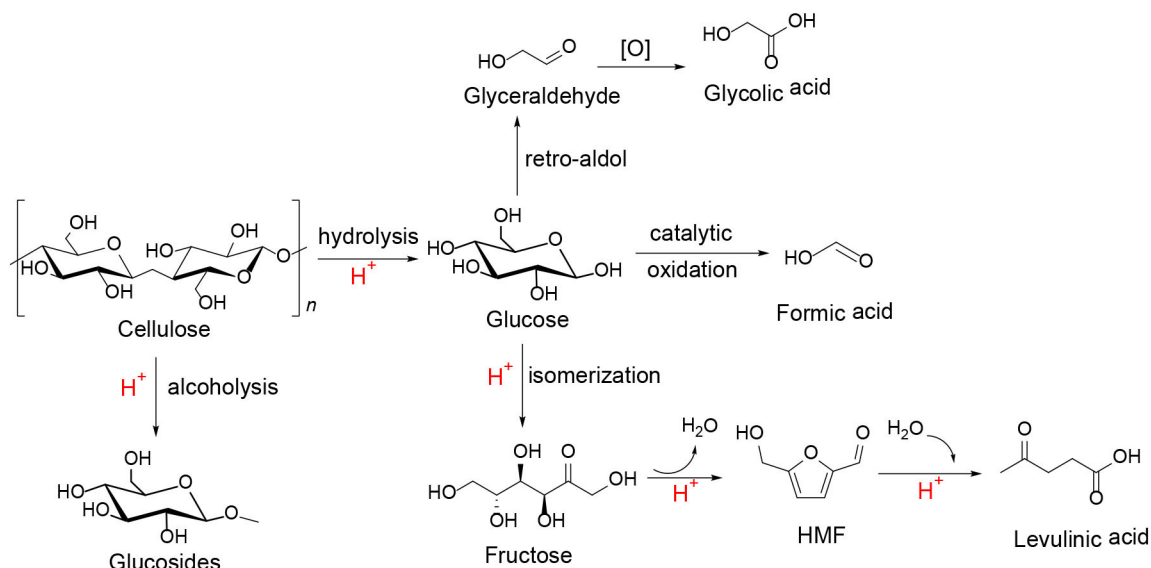
catalytic process in the presence of Mo-V-P HPA catalysts. In addition, the temperature of 150–160°C and air pressure of 10–20 Mpa (20% O_2 and 80% N_2) were found to be the optimal reaction conditions.

The Keggin-type (Mo-V-P)-HPAs were used to catalyze the hydrolysis of hemicellulose in a diluted aqueous solution that was reported by Shatalov (2019). HPAs of series $\text{H}_{(n+3)}[\text{PMo}_{(12-n)}\text{VnO}_{40}]$ used as the bifunctional catalysts were studied. For example (Mo-V-P)-HPAs-catalyzed hydrolysis of model xylan, which confirmed the established order of HPAs catalytic activity in hydrolysis reaction ($\text{H}_3\text{PMo}_{12}\text{O}_{40} > \text{H}_6[\text{PMo}_{8.9}\text{V}_{3.1}\text{O}_{40}] > \text{H}_7[\text{PMo}_{7.9}\text{V}_{4.2}\text{O}_{40}] >> \text{H}_2\text{SO}_4$). In addition (Mo-V-P)-HPAs, showed remarkable activity in both the acid-catalyzed reactions and the oxidative degradation of lignin. Therefore (Mo-V-P)-HPAs, as the green bifunctional catalysts have the potential to be an alternative to common mineral acids for selective hydrolysis and oxidative degradation of a variety of polysaccharides.

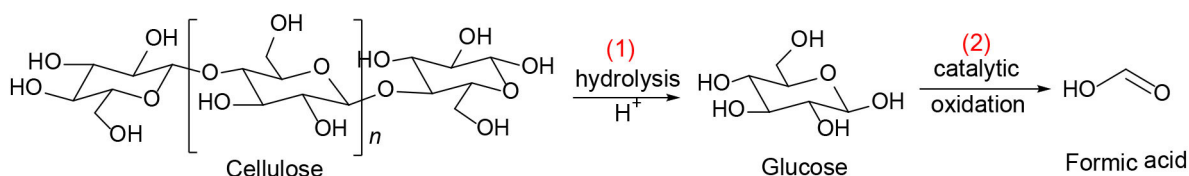
Cellulose Conversion to Other Substances

In the oxygen environment, HPAs can also catalyze cellulose being converted to glycolic acid. In 2019, Zhang et al. reported the conversion of cellulose to glycolic acid by phosphomolybdic acid catalyst (Zhang et al., 2012). In this reaction system, the heteromolybdic acid acted as multifunctional catalysts that first hydrolyzed cellulose to glucose, followed by oxidation to glycolic acid in a water medium, which combines the advantages of homogeneous and heterogeneous catalysts. The proposed reaction pathways for the conversion of cellulose to glycolic acid are shown in **Scheme 13**. Cellulose was hydrolyzed to glucose, which was converted to glycolaldehyde by the continuous retro-aldol reaction, and then to glyoxal by oxidation. Simultaneously, the isomerization of glucose produced fructose, which was converted to glycolaldehyde and formaldehyde via the retro-aldol reaction, which was then oxidized to glycolic acid and formic acid, respectively. In addition, the authors investigated the reusability of the phosphomolybdic acid catalyst in cellulose conversion (**Figure 8**). The results indicated that the catalyst exhibited constant catalytic performance. X-ray photoelectron spectroscopy (XPS) showed that the oxidation state of Mo in the heteromolybdic acid catalyst was unchanged after successive reactions (**Figure 9**). It can be concluded that Mo-containing HPAs can effectively promote the conversion of various kinds of cellulosic biomass materials to glycolic acid.

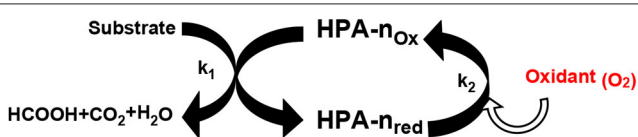
The effective alcoholysis of cellulose to monosaccharide is of great significance for fuel production. The $\text{H}_3\text{PW}_{12}\text{O}_{40}$ catalyst can promote cellulose transformation into methyl glucosides after pretreatment of microcrystalline cellulose by the ionic liquid 1-allyl-3-methylimidazolium chloride, as reported by Zheng et al. (2018). In their work, cellulose was firstly obtained by pretreatment with the ionic liquid 1-allyl-3-methylimidazolium chloride, followed by cellulose alcoholysis using $\text{H}_3\text{PW}_{12}\text{O}_{40}$ as the bifunctional catalyst. It was found that cellulose was easier to be saccharified after pretreatment by the ionic liquid. Meanwhile, prolonging the pretreatment time with the increased temperature is beneficial to the succedent alcoholysis reaction. Whereafter, the authors investigated the effects of various parameters on the alcoholysis reaction, including the alcoholizing time, the alcoholizing temperature, and different concentrations of



SCHEME 9 | Conversion of cellulose to other substance with an HPA catalyst (H^+ , HPA catalyst).



SCHEME 10 | The stages of converting cellulose into formic acid.



SCHEME 11 | The redox cycle of the catalyst $H_5PV_2Mo_{10}O_{40}$.

$H_3PW_{12}O_{40}$ catalyst. It was observed that under the optimum conditions (110°C, 60 min), the yield of methyl glucosides could be up to 70.2% with this system. Therefore, using some processes such as pretreatment of cellulose with ionic liquid can make it easier to saccharify, thus better-promoting HPA catalytic conversion of cellulose into the desired products. However, the reusability of the catalyst is not satisfactory. As shown in **Figure 10**, the activity of the $H_3PW_{12}O_{40}$ catalyst decreased gradually in the repeated experiment, indicating the low catalyst stability.

In addition, the HPA is also an important catalyst for the formation of glucose from other saccharides. In 2015, Klein et al. found that HPA can catalyze the hydrolysis of glycogen to glucose (Klein et al., 2015). Through a series

TABLE 4 | The comparison of the yields of glucose to formic acid with different HPA catalysts (Albert et al., 2014).

Catalyst	Combined yield FA + CO ₂ (%)	pH before reaction	pH after reaction	Selectivity FA + CO ₂ (%)
HPA-0	10	3.32	1.54	40 : 60
HPA-1	12	3.34	1.52	50 : 50
HPA-2	91	3.51	1.30	52 : 48
HPA-3	100	3.39	1.27	56 : 44
HPA-4	97	3.45	1.41	54 : 46
HPA-5	94	3.45	1.41	61 : 39
HPA-6	97	3.24	1.41	58 : 42
$H_9PV_{14}O_{42}$	88	3.68	1.41	58 : 42

Reaction conditions: 5.0 g (27.8 mmol) glucose and 0.8 mmol catalyst, 100.0 mL H₂O, 90°C, 8 h, 1,000 rpm. HPA- n , $H_{3+n}[PV_nMo_{12-n}O_{40}]$.

of experiments, it can be concluded that glycogen could be completely converted to glucose by using $H_3PW_{12}O_{40} \cdot nH_2O$ and $H_4SiW_{12}O_{40} \cdot nH_2O$ as the catalyst, respectively, and the optimized hydrothermal conditions are a mass fraction of catalyst 2.4%, 100°C temperature, and 2 h reaction time. In addition to hydrolysis in an autoclave, the authors also investigated

microwave irradiation and sonication heating mode for glucose synthesis (Table 6). The results showed that using $\text{H}_4\text{SiW}_{12}\text{O}_{40}$ as a catalyst, glycogen could be completely converted into glucose by the autoclave method and sonication method without other by-products, so relatively high selectivity toward glucose (>99%) was obtained using these two methods. On the other hand, when glycogen was hydrolyzed by microwave method, glycogen was completely transformed in 0.25 h, but giving by-products like levulinic acid and formic acid, which showed lower selectivity of glucose than the other two methods. More importantly, under microwave irradiation, the formation of glucose was the result of the increase of reaction temperature in the process of microwave irradiation (Klein et al., 2012). In the process

of sonochemical irradiation, the acoustic bubble collapsed at a faster speed, causing local high temperatures, thus promoting the hydrolysis of glycogen to glucose (Klein et al., 2012). Therefore, high temperature is the key factor of glycogen hydrolysis, and the HPAs are highly efficient, environmentally friendly, and

TABLE 5 | Synthesis of formic acid (FA) from cellulose at different pH (Lu et al., 2016).

Catalyst	Temp/°C	Time/h	pH	FA yield/%
HPA	90	66	1.79	9
HPA + TSA	90	66	0.91	22
HPA	170	9	1.96	3
HPA + HCl	170	9	1.87	34
HPA	180	3	1.80	45
HPA	180	1/12	1.79	28
HPA + H_2SO_4	180	1/12	0.56	61

HPA, $\text{H}_5\text{PV}_2\text{Mo}_{10}\text{O}_{40}$; TSA, *p*-toluenesulfonic acid.

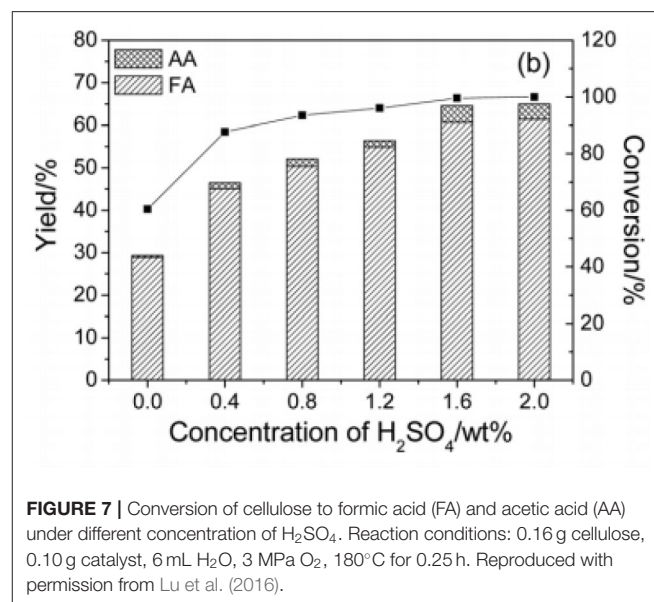
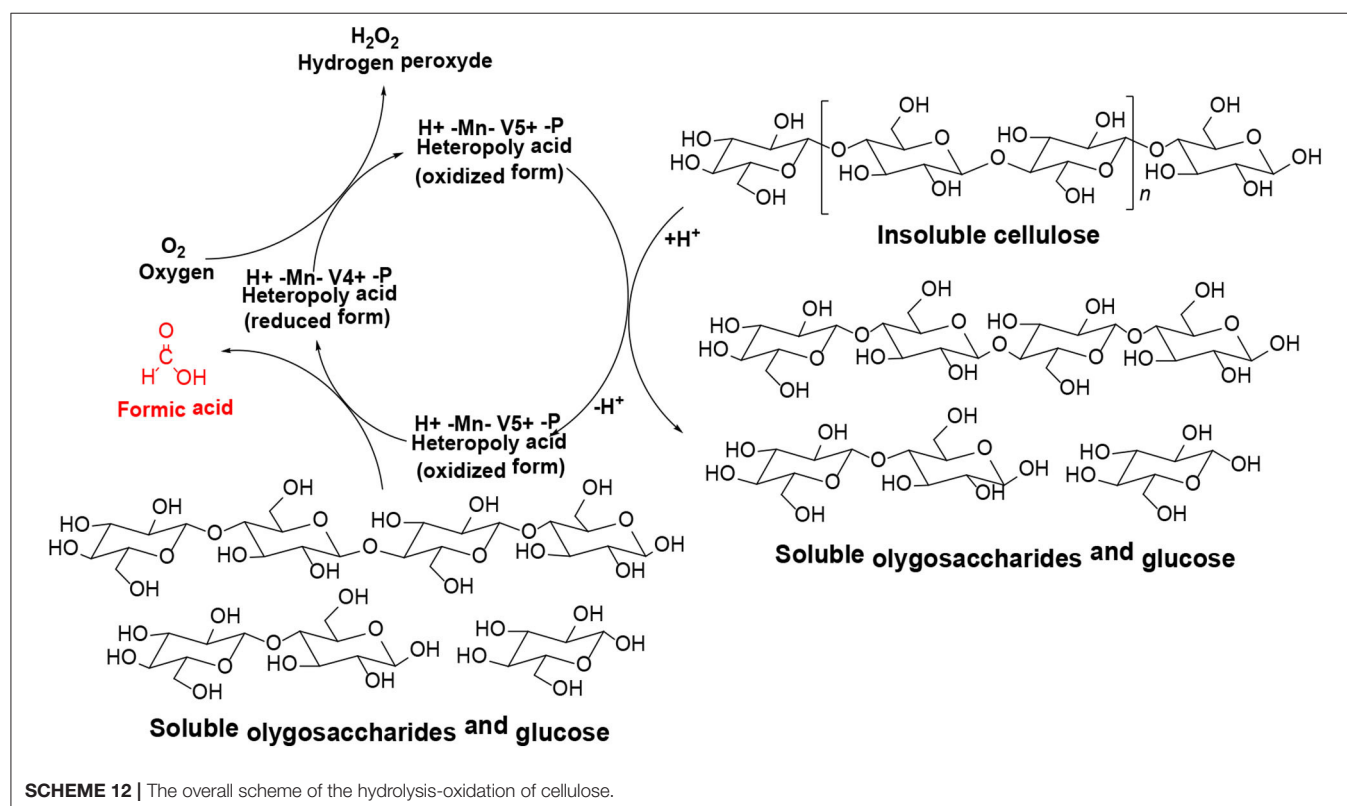
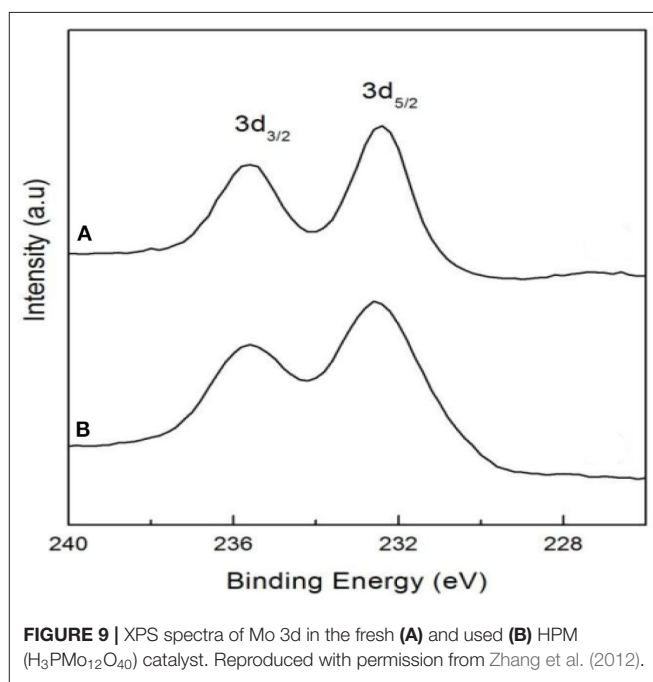
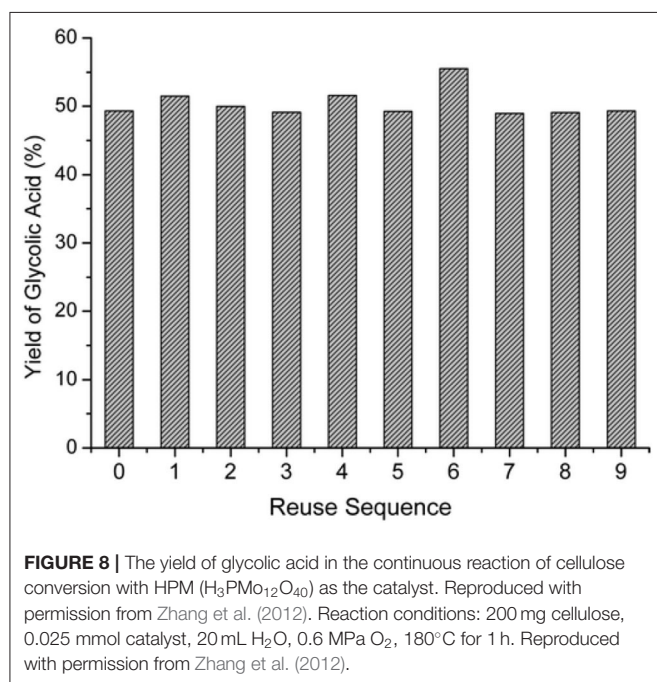
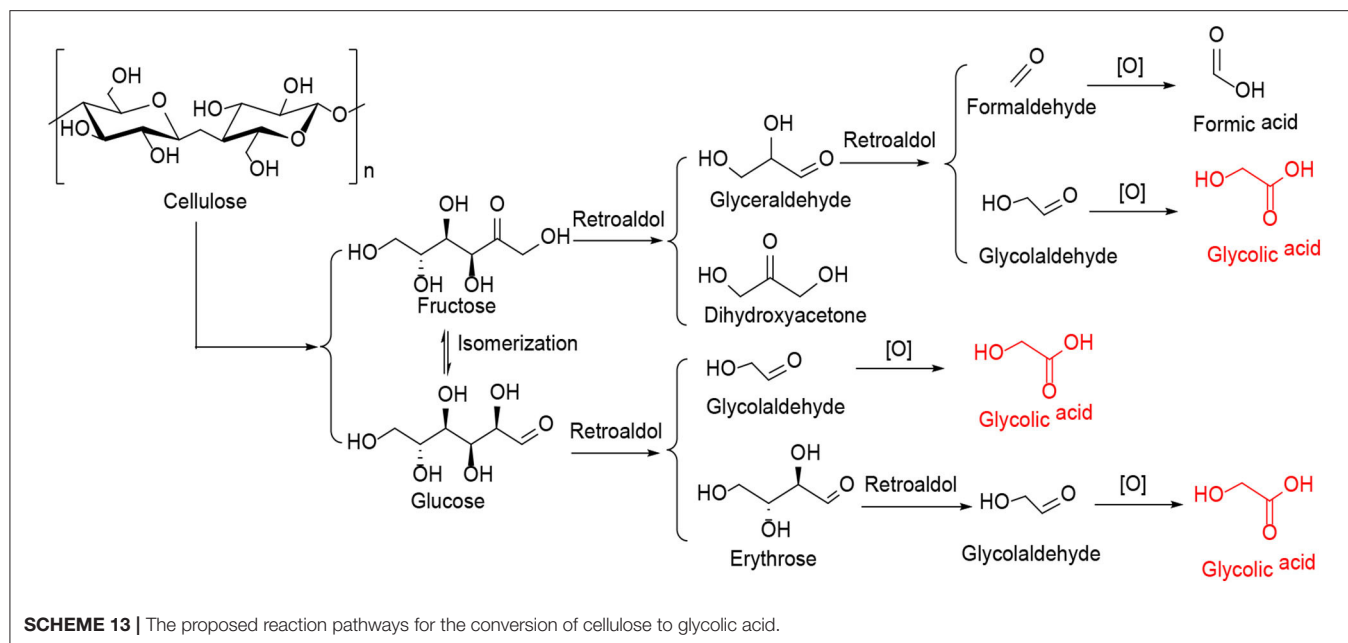


FIGURE 7 | Conversion of cellulose to formic acid (FA) and acetic acid (AA) under different concentration of H_2SO_4 . Reaction conditions: 0.16 g cellulose, 0.10 g catalyst, 6 mL H_2O , 3 MPa O_2 , 180°C for 0.25 h. Reproduced with permission from Lu et al. (2016).





reusable catalysts that can catalyze the hydrolysis of glycogen to glucose.

Substituted HPAs

Substituted HPAs are formed when H^+ ions on conventional HPAs are substituted by monovalent cations, such as Cs^+ ions. One of the typical substitutional HPAs, $\text{Cs}_x\text{H}_{3-x}\text{PW}_{12}\text{O}_{40}$ has the advantages of super acidity, microporous structure, shape selectivity, and hydrophobicity, which is conducive to the hydrolysis of cellulose (Okuhara, 2002).

Cellulose Conversion to Glucose

In 2010, Tian et al. reported hydrolysis of cellulose over the $\text{Cs}_x\text{H}_{3-x}\text{PW}_{12}\text{O}_{40}$ ($x = 1-3$) catalysts, which were active in the hydrolysis of cellulose into glucose. Notably, cellulose can be hydrolyzed to glucose in the presence of $\text{Cs}_x\text{H}_{3-x}\text{PW}_{12}\text{O}_{40}$ catalysts due to the breaking of β -1,4-glycoside bond (Scheme 14).

After a series of catalyst tests, it was found that $\text{Cs}_1\text{H}_2\text{PW}_{12}\text{O}_{40}$ showed the best catalytic performance in terms of cellulose conversion (54.0%) and glucose yield (27.2%),

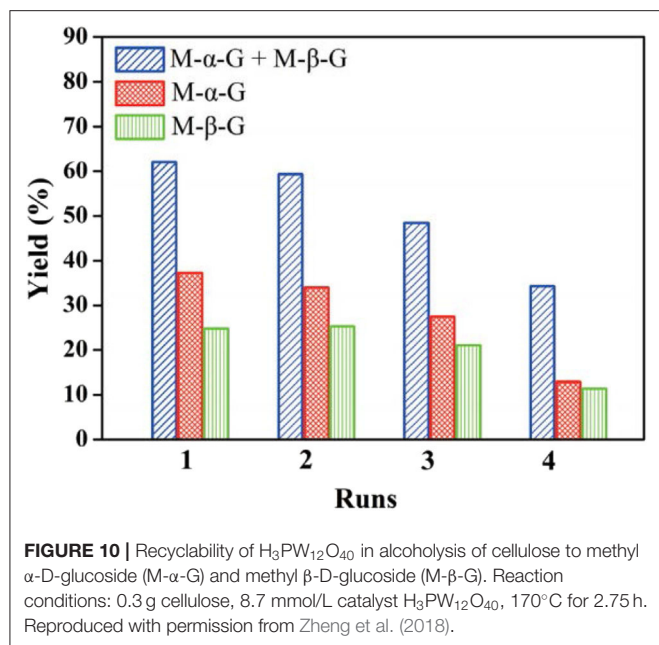


TABLE 6 | Effect of $\text{H}_4\text{SiW}_{12}\text{O}_{40}$ on glycogen hydrolysis using different methods (Klein et al., 2012).

Method	Reactant	Reaction products		
	Glycogen	Glucose	LA ^a	FA ^b
Autoclave ^c	– ^f	+ ^g	–	–
Microwave ^d	–	+	+	+
Sonication ^e	–	+	–	–

^aLA, levulinic acid.

^bFA, formic acid.

^cGlycogen: 50 mg, HSiW: 50 mg, water: 2 mL, 2 h, 100°C .

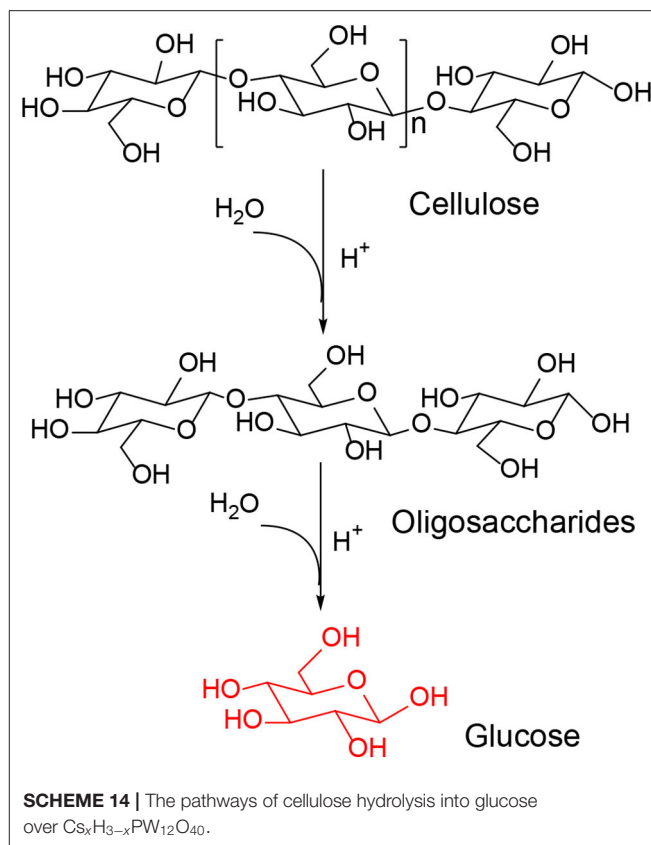
^dGlycogen: 200 mg, HSiW: 1.2 g, water: 10 mL, 0.25 h.

^eGlycogen: 250 mg, HSiW: 1.5 g, water: 10 mL, 3 h.

^f–, absent.

^g+, present.

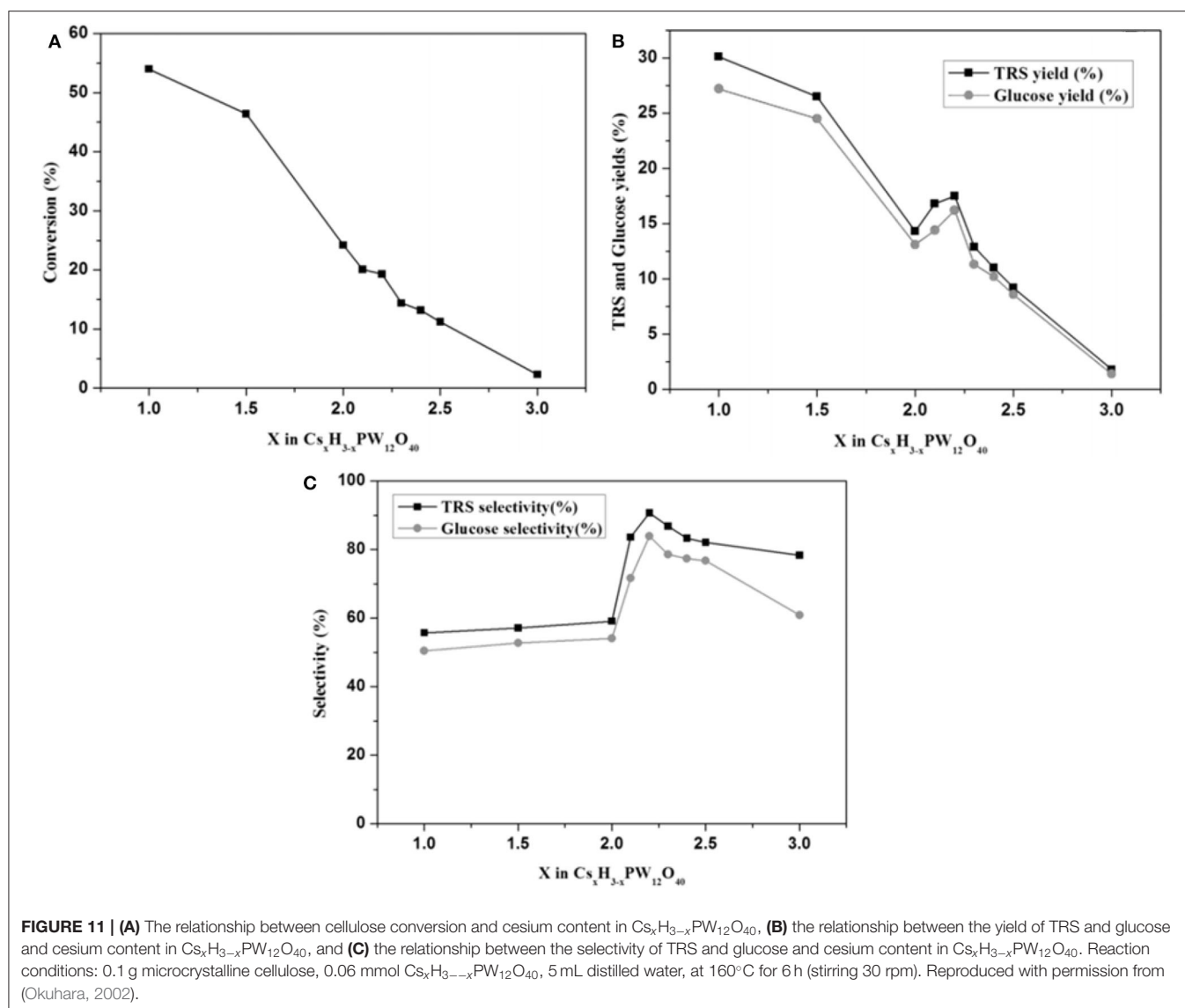
while $\text{Cs}_{2.2}\text{H}_{0.8}\text{PW}_{12}\text{O}_{40}$ showed the highest selectivity toward glucose (83.9%). The test results are shown in **Figures 11A–C**. In the meantime, they also studied the effect of $\text{Cs}_x\text{H}_{3-x}\text{PW}_{12}\text{O}_{40}$'s properties on cellulose hydrolysis. $\text{Cs}_1\text{H}_2\text{PW}_{12}\text{O}_{40}$ with the strongest protonic acid site was found to have the best catalytic performance for the hydrolysis and transformation of cellulose. However, the catalyst surface area and porous structure have little effect on the conversion of cellulose (Tian et al., 2010). Stronger Brønsted acid is more beneficial to the hydrolysis of β -1,4-glycoside bond in cellulose (Furukawa et al., 2009). It is further proved that $\text{Cs}_1\text{H}_2\text{PW}_{12}\text{O}_{40}$ with the strongest acidity is more conducive to the degradation of cellulose. When the catalyst and the unreacted cellulose were in the same reaction, the catalyst kept high activity during the hydrolysis of cellulose to TRS and glucose with the yields was 30.1 and 27.2%, respectively. Therefore, the tested acid catalyst is stable and can be reused.



Cellulose Conversion to Other Products

In 2011, Geboers et al. studied the hydrotreated cesium salts of HPAs in combination with Ru/C which can be used to degrade cellulose for the synthesis of hexitol (Geboers et al., 2011). The authors discussed the effects of calcination temperature and cesium HPAs hydrotreating conditions on cellulose conversion. The catalytic properties of several cesium HPAs were discussed and compared with conventional HPAs (**Table 7**). The synthesized cesium salts of HPAs were more active than the natural HPA salts, and their hydrolysis activity was further improved by increasing the calcination and hydrotreating temperature in the synthesis process.

As compared with their fully protonated counterparts ($\text{Cs}_{2.5}\text{PW}$ and Ru/C or $\text{Cs}_{3.5}\text{SiW}$ and Ru/C), the cesium HPAs have higher proton activity due to their higher surface acidity and hydrophobicity. After a hydrotreatment of cesium HPAs catalysts in water at 190°C was performed, the activity and selectivity of the catalysts were improved obviously due to the increase of crystallinity and hydrophobicity of samples. Finally, they found that these cesium HPAs could be completely recovered under certain conditions by a simple recrystallization method (Geboers et al., 2011). In 2011, they had studied the catalysts formed by natural HPAs in combination with Ru/C for cellulose degradation to hexitols (90%). These catalysts also had extraordinary catalytic performance, but they were difficult to recovery and reuse because of the limitation of reaction



temperature (Geboers et al., 2010). Therefore, the hydrotreated cesium salts of HPAs in combination with Ru/C are more ideal for cellulose degradation.

In 2014, Zhang et al. synthesized a series of HPA catalysts $(\text{HOCH}_2\text{CH}_2\text{N}(\text{CH}_3)_3)_x\text{H}_{3-x}\text{PW}_{12}\text{O}_{40}$ (abbreviated as Ch), which could be used as heterogeneous catalysts for degradation of cellulose to 5-hydroxymethylfurfural (HMF) (Zhang et al., 2016). By comparing several different types of acid catalysts (Figure 12), they found that the conversion of cellulose with Brønsted acid in HCl and $\text{H}_3\text{PW}_{12}\text{O}_{40}$ was 41.5 and 89.2%, respectively, while that of ChCl and $\text{Ch}_3\text{PW}_{12}\text{O}_{40}$ without Brønsted acid was 2.0 and 12.2%, respectively. So the strong Brønsted acidity of the catalyst was the necessary condition for cellulose hydrolysis. And $(\text{HOCH}_2\text{CH}_2\text{N}(\text{CH}_3)_2)_2\text{H}_2\text{PW}_{12}\text{O}_{40}$ had the highest catalytic activity among the previous catalysts. The yield

of HMF can reach 75% when cellulose was catalyzed by $(\text{HOCH}_2\text{CH}_2\text{N}(\text{CH}_3)_2)_2\text{H}_2\text{PW}_{12}\text{O}_{40}$ within 8 h at 140°C. Besides, the temperature-responsive property and high stability of the catalyst made the recovery and reuse benefit reach 10 times without obvious activity loss (Figure 13).

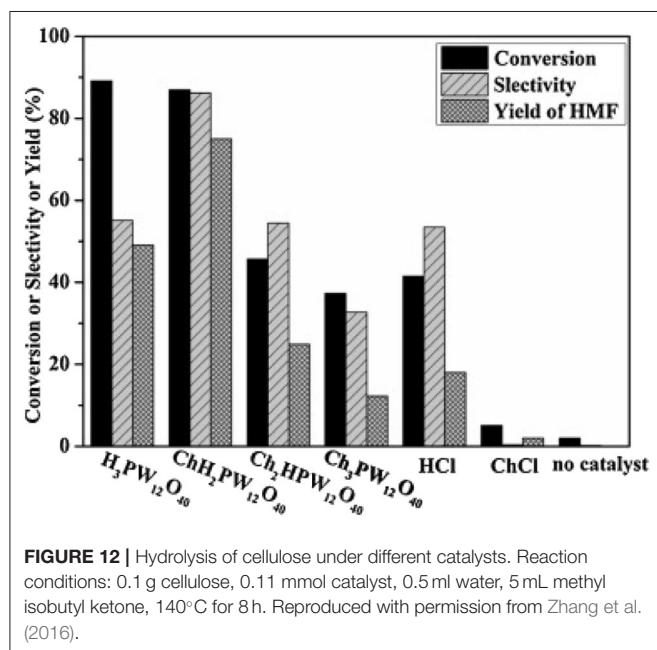
Overall, it can be seen that the substituted HPA catalysts showed high activity in the conversion of cellulose and they were stable and reusable. Therefore, the substituted HPA catalysts have good application prospects in cellulose degradation. However, the substituted HPA catalysts still suffer the disadvantage of low target product yield or selectivity, possibly due to the resistance of mass transfer.

Supported HPAs

So far, more and more attention has been paid to the supported acid catalysts, especially the supported HPAs. The

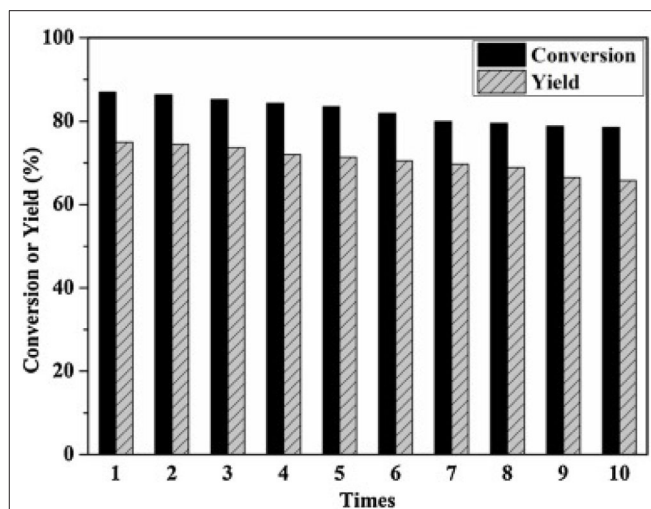
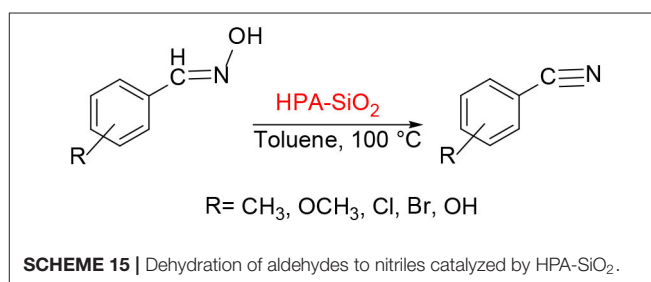
TABLE 7 | Hydrolysis and hydrogenation of cellulose with Ru/C and different HPAs at 190°C and 5 MPa H₂ (Geboers et al., 2011).

Entry	Acid catalyst	Reaction time/h	Conversion (%)	Hexitol yield
1	Cs _{3.5} SiW ₃₀₀ ^a	24	100	55
2	Cs _{3.5} SiW ₆₀₀ ^a	13	100	56
3	Cs _{2.5} PW ₃₀₀ ^a	8	91	45
4	Cs _{2.5} PW ₆₀₀ ^a	8	95	59
5	Cs _{2.5} PW ₆₀₀ ^b	11	93	46
6	H ₄ SiW ^c	24	100	18
7	H ₃ PW ^c	24	81	41

^a 1 g cellulose, 0.5 g CsHPA ([H⁺] = 1.5 mM), 0.25 g Ru/C, 50 mL water.^b 5 g cellulose, 2.5 g CsHPA ([H⁺] = 7.5 mM), Ru/C = 1.25 g, water 50 mL.^c Adjust the HPA amount to make the proton concentration consistent with CsHPA.**FIGURE 12** | Hydrolysis of cellulose under different catalysts. Reaction conditions: 0.1 g cellulose, 0.11 mmol catalyst, 0.5 mL water, 5 mL methyl isobutyl ketone, 140°C for 8 h. Reproduced with permission from Zhang et al. (2016).

dispersion of these catalysts on the support material increases the specific surface area, thus improving the catalytic activity. Some supported HPAs have been used in the degradation of cellulose. In 1981, Yusuke and Urabe found that activated carbon can encapsulate a certain amount of HPA, thus producing solid acid catalysts, which provided a convenient method for liquid phase etherification and gas-phase selective esterification of alcohols (Yusuke and Urabe, 1981). In 1989, the nuclear magnetic resonance (NMR) technology had been used in the structural research of HPAs and H₃PW₁₂O₄₀ supported on SiO₂ (Mastikhin et al., 1990).

HPAs are usually used as soluble catalysts in the liquid phase and as supported catalysts in the gas phase. From a practical point of view, it is useful to develop those supported HPA catalysts, which can be applied to a variety of reactions through fixed catalysts without leakage of HPA in the liquid, such as acylation of anisole with acetic anhydride (Bachillerbaeza and Anderson, 2004), the electrophilic substitution of phenols and

**FIGURE 13** | The recycle reaction test of catalyst. Reaction conditions: 0.1 g cellulose, 0.11 mmol ChH₂PW₁₂O₄₀, 0.5 mL water, 5 mL methyl isobutyl ketone, 140°C for 8 h. Reproduced with permission from Zhang et al. (2016).**SCHEME 15** | Dehydration of aldehydes to nitriles catalyzed by HPA-SiO₂.

aldehydes with HPA/MCM-41 (Udayakumar et al., 2007), and dehydration of aldehydes to nitriles catalyzed by silica-supported HPAs (Scheme 15; Parghi et al., 2011), and so on.

In 2007, Guo et al. studied a sol-gel co-condensation technology that can be used to prepare the green supported heteropoly acid catalysts (H₃PW₁₂O₄₀-silica), which was an efficient and reusable solid acid catalyst for the catalytic esterification of levulinic acid (LA) with phenol (Guo et al., 2007). The SBA-15 silica-supported H₃PW₁₂O₄₀ catalysts exhibited unique surface physicochemical properties, such as high porosity, larger pore size, and larger surface area (Table 8) that is attractive for the study of acid-catalyzed reactions. Figure 14 shows the nitrogen adsorption-desorption isotherms of the H₃PW₁₂O₄₀/SBA-15 catalyst, indicating a clear mesoporous structure and relatively narrow pore size distribution. It is shown in Figure 14 that all isotherms are type IV and the results show that the capillary condensation occurs at high relative pressure ($P/P_0 = 0.45-0.85$), indicating that the mesoporous structure is clear and the pore size distribution is relatively good.

In 2011, silica-supported HPA, a heterogeneous and environmentally benign catalyst was found by Parghi et al. (2011). And it was characterized by many analytical techniques. The effect of catalysts on aldosterone dehydration is shown in Table 9. The results showed that the silica-supported

TABLE 8 | Comparison of surface properties and catalytic activities of different catalysts in the esterification of levulinic acid (LA) with phenol (Guo et al., 2007).

Catalyst	$2\theta/^\circ$	$S_{BET}/m^2\ g^{-1}$	D_p^a/nm	Porosity ^b	LA conversion (%)	TOF
H ₃ PW ₁₂ O ₄₀ /SBA-15-E-4.0	0.95	691.6	7.1	1.20	23.6	6.9
H ₃ PW ₁₂ O ₄₀ /SBA-15-E-14.8	0.92	683.0	7.4	0.95	74.8	46.4
H ₃ PW ₁₂ O ₄₀ /SBA-15-E-17.5	0.90	630.4	8.6	0.91	80.1	51.0
H ₃ PW ₁₂ O ₄₀ /SBA-15-C-7.5	0.95	753.0	6.0	1.10	19.2	3.5
H ₃ PW ₁₂ O ₄₀ /SBA-15-C-11.3	0.91	713.2	6.4	0.85	72.3	48.5
H ₃ PW ₁₂ O ₄₀ /SBA-15-C-15.7	0.96	604.5	6.6	0.75	80.3	53.9
H ₃ PW ₁₂ O ₄₀ /SiO ₂ -D-15.4	—	317.6	1.2	0.34	5.3	0.65
H ₃ PW ₁₂ O ₄₀	—	5.5	—	—	60.1	1.04
HCl	—	—	—	—	65.4	0.73
SBA-15-E	0.99	858.2	5.2	0.71	0	0
SBA-15-C	0.96	750.1	5.3	0.51	0	0

^aPore diameters are estimated from BJH desorption determination.

^bThe porosity is estimated from the pore volume determined using the adsorption branch of the N₂ isotherm curve.

Reaction conditions: 3.4 mmol LA, 13.6 mmol phenol, 0.05 g catalyst, 100°C for 8 h.

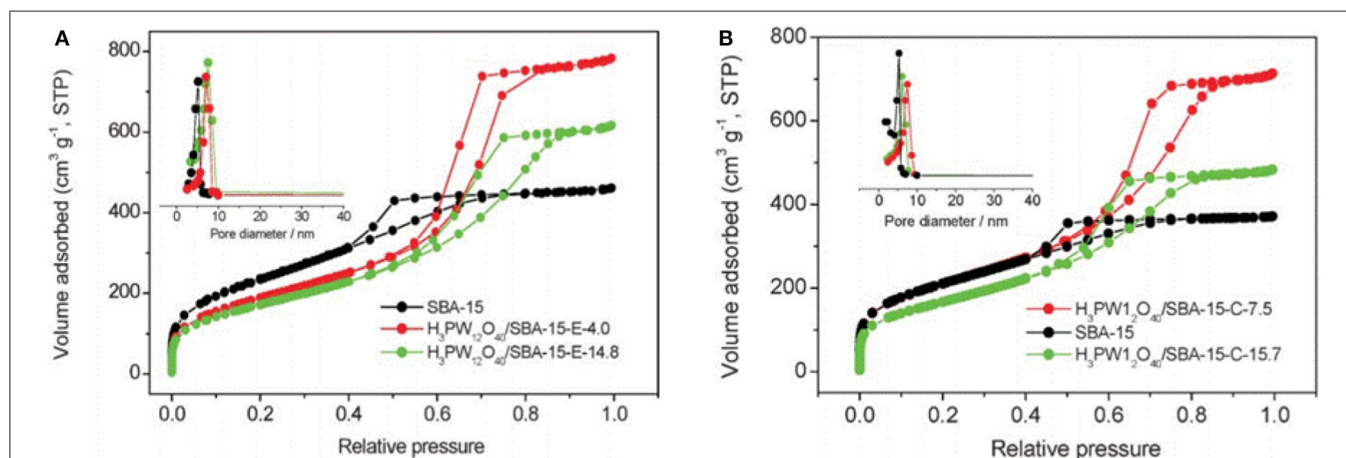


FIGURE 14 | Nitrogen adsorption-desorption isotherms and pore size distribution profiles (inset) of H₃PW₁₂O₄₀/SBA-15 materials. **(A)** Removal of H₃PW₁₂O₄₀/SBA-15 by extraction with acidic ethanol, and **(B)** removal of H₃PW₁₂O₄₀/SBA-15 by calcination at 400°C. Reproduced with permission from Guo et al. (2007).

TABLE 9 | Aldosterone dehydration with different catalysts (Parghi et al., 2011).

Entry	Catalyst	Benzonitrile yield/%
1	SiO ₂	10
2	HPW	51
3	HPW	40
4	HPW-SiO ₂	85
5	HPW-SiO ₂	72
6	—	—

Reaction condition: 2 mmol benzaldehyde oxime, catalyst (20 wt%); 3 mL toluene, 100°C for 4.5 h.

phosphotungstic acid catalyst was the most favorable catalyst for the aldosterone dehydration reaction they studied. The reusability of the catalyst was investigated, and it was found that the catalyst was stable in five consecutive recycles with benzonitrile yield slightly decreasing from 85 to 79%.

In 2012, An et al. reported on the conversion of cellulose and cellobiose by polyoxometalate-supported gold nanoparticles (An et al., 2012). The catalysts, Cs_xH_{3x}PW₁₂O₄₀ supported Au nanoparticles can convert cellulose and cellobiose into gluconic acid that is widely used in the pharmaceutical and food industry. The reaction pathways of cellulose to gluconic acid are shown in **Scheme 16**. Cellulose was first hydrolyzed to glucose, which was then oxidized to gluconic acid by oxygen. The selectivity of Au/Cs_xH_{3x}PW₁₂O₄₀ to gluconic acid was significantly higher than that of Au catalysts supported on typical metal oxides, carbon nanotubes, and zeolites (**Table 10**; An et al., 2012). The possible reasons were the acidity of polyoxometalates and the average particle size of Au nanoparticles. The strong acidity of polyoxometalates not only benefited the conversion of cellobiose but also promoted desorption to improve the selectivity of gluconic acid. And smaller Au nanoparticles expedited the oxidation of glucose to gluconic acid, thus increasing the conversion of cellobiose (**Figure 15**).

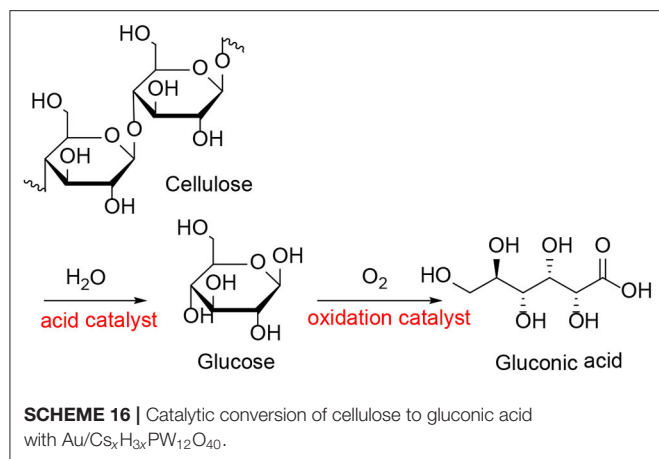


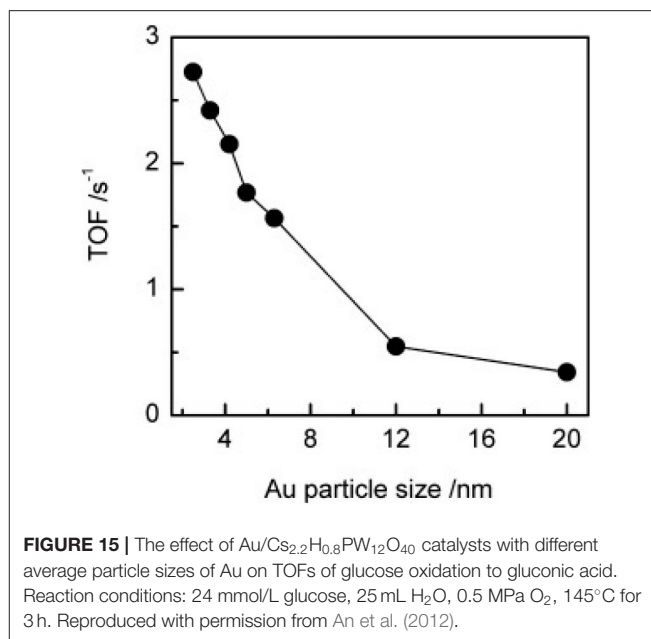
TABLE 10 | Transformation of cellobiose with different supported catalysts (An et al., 2012).

Catalyst	Conversion (%)	GA ^a selectivity (%)	GA yield (%)
Au/Cs _{1.2} H _{1.8} PW ₁₂ O ₄₀	97	>99	97
Au/Cs _{1.7} H _{1.3} PW ₁₂ O ₄₀	98	96	94
Au/Cs _{2.2} H _{0.8} PW ₁₂ O ₄₀	96	95	91
Au/Cs _{2.6} H _{0.4} PW ₁₂ O ₄₀	97	90	87
Au/Cs _{3.0} PW ₁₂ O ₄₀	95	85	81
Au/SiO ₂	67	61	41
Au/Al ₂ O ₃	95	31	29
Au/TiO ₂	96	63	60
Au/H-ZSM-5	45	76	34
Au/HY	64	62	40
Au/CNT	84	86	72

^aGA, GLUCONIC acid. Reaction conditions: 12 mmol/L cellobiose, 0.050 g catalyst (Au loading: 1.0 wt%), 25 mL H₂O, 0.5 MPa O₂, 145°C for 3 h. Reproduced with permission from An et al. (2012).

In 2012, Lanzafame et al. reported that some solid acid catalysts can convert cellulose into glucose, HMF, and other soluble by-products in 190°C aqueous solution for 5 h or <5 h (Lanzafame et al., 2012). They mainly studied supported solid acid catalysts, including sulphated zirconia supported over HPAs, which were found to effectively transform cellulose at a reaction temperature of 190°C (Figure 16). It can be seen that all the catalysts were active in the hydrolysis of cellulose to glucose. However, a significant disadvantage is that the conversion of cellulose with a solid acid catalyst produces more by-products, resulting in low glucose selectivity.

In 2014, Hafizi et al. found a unique heterogeneous silica-supported Preyssler heteropoly acid catalyst (H₁₄NaP₅W₃₀O₁₂₀), which can be used for alkylation of benzene (Hafizi et al., 2014). Preyssler HPA has the advantages of high thermal stability, high hydrolysis stability, regeneration, safety, easy separation, and so on (Bamoharram et al., 2004; Heravi et al., 2007, 2008). It combines with silica to form a supported heteropoly acid catalyst, which is active for the alkylation of benzene. In 2019, Zhang et al. developed a series of highly efficient heterogeneous catalysts



with good stability and reusability for the catalytic conversion of cellulose to glucose. A typical Keggin type HPA (H₃PW₁₂O₄₀) was immobilized on the surface and pore of carbon foam (CF) to prepare supported HPA catalyst (H₃PW₁₂O₄₀/CF) for cellulose conversion to glucose (Zhang et al., 2019). After comparing with different CFs that were prepared from damaged starch and gluten protein (*s* is the percentage of gluten protein), it was found that CF30 was considered as the best porous support material for fixing the HPW catalyst because of its higher specific surface area (Table 11). In addition, H₃PW₁₂O₄₀/CF30 catalyst had good reusability and was easy to separate and recover from the reaction system (Figure 17). It was shown that the supported catalyst could effectively catalyze the conversion of cellulose to glucose, and the supported technology could improve the catalytic performance and high-efficiency reusability of the catalyst.

Based on the studies of these supported HPA catalysts, it can be seen that the supported HPAs have a higher specific surface area than conventional HPAs. Also, the supported HPAs can be used in the heterogeneous reaction, which is more convenient for product separation and can be reused. It is worth noting that there are still some shortcomings of the catalysts, such as low selectivity of the target product and gradual decline of stability of the catalysts in recycles.

Assembled HPAs

In recent years, people began to explore new efficient catalysts for cellulose conversion. The assembled HPA catalysts have also become one of the research directions. It is noteworthy that the assembled HPA catalysts were studied for the degradation of cellulose in biomass and other valuable catalytic reactions. For example, in 2010, Wee et al. proposed a simple and highly repetitive synthesis method for the assembly of

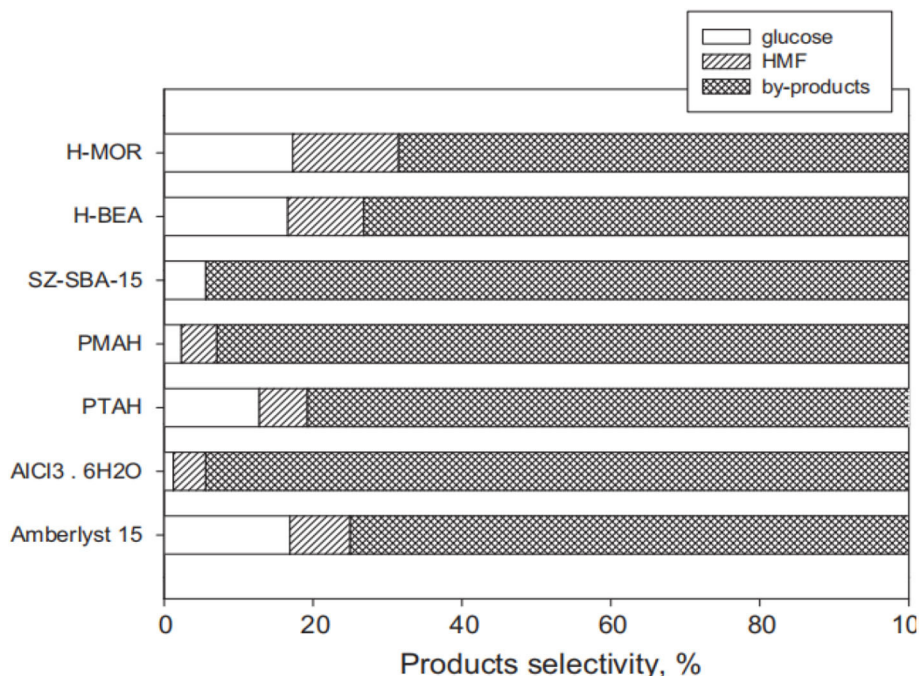


FIGURE 16 | Activity comparison of different solid acid catalysts for cellulose conversion. Reaction conditions: 2 g cellulose, 0.2 g catalyst, 55 mL distilled water, 190°C for 5 h. Reproduced with permission from Lanzafame et al. (2012).

TABLE 11 | Selected properties of different catalysts (Zhang et al., 2019).

Sample	Compressive strength (MPa)	Specific surface area (m ² g ⁻¹)	Pore volume (cm ³ g ⁻¹)	Mean pore size (nm)
CF0	—	201.2	0.208	9.72
CF10	0.096	225.6	0.221	7.95
CF20	0.126	253.9	0.232	4.36
CF30	0.147	302.5	0.259	4.03
CF40	0.146	255.2	0.242	3.65
Original HPW/CF30	0.148	200.9	0.222	3.73
Reused HPW/CF30	0.140	221.9	0.223	2.01

nanomaterial catalyst H₃PW₁₂O₄₀/Cu₃(BTC)₂ (BTC = benzene tricarboxylic acid). Cu₃(BTC)₂ was encapsulated into Keggin HPA H₃PW₁₂O₄₀ for application in catalysis (Wee et al., 2010). And this assembled HPA nanomaterial catalyst can be used in acid-catalyzed esterification (Figure 18).

In 2011, Cheng et al. reported that a micellar HPA catalyst [C₁₆H₃₃N(CH₃)₃]H₂PW₁₂O₄₀ (C₁₆H₂PW) was designed to hydrolyze cellulose and starch into glucose. The micellar HPA catalyst can allow cellulose molecules to enter into the catalytic sites, so as to improve the reaction rate and cellulose conversion rate (Dwars et al., 2005; Cheng et al., 2011). As a heterogeneous catalyst [C₁₆H₃₃N(CH₃)₃]H₂PW₁₂O₄₀ exhibited remarkable catalytic performance for cellulose degradation, and the yield and selectivity of glucose were 39.3 and 89.1% respectively (Table 12).

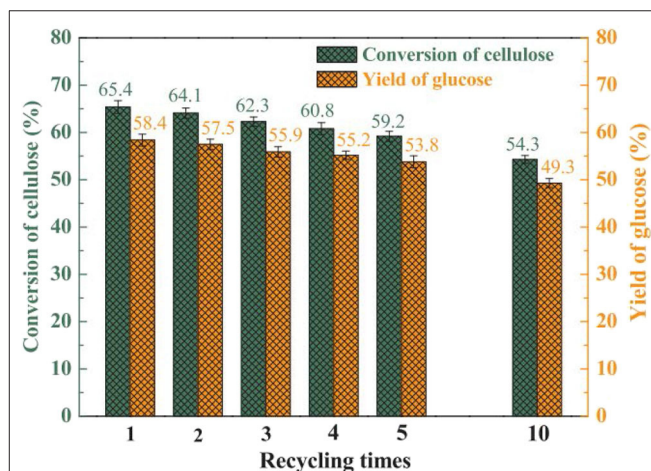


FIGURE 17 | Reusability test of the HPW/CF30 catalyst for cellulose hydrolysis. Reaction conditions: 0.1 g MAMCC (mechanical activation microcrystalline cellulose), 1.0 g HPW/CF30, 10 mL H₂O, 170°C for 9 h. Reproduced with permission from Zhang et al. (2019).

In addition, the catalyst was easily recovered by centrifuge and had good reusability (Figure 19). Therefore, the heterogeneous micelle HPA catalyst is a clean, economical and environmentally friendly catalyst for hydrolysis of cellulose.

In 2012, Sun et al. investigated a kind of HPA-ionic liquid catalysts [C₄H₆N₂(CH₂)₃SO₃H]_{3-n}H_nPW₁₂O₄₀ (*n* = 1, 2, 3) (abbreviated as [MIMPSH]_{*n*}H_{32*n*}PW), which can be used to

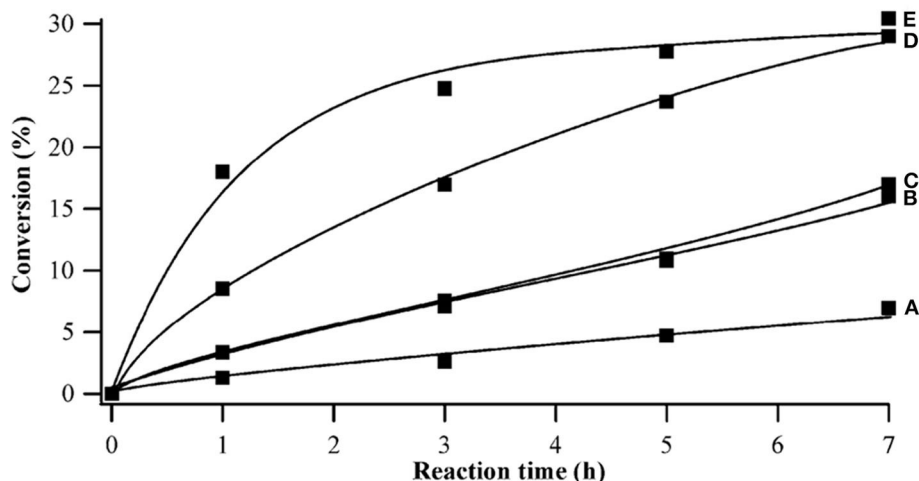


FIGURE 18 | Effect of catalysts on conversion of acetic acid in esterification. Catalysts: **(A)** without catalyst, **(B)** micron-sized HPW/Cu₃(BTC)₂, **(C)** ultrastable Y zeolite (CBV 720), **(D)** 65 nm HPW/Cu₃(BTC)₂, and **(E)** 50 nm HPW/Cu₃(BTC)₂. Reaction conditions: 1 mol acetic acid, 40 mol 1-propanol, 2.23 wt% catalyst, 60°C. Reproduced with permission from Wee et al. (2010).

TABLE 12 | Hydrolysis of cellulose over different catalysts (Cheng et al., 2011).

Catalyst (mmol)	Reaction time (h)	Amount of water (mL)	Cellulose conversion (%)	TRS yield (%)	Glucose yield (%)	Glucose selectivity (%)	TOF (g mmol ⁻¹ h ⁻¹)
CTAB (0.07)	8	7	0	0	0	0	0
H ₃ PW ₁₂ O ₄₀ (0.07)	5	5	70.4	68.1	59.9	85.1	0.201
Cs _{2.5} H _{0.5} PW (0.07)	6	5	23.7	22.2	21.3	89.9	0.056
C ₁₆ H ₂ PW (0.08)	8	7	45.7	36.3	35.1	76.8	0.071
C ₁₆ H ₂ PW (0.07)	8	8	43.7	35.7	34.2	78.3	0.078
C ₁₆ H ₂ PW (0.07)	8	7	44.1	40.2	39.3	89.1	0.079
C ₁₆ H ₂ PW (0.07)	8	6	42.6	40.5	37.0	86.9	0.076
C ₁₆ H ₂ PW (0.07)	8	5	39.3	34.4	33.5	85.2	0.070
C ₁₆ H ₂ PW (0.07)	8	4	34.7	30.7	29.3	84.4	0.062
C ₁₆ H ₂ PW (0.06)	8	7	42.8	38.5	37.6	87.9	0.089
C ₁₆ H ₂ PW (0.05)	8	7	37.4	31.3	30.2	80.7	0.093

Reaction conditions: 0.1 g cellulose, 170°C. Reproduced with permission from Cheng et al. (2011).

degrade cellulose into water-soluble products such as glucose and levulinic acid (Sun et al., 2012). Glucose was the main product of hydrolysis of cellulose by the HPA-based on the ionic liquid catalyst, and the conversion of cellulose and the yield of glucose was 55.1 and 36.0%, respectively at 140°C for 5 h in a biphasic system (water–MIBK). Compared with the previously reported HPA catalysts, such as H₃PW₁₂O₄₀ and Cs_{2.5}H_{0.5}PW₁₁₂O₄₀, the assembled catalyst showed much better catalytic performance because of its better solubility in water (Table 13). Moreover, the HPA-ionic liquids catalyst can also depolymerize other polysaccharides, from which high yields of glucose can be obtained (Scheme 17). More importantly, the HPA-ionic liquids catalyst can be completely recovered and reused six times without significant performance loss (Figure 20).

In 2013, Chen et al. synthesized the polyvinylpyrrolidone-stabilized heteropolyacids (PVP–HPAs), a kind of reusable

self-assembling catalysts for conversion of cellulose (Chen et al., 2013). A model for the synthesis of PVP–HPAs is shown in Scheme 18 and the alcoholysis diagram of cellulose is shown in Scheme 19. First, cellobiose alcoholysis, then dehydration between glucose and alcohol molecules, and final interconversion between β-alkylglucoside and α-alkylglucoside gives the product. The authors used a variety of characteristic techniques (e.g., FT-IR and Solid MAS ¹H-NMR) to study the structure of the self-assembling catalysts (Figures 21A,B), and they found that HPAs can protonate PVP and the protonated PVP can form the structure similar to the ionic liquid and interact with heteropolyanion (Chen et al., 2013). Moreover, the structure of PVP assembled with HPA contributes to the easy separation and reuse of catalysts. After optimizing the content of PVP and HPA, the results showed that the self-assembling catalyst PVP–H₄SiW₁₂O₄₀·0.5H₂O (1/5:3/4) had excellent catalytic performance

for the alcoholization of cellulose, and the conversion of cellulose was more than 60% (Chen et al., 2013). The application of the self-assembled catalyst is expected to expand to other reactions.

In 2015, Sun et al. synthesized an assembled HPA catalyst $[\text{C}_{16}\text{H}_{33}\text{N}(\text{CH}_3)_3]_x\text{H}_{6-x}\text{P}_2\text{W}_{18}\text{O}_{62}$ (abbreviated as $(\text{C}_{16}\text{TA})_n\text{H}_{6-n}\text{P}_2\text{W}_{18}\text{O}_{62}$). Wells–Dawson heteropolyacid

$\text{H}_6\text{P}_2\text{W}_{18}\text{O}_{62}$ was used to synthesize the micellar assembly catalyst, which can catalyze the hydrolysis of cellulose to glucose (Sun et al., 2015). The mechanism of cellulose conversion by $(\text{C}_{16}\text{TA})_n\text{H}_{6-n}\text{P}_2\text{W}_{18}\text{O}_{62}$ catalysts is shown in **Scheme 20**. The micelle catalyst first partially hydrolyzes cellulose to the oligomer, and then further degrades cellulose to glucose. Meanwhile, this catalyst can also promote the conversion of other polysaccharides, such as starch and cellobiose (Sun et al., 2015). The $(\text{C}_{16}\text{TA})\text{H}_5\text{P}_2\text{W}_{18}\text{O}_{62}$ ($n = 1$) catalyst exhibited higher catalytic activity than ordinary Keggin heteropoly acid catalyst $\text{H}_3\text{PW}_{12}\text{O}_{40}$ (Table 14).

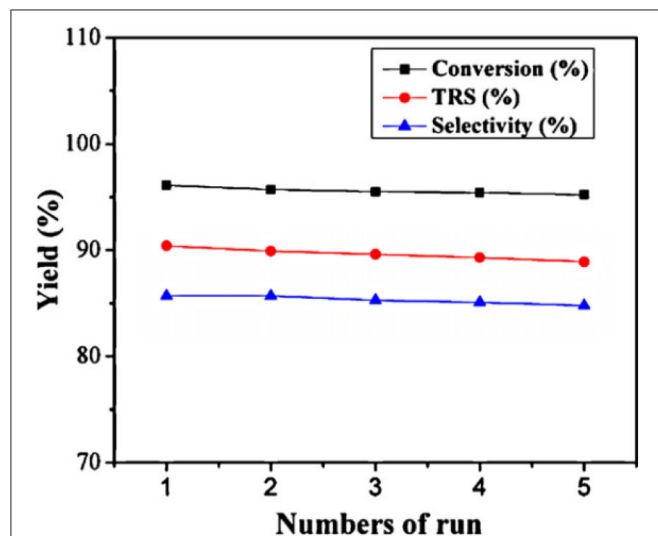


FIGURE 19 | Recycling test of the $[\text{C}_{16}\text{H}_{33}\text{N}(\text{CH}_3)_3]\text{H}_2\text{PW}_{12}\text{O}_{40}$ catalyst. Reaction conditions: 0.1 g cellulose, 0.07 mmol catalyst, 7 mL water, 170°C for 8 h. Reproduced with permission from Cheng et al. (2011).

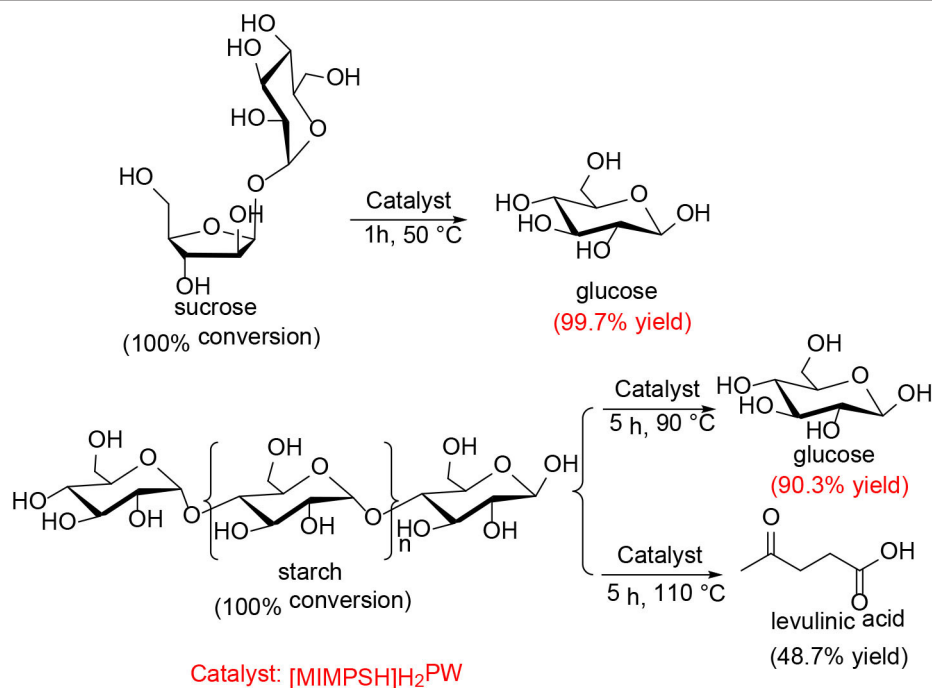
TABLE 13 | Hydrolysis of cellulose with different catalysts^a (Sun et al., 2012).

Catalyst	Conversion/%	TRS yield/%	Glucose yield (%)	TOF/g mmol ⁻¹
MIMPSH	0	0	0	0
$\text{H}_3\text{PW}_{12}\text{O}_{40}$	54.1	31.6	27.0	0.12
$\text{H}_3\text{PW}_{12}\text{O}_{40} + \text{IL}^b$	57.3	33.8	27.1	0.12
$[\text{MIMPSH}]\text{H}_2\text{PW}$	55.1 ± 1.7	40.2 ± 1.7	36.0 ± 2.6	0.17
$[\text{MIMPSH}]\text{H}_2\text{PW}^c$	13.1 ± 1.6	9.6 ± 2.0	8.4 ± 2.3	0.14
$[\text{MIMPSH}]\text{H}_2\text{PW}$	42.7 ± 1.3	35.9 ± 1.9	27.3 ± 1.8	0.13
$[\text{MIMPSH}]\text{H}_3\text{PW}$	28.4 ± 1.4	25.2 ± 1.5	23.2 ± 2.5	0.11
$\text{Cs}_{2.5}\text{H}_{0.5}\text{PW}_{12}\text{O}_{40}$	12.3	10.0	8.1	

^aReaction conditions: 0.1 g cellulose, 0.07 mmol catalyst, 0.5 mL water and 5 mL MIBK (methyl isobutyl ketone) at 140°C for 5 h.

^b0.07 mmol $\text{H}_3\text{PW}_{12}\text{O}_{40}$ and 0.07 mmol IL as the catalyst.

^cNo MIBK, just 5.5 mL water. Reproduced with permission from Sun et al. (2012).



SCHEME 17 | Conversion of other polysaccharides over the $[\text{MIMPSH}]\text{H}_2\text{PW}$ catalyst. Reaction conditions: 0.077 mmol catalyst, 0.5 mL water, and 5.0 mL MIBK.

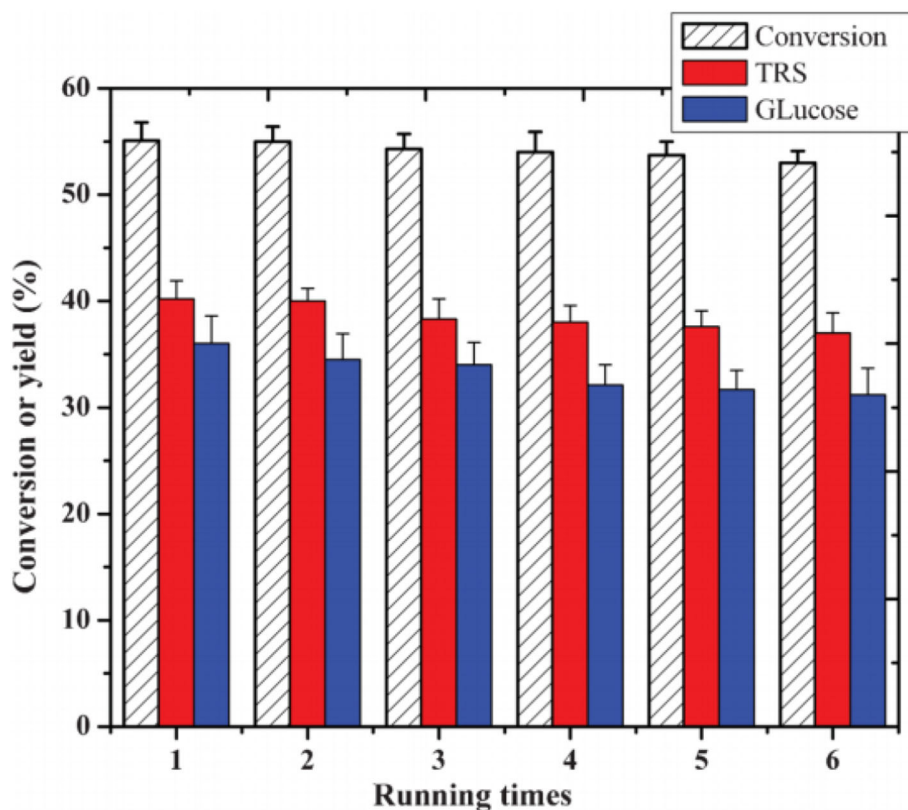
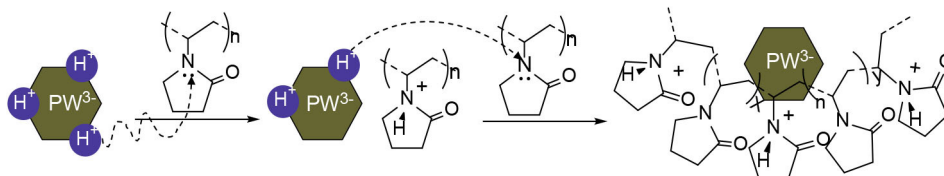


FIGURE 20 | Reusability test of the [MIMPSH]-H₂PW catalyst. Reaction conditions: 0.1 g cellulose, 0.07 mmol catalyst, 0.5 mL H₂O, 5 mL MIBK, 140°C for 5 h. Reproduced with permission from Sun et al. (2012).



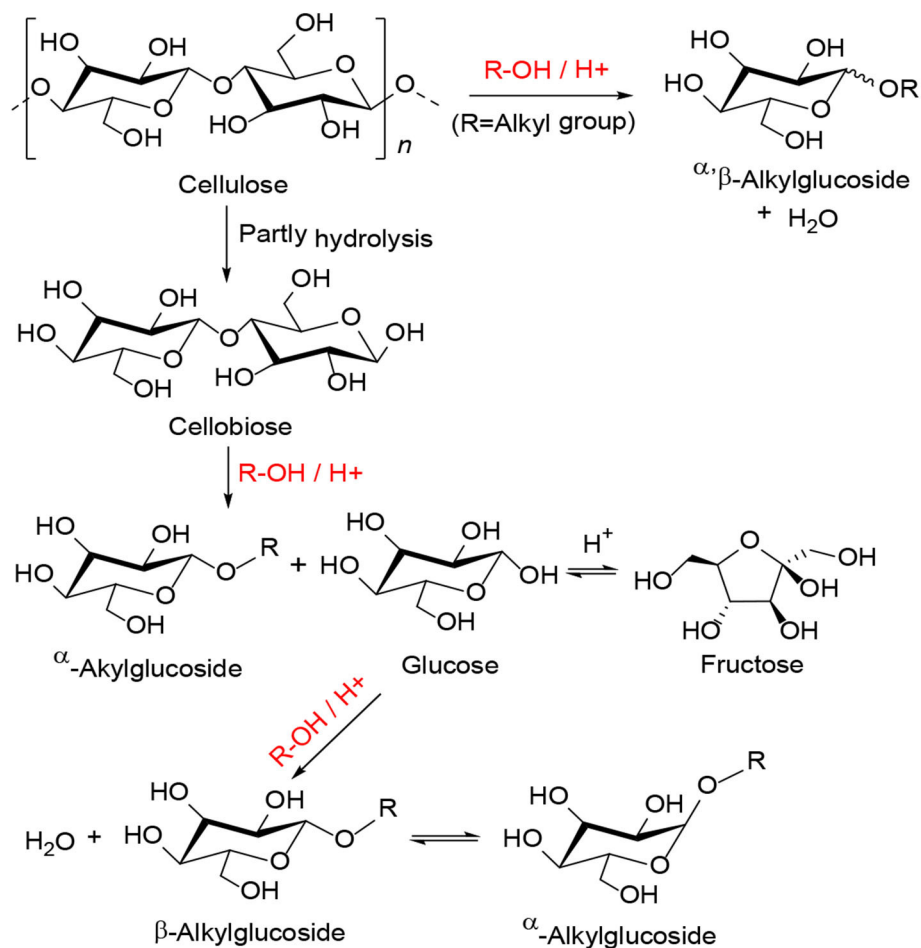
SCHEME 18 | Synthetic routes to PVP-HPAs model.

Sun et al. found that the high catalytic activity of the catalyst was due to the interaction of a high concentration of acid sites, which provided more opportunities for the substrate to enter the catalytic sites and the oxidation ability of (C₁₆TA)_nH_{6-n}P₂W₁₈O₆₂ (Sun et al., 2015). Moreover, this micellar assembled HPA catalyst was used as a heterogeneous catalyst and recycled by simple centrifuge (Figure 22).

Lu et al. prepared heterogeneous catalysts (C_nH_{2n+1}N(CH₃)₃)H₄PW₁₁TiO₄₀ ($n = 4, 8, 12, 14, 16$, and 18) composed of HPAs and amphiphilic quaternary ammonium salt by self-assembly method (Lu et al., 2015). The results showed that the heterogeneous catalyst (C₁₆H₃₃N(CH₃)₃)H₄PW₁₁TiO₄₀ had the strongest acidity and exhibited excellent activity in the conversion of saccharides to other useful substances, with

HMF yield of 53.7 and 50.8% from fructose and glucose, respectively (Figure 23). Meanwhile, the self-assembled structure of (C₁₆H₃₃N(CH₃)₃)H₄PW₁₁TiO₄₀ in water could make cellulose and other polysaccharides gather to the catalytic sites, thus improving the catalytic efficiency. Also, the catalyst can be easily separated from the reactant, and the activity was almost no loss after recycling for many times (Figure 24).

It can be seen that the assembled HPA catalysts can convert cellulose into glucose or other substances. Their unique structure can make cellulose aggregate to the catalytic sites, thus improving the catalytic efficiency. And almost all of them can be recycled by simple instruments. These advantages make their research more meaningful.



SCHEME 19 | The conversion pathways and mechanism for the alcoholysis of cellulose.

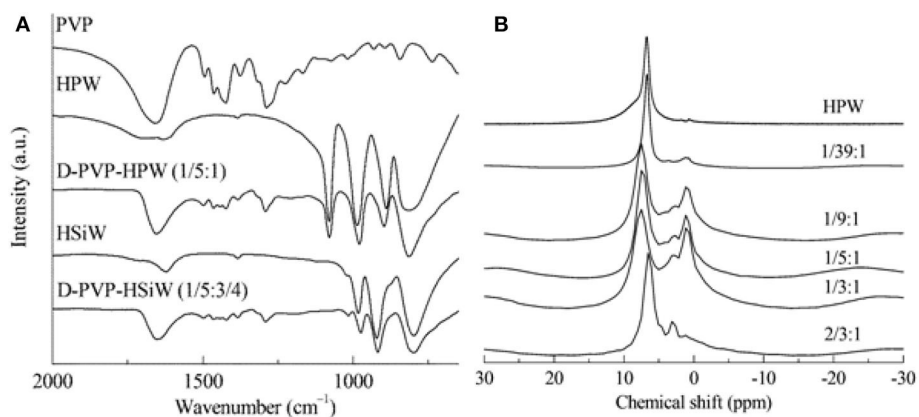
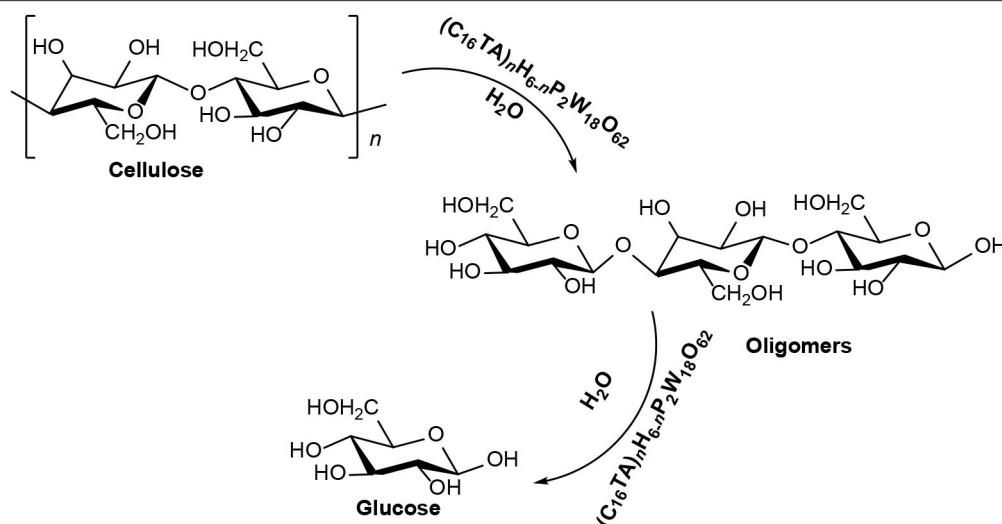


FIGURE 21 | (A) The FT-IR spectra of PVP, HPAs, and PVP-HPAs, and **(B)** solid MAS ¹H-NMR spectra of PVP-HPW catalysts. Reproduced with permission from Chen et al. (2013).

However, it can not be ignored that some supported catalysts have low selectivity and yield for glucose, such as (C₁₆TA)H₅P₂W₁₈O₆₂ and [MIMPSH]H₂PW. Moreover,

the stability of some HPA catalysts decreased after reuse, which should be improved by the exploration of novel preparation methods.



SCHEME 20 | The mechanism of cellulose conversion by $(C_{16}TA)_nH_{6-n}P_2W_{18}O_{62}$ catalyst.

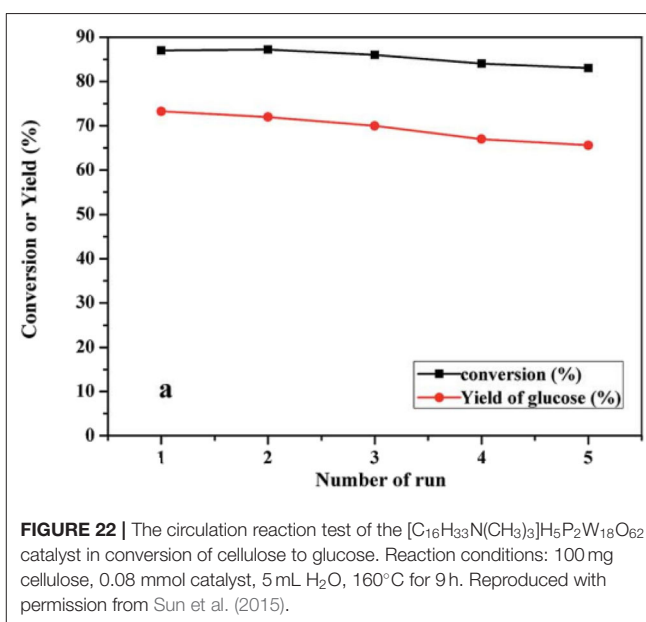
TABLE 14 | Conversion of cellulose over different catalysts (Sun et al., 2015).

Catalyst	Conversion/%	TRS yield/%	Glucose yield (%)	TOF/g $mmol^{-1}$
$H_6P_2W_{18}O_{62}$	93.5	52.6	45.6	12.9×10^{-2}
$(C_{16}TA)H_5P_2W_{18}O_{62}$	87.2	72.4	69.1	12.1×10^{-2}
$(C_{16}TA)_2H_4P_2W_{18}O_{62}$	75.5	64.4	61.7	10.5×10^{-2}
$(C_{16}TA)_3H_3P_2W_{18}O_{62}$	63.8	58.7	53.4	8.9×10^{-2}
$(C_{16}TA)_4H_2P_2W_{18}O_{62}$	58.3	53.0	49.4	8.1×10^{-2}
$(C_{16}TA)_5HP_2W_{18}O_{62}$	43.5	40.3	37.8	6.0×10^{-2}
$(C_{16}TA)_6P_2W_{18}O_{62}$	30.6	28.5	25.7	4.3×10^{-2}
$(C_{16}TA)H_2PW_{12}O_{40}$	81.6	75.3	63.3	11.3×10^{-2}
$H_3PW_{12}O_{40}$	55.7	46.3	44.2	7.7×10^{-2}

Reaction conditions: 100 mg cellulose, 0.08 mmol catalyst, 5 mL H_2O , 160°C, 9 h. Reproduced with permission from Sun et al. (2015).

Other HPA Catalysts

In addition to the HPA catalysts mentioned above, many other HPACatalysts have also been developed and utilized for cellulose degradation. For example, HPAs can be combined with other catalysts to facilitate cellulose conversion. Palkovits et al. proved that the combination of HPAs and supported Ru catalysts can directly convert cellulose into glycols with a yield of 81% (Palkovits et al., 2011). And the catalyst is very easy to recycle. In 2014, Xie et al. used HPA to synthesize a new catalyst $Ru/[Bmim]_3PW_{12}O_{40}$, which can selectively convert microcrystalline cellulose to hexanol under mild conditions (Xie et al., 2014). The catalyst was synthesized by supporting Ru on ionic liquid ($BmimPF_6$)-heteropoly acid ($H_3PW_{12}O_{40} \cdot nH_2O$), which resulted in the formation of Brønsted acid sites. It improves the performance of the catalyst and is an important reason for the remarkable activity of the catalyst in the conversion of cellulose. Su et al. used HPA and ZrO_2 to synthesize a kind of



dual-functional heterogeneous catalyst ($H_3PW_{12}O_{40}/ZrO_2$ -Et-HNS), which was composed of organosilicon hollow nanospheres and can be used in esterification (Su et al., 2014). The unique hollow nanospherical morphology of the catalyst increases its surface acidity and thus improves its catalytic activity. Basahel et al. (2016) synthesized a heterogeneous catalyst $Al_xH_{3x}PW_{12}O_{40}$ by ion-exchange method. The HPA catalysts formed by the exchange of hydrogen and aluminum ions showed higher activity because of the increase of Lewis acid sites on the surface of the catalysts. These catalysts proved to be able to synthesize bioactive pyrido[1,2-a]pyrimidines with yields above 90%. In 2017, Wu et al. synthesized a new luryamine-modified phosphotungstic acid catalyst. They used several characterization instruments to characterize the catalyst and found that the

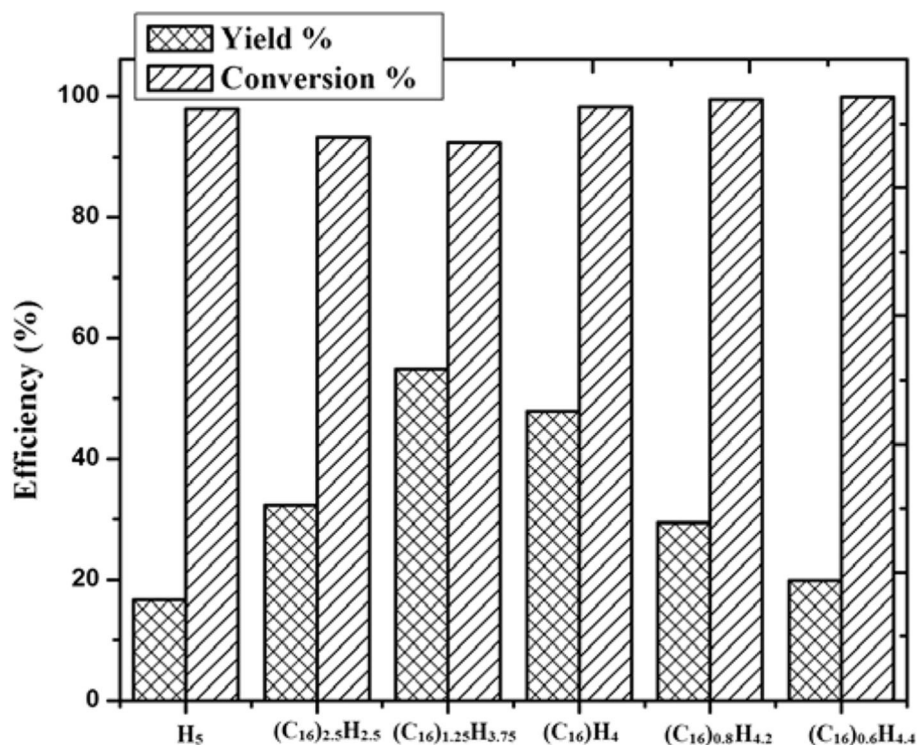


FIGURE 23 | The efficiency of different catalysts for fructose transformation. Reaction conditions: 0.6 g fructose, 0.01 mmol catalyst, 2 mL H₂O, 130°C for 1.5 h. Reproduced with permission from Lu et al. (2015).

modified heteropoly acid was still the Keggin structure (Wu et al., 2017). As compared with conventional phosphotungstic acid, the luryamine-modified HPA catalyst showed more stable and higher catalytic activity. It's worth mentioning that the yield of glucose reached 100% by hydrolysis of sucrose with the modified catalyst which can provide a way to study cellulose hydrolysis in the future. All the HPA catalysts reported above are heterogeneous. They have a common feature that they are easy to separate from reactants and can be reused with almost no loss of catalytic activity.

Comparison of Different HPA-Based Catalysts

As discussed above, it can be concluded that the Keggin HPA-based catalysts are one of the most common cellulose degradation catalysts. Due to their dual functional properties, the HPA-based catalysts can further promote the oxidation of hydrolysates into valuable compounds. However, their specific surface areas are relatively low, which is not conducive to the catalytic activity. To solve this deficiency, some substituted and supported heteropoly acid catalysts were developed, which are demonstrated to have higher specific surface areas, higher reactivity, and better thermal stability, and are more conducive to the separation because they are commonly used in the heterogeneous systems. It is worth noting that the preparation of these catalysts is complicated and the synthesis cycle is long. In order to further improve the catalytic activity of HPAs, the

assembled HPAs and other modified HPA catalysts have been developed. With unique structures, these catalysts exhibit high catalytic performance in cellulose conversion. More importantly, they are all heterogeneous catalysts, providing convenience for the catalyst separation and recycling processes. Therefore, different HPA catalysts have their own characteristics, advantages and disadvantages, and the catalytic upgrading of cellulosic biomass can be effectively enabled with these HPA-based catalysts as long as their properties are properly switched.

CONCLUSIONS AND OUTLOOK

With the rapid development and utilization of chemical fuels, depolymerization of cellulosic biomass has become one of the ways to provide organic carbon sources. It is reported that cellulose can be converted into a variety of useful platform molecules that can be applied in various fields. In this review, the focus is placed on finding homogeneous and heterogeneous HPA catalysts for cellulose degradation.

HPAs, as a kind of efficient, environmentally friendly, and safe catalysts, show high catalytic activity for cellulose degradation. HPA catalysts have higher catalytic activity than conventional solid acid catalysts, which are more conducive to the degradation of cellulose into valuable platform molecules, such as glucose. Meanwhile, due to its unique physical and chemical properties, HPAs can be used in homogeneous and heterogeneous systems.

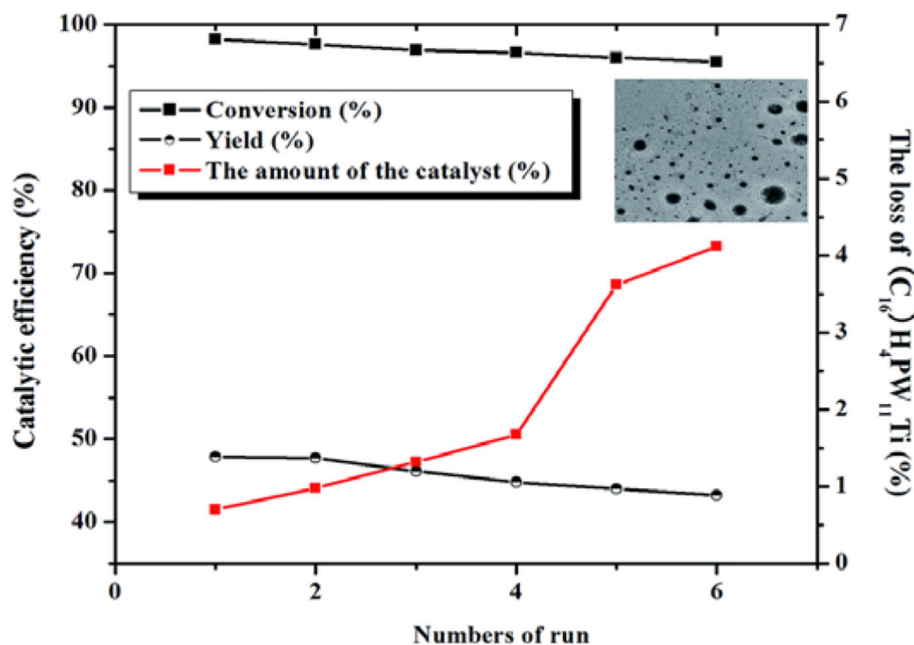


FIGURE 24 | Recycling test of the $(C_{16}H_{33}N(CH_3)_3)H_4PW_{11}TiO_{40}$ catalyst in the conversion of fructose to HMF. Reaction conditions: 0.6 g fructose, 0.01 mmol catalyst, 2 mL H_2O , $130^\circ C$ for 1.5 h. Reproduced with permission from Lu et al. (2015).

And they can all be reused after separation in the reactor with almost no loss of catalytic activity.

Several methods have been developed to synthesize HPA catalysts. (1) The acidification process coupled with an ether extraction is the most commonly used method, which is mainly used for the synthesis of common HPAs (e.g., $H_3PW_{12}O_{40}$, $H_3SiW_{12}O_{40}$), but its safety is low due to the use of some toxic substances. (2) The ion-exchange method has high safety, but it has the disadvantage of a long production cycle. (3) The impregnation method is simple and safe but suffers the disadvantage of the loss of catalyst activity and limited recycling ability. (4) The sol-gel method can prepare HPA catalysts at low temperatures or mild conditions, which is widely used in the synthesis of HPA-based nanomaterial catalysts. However, this method has the disadvantages of low security and long cycle. Therefore, it is very important and urgent to develop more efficient methods for the preparation of HPA-based catalysts.

As depicted in previous studies, typical Keggin-type HPA catalysts are the most common ones for cellulose degradation, and they can further catalyze the oxidation of the hydrolysates to valuable substances due to their dual functional properties. Then, the supported and substituted HPA catalysts always exist in heterogeneous form. After supporting and substituting disposal, the acid site number, the acid strength, and the specific surface area of the HPA catalysts increase, which improves the catalytic properties of the catalysts. In addition, the assembled HPA catalysts and other modified HPA catalysts show good catalytic performance in cellulose conversion because of their unique structure. Therefore, HPA-based catalysts provide convenience for cellulose degradation and more possibilities for

the development of chemical fuels in the future. But it cannot be neglected that some of HPAs have the disadvantages of high catalyst dosage and relatively low catalytic activity with respect to the reaction conversion, product selectivity, and catalyst stability. For example, the selectivity of substituted and supported HPAs toward target products is lower than that of Keggin-type HPAs. Also, the stability of the supported HPAs is lower than that of common HPAs.

Although HPAs-based catalysts in either homogeneous or heterogeneous state have made great progress in the degradation of biomass cellulose, there are still many deficiencies to be improved:

(1) Study on the relationship between the properties of HPA catalysts and the degradation of cellulose to further improve the catalytic activity.

(2) Design of a cleaner, safer, and more effective HPA catalyst with simple preparation methods to promote cellulose degradation.

(3) Development of more new HPA catalysts with special structure, and ensure no or fewer side reactions in the reaction process, with the focus on the improvement of the HPA catalyst disadvantages especially unsatisfactory conversion, selectivity, and stability.

(4) Further understanding the structural characteristics of HPAs, study of the reaction mechanism catalyzed by HPAs, and promotional completion of the target reaction by linking the relationship between them.

(5) Extension of HPA catalysts to other biomass feedstocks, providing more help for the future development of fuels and HPAs in the field of catalysis.

In summary, this review mainly summarizes some examples of the degradation of cellulose by some kinds of HPA catalysts. The HPA catalysts are considered to have great application prospects in the degradation of cellulose and the conversion of other relevant research fields.

AUTHOR CONTRIBUTIONS

XL and HL initiated the project. XL, HW, CL, ZL, HL, HZ, YL, YS, and SY searched the data and wrote, revised, and

completed the manuscript. All authors contributed to the article and approved the submitted version.

FUNDING

The authors thank the financial support from the National Natural Science Foundation of China (21666008, 21908033, and 21576059), Fok Ying-Tong Education Foundation (161030), Guizhou Science & Technology Foundation ([2018]1037), and Program of Introducing Talents of Discipline to Universities of China (111 Program, D20023).

REFERENCES

- Ahmed, A. I., El-Hakam, S. A., Elghany, M. A. A., and El-Yazeed, W. S. A. (2011). Synthesis and characterization of new solid acid catalysts, $\text{H}_3\text{PW}_{12}\text{O}_{40}$ supported on nanoparticle tin oxide: An efficient catalyst for the preparation of 7-hydroxy-4-methylcoumarin. *Appl. Catal. A Gen.* 407, 40–48. doi: 10.1016/j.apcata.2011.08.020
- Akiyama, G., Matsuda, R., Sato, H., Takata, M., and Kitagawaet, S. (2011). Cellulose hydrolysis by a new porous coordination polymer decorated with sulfonic acid functional groups. *Adv. Mater.* 23, 3294–3297. doi: 10.1002/adma.201101356
- Albert, J., Luders, D., Bosmann, A., Guldi, D. M., and Wasserscheid, P. (2014). Spectroscopic and electrochemical characterization of heteropoly acids for their optimized application in selective biomass oxidation to formic acid. *Green Chem.* 16, 226–237. doi: 10.1039/C3GC41320A
- Albert, J., Wolfel, R., Bosmann, A., and Wasserscheid, P. (2012). Selective oxidation of complex, water-insoluble biomass to formic acid using additives as reaction accelerators. *Energy Environ. Sci.* 5, 7956–7962. doi: 10.1039/c2ee21428h
- An, D., Ye, A., Deng, W., Zhang, Q., and Wang, Y. (2012). Selective conversion of cellobiose and cellulose into gluconic acid in water in the presence of oxygen, catalyzed by polyoxometalate-supported gold nanoparticles. *Chem. Eur. J.* 18, 2938–2947. doi: 10.1002/chem.201103262
- Bachillerbaeza, B., and Anderson, J. (2004). FTIR and reaction studies of the acylation of anisole with acetic anhydride over supported hpa catalysts. *J. Catal.* 228, 225–233. doi: 10.1016/j.jcat.2004.08.010
- Bamoharram, F. F., Heravi, M. M., Heravi, H. M., and Dehghan, M. (2004). Photocatalytic oxidation of benzyl alcohols in the presence of $\text{H}_{14}[\text{NaP}_5\text{W}_{30}\text{O}_{110}]$ as a green and reusable catalyst. *Synth. React. Inorg. Metal Org. Nano Metal Chem.* 39, 394–399. doi: 10.1080/15533170903129745
- Basahel, S. N., Ahmed, N. S., Narasimharao, K., and Mokhtar, M. (2016). Simple and efficient protocol for synthesis of pyrido [1, 2-a] pyrimidin-4-one derivatives over solid heteropolyacid catalysts. *RSC Adv.* 6, 11921–11932. doi: 10.1039/C5RA22180C
- Bechtold, M. F., and Square, K. (1950). *Method of Preparing Heteropolyacids Containing a Heavy Metal*. U.S. Patent No. 2503991.
- Bennardi, D., Romanelli, G., Autino, J., Pizzio, L., Vázquez, P., Cáceres, C., et al. (2010). Comparative study of the catalytic preparation of flavones using keggins heteropolyacids under homogeneous, heterogeneous and solvent free conditions. *React. Kinet. Mech. Catal.* 100, 165–174. doi: 10.1007/s11144-010-0172-4
- Cardoso, L. A. M., Alves, W., Gonzaga, A. R. E., Aguiar, L. G., and Andrade, H. M. C. (2004). Friedel-crafts acylation of anisole with acetic anhydride over silica-supported heteropolyphosphotungstic acid (HPW/SiO_2). *J. Mol. Catal. A Chem.* 209, 189–197. doi: 10.1016/j.molcata.2003.08.022
- Chang, F., Hanna, M. A., Zhang, D., Li, H., Zhou, Q., Song, B., et al. (2013). Production of biodiesel from non-edible herbaceous vegetable oil: *Xanthium sibiricum* Patr. *Bioresour. Technol.* 140, 435–438. doi: 10.1016/j.biortech.2013.04.111
- Chen, J., Fang, X., Duan, X., Ye, L., Lin, H., and Yuan, Y. (2013). PVP-stabilized heteropolyacids as reusable self-assembling catalysts for alcoholysis of cellulosic saccharides. *Green Chem.* 16, 294–302. doi: 10.1039/C3GC40994E
- Cheng, M., Tian, S., Guan, H., Wang, S., Wang, X., and Jiang, Z. J. (2011). Clean production of glucose from polysaccharides using a micellar heteropolyacid as a heterogeneous catalyst. *Appl. Catal. B Environ.* 107, 104–109. doi: 10.1016/j.apcatb.2011.07.002
- Chheda, J. N., Huber, G. W., and Dumesic, J. A. (2007). Liquid-phase catalytic processing of biomass-derived oxygenated hydrocarbons to fuels and chemicals. *Angew. Chem. Int. Ed.* 46, 7164–7183. doi: 10.1002/anie.200604274
- Chiola, V., and Lawrence, J. G. (1969). *Preparation of Heteropoly Molybdic Acids*. U.S. Patent No. 3425794. Washington, DC: U.S. Patent and Trademark Office.
- Chiola, V., vanderpool, C. D., and Towanda, P. (1969). *Method of Preparing Heteropoly Compounds*. U.S. Patent No. 3446575. Washington, DC: U.S. Patent and Trademark Office.
- Climent, M. J., Corma, A., and Iborra, S. (2014). Conversion of biomass platform molecules into fuel additives and liquid hydrocarbon fuels. *Green Chem.* 16, 516–547. doi: 10.1039/c3gc41492b
- de Op Beeck, B., Geboers, J., and van de Vyver, S. (2013). Conversion of (ligno)cellulose feeds to isosorbide with heteropoly acids and Ru on carbon. *ChemSusChem* 6, 199–208. doi: 10.1002/cssc.201200610
- Deng, W., Zhang, Q., and Wang, Y. (2012). Polyoxometalates as efficient catalysts for transformations of cellulose into platform chemicals. *Dalton Trans.* 41, 9817–9831. doi: 10.1039/c2dt30637a
- Dhepe, P. L., and Fukuoka, A. (2008). Cellulose conversion under heterogeneous catalysis. *ChemSusChem* 1, 969–975. doi: 10.1002/cssc.200800129
- Duan, X., Sun, G., Sun, Z., Li, J., Wang, S., Wang, X., et al. (2013). A heteropolyacid-based ionic liquid as a thermoregulated and environmentally friendly catalyst in esterification reaction under microwave assistance. *Catal. Commun.* 42, 125–128. doi: 10.1016/j.catcom.2013.08.014
- Dwars, T., Paetzold, E., and Oehme, G. (2005). Reactions in micellar systems. *Angew. Chem. Int. Ed.* 44, 7174–7199. doi: 10.1002/anie.200501365
- Feng, J., Zhu, Q., Ding, M., Liu, X., and Han, X. (2011). Direct conversion and nmr observation of cellulose to glucose and 5-hydroxymethylfurfural (HMF) catalyzed by the acidic ionic liquids. *J. Mol. Catal. A Chem.* 334, 8–12. doi: 10.1016/j.molcata.2010.10.006
- Furukawa, H., Kobayashi, N., Itaya, Y., Satsuma, A., and Shimizu, K. (2009). Effects of Brønsted and Lewis acidities on activity and selectivity of heteropolyacid-based catalysts for hydrolysis of cellobiose and cellulose. *Green Chem.* 11, 1627–1632. doi: 10.1039/b913737h
- Geboers, J., van de Vyver, S., Carpentier, K., de Blochouse, K., Jacobs, P., and Sels, B. (2010). Efficient catalytic conversion of concentrated cellulose feeds to hexitols with heteropoly acids and Ru on carbon. *Chem. Commun.* 46, 3577–3580. doi: 10.1039/c001096k
- Geboers, J., van de Vyver, S., Carpentier, K., Jacobs, P., and Sels, B. (2011). Hydrolytic hydrogenation of cellulose with hydrotreated caesium salts of heteropoly acids and Ru/C. *Green Chem.* 13, 2167–2174. doi: 10.1039/c1gc15350a
- Gromov, N. V., Taran, O. P., Delidovich, I. V., Pestunov, A. V., Rodikova, Y. A., Yatsenko, D. A., et al. (2016). Hydrolytic oxidation of cellulose to formic acid in the presence of Mo-V-P heteropoly acid catalysts. *Catal. Today* 278, 74–81. doi: 10.1016/j.cattod.2016.03.030
- Guo, Y., Li, K., and Clark, J. H. (2007). The synthesis of diphenolic acid using the periodic mesoporous $\text{H}_3\text{PW}_{12}\text{O}_{40}$ -silica composite catalysed reaction of levulinic acid. *Green Chem.* 9, 839–841. doi: 10.1039/b702739g

- Hafizi, A., Ahmadvour, A., Heravi, M. M., and Bamoharram, F. F. (2014). The application of silica-supported preysler hpa as a heterogeneous and green catalyst for the alkylation of benzene. *Petrol. Sci. Technol.* 32, 1022–1027. doi: 10.1080/10916466.2011.637534
- Harada, T., Tokai, Y., Kimura, A., Ikeda, S., and Matsumura, M. (2014). Hydrolysis of crystalline cellulose to glucose in an autoclave containing both gaseous and liquid water. *RSC Adv.* 4, 26838–26842. doi: 10.1039/c4ra02396j
- He, J., Li, H., Riisager, A., and Yang, S. (2018). Catalytic transfer hydrogenation of furfural to furfuryl alcohol with recyclable Al-Zr@Fe mixed oxides. *ChemCatChem* 10, 430–438. doi: 10.1002/cctc.201701266
- Heravi, M. M., Jani, B. A., Derikvand, F., Bamoharram, F. F., and Oskooie, H. A. (2008). Three component, one-pot synthesis of dihydropyrano[3,2-c]chromene derivatives in the presence of $H_6P_2W_{18}O_{62} \cdot 18H_2O$ as a green and recyclable catalyst. *Catal. Commun.* 10, 272–275. doi: 10.1016/j.catcom.2008.08.023
- Heravi, M. M., Khorasani, M., Derikvand, F., Oskooie, H. A., and Bamoharram, F. F. (2007). Highly efficient synthesis of coumarin derivatives in the presence of $H_{14}[NaP_5W_{30}O_{110}]$ as a green and reusable catalyst. *Catal. Commun.* 8, 1886–1890. doi: 10.1016/j.catcom.2007.02.030
- Hu, S., Jiang, F., and Hsieh, Y. L. (2015). 1D lignin-based solid acid catalysts for cellulose hydrolysis to glucose and nanocellulose. *ACS Sustain. Chem. Eng.* 3, 2566–2574. doi: 10.1021/acssuschemeng.5b00780
- Huber, G. W., Iborra, S., and Corma, A. (2006). Synthesis of transportation fuels from biomass: chemistry, catalysts, and engineering. *Chem. Rev.* 106, 4044–4098. doi: 10.1021/cr068360d
- Izumi, Y., Matsuo, K., and Urabe, K. (1983). Efficient homogeneous acid catalysis of heteropoly acid and its characterization through ether cleavage reactions. *J. Mol. Catal.* 18, 299–314. doi: 10.1016/S0304-5102(83)80004-2
- Izumi, Y., Ono, M., Kitagawa, M., Yoshida, M., and Urabe, K. (1995). Silica-included heteropoly compounds as solid acid catalysts. *Microporous Mater.* 5, 255–262. doi: 10.1016/0927-6513(95)00059-3
- Kamm, B., and Kamm, M. (2004). Principles of biorefineries. *Appl. Microbiol. Biotechnol.* 64, 137–145. doi: 10.1007/s00253-003-1537-7
- Kaur, J., and Kozhevnikov, I. V. (2002). Efficient acylation of toluene and anisole with aliphatic carboxylic acids catalysed by heteropoly salt $Cs_{2.5}H_{0.5}PW_{12}O_{40}$. *Chem. Commun.* 8, 2508–2509. doi: 10.1039/b207915c
- Klein, M., Pulidindi, I. N., Perkas, N., and Gedanken, A. (2015). Heteropoly acid catalyzed hydrolysis of glycogen to glucose. *Biomass Bioenergy* 76, 61–68. doi: 10.1016/j.biombioe.2015.02.036
- Klein, M., Pulidindi, I. N., Perkas, N., Meltzer-Mats, E., Gruzman, A., and Gedanken, A. (2012). Direct production of glucose from glycogen under microwave irradiation. *RSC Adv.* 2, 7262–7267. doi: 10.1039/c2ra21066e
- Klemm, D., Heublein, B., Fink, H. P., and Bohn, A. (2005). Cellulose: fascinating biopolymer and sustainable raw material. *Angew. Chem. Int. Ed.* 44, 3358–3393. doi: 10.1002/anie.200460587
- Kobayashi, H., Komanoya, T., Hara, K., and Fukuoka, A. (2010). Water-tolerant mesoporous-carbon-supported ruthenium catalysts for the hydrolysis of cellulose to glucose. *ChemSusChem* 3, 440–443. doi: 10.1002/cssc.200900296
- Komanoya, T., Kobayashi, H., Hara, K., Chun, W. J., and Fukuoka, A. (2011). Catalysis and characterization of carbon-supported ruthenium for cellulose hydrolysis. *Appl. Catal. A Gen.* 407, 188–194. doi: 10.1016/j.apcata.2011.08.039
- Kozhevnikov, I. V. (1987). Advances in catalysis by heteropolyacids. *Russ. Chem. Rev.* 56, 811–825. doi: 10.1070/RC1987v056n09ABEH003304
- Kozhevnikov, I. V. (1998). Catalysis by heteropoly acids and multicomponent polyoxometalates in liquid-phase reactions. *Chem. Rev.* 98, 171–198. doi: 10.1021/cr960400y
- Laferty, J. M., and John, M. (1966). *Method of Preparing Phosphotungstic Acid*. U.S. Patent No. 3288562. Washington, DC: U.S. Patent and Trademark Office.
- Lai, D. M., Deng, L., Guo, Q. X., and Fu, Y. (2011). Hydrolysis of biomass by magnetic solid acid. *Energy. Environ. Sci.* 4, 3552–3557. doi: 10.1039/c1ee01526e
- Lanzafame, P., Temi, D. M., Perathoner, S., Spadaro, A. N., and Centi, G. (2012). Direct conversion of cellulose to glucose and valuable intermediates in mild reaction conditions over solid acid catalysts. *Catal. Today* 179, 178–184. doi: 10.1016/j.cattod.2011.07.018
- Leng, Y., Wang, J., Zhu, D., Ren, X., Ge, H., and Shen, L. (2010). Heteropolyanion-based ionic liquids: reaction-induced self-separation catalysts for esterification. *Angew. Chem.* 48, 168–171. doi: 10.1002/anie.200803567
- Li, H., Fang, Z., and Yang, S. (2016). Direct catalytic transformation of biomass derivatives into biofuel component γ -valerolactone with magnetic nickel-zirconium nanoparticles. *ChemPlusChem* 81, 135–142. doi: 10.1002/cplu.201500492
- Li, H., He, X., Zhang, Q., Chang, F., Xue, W., Zhang, Y., et al. (2013). Polymeric ionic hybrid as solid acid catalyst for the selective conversion of fructose and glucose to 5-hydroxymethylfurfural. *Energy Technol.* 1, 151–156. doi: 10.1002/ente.201200041
- Li, H., Liu, X., Yang, T., Zhao, W., Saravanamurugan, S., and Yang, S. (2015). Porous zirconium-furandicarboxylate microspheres for efficient redox conversion of biofurans. *ChemSusChem* 10, 1761–1770. doi: 10.1002/cssc.201601898
- Li, H., Zhang, Q., Bhadury, P. S., and Yang, S. (2014). Furan-type compounds from carbohydrates via heterogeneous catalysis. *Curr. Org. Chem.* 18, 547–597. doi: 10.2174/13852728113176660138
- Liu, B., and Zhang, Z. H. (2015). Catalytic conversion of biomass into chemicals and fuels over magnetic catalysts. *ACS Catal.* 6, 326–338. doi: 10.1021/acscatal.5b02094
- Liu, Q. Y., Wu, W. L., Wang, J., Ren, X. Q., and Wang, Y. R. (2004). Characterization of 12-tungstophosphoric acid impregnated on mesoporous silica SBA-15 and its catalytic performance in isopropylation of naphthalene with isopropanol. *Micropor. Mesopor. Mater.* 76, 51–60. doi: 10.1016/j.micromeso.2004.08.001
- Liu, X., Li, H., Pan, H., Zhang, H., Huang, S., Yang, K., et al. (2016). Efficient catalytic conversion of carbohydrates into 5-ethoxymethylfurfural over MIL-101-based sulfated porous coordination polymers. *J. Energy Chem.* 25, 523–530. doi: 10.1016/j.jechem.2016.01.015
- Lu, T., Niu, M., Hou, Y., Wu, W., Ren, S., and Yang, F. (2016). Catalytic oxidation of cellulose to formic acid in $H_5PV_2Mo_{10}O_{40} + H_2SO_4$ aqueous solution with molecular oxygen. *Green Chem.* 18, 4725–4732. doi: 10.1039/C6GC01271J
- Lu, Y., Sun, Z., and Huo, M. (2015). Fabrication of a micellar heteropolyacid with lewis-brønsted acid sites and application for the production of 5-hydroxymethylfurfural from saccharides in water. *RSC Adv.* 5, 30869–30876. doi: 10.1039/C4RA16952B
- Macht, J., Janik, M. J., Neurock, M., and Iglesia, E. (2008). Mechanistic consequences of composition in acid catalysis by polyoxometalate keggins clusters. *J. Am. Chem. Soc.* 130, 10369–10379. doi: 10.1021/ja803114r
- Mastikhin, V. M., Kulikov, S. M., Nosov, A. V., Kozhevnikov, I. V., and Timofeeva, M. N. (1990). 1H and ^{31}P mas nmr studies of solid heteropolyacids and $H_3PW_{12}O_{40}$ supported on SiO_2 . *J. Mol. Catal. A Chem.* 60, 65–70. doi: 10.1016/0304-5102(90)85068-S
- Mizuno, N., and Misono, M. (1994). Heteropolyanions in catalysis. *J. Mol. Catal.* 86, 319–342. doi: 10.1016/0304-5102(93)E0155-A
- Mrowiec-Białoń, J., Turek, W. A., and Jarzebski, B. (2002). Preparation of highly active heteropolyacid-silica composite catalysts using the sol-gel method. *React. Kinet. Catal. Lett.* 76, 213–219. doi: 10.1023/A:1016515407161
- Nowinska, K., Dudko, D., and Golon, R. (1996). $Pd_2 + Mn_2 + HPA$: a heterogeneous wacker system catalyst. *Chem. Commun.* 2, 277–297. doi: 10.1039/CC9960000277
- Odyakov, V. F., and Zhizhina, E. G. (2009). New process for preparing aqueous solutions of mo-v-phosphoric heteropoly acids. *Russ. J. Inorg. Chem.* 54, 361–367. doi: 10.1134/S003602360903005X
- Ogasawara, Y., Itagaki, S., Yamaguchi, K., and Mizuno, N. (2011). Saccharification of natural lignocellulose biomass and polysaccharides by highly negatively charged heteropolyacids in concentrated aqueous solution. *ChemSusChem* 4, 519–525. doi: 10.1002/cssc.201100025
- Okuhara, T. (2002). Water-tolerant solid acid catalysts. *Chem Rev.* 102, 3641–3665. doi: 10.1021/cr0103569
- Okuhara, T., Nishimura, T., and Misono, M. (1996). Novel microporous solid “superacids”: $Cs_xH_{3-x}PW_{12}O_{40}$ ($2 < x < 3$). *Stud. Surf. Sci. Catal.* 101, 581–590. doi: 10.1016/S0167-2991(96)80269-2
- Okuhara, T., Nishimura, T., Watanabe, H., and Misono, M. (1992). Insoluble heteropoly compounds as highly active catalysts for liquid-phase reactions. *J. Mol. Catal.* 74, 247–256. doi: 10.1016/0304-5102(92)80242-9

- Okuhara, T., Watanabe, H., Nishimura, T., Inumaru, K., and Misono, M. (2000). Microstructure of cesium hydrogen salts of 12-tungstophosphoric acid relevant to novel acid catalysis. *Chem. Mater.* 12, 2230–2238. doi: 10.1021/cm9907561
- Palkovits, R., Tajvidi, K., Ruppert, A., and Procelewska, J. (2011). Heteropoly acids as efficient acid catalysts in the one-step conversion of cellulose to sugar alcohols. *Chem. Commun.* 47, 576–578. doi: 10.1039/C0CC02263B
- Pan, T., Deng, J., Xu, Q., Zuo, Y., Guo, Q. X., and Fu, Y. (2013). Catalytic conversion of furfural into a 2,5-furandicarboxylic acid-based polyester with total carbon utilization. *ChemSusChem* 6, 47–50. doi: 10.1002/cssc.201200652
- Pang, J., Wang, A., Zheng, M., and Zhang, T. (2010). Hydrolysis of cellulose into glucose over carbons sulfonated at elevated temperatures. *Chem. Commun.* 46, 6935–6937. doi: 10.1039/c0cc02014a
- Parghi, K. D., Satam, J. R., and Jayaram, R. V. (2011). Silica supported heteropolyacid catalyzed dehydration of aldioximes to nitriles and alcohols to alkenes. *Green Chem. Lett. Rev.* 4, 143–149. doi: 10.1080/17518253.2010.523015
- Reddy, B. S., Narasimhulu, G., Lakshumma, P. S., Reddy, Y. V., and Yadav, J. S. (2012). Phosphomolybdic acid: a highly efficient solid acid catalyst for the synthesis of trans-4, 5-disubstituted cyclopentenones. *Tetrahedron Lett.* 53, 1776–1779. doi: 10.1016/j.tetlet.2012.01.115
- Ren, H., Girisuta, B., Zhou, Y., and Liu, L. (2015). Selective and recyclable depolymerization of cellulose to levulinic acid catalyzed by acidic ionic liquid. *Carbohydr. Polym.* 117, 569–576. doi: 10.1016/j.carbpol.2014.09.091
- Rinaldi, R., Palkovits, R., and Schüth, F. (2010). Depolymerization of cellulose using solid catalysts in ionic liquids. *Angew. Chem. Int. Ed.* 47, 8047–8050. doi: 10.1002/anie.200802879
- Shatalov, A. A. (2019). Highly efficient hydrolysis of plant hemicelluloses by mixed-addenda keggins-type (Mo-V-P)-heteropolyacids in diluted aqueous solution. *Carbohydr. Polym.* 206, 80–85. doi: 10.1016/j.carbpol.2018.10.106
- Sheldon, R. A. (2014). Green and sustainable manufacture of chemicals from biomass: state of the art. *Green Chem.* 16, 950–963. doi: 10.1039/C3GC41935E
- Shimizu, K., and Satsuma, A. (2011). Toward a rational control of solid acid catalysis for green synthesis and biomass conversion. *Energy Environ. Sci.* 4, 3140–3153. doi: 10.1039/c1ee01458g
- Song, I. K., and Lee, W. Y. (2004). Heteropolyacid (HPA)-polymer composite films as heterogeneous catalysts and catalytic membranes. *Appl. Catal. A Gen.* 256, 77–98. doi: 10.1016/S0926-860X(03)00390-9
- Su, F., An, S., Song, D., Zhang, X., Lu, B., and Guo, Y. (2014). Heteropoly acid and ZrO₂ bifunctionalized organosilica hollow nanospheres for esterification and transesterification. *J. Mater. Chem.* 2, 14127–14138. doi: 10.1039/C4TA02257B
- Sun, Z., Cheng, M., Li, H., Shi, T., Yuan, M., Wang, X., et al. (2012). One-pot depolymerization of cellulose into glucose and levulinic acid by heteropolyacid ionic liquid catalysis. *RSC Adv.* 2, 9058–9065. doi: 10.1039/c2ra01328b
- Sun, Z., Zhang, X., Wang, S., Li, X., Wang, X., and Shi, J. (2015). Hydrolysis and alcoholysis of polysaccharides with high efficiency catalyzed by a (C₁₆TA)_xH_{6-x}P₂W₁₈O₆₂ nanoassembly. *RSC Adv.* 5, 94155–94163. doi: 10.1039/C5RA15047G
- Tian, J., Fang, C., Cheng, M., and Wang, X. (2011). Hydrolysis of cellulose over Cs_xH_{3-x}PW₁₂O₄₀ (x = 1–3) heteropoly acid catalysts. *Chem. Eng. Technol.* 34, 482–486. doi: 10.1002/ceat.201000409
- Tian, J., Wang, J. H., Zhao, S., Jiang, C. Y., Zhang, X., and Wang, X. H. (2010). Hydrolysis of cellulose by the heteropoly acid H₃PW₁₂O₄₀. *Cellulose* 17, 587–594. doi: 10.1007/s10570-009-9391-0
- To, A. T., Chung, P. W., and Katz, A. (2015). Weak-acid sites catalyze the hydrolysis of crystalline cellulose to glucose in water: importance of post synthetic functionalization of the carbon surface. *Angew. Chem. Int. Ed.* 127, 11202–11205. doi: 10.1002/ange.201504865
- Udayakumar, S., Ajaikumar, S., and Pandurangan, A. (2007). Electrophilic substitution reaction of phenols with aldehydes: enhance the yield of bisphenols by hpa and supported HPA. *Catal. Commun.* 8, 366–374. doi: 10.1016/j.catcom.2006.05.054
- Vázquez, P., Pizzio, L., Cáceres, C., Blanco, M., Thomas, H., Alessio, E., et al. (2000). Silica-supported heteropolyacids as catalysts in alcohol dehydration reactions. *J. Mol. Catal. A Chem.* 16, 223–232. doi: 10.1016/S1381-1169(00)00346-0
- Wang, H., Gurau, G., and Rogers, R. D. (2012). Ionic liquid processing of cellulose. *Chem. Soc. Rev.* 41, 1519–1537. doi: 10.1039/c2cs15311d
- Wee, L. H., Bajpe, S. R., Janssens, N., Hermans, I., and Martens, J. A. (2010). Convenient synthesis of Cu₃(BTC)₂ encapsulated keggins heteropolyacid nanomaterial for application in catalysis. *Chem. Commun.* 46, 8186–8188. doi: 10.1039/c0cc01447h
- Wölfel, R., Taccardi, N., Bösmann, A., and Wasserscheid, P. (2011). Selective catalytic conversion of biobased carbohydrates to formic acid using molecular oxygen. *Green Chem.* 13, 2759–2763. doi: 10.1039/c1gc15434f
- Wu, L., Zhu, B., and Wu, Y. (2017). “Hydrophobic lurylamine modified heteropoly acid as an efficient and recyclable catalyst for the hydrolysis reaction in aqueous solution under microwave,” in *The 4th Annual International Conference on Information Technology and Applications (ITA 2017)* (Guangzhou), 12:04026. doi: 10.1051/itmconf/20171204026
- Wu, Y., Fu, Z., Yin, D., Xu, Q., Liu, F., Lu, C., et al. (2010). Microwave-assisted hydrolysis of crystalline cellulose catalyzed by biomass char sulfonic acids. *Green Chem.* 12, 696–700. doi: 10.1039/b917807d
- Xie, X., Han, J., Wang, H., Zhu, X., Liu, X., Niu, Y., et al. (2014). Selective conversion of microcrystalline cellulose into hexitols over a Ru/[Bmim]₃PW₁₂O₄₀ catalyst under mild conditions. *Catal. Today* 233, 70–76. doi: 10.1016/j.cattod.2013.09.061
- Yabushita, M., Kobayashi, H., and Fukuoka, A. (2014). Catalytic transformation of cellulose into platform chemicals. *Appl. Catal. B Environ.* 145, 1–9. doi: 10.1016/j.apcatb.2013.01.052
- Yan, L., Greenwood, A. A., Hossain, A., and Yang, B. (2014). A comprehensive mechanistic kinetic model for dilute acid hydrolysis of switchgrass cellulose to glucose, 5-HMF and levulinic acid. *RSC Adv.* 4, 23492–23478. doi: 10.1039/c4ra01631a
- Yang, L., Qi, Y., Yuan, X., Shen, J., and Kim, J. (2005). Direct synthesis, characterization and catalytic application of SBA-15 containing heteropolyacid H₃PW₁₂O₄₀. *J. Mol. Catal. A Chem.* 22, 199–205. doi: 10.1016/j.molcata.2004.11.024
- Yang, P., Kobayashi, H., and Fukuoka, A. (2011). Recent developments in the catalytic conversion of cellulose into valuable chemicals. *Chin. J. Catal.* 32, 716–722. doi: 10.1016/S1872-2067(10)60232-X
- Yu, F., Kong, X. J., Zheng, Y. Y., Ren, Y. P., Long, L. S., Huang, R. B., et al. (2009a). Ph-dependent assembly of 0D to 3D keggins-based coordination polymers: structures and catalytic properties. *Dalton Trans.* 43, 9503–9509. doi: 10.1039/b911606k
- Yu, S., Brown, H. M., Huang, X., Zhou, X.-d., Amonette, J. E., and Zhang, Z. (2009b). Single-step conversion of cellulose to 5-hydroxymethylfurfural (HMF), a versatile platform chemical. *Appl. Catal. A Gen.* 361, 117–122. doi: 10.1016/j.apcata.2009.04.002
- Yusuke, K., and Urabe, K. (1981). Catalysis of heteropoly acids entrapped in activated carbon. *Chem. Lett.* 10, 663–666. doi: 10.1246/cl.1981.663
- Zhang, F., Deng, X., Fang, Z., Zeng, H., Tian, X., and Kozinski, J. (2011). Hydrolysis of microcrystalline cellulose over Zn-Ca-Fe oxide catalyst. *Petrochem. Technol.* 40, 43–48. doi: 10.1016/S1872-5805(11)60067-X
- Zhang, H., Li, H., Pan, H., Wang, A., Souzanchi, S., Xu, C., et al. (2018). Magnetically recyclable acidic polymeric ionic liquids decorated with hydrophobic regulators as highly efficient and stable catalysts for biodiesel production. *Appl. Energ.* 223, 416–429. doi: 10.1016/j.apenergy.2018.04.061
- Zhang, H., Zhou, Q., Chang, F., Pan, H., Liu, X., Li, H., et al. (2015). Production and fuel properties of biodiesel from Firmiana platanifolia L.f. as a potential non-food oil source. *Ind. Crop. Prod.* 76, 768–771. doi: 10.1016/j.indcrop.2015.08.002
- Zhang, J., Liu, X., Sun, M., Ma, X., and Han, Y. (2012). Direct conversion of cellulose to glycolic acid with a phosphomolybdic acid catalyst in a water medium. *ACS Catal.* 2, 1698–1702. doi: 10.1021/cs300342k
- Zhang, J., Sun, M., Liu, X., and Han, Y. (2014). Catalytic oxidative conversion of cellulosic biomass to formic acid and acetic acid with exceptionally high yields. *Catal. Today* 233, 77–82. doi: 10.1016/j.cattod.2013.12.010
- Zhang, X., Zhang, D., Sun, Z., Xue, L., Wang, X., and Jiang, Z. (2016). Highly efficient preparation of HMF from cellulose using temperature-responsive heteropolyacid catalysts in cascade reaction. *Appl. Catal. B Environ.* 196, 50–56. doi: 10.1016/j.apcatb.2016.05.019
- Zhang, Y., Zhao, M., Wang, H., Hu, H., Liu, R., Huang, Z., et al. (2019). Damaged starch derived carbon foam-supported heteropolyacid for catalytic conversion of cellulose: improved catalytic performance and efficient reusability. *Bioresour. Technol.* 288:121532. doi: 10.1016/j.biortech.2019.121532

- Zhao, Q., Wang, H., Zheng, H., Sun, Z., Shi, W., Wang, S., et al. (2013). Acid–base bifunctional hpa nanocatalysts promoting heterogeneous transesterification and esterification reactions. *Catal. Sci. Tech.* 3, 2204–2209. doi: 10.1039/c3cy20868k
- Zheng, W., Cui, Y., Xu, Z., Zhao, L., and Sun, W. (2018). Cellulose transformation into methyl glucosides catalyzed by $H_3PW_{12}O_{40}$: enhancement of ionic liquid pretreatment. *Can. J. Chem. Eng.* 96, 1250–1255. doi: 10.1002/cjce.23057
- Zhizhina, E. G., and Odyakov, V. F. (2008). Alteration of the physicochemical properties of catalysts based on aqueous solutions of mo-v-p heteropoly acids in redox processes. *Reac. Kinet. Catal. Lett.* 95, 301–312. doi: 10.1007/s11144-008-5423-2

Conflict of Interest: The authors declare that the research was conducted in the absence of any commercial or financial relationships that could be construed as a potential conflict of interest.

Copyright © 2020 Luo, Wu, Li, Li, Li, Zhang, Li, Su and Yang. This is an open-access article distributed under the terms of the Creative Commons Attribution License (CC BY). The use, distribution or reproduction in other forums is permitted, provided the original author(s) and the copyright owner(s) are credited and that the original publication in this journal is cited, in accordance with accepted academic practice. No use, distribution or reproduction is permitted which does not comply with these terms.



The Effect of Ni-ZSM-5 Catalysts on Catalytic Pyrolysis and Hydro-Pyrolysis of Biomass

Ya-Long Ding¹, Hua-Qin Wang¹, Mei Xiang², Pei Yu¹, Rong-Qiang Li^{1*} and Qing-Ping Ke^{3*}

¹ College of Chemistry and Pharmaceutical Engineering, Huanghuai University, Zhumadian, China, ² School of Chemical Engineering and Materials, Changzhou Institute of Technology, Changzhou, China, ³ College of Chemistry and Chemical Engineering, Anhui University of Technology, Ma'anshan, China

OPEN ACCESS

Edited by:

Hu Li,
Guizhou University, China

Reviewed by:

Yujing Weng,
Henan Polytechnic University, China
Zhibing Shen,
Xi'an Shiyou University, China

*Correspondence:

Rong-Qiang Li
rqli@iccas.ac.cn
Qing-Ping Ke
qingke@ahut.edu.cn

Specialty section:

This article was submitted to
Catalysis and Photocatalysis,
a section of the journal
Frontiers in Chemistry

Received: 21 May 2020

Accepted: 28 July 2020

Published: 25 September 2020

Citation:

Ding Y-L, Wang H-Q, Xiang M, Yu P,
Li R-Q and Ke Q-P (2020) The Effect
of Ni-ZSM-5 Catalysts on Catalytic
Pyrolysis and Hydro-Pyrolysis of
Biomass. *Front. Chem.* 8:790.
doi: 10.3389/fchem.2020.00790

With the demand of energy and re-utilization of wastes, the renewable lignocellulosic biomass, has attracted increasing and significant attention for alleviating the growing energy crisis and environment problems. As main components of lignocellulosic biomass, lignin, cellulose, and hemicellulose are connected by hydrogen bond to form a compact skeleton structure, resulting the trenchant condition of biomass pyrolysis. Also, pyrolysis products of above three main constituents contain a large amount of oxygenates that cause low heating value, high corrosiveness, high viscosity, and instability. Meanwhile, zeolites are of considerable significance to the conversion of lignocellulosic biomass to desirable chemical products on account of fine shape selectivity and moderate acid sites and strength. Among numerous zeolites, ZSM-5-based catalysts have been most extensively studied, and the acidity and porosity of ZSM-5 can be tuned by changing the content of Si or Al in zeolite. Beyond that, doping of other metal elements, such as Mn, Co, Ni, Ga, Ce, Pt, into ZSM-5 is also an efficient way to regulate the strength and density of acid sites in zeolite precisely. This review focused on the recent investigation of Ni-modified microporous ZSM-5 used in catalytic pyrolysis of lignin and cellulose. The application of metal-modified hierarchical ZSM-5 is also covered.

Keywords: lignocellulose, microporous, Ni-ZSM-5, catalytic pyrolysis, hydro-pyrolysis

INTRODUCTION

With the rapid development of world economy and the continuous increase of population, human is facing unprecedented energy demand (Department of Economic Social Affairs United Nations, 2019; Energy Information Administration United States, 2019). Petroleum-based resources are currently society's primary source of chemicals and transportation fuels. However, due to limited oil reserves, uneven geographical distribution and environmental motivation to reduce carbon dioxide emissions and other factors, renewable energy such as lignocellulosic biomass has become a promising candidate resource for the production of renewable fuels and chemicals (Huber et al., 2006; Demirbas, 2008; Saxena et al., 2009; Zakzeski et al., 2010). Although fossil fuels continue to meet most of the world's energy demand, renewable energy is the world's fastest growing form of energy and its worldwide consumption will increase by 3% per year between 2018 and 2050 (Energy Information Administration United States, 2019). As carbon-neutral and the most abundant renewable energy resource for production of biofuels and valuable chemicals, biomass

energy has attracted great attention, and developed rapidly in the last two decades (Jürgen, 2006; Ragauskas et al., 2006; Chheda et al., 2007; Huber and Corma, 2007). Biomass consists of a mixture of strongly bonded natural polymers such as cellulose (40–50%), hemicelluloses (25–30%), lignin and non-carbohydrate (Zhang et al., 2006; Menon and Rao, 2012). One most recent emerging focus of biomass utilization was the use of bio-oil generated from sustainable biomass feedstocks.

Biomass conversion is generally carried out in two ways: thermochemical decomposition, including gasification, biological carbonization, liquefaction, thermal decomposition (pyrolysis) process, and biological digestion process (essentially microbial digestion and fermentation) (Rocca et al., 1999; Lewandowski et al., 2011). Biomass conversion through thermochemical processes is considered to be a very promising biofuel carrier, because obtained bio-oil can be easily transported, burned directly in a thermal power station or gas turbine, and used in traditional refineries to produce high-quality light hydrocarbon fuels. Fast pyrolysis technology, firstly appeared in the late 1970s, is a promising way to convert biomass into bio-oil, for its high liquid oil production (up to 80% of dry feed) (Bridgwater and Peacocke, 2000; Onay, 2007). Bio-oil has many potential applications in the field of energy including being used for static application, and also can be upgraded to transportation fuel (Bridgwater and Cottam, 1992; Czernik and Bridgwater, 2004; Bridgwater, 2012). However, bio-oil usually presents several shortcomings, among which high water and oxygen content, corrosiveness, heat storage instability, immiscibility with petroleum fuel, high acidity, high viscosity, and low calorific value are main obstacles for its direct application as fuel (Michael, 2008; Park et al., 2011). The major product from non-catalytic fast pyrolysis are acids including linoleic acid, nitrogen containing compounds such as amines, amides, indoles, and pyrroles. Other organic compounds are ketones, alcohols, esters, ethers, phenols, and sugars. Acid is related to the high acidity of bio oil, and ketone is the cause of the instability of bio oil. Ethers and esters will reduce the heating values of bio oil, and nitrogen compounds cause environmental problems. In order to improve fuel quality, the process used must remove oxygen, convert carboxylic acid and other active substances into milder products, and add hydrogen to bio oil (Corma et al., 2007a; Gallezot, 2007; Alonso et al., 2010). Catalytic pyrolysis is the process of pyrolysis with assistance of catalyst and recombination of organic steam obtained from rapid pyrolysis of biomass into a class of compounds under the action of catalysts. Meanwhile, liquid fuels such as aromatic compounds within the gasoline range can be directly pyrolyzed by biomass materials (Chen and Degnan, 1988). However, due to the existence of lignin and hemicellulose structure, it is difficult to transform lignocellulose into liquid fuels by simple chemical or enzymatic hydrolysis, and finally into biofuels. Many pyrolysis parameters, such as temperature, pressure, heating rate, reactor structure, biomass type, particle size, and so on, have been widely studied and summarized (Melligan et al., 2011; Bridgwater, 2012).

Catalysts play an important role in the upgrading of bio-oil (Horne and Williams, 1996; Zhang et al., 2011). The primary catalysts mainly consist of supported noble metals Pt and Pd,

transition metals Mo, Ni-Mo, Co-Mo, Ni-W, and Co-W (Viljava et al., 2000; Olivas et al., 2008; Yang et al., 2008). Although the noble metal catalysts have excellent catalytic performance, their high cost limit their large-scale application (Kubičková et al., 2005). To maintain the activity and stability of catalysts modified with metal Co and Ni, sulfurization of these catalysts is necessary during catalysts activation and bio-oil upgrading process, which will result in sulfur pollution of final products (Ryymän et al., 2010). In order to prevent sulfur pollution, it is of great significance to explore the non-sulfurized transition metal catalyst (Hu et al., 2018). ZSM-5 has been widely applied in crude oil refinery and gas adsorption-separation industry due to its strong acidity as well as shape selectivity. ZSM-5 is a kind of crystalline aluminosilicate material, which has unique two-dimensional channel-like pore structure with intersecting channels of ~0.55 nm in diameter favoring hydrocarbons of <10 carbon atoms, good thermal and hydrothermal stability, strong acid resistance, and carbon deposition resistance, adjustable acidity (Brønsted acid sites and Lewis acid sites), excellent shape selectivity, isomerization, hydrodeoxidization, and other catalytic properties (Sharma and Bakhshi, 1991; Chen et al., 2020). It has been successfully used in the hydrolysis of lignocellulose (Corma et al., 2007b; Mortensen et al., 2011; Park et al., 2011). ZSM-5 has also been widely used as a catalyst for biomass pyrolysis, and found to greatly change the composition of bio oil via dramatically reducing oxygenated compounds by deoxidization reactions, increasing aromatic species, and producing more organic matters (bio-oil) which can be upgraded to gasoline and diesel fuel (Vitolo et al., 2001; Cheng and Huber, 2011; Mortensen et al., 2011; Park et al., 2011; Taarning et al., 2011). Oxygen is removed through formation of water due to strong dehydration tendency promoted by the strong acidity of H⁺-exchanged ZSM-5 (HZSM-5) (Topsøe et al., 1981; Kapustin et al., 1988; Triantafyllidis et al., 2001; Lappas et al., 2009). However, the strong acidity of ZSM-5 may lead to the decrease of organic components of bio oil by over-cracking to hydrocarbon, gas, or coke. Therefore, tuning of the acid sites is essential to utilization of catalyst (Huang et al., 2009).

Transition metal dopants are believed to affect the oxygen exclusion pattern by producing more carbon oxides and less water, so that more hydrogen can be incorporated into hydrocarbons. Different metal-modified ZSM-5 catalysts (Ce-ZSM-5, Co-ZSM-5, FeZSM-5, Ga-ZSM-5, HZSM-5, Ni-ZSM-5) have been used in biomass pyrolysis to verify whether these metal promoted low acid zeolites produce higher hydrocarbon yield and less coke than the commercial ZSM-5 catalysts previously tested (Park et al., 2007; French and Czernik, 2010; Valle et al., 2010; Cheng et al., 2012; Neumann and Hicks, 2012). Among them, French and Czernik (2010) studied 40 different catalysts and found that Ni-ZSM-5 catalyst has the highest hydrocarbon yield. The incorporation of transition metals (such as nickel) can increase the yield of aromatics, and they found that the hydrothermal stability of ZSM-5 will be improved by metal impregnation (Valle et al., 2005). Considering the importance of hydrodeoxygenation of bio-oil for biomass utilization and the hydrogenation ability of transition metals such as Ni, this paper mainly reviews the research progress of Ni supported ZSM-5

zeolite in catalytic conversion of biomass, and comprehensively summarizes the following aspects: (1) the catalytic conversion of biomass promoted by single metal Ni supported ZSM-5 in the absence of hydrogen; (2) the promotion of Ni supported ZSM-5 in biomass catalytic conversion in hydrogen atmosphere; (3) the utilization of bimetal supported ZSM-5 composed of Ni and other metals in biomass catalytic conversion.

NI MODIFIED ZSM-5

The most representative organic compounds in pyrolytic bio-oil can be divided into 13 major functional groups: aromatic hydrocarbons, aliphatic hydrocarbons, phenols, furans, acids, esters, alcohols, ethers, aldehydes, ketones, polyaromatic hydrocarbons (PAHs), nitrogen compounds, and heavier compounds (Iliopoulou et al., 2012). Among them, aromatic hydrocarbon, aliphatic hydrocarbon, and alcohol are considered as ideal biofuel products, and phenols and furans are considered as high value-added chemicals. Carbonyl compounds, such as acids, ketones, aldehydes, ketones, esters, ethers are undesirable products for their relation to corrosiveness, instability and reduce the heating value of bio oils. Other undesirable products includes polyaromatic hydrocarbons and nitrogen compounds due to environmental reasons.

The aromatics produced by catalytic pyrolysis can be divided into two types including (1) monocyclic aromatics (MAHs), such as benzene, toluene, ethylbenzene (EB), xylene, indene and other substituted benzenes as styrene, ethyl-methyl-benzene, etc. (2) polycyclic aromatics (PAHs: naphthalene, anthracene, phenanthrene, fluorene). The metal on ZSM-5 helps to catalyze the formation of monocyclic aromatics and retards the further polymerization of PAHs and other oxygenates, which is a competitive reaction and leads to the formation of PAHs.

The conversion of biomass to bio oil (X_A) and selectivity to product i (S_i) was defined as:

$$X_A(\text{wt.}\%) = \frac{w_0 - w_1}{w_0} \times 100\%$$

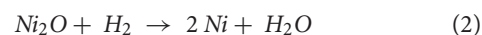
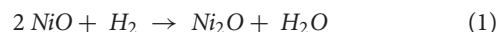
$$S_i(\text{mol.}\%) = \frac{n_i \times a_i}{\sum_1^i n_i \times a_i} \times 100\%$$

Where w_0 refers to the initial weight of biomass, w_1 means the weight of bio oil after catalytic pyrolysis; n_i refers to moles of the product i , and a_i is the carbon atom numbers for product i .

The addition of Ni metal to ZSM-5 zeolite is believed to promote the conversion of oxygenated and nitrogen compounds to aliphatics and aromatics and improve the hydrothermal stability of the catalyst, due to the synergistic effect of the dehydrogenation activity of nickel and the moderate acid strength of the catalyst (Valle et al., 2010). The formation of aliphatic compounds may be due to the fact that the metal part slows down the reaction between aromatics and other oxygenated compounds during the catalytic pyrolysis, forming alkylated benzene or polycyclic aromatic hydrocarbons (PAHs) (Carlson et al., 2010; Thangalazhy-Gopakumar et al., 2012).

Monometallic Ni-Modified ZSM-5

Huynh et al. (2014) synthesized Ni-ZSM-5 for 4, 12, 21 wt.% Ni loadings. The N_2 adsorption studies revealed a steady decline in adsorption capacities with the increase in Ni content, as the N_2 adsorbed volume were 94.5, 75.2, 73.4, and 65.4 $\text{cm}^3 \cdot \text{g}^{-1}$ at standard temperature and pressure for 4, 12, 21 wt.% Ni loadings ZSM-5, respectively. This finding could be attributed to pore blocking by the increasing proportion of loaded metal species, which is in consistence with the results of Gayubo et al. (2010). The H_2 temperature-programmed reduction (TPR) profile of 21 wt.% Ni-ZSM-5 consists of two peaks at low temperature (350–450°C) and high temperature (500–600°C). There are two possible explanations for this result. One is that nickel oxide can be reduced to two-step reaction as shown in formula (1) and formula (2), as Hadjiivanov et al. (2002) confirmed. The other explanation is the intensities of interaction between Ni^{2+} and HZSM-5 at different positions are different, which may lead to different reducibility, which is in line with conclusion from Maia et al. (2010). According to the elemental compositions analysis by X-ray photoelectron spectroscopy, the surface Ni/Si ratio decrease from 0.24 to 0.11 during the reduction of 21 wt.% Ni-ZSM-5, and this result may be due to the sintering or migration of Ni into the pore (volume) during reduction. Results from IR spectra of neat and reduced 21 wt.% Ni-ZSM-5 showed that the total acidity remains the same (619 and 588 $\mu\text{mol} \cdot \text{g}^{-1}$ for neat and reduced 21 wt.% Ni-ZSM-5). However, after impregnation with Ni species, the overall Brönsted acidity significantly decreased from 451 to 243 $\mu\text{mol} \cdot \text{g}^{-1}$ whereas the overall Lewis acidity increased from 168 to 345 $\mu\text{mol} \cdot \text{g}^{-1}$. The variation of overall Brönsted acidity and Lewis acidity may be attributed to substitution of protons at Brönsted sites by exchangeable cations, that is Ni^{2+} (Huynh et al., 2014). The overall Lewis acidity could be produced by dehydration of protonated oxide bridge after high temperature treatment in the calcination or reduction step (Hooff and Roelofsen, 1991). This combination of Brönsted acid sites and Lewis acid sites is more suitable for HDO reaction because the acid center can cleave C-O bond through protonation, while the metal center can activate H_2 and reduce aromatic ring.



Catalytic Pyrolysis

Catalytic pyrolysis with cracking catalyst is an emerging technology to directly convert the oxygenated compounds produced in the pyrolysis of biomass into hydrocarbons, so as to improve the quality of bio-oil. Catalytic pyrolysis can be carried out in the atmosphere without high hydrogen pressure, which reduces the operation cost. The volatile oxygenated species in the pyrolysis gas enter into ZSM-5 pores and react with the protons in the active sites through dehydration, decarboxylation, decarbonylation, oligomerization, and dehydrogenation to generate aromatic compounds, carbon monoxide, carbon dioxide, and water.

The results from Huynh et al. revealed that phenol conversion of 14, 82, and 98% were obtained with 4, 12, 21 wt.% Ni-ZSM-5, respectively. For 21 wt.% Ni-ZSM-5, selectivity toward deoxygenated products reached 98%, which included ~88% for cyclohexane and 8% for benzene, indicating that the combination of metal and acid is needed to effectively remove oxygen from phenol. Tuning of the metal sites can provide additional control over the severity of hydrogenation (whether it is an attack on a substituent or aromatic ring system) and selectivity. Iliopoulou et al. (2012) investigated the catalytic upgrading of biomass pyrolysis vapors using different loadings (1, 5, 10 wt.%) Ni-modified commercial equilibrium ZSM-5 diluted with silica-alumina (containing 30 wt.% crystalline zeolite) via typical wet impregnation method. There is no significant loss of surface area at low loadings (1 and 5 wt.%). However, high loading (10 wt.%) results in a 15% decrease of surface area, which is mainly due to the blocking of micropores in ZSM-5 crystal when metal phases are formed (Vitolo et al., 2001). On the other hand, compared with porosity, the effect of metals on the acidity of ZSM-5 zeolite catalyst is more significant. The presence of 1 and 5 wt.% Ni reduced the number of Brønsted acid sites by 40%, and higher loading (10 wt.%) induced further reduction (47 wt.%). The significant decrease of Brønsted acid sites indicated that the acidic protons in ZSM-5 zeolite were exchanged by Ni ions during the dry impregnation process, and the quantity of Lewis was increased by 2–3 times, possibly due to the formation of the corresponding oxide, i.e., NiO, which can serve as Lewis acid center. Basing on X-ray diffraction (XRD) pattern, crystallite size of NiO increases from 28.5 to 39.5 nm for the 5 and 10 wt.% loaded catalyst, while it is difficult to identify the XRD peaks caused by NiO in Ni (1%) ZSM-5 catalyst. For 10 wt.% Ni-ZSM-5, the rectangular or cubic NiO particles were highly dispersed on catalysts and showed a mean size of ~40–45 nm.

The results of deoxy-liquefaction of *Laminaria japonica* to liquid oil over Ni-ZSM-5 showed that Ni-ZSM-5 catalyst could increase the liquid oil yield and the contents of aromatics and long-chain alkanes, and decrease the amounts of phenols, other oxygen and nitrogen containing species (Li et al., 2013). Vichaphund et al. (2015) investigate the catalytic pyrolysis of *Jatropha* residues including 59.2% cellulose, 18.0% hemicelluloses, and 22.8% lignin with 3 wt.% Ni-ZSM-5 catalysts. The combination of Ni and acid sites provides an ideal environment for the oligomerization, cyclization, and dehydrogenation of small olefins, and improves the formation rate of aromatic compounds. The main product is toluene with selectivity of 36.4% while the selectivity of benzene is only 10%, owing to the alkylation of benzene and other oxygenated compounds to form alkylated benzene. In addition, the 3 wt.% Ni-ZSM-5 catalysts with different preparation method of ion-exchange and wet impregnation are compared in catalytic pyrolysis of *Jatropha* residues. For ion-exchanged HZSM-5, the MAHs selectivity is 85–88% and PAHs can be reduced to 12–16%, while for impregnated HZSM-5, the MAHs selectivity is 85–90% and PAHs can be reduced to 10–15%.

The upgrading of bio-oil with Ni modified hierarchical ZSM-5 catalyst is also studied, and results showed that the preferential mechanism for O-removal using hierarchically structured Ni-ZSM-5 zeolite catalysts seems to proceed through

decarbonylation and decarboxylation reactions at the Lewis acid sites evolved after metal incorporation (Veses et al., 2016). However, the main product in obtained bio-oil is phenols (42.8 wt%). Chen et al. synthesize hierarchical ZSM-5 catalyst by NaOH desilication and HCl treatment and investigate the catalytic pyrolysis of rice straw to aromatics with Ni modified ZSM-5. High yields of aromatics (28%) can be obtained at very low Ni loading (0.1 wt.%), and there is no difference in the selectivity of aromatic products when the amount of Ni added is 0.1, 0.5, or 1.0% (Chen et al., 2018). The study on effect of reaction temperature on conversion of phenol with hierarchical Ni-ZSM-5 shows that the main products were mostly benzene and cyclohexene formed by phenol deoxygenation at low and intermediate temperatures (393 and 423 K) whereas a shift in the reaction pathways occurred at higher temperature (448 K), leading to high selectivity of valuable alkylphenols (mostly cresols and cyclohexylphenols) generated by the occurrence of alkylation reactions catalyzed by the zeolite acid sites (García-Minguillan et al., 2020). The mixture of microporous ZSM-5 and another mesoporous zeolite is also employed for catalytic pyrolysis of biomass. Hu et al. (2020) investigate the catalytic co-pyrolysis of seaweeds and cellulose using mixed ZSM-5 and MCM-41, the yield of main product (furans) is 52.2%, which is higher than that using single ZSM-5 or MCM-41. Because of the interaction between the free radicals of seaweeds/cellulose and ZSM-5/MCM-41, as well as the synergism between the joint channel advantage of mesoporous molecular sieve and the acidity of microporous molecular sieve, the yield and composition of bio oil are improved.

The biomass pyrolysis experiments were performed on a bench-scale fixed bed tubular reactor, and catalytic pyrolysis experiment with NiO was also conducted for comparison (Iliopoulou et al., 2007; Triantafyllidis et al., 2007). Compared with the non-catalytic experiment, all the catalysts reduced the total liquid yield, increased the gas products and coke at the expense of organic yield. This behavior is due to various hydrocarbon conversion reactions, such as cracking, dehydrogenation, and cyclization/aromatization, which are catalyzed by zeolite protonic acid sites. Besides that, water formation was promoted by dehydration/decarboxylation of oxygenated compound on acid sites of ZSM-5 (Lappas et al., 2009). What is needed to point out is that the addition of Ni in to ZSM-5 does not influence the formation of water and leads mainly to increased production of H₂ and C₂–C₆ gaseous hydrocarbons. Iliopoulou et al. (2012) suggested two important reaction routes: (1) bio oil deoxidized by decarboxylation, producing a small amount of water and *in situ* generating hydrogen; (2) *in situ* generated hydrogen atoms participate in the hydrogen transfer reaction on NiO atoms, increasing the generation of saturated hydrocarbon through the carbonium intermediate on the acid sites of zeolite. The almost unaffected water production indicates that the oxygen of bio oil compounds is not removed by hydrogen deoxidation, which can be promoted by Ni supported metals, but mainly by decarboxylation reactions. The increase of aromatics may be due to the enhancement of dehydrogenation of Ni metal, and the increase of phenolic content may be related to the decrease of Brønsted acid sites which are covering by Ni metal ions. After pyrolysis experiment,

a majority of NiO particles converted to metallic Ni particles which showed smaller spherical or rectangular particles with an average size of ~ 17 nm, and the catalyst particle were covered by a layer of graphitized carbon, which may be due to the strong dehydrogenation effect of Ni species (related to the formation of coke) during pyrolysis. This is the first report of observation of reduction of Ni oxides to metallic Ni during biomass catalytic pyrolysis. And this result may play an important role in commercial use of Ni-ZSM-5, because the catalyst will continue to circulate between the pyrolysis reactor (reduction of Ni oxides) and the regenerator (oxidization of metal Ni) which is used to burn off char (coke deposited on the catalyst and possibly unreacted biomass). In addition, the *in-situ* formation of reduced Ni metal phase can also promote the hydrogen transfer reaction using the *in situ* produced H_2 on metallic Ni or external supplied H_2 in a hydro-pyrolysis process (Yung et al., 2016). Porosity and acidity of different Ni-ZSM-5 catalysts and their catalytic pyrolysis performance are shown in Table 1.

Catalytic Hydro-Pyrolysis

When hydrogen is added in the pyrolysis process, very active $H\cdot$ radicals will be produced. $H\cdot$ radicals are easy to react to form biomass fragments, while removing oxygen and covering free radicals, thus increasing the hydrocarbons production. Hydro-pyrolysis has been widely used in coal pyrolysis, and the

results show that under high hydrogen pressure, cracking, and hydrogenation of bio oil compounds will occur simultaneously (Canel et al., 2005). To study the deoxidization effect of Ni-ZSM-5 catalyst in the process of catalytic hydro-pyrolysis, Thangalazhy-Gopakumar et al. (2012) investigated the catalytic hydro-pyrolysis of pine wood sample (particle size of 149–177 μm) using HZSM-5 and 5 wt.% Ni-HZSM-5 under different hydrogen pressure of 10, 20, 30, and 40 MPa.

For HZSM-5 catalysts, the aromatic yields have no change in the hydrogen pressure of 10–40 MPa, and the catalyst may only play the role of cracking catalyst, not the role of promoting hydrogenation (Pindoria et al., 1998). Lower amounts of the higher molecular weight phenolic compounds and larger amounts of the lighter phenols were observed in the presence of Ni supported ZSM-5 (Melligan et al., 2012). The possible reaction mechanism for the formation of phenols, benzene, toluene, and ethylbenzene is shown in Scheme 1. Compared with ZSM-5 catalyst, Ni-ZSM-5 lowered the ethanoic acid content, and a further decrease of 20% in ethanoic acid was observed after introduction of H_2 to the reaction.

The hydrodeoxygenation of guaiacol and 2-phenoxy-1-phenylethanol as model compounds of lignin are performed with different Ni loadings (5, 10, 12.5, 15, 20 wt.%) Ni-ZSM-5 under 5 MPa of hydrogen pressure (Barton et al., 2018). Regardless of Ni loading, the conversions of guaiacol are nearly 100% and

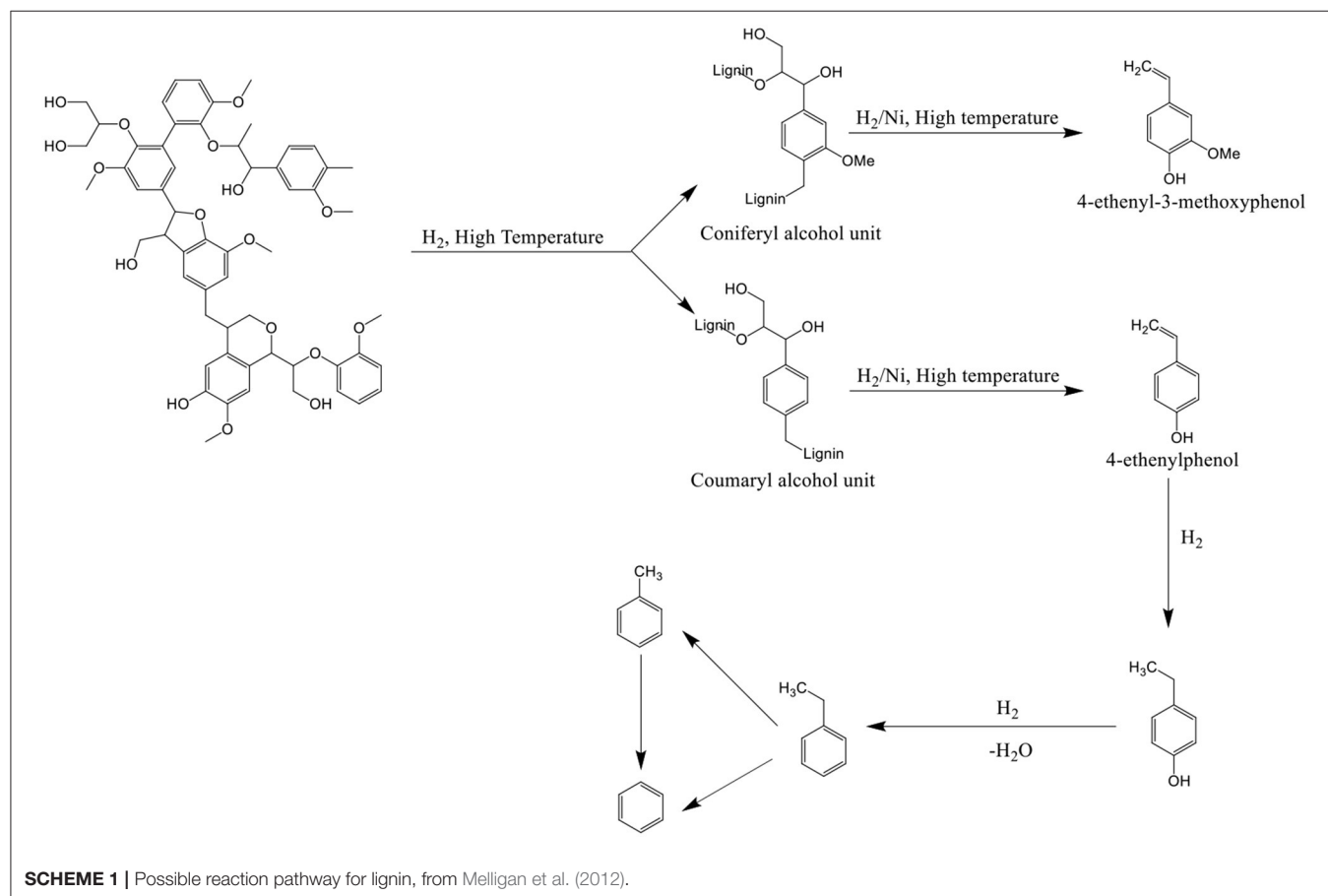


TABLE 1 | Porosity and acidity characteristics of catalysts and catalytic pyrolysis performance of different catalysts.

Catalyst	Surface area (m ² /g) ^a	Acidic properties (μmol/g)			Raw material	Primary product in liquid phase (wt.%)	References
		Brønsted acidity	Lewis acidity	Total acidity			
ZSM-5 ^b	138	36.5 ^c	18.1 ^c	54.6 ^c	Beech wood ^d	Phenols (35.0)	Iliopoulou et al., 2012
5 wt.% Ni-ZSM-5 ^b	132	21.9 ^c	54.6 ^c	76.5 ^c	Beech wood ^d	Phenols (39.0)	Iliopoulou et al., 2012
Ni-ZSM-5 ^e	306	None	None	401 ^f	Laminaria japonica	C ₁₂ -C ₂₁ alkanes (22.9) Phenols (23.0)	Li et al., 2013
3 wt.% Ni-ZSM-5 ^g	608	None	None	None	Jatropha residues	Aromatics (30.6), Acid (15.7)	Vichaphund et al., 2015
3 wt.% Ni-ZSM-5 ^h	358	None	None	None	Eucalyptus urophylla	N-compounds (28.9) BETX ⁱ (NM ^j) Naphthalenes (NM ^j)	Schultz et al., 2016
12 wt.% Ni-ZSM-5	386	None	None	None	Prairie cordgrass	C ₄ -C ₁₂ hydrocarbons (32.45)	Cheng et al., 2016
1 wt.% Ni-ZSM-5	500	148 ^c	270 ^c	418 ^c	Pine wood	Phenols (42.8)	Veses et al., 2016
0.1 wt.% Ni-ZSM-5 ^k	None	None	None	None	Rice straw	Aromatics (28)	Chen et al., 2018

^aMulti-point BET method.^bCommercial equilibrium ZSM-5 zeolite catalyst diluted with silica-alumina (~30 wt.% zeolite).^cFourier-Transform Infrared (FTIR) measurements.^dA commercial lignocellulosic biomass originating from beech wood consists of 1.35% ash, 3.74% extractives, 21.75% lignin, 33.91% hemicellulose and 39.25% cellulose.^eZSM-5 (Si/Al = 100) was commercially purchased.^fThe result was obtained from NH₃ temperature programmed desorption.^gThe ZSM-5 zeolite is synthesized at 160°C for 72 h with raw materials ratio as SiO₂: Al₂O₃: TPABr: Na₂O: H₂O = 1: 40: 10: 1.0: 0.02.^hZSM-5 (Si/Al = 46) was commercially purchased.ⁱBETX: sum of benzene, toluene, ethylbenzene, and xylenes.^jNM: not measured.^kThe ZSM-5 is deal with NaOH solution and HCl, with surface area of 354 m²/g, total acidity of 103.9 μmol/g.

three main products are 2-methoxycyclohexanol, cyclohexanol, and cyclohexane. But the time required to reach 100% conversion decreased with increased Ni loading. The Ni-ZSM-5 was also used to investigate the hydrodeoxygenation of vegetable oils to liquid alkane fuels, where the selectivity of *n*-C₅-C₁₆ alkane was 71.0% (Na et al., 2012). Porosity and acidity of different Ni-ZSM-5 catalysts and their catalytic hydro-pyrolysis performance are shown in Table 2.

Bimetallic Ni Modified ZSM-5

Although the activity of nickel-based catalysts is higher than that of other catalysts, there are still many problems that limit the utilization of Ni-ZSM-5 catalysts, such as carbon deposition. Zhang et al. (2013) observed that 36 wt.% of residue such as coke was deposited on the surface after hydrotreatment. Zhao et al. (2012) observed the deactivation of Ni-ZSM-5 catalysts owing to sintering during the hydrothermal treatment and recycling process as well as partly Ni leaching from the catalyst into water (Zhao et al., 2012). The deactivation of catalysts mainly depends on the zeolite pore structure, acidic properties, reaction temperature, and properties of reactants. The main function of Lewis acid sites is to bind substances to the catalyst surface; Brønsted acid sites is to transfer protons to related compounds to form carbon positive ions, which is considered to be the main reason for coking (Mortensen et al., 2011). The process of carbon deposition is very complex, in which the intramolecular and intermolecular condensation reactions of reactants and/or products play a key role. These condensation reactions usually undergo nearly irreversible second reaction of dehydrogenation

or hydrogen transfer to form stable oligomer or graphite carbon, which is difficult to remove from the acid catalyst. Li et al. (2015) investigate the coke deposition on 15 wt.% Ni-ZSM-5 in bio-oil hydrodeoxygenation process under 523–603 K and 2.0 MPa of hydrogen pressure. The results showed that most of the deposited filamentous carbon is converted into carbon-rich flat plate as the temperature rises from 250 to 330°C. The filamentous carbon and carbon-rich flat plate both possess low volatility and solubility and are often retained within pores or on the outer surface of the catalysts, which could potentially block reactant molecules from reaching acid sites and result in catalysts deactivation. The deposition coked at 250°C is soft carbon which is soluble in organic solvents, the deposition coked at 280°C shows that some soluble carbon burned off or is transformed into derivatives with higher molecular weights, the deposition coked at 300°C shows deposited hard coke (or amorphous graphite) which is insoluble in organic solvents, and the deposition coked at 330°C shows deposited graphite or amorphous graphite (Rossetti et al., 2005; Xu et al., 2009). Thermogravimetry analysis of catalysts after hydrodeoxygenation process shows four stages of mass loss from 50 to 250°C, from 250 to 450°C, from 450 to 600°C, and from 600 to 750°C, which corresponds to the loss of moisture, physical absorbents, the formation of soft coke, hard coke, and graphite, respectively.

Bimetallic catalysts often show properties different from those of the corresponding monometallic catalysts (Alonso et al., 2012). Therefore, bimetallic catalysts have also attracted much attention from researchers in recent years. Huynh et al. (2014) discovered that when using monometallic Ni-ZSM-5 and

TABLE 2 | Porosity and acidity characteristics of catalysts and catalytic hydro-pyrolysis performance of different catalysts.

Catalysts	Surface area (m ² /g) ^a	Acidic properties (μmol/g)			Experimental conditions		Primary product in liquid phase (wt.%)	References
		Brønsted acidity	Lewis acidity	Total acidity	Raw material	H ₂ pressure (MPa)		
5 wt.% Ni-ZSM-5 ^b	292	None	None	None	Pine wood ^c	40	Aromatic compounds (41.3±4.5)	Thangalazhy-Gopakumar et al., 2012
10 wt.% Ni-ZSM-5 ^d	331	1,900 ^e	None	None	Scots Pine	AP ^e	Low molecule weight Phenols (13.19) Aromatic hydrocarbons (21.86)	Melligan et al., 2012
10 wt.% Ni-ZSM-5 ^d	331	1,900 ^f	None	None	Mahogany	AP	Low molecule weight Phenols (16.13) Aromatic hydrocarbons (31.67)	Melligan et al., 2012
10 wt.% Ni-ZSM-5 ^d	331	1,900 ^f	None	None	Miscanthus × giganteus	AP	Low molecule weight Phenols (31.11) Aromatic hydrocarbons (21.73)	Melligan et al., 2012
40 wt.% Ni-ZSM-5 ^g	None	None	None	None	Cellulose	2.0	Hexitols (~48.6)	Liang et al., 2012
10 wt.% Ni-ZSM-5	254	None	None	None	Guaiacol	5.0	2-methoxycyclohexanol (12)	Barton et al., 2018
7 wt.% Ni-ZSM-5 ^h	173	None	None	None	Methyl hexadecanoate ⁱ	2.0	<i>n</i> -C ₅ -C ₁₆ alkane (71.0)	Na et al., 2012

^aMulti-point BET method.^bZSM-5 is commercially purchased, whose BET surface area is 301.9 m²/g.^cPine wood particle size is 149–177 μm.^dZSM-5 (Si/Al = 23) is commercially purchased, whose BET surface area is 425 m²/g.^eRefers to atmosphere pressure.^fThe Brønsted acidity was measured by titration method with standardized 0.1 M NaOH (aq) after catalyst equilibrating with 0.1 M NaCl solution.^gZSM-5 (Si/Al = 25).^hThe ZSM-5 (Si/Al = 38) was commercially purchased.ⁱThe Methyl hexadecanoate was choose as model compound of vegetable oil.

bimetallic Ni-Cu or Ni-Co-ZSM-5 as catalysts, no differences in adsorption capacities were observed irrespective of mono- or bimetallic catalysts with 20 wt.% loading. Thus, the difference of catalytic performance must be related to other reasons besides pore size effect, because all of these samples have similar micropore volumes. After calcination and reduction of Ni-Cu-ZSM-5 and Ni-Co-ZSM-5, Ni-Cu alloy and possible Ni-Co alloy are detected. What should be pointed is that a new phase of NiCo₂O₄ is detected in the calcined Ni-Co-ZSM-5. During the H₂ temperature-programmed reduction (TPR) experiments, the Ni-Cu-ZSM-5 shows lower reduction temperature, possibly due to synergistic interaction between the oxide phases and even physical mixing of NiO and CuO (Carrero et al., 2007; Rogatis et al., 2009), whereas the effect of Co addition to Ni on reducibility is not as strong as that of Cu on Cu-Ni bimetallic precursors. The above TPR results reveal that the addition of Cu and Co promotes the reduction of nickel oxide. For catalytic hydro-pyrolysis of phenol with Ni-Cu-ZSM-5 catalyst, the phenol conversion decreases substantially along with exchange of Ni with Cu, while the selectivity to cyclohexanol increases. Considering the decrease in the number of Ni active sites and acid sites, it can be concluded that the combination of metal and acid sites can effectively remove oxygen from phenol,

and tuning of metal sites can provide additional control over the severity and selectivity of hydrogenation. For catalytic hydro-pyrolysis of phenol with Ni-Co-ZSM-5 catalyst, the phenol conversion is complete for 10 wt.% Ni-10 wt.% Co-ZSM-5 and the selectivity toward deoxygenated products (benzene and cyclohexene) is 99.3%, which is probably due to the formation of a NiCo₂O₄ spinel phase in the catalyst precursor resulting in the high dispersion of metal species. The Ni-Cu biometallic zeolite also is investigated by Kumal et al., where CuNi/zeolite showed better deoxygenation efficiency than mono-metallic catalysts (Cu/zeolite and Ni/zeolite) and produced comparatively higher percentage of aromatic hydrocarbons at 14.3% and aliphatic hydrocarbons at 39.9% (Kumar et al., 2019, 2020).

The addition of noble metals to Ni-ZSM-5 show excellent catalytic performance in hydrogenation of microcrystalline cellulose (Liang et al., 2014). All investigated noble-metal-modified Ni-ZSM-5 gave enhanced hexitols yields in an order of Ir-Ni-ZSM-5 (49.2%) < Ru-Ni-ZSM-5 (55.6%) < Pd-Ni-ZSM-5 (58.9%) < Rh-Ni-ZSM-5 (60.6%) < Pt-Ni-ZSM-5 (76.9%). The TPR results show that the reduction of NiO is promoted by the addition of noble metals, and this promotion is due to hydrogen spillover, i.e., free hydrogen migrates from noble metals to NiO surfaces. The close interaction between platinum

TABLE 3 | Porosity and acidity characteristics of catalysts and catalytic performance of different bimetallic Ni-ZSM-5.

Catalysts	Surface area (m ² /g) ^a	Acidic properties (μmol/g)			Experimental conditions		Primary product (wt.%)	References
		Brønsted acidity	Lewis acidity	Total acidity	Raw material	H ₂ pressure (MPa)		
17 Ni 2 Cu ^b	63.0 ^c	None	None	None	Phenol	AP ^d	Cyclohexane (77)	Huynh et al., 2014
16 Ni 4 Cu	65.3 ^c	None	None	None	Phenol	AP	Cyclohexane (60)	Huynh et al., 2014
10 Ni 10 Co	65.4 ^c	162	509	672	Phenol	AP	Cyclohexane (92)	Huynh et al., 2014
5 Ni 14 Co	63.5 ^c	166	527	693	Phenol	AP	Cyclohexane (90)	Huynh et al., 2014
17 Ni 1 Pt	None	None	None	None	Cellulose	4.0	Hexitols (76.9)	Liang et al., 2014
1.3 Ni 3.1 Ga	328	None	None	None	Eucalyptus urophylla	None	BTEX ^e (NM ^f)	Schultz et al., 2016
8 Ni 8 Ce	257	None	None	None	Phenol	None	H ₂ (NM)	Li et al., 2017
45 Ni 5 Ca	None	31.8	157.6	189.4	2-methoxyphenyl anisole	1.0	Phenol (31.3)	Guo et al., 2019
45 Ni 5 Ca	None	31.8	157.6	189.4	2-(2-methoxyphenoxy)-1-phenylethanol	1.0	1-Phenyl ethanol (37.6) Guaiacol (43.7)	Guo et al., 2019
45 Ni 5 Ca	None	31.8	157.6	189.4	4-phenoxyphenol	1.0	Toluene (49.4) Guaiacol (50.5)	Guo et al., 2019

^aMulti-point BET method.^bRefers to 17 wt.% Ni 2% Cu-ZSM-5, and the other representations have the same meaning.^cRefers to the N₂ adsorbed volume (cm³ · g⁻¹) at standard temperature and pressure (0.1 MPa, 0°C).^dRefers to atmosphere pressure.^eBTEX: sum of benzene, toluene, ethylbenzene, and xylenes.^fNM, not measured.

clusters and nickel clusters leads to homogeneous reduction, forming Pt-Ni alloy. In addition, the size of metal particles decreases to 13 nm in the presence of Pt, indicating that the addition of Pt results in higher dispersion of Pt-Ni particles, as same as the effect of addition of Ce (Li et al., 2017). The Pt-enriched alloy surface can inhibit the oxidation of nickel and suppress the leaching of active nickel, which leads to excellent hydrothermal stability. Guo et al. (2019) investigate the cleavage C-O ether bond of lignin model compounds (2-methoxyphenyl anisole, 2-(2-methoxyphenoxy)-1-phenylethanol, and 4-phenoxyphenol) over Ni/CaO-ZSM-5 catalyst and conclude that low H₂ pressure favored hydrogenolysis, while high H₂ pressure favored hydrogenation. Porosity and acidity of different bimetallic Ni-ZSM-5 catalysts and their catalytic hydro-pyrolysis performance are shown in **Table 3**.

OUTLOOK

Despite the praiseworthy achievements in catalytic pyrolysis and catalytic hydro-pyrolysis of bio oil have been studied extensively, there are still some disadvantages, such as harsh conditions (high temperature and high pressure), the use of molecular H₂ as hydrogen donor, and the high cost of developing catalysts (generally noble metal catalyst is needed), low selectivity to target products and low catalyst stability. Special attention should be paid to the stability of bifunctional ZSM-5 catalysts containing different catalytic sites (metal and acid sites), which get deactivated due to different mechanisms. The metal particles on ZSM-5 suffer from leaching out while the ZSM-5 suffers from phase transformation and surface area loss. However, there

are limited methods to stabilize each type of catalytic active sites. Though surface functionalization can be used to stabilize ZSM-5 catalyst, it is difficult to prepare bifunctional catalysts by different methods. Considering that improving the stability of catalyst can help to solve the problem of high catalyst cost, further study on the stability of bifunctional sites is needed. It is also necessary to study the long-term operation of continuous reactor system, because the batch reactor used in most studies is not the appropriate choice to evaluate the stability of catalyst. In order to obtain higher quality bio oil, most processes need to add a lot of molecular H₂, which is usually obtained from non-renewable resources (such as steam reforming of coal). The use of gaseous hydrogen has brought challenges to the process economy and transportation. More importantly, its low solubility in most solvents requires high operating pressure, which will cause serious safety problems.

Excessive metal loading reduces the acidity and physical properties of ZSM-5, and then reduces the diffusivity and catalytic activity of the reactants. High mesopore content will increase coke formation and catalyst deactivation, so it is necessary to determine the mesoporous content of ZSM-5 and the optimal metal loading. Considering the cost of catalyst, the regeneration of ZSM-5 is still the focus of future research. Co-pyrolysis of biomass needs to be taken into account as an effective way to improve the quality as well as quantity of bio-oil, in which two or more materials will be used as feedstock. In general, the use of catalysts for biomass conversion has achieved valuable results, but there is still much room for us to understand the design of catalysts for the selective preparation of target products from biomass. Therefore, the reasonable design

of catalyst is of great significance to the innovation of biomass conversion technology.

AUTHOR CONTRIBUTIONS

R-QL: conceptualization and supervision. Y-LD and H-QW: investigation and original draft. Q-PK: methodology. MX and PY: review and editing. All authors: contributed to the article and approved the submitted version.

REFERENCES

- Alonso, D. M., Bond, J. Q., and Dumesic, J. A. (2010). Catalytic conversion of biomass to biofuels. *Green Chem.* 12, 1493–1513. doi: 10.1039/c004654j
- Alonso, D. M., Wettstein, S. G., and Dumesic, J. A. (2012). Bimetallic catalysts for upgrading of biomass to fuels and chemicals. *Chem. Soc. Rev.* 41:8075. doi: 10.1039/c2cs35188a
- Barton, R. R., Carrier, M., Segura, C., Garcia, F. J. L., Park, S., Lamb, H. H., et al. (2018). Ni/HZSM-5 catalyst preparation by deposition-precipitation. Part 2. catalytic hydrodeoxygenation reactions of lignin model compounds in organic and aqueous systems. *Appl. Catal. A General* 562, 294–309. doi: 10.1016/j.apcata.2018.06.012
- Bridgwater, A. V. (2012). Review of fast pyrolysis of biomass and product upgrading. *Biomass Bioenergy* 38, 68–94. doi: 10.1016/j.biombioe.2011.01.048
- Bridgwater, A. V., and Cottam, M. L. (1992). Opportunities for biomass pyrolysis liquids production and upgrading. *Energy Fuels* 6, 113–120. doi: 10.1021/ef00032a001
- Bridgwater, A. V., and Peacocke, G. V. C. (2000). Fast pyrolysis processes for biomass. *Renew. Sustain. Energy Rev.* 4, 1–73. doi: 10.1016/S1364-0321(99)00007-6
- Canel, M., Misirlioglu, Z., and Sinag, A. (2005). Hydrolysis of a turkish lignite (tuncbilek) and effect of temperature and pressure on product distribution. *Energy Convers. Manage.* 46, 2185–2197. doi: 10.1016/j.enconman.2004.10.007
- Carlson, T. R., Cheng, Y. T., Jae, J., and Huber, G. W. (2010). Production of green aromatics and olefins by catalytic fast pyrolysis of wood sawdust. *Energy Environ. Sci.* 4, 145–161. doi: 10.1039/C0EE00341G
- Carrero, A., Calles, J. A., and Vizcaino, A. J. (2007). Hydrogen production by ethanol steam reforming over Cu-Ni/SBA-15 supported catalysts prepared by direct synthesis and impregnation. *Appl. Catal. A General* 327, 82–94. doi: 10.1016/j.apcata.2007.04.030
- Chen, H., Cheng, H., Zhou, F., Chen, K., Qiao, K., Lu, X., et al. (2018). Catalytic fast pyrolysis of rice straw to aromatic compounds over hierarchical HZSM-5 produced by alkali treatment and metal-modification. *J. Anal. Appl. Pyrol.* 131, 76–84. doi: 10.1016/j.jaap.2018.02.009
- Chen, N. Y., and Degnan, T. F. (1988). Cheminform abstract: industrial catalytic applications of zeolites. *ChemInform* 84, 32–41. doi: 10.1002/chin.198826353
- Chen, Y., Aanjaneya, K., and Atreya, A. (2020). Catalytic pyrolysis of centimeter-scale pinewood particles to produce hydrocarbon fuels: the effect of catalyst temperature and regeneration. *Energy Fuels* 34, 1977–1983. doi: 10.1021/acs.energyfuels.9b04314
- Cheng, S., Wei, L., and Zhao, X. (2016). Development of a bifunctional Ni/HZSM-5 catalyst for converting prairie cordgrass to hydrocarbon biofuel. *Energy Sources* 38, 2433–2437. doi: 10.1080/15567036.2015.1065298
- Cheng, Y. T., and Huber, G. W. (2011). Chemistry of furan conversion into aromatics and olefins over HZSM-5: a model biomass conversion reaction. *ACS Catal.* 1, 611–628. doi: 10.1021/cs200103j
- Cheng, Y. T., Jae, J., Shi, J., Fan, W., and Huber, G. W. (2012). Production of renewable aromatic compounds by catalytic fast pyrolysis of lignocellulosic biomass with bifunctional Ga/ZSM-5 catalysts. *Angew. Chemie* 51, 1387–1390. doi: 10.1002/anie.201107390
- Chheda, J., Huber, G. W., and Dumesic, J. (2007). Liquid-phase catalytic processing of biomass-derived oxygenated hydrocarbons to fuels and chemicals. *Angew. Chemie Int. Ed.* 46, 7164–7183. doi: 10.1002/anie.200604274

ACKNOWLEDGMENTS

We are grateful for the support of Henan Province Science and Technology Research and Development Projects (192102210025 and 202102310279); the Key Program for International S&T Cooperation Projects of China from the Ministry of Science and Technology of China (2017YFE0124300); and Anhui Provincial Natural Science Foundation of China (200808M47).

- Corma, A., Huber, G. W., Sauvanaud, L., and Oconnor, P. (2007a). Processing biomass-derived oxygenates in the oil refinery: catalytic cracking (FCC) reaction pathways and role of catalyst. *J. Catal.* 247, 307–327. doi: 10.1016/j.jcat.2007.01.023
- Corma, A., Iborra, S., and Velty, A. (2007b). Chemical routes for the transformation of biomass into chemicals. *Chem. Rev.* 107, 2411–2502. doi: 10.1021/cr050989d
- Czernik, S., and Bridgwater, A. V. (2004). Overview of applications of biomass fast pyrolysis oil. *Energy Fuels* 18, 590–598. doi: 10.1021/ef034067u
- Demirbas, A. (2008). Biofuels sources, biofuel policy, biofuel economy and global biofuel projections. *Energy Convers. Manage.* 49, 2106–2116. doi: 10.1016/j.enconman.2008.02.020
- Department of Economic and Social Affairs United Nations (2019). *World Population Prospects*. Available online at: <https://population.un.org/wpp/>
- Energy Information Administration and United States (2019). *International Energy Outlook*. Available online at: <https://www.eia.gov/outlooks/ieo/>
- French, R., and Czernik, S. (2010). Catalytic pyrolysis of biomass for biofuels production. *Fuel Process. Technol.* 91, 25–32. doi: 10.1016/j.fuproc.2009.08.011
- Gallezot, P. (2007). Catalytic routes from renewables to fine chemicals. *Catal. Today* 121, 76–91. doi: 10.1016/j.cattod.2006.11.019
- García-Minguillán, A. M., Briones, L., Serrano, D. P., Botas, J. A., and Escola, J. M. (2020). Shifting pathways in the phenol/2-propanol conversion over the tandem Raney Ni + ZSM-5 catalytic system. *Ind. Eng. Chem. Res.* 59, 3375–3382. doi: 10.1021/acs.iecr.9b07015
- Gayubo, A. G., Alonso, A., Valle, B., Aguayo, A. T., Olazar, M., and Bilbao, J. (2010). Hydrothermal stability of HZSM-5 catalysts modified with Ni for the transformation of bioethanol into hydrocarbons. *Fuel* 89, 3365–3372. doi: 10.1016/j.fuel.2010.03.002
- Guo, J., Ma, Y. L., Yu, J. Y., Gao, Y. J., and Wu, X. Y. (2019). Highly selective cleavage C-O ether bond of lignin model compounds over Ni/CaO-H-ZSM-5 in ethanol. *BMC Chem.* 13, 1–15. doi: 10.1186/s13065-019-0557-z
- Hadjiivanov, K., H., and Knözinger, M., Mihaylov, M. (2002). FTIR study of co adsorption on Ni-ZSM-5. *J. Phys. Chem. B* 106, 331–338. doi: 10.1021/jp0132782
- Hooff, J. H. C. V., and Roelofsen, J. W. (1991). Chapter 7: Techniques of zeolite characterization. *Stud. Surf. Sci. Catal.* 58, 241–283. doi: 10.1016/S0167-2991(08)63605-8
- Horne, P. A., and Williams, P. T. (1996). Upgrading of biomass-derived pyrolytic vapours over zeolite ZSM-5 catalyst: effect of catalyst dilution on product yields. *Fuel Energy Abstracts* 75, 1043–1050. doi: 10.1016/0016-2361(96)00082-8
- Hu, M., Safarifar, V., Doustkhah, E., Rostamnia, S., Morsali, A., Nouruzi, N., et al. (2018). Taking organic reactions over metal-organic frameworks as heterogeneous catalysis. *Microporous Mesoporous Mater.* 256, 111–127. doi: 10.1016/j.micromeso.2017.07.057
- Hu, Y., Wang, H., Lakshmikanandan, M., Wang, S., Wang, Q., He, Z., et al. (2020). Catalytic co-pyrolysis of seaweeds and cellulose using mixed ZSM-5 and MCM-41 for enhanced crude bio-oil production. *J. Thermal Anal. Calorimetry*. doi: 10.1007/s10973-020-09291-w
- Huang, J., Long, W., Agrawal, P. K., and Jones, C. W. (2009). Effects of acidity on the conversion of the model bio-oil ketone cyclopentanone on H-Y zeolites. *J. Phys. Chem. C* 113, 16702–16710. doi: 10.1021/jp905661w

- Huber, G. W., and Corma, A. (2007). Synergies between bio- and oil refineries for the production of fuels from biomass. *Angew. Chemie Int. Ed.* 46, 7184–7201. doi: 10.1002/anie.200604504
- Huber, G. W., Iborra, S., and Corma, A. (2006). Synthesis of transportation fuels from biomass: chemistry, catalysts, and engineering. *Chem. Rev.* 106, 4044–4098. doi: 10.1021/cr068360d
- Huynh, T. M., Armbruster, U., Pohl, M. M., Schneider, M., Radnik, J., Hoang, D. L., et al. (2014). Hydrodeoxygenation of phenol as a model compound for bio-oil on non-noble bimetallic nickel-based catalysts. *ChemCatChem* 6, 1940–1951. doi: 10.1002/cctc.201402011
- Iliopoulou, E. F., Antonakou, E. V., Karakoulia, S. A., Vasalos, I. A., Lappas, A. A., and Triantafyllidis, K. S. (2007). Catalytic conversion of biomass pyrolysis products by mesoporous materials: effect of steam stability and acidity of Al-MCM-41 catalysts. *Chem. Eng. J.* 134, 51–57. doi: 10.1016/j.cej.2007.03.066
- Iliopoulou, E. F., Stefanidis, S. D., Kalogiannis, K. G., Delimitis, A., Lappas, A. A., and Triantafyllidis, K. S. (2012). Catalytic upgrading of biomass pyrolysis vapors using transition metal-modified ZSN-5 zeolite. *Appl. Catal. B Environ.* 127, 281–290. doi: 10.1016/j.apcatb.2012.08.030
- Jürgen, O. M. (2006). Production of liquid hydrocarbons from biomass. *Angew. Chemie Int. Ed.* 45, 696–698. doi: 10.1002/anie.200502895
- Kapustin, G. I., Brueva, T. R., Klyachko, A. L., Beran, S., and Wichterlova, B. (1988). Determination of the number and acid strength of acid sites in zeolites by ammonia adsorption: comparison of calorimetry and temperature-programmed desorption of ammonia. *Appl. Catal.* 42, 239–246. doi: 10.1016/0166-9834(88)80005-8
- Kubičková, I., Šnáre, M., Eränen, K., Mäki-Arvela, P., and Murzin, D. (2005). Hydrocarbons for diesel fuel via decarboxylation of vegetable oils. *Catal. Today* 106, 197–200. doi: 10.1016/j.cattod.2005.07.188
- Kumar, R., Strezov, V., Kan, T., Weldekidan, H., He, J., and Jahan, S. (2020). Investigating the effect of mono and bimetallic/zeolite catalysts on hydrocarbon production during bio-oil upgrading from ex-situ pyrolysis of biomass. *Energy Fuels* 34, 389–400. doi: 10.1021/acs.energyfuels.9b02724
- Kumar, R., Strezov, V., Lovell, E., Kan, T., Weldekidan, H., He, J., et al. (2019). Bio-oil upgrading with catalytic pyrolysis of biomass using copper/zeolite-nickel/zeolite and copper-nickel/zeolite catalysts. *Bioresour. Technol.* 279, 404–409. doi: 10.1016/j.biortech.2019.01.067
- Lappas, A. A., Bezergianni, S., and Vasalos, I. A. (2009). Production of biofuels via co-processing in conventional refining processes. *Catal. Today* 145, 55–62. doi: 10.1016/j.cattod.2008.07.001
- Lewandowski, W. M., Klugmann-Radziemska, E., Rymas, M., and Ostrowski, P. (2011). Modern methods of thermochemical biomass conversion into gas, liquid and solid fuels. *Ecol. Chem. Eng.* 18, 39–47.
- Li, J., Wang, G., Gao, C., Lv, X., Wang, Z., and Liu, H. (2013). Deoxy-liquefaction of laminaria japonica to high-quality liquid oil over metal modified ZSM-5 catalysts. *Energy Fuels* 27, 5207–5214. doi: 10.1021/ef4004208
- Li, X., Yan, B., Zhang, J., Xu, N., Tao, J., Zhang, R., et al. (2017). Hydrogen production by aqueous phase reforming of phenol derived from lignin pyrolysis over NiCe/ZSM-5 catalysts. *Int. J. Hydr. Energy* 43, 649–658. doi: 10.1016/j.ijhydene.2017.09.096
- Li, Y., Zhang, C., Liu, Y., Hou, X., Zhang, R., and Tang, X. (2015). Coke deposition on Ni/HZSM-5 in bio-oil hydrodeoxygenation processing. *Energy Fuels* 29, 1722–1728. doi: 10.1021/ef5024669
- Liang, G., Cheng, H., Li, W., He, L., Yu, Y., and Zhao, F. (2012). Selective conversion of microcrystalline cellulose into hexitols on nickel particles encapsulated within ZSM-5 zeolite. *Green Chem.* 14, 2146–2149. doi: 10.1039/c2gc35685f
- Liang, G., He, L., Arai, M., and Zhao, F. (2014). The Pt-enriched PtNi alloy surface and its excellent catalytic performance in hydrolytic hydrogenation of cellulose. *ChemSusChem* 7, 1415–1421. doi: 10.1002/cssc.201301204
- Maia, A. J., Louis, B., Lam, Y. L., and Pereira, M. M. (2010). Ni-ZSM-5 catalysts: detailed characterization of metal sites for proper catalyst design. *J. Catal.* 269, 103–109. doi: 10.1016/j.jcat.2009.10.021
- Melligan, F., Auccaise, R., Novotny, E. H., Leahy, J. J., Hayes, M. H. B., and Kwapinski, W. (2011). Pressurised pyrolysis of miscanthus using a fixed bed reactor. *Bioresour. Technol.* 102, 3466–3470. doi: 10.1016/j.biortech.2010.10.129
- Melligan, F., Hayes, M. H. B., Kwapinski, W., and Leahy, J. J. (2012). Hydro-pyrolysis of biomass and online catalytic vapor upgrading with Ni-ZSM-5 and Ni-MCM-41. *Energy Fuels* 26, 6080–6090. doi: 10.1021/ef301244h
- Menon, V., and Rao, M. (2012). Trends in bioconversion of lignocellulose: biofuels, platform chemicals & biorefinery concept. *Progress in Energy Combust. Sci.* 38, 522–550. doi: 10.1016/j.pecs.2012.02.002
- Michael, S. (2008). Biofuels and biomass-to-liquid fuels in the biorefinery: catalytic conversion of lignocellulosic biomass using porous materials. *Angew. Chemie Int. Ed.* 47, 9200–9211. doi: 10.1002/anie.200801476
- Mortensen, P. M., Grunwaldt, J. D., Jensen, P. A., Knudsen, K. G., and Jensen, A. D. (2011). A review of catalytic upgrading of bio-oil to engine fuels. *Appl. Catal. A General* 407, 1–19. doi: 10.1016/j.apcata.2011.08.046
- Na, S., Qi-Ying, L., Ting, J., Tie-Jun, W., Long-Long, M., Qi, Z., et al. (2012). Hydrodeoxygenation of vegetable oils to liquid alkane fuels over Ni/HZSM-5 catalysts: methyl hexadecanoate as the model compound. *Catal. Commun.* 20, 80–84. doi: 10.1016/j.catcom.2012.01.007
- Neumann, G. T., and Hicks, J. C. (2012). Effects of cerium and aluminum in cerium-containing hierarchical HZSM-5 catalysts for biomass upgrading. *Topics Catal.* 55, 196–208. doi: 10.1007/s11244-012-9788-0
- Olivas, A., Zepeda, T. A., Villalpando, I., and Fuentes, S. (2008). Performance of unsupported Ni(Co, Fe)/MoS₂ catalysts in hydrotreating reactions. *Catal. Commun.* 9, 1317–1328. doi: 10.1016/j.catcom.2007.11.025
- Onay, O. (2007). Fast and catalytic pyrolysis of pistacia khinjuk seed in a well-swept fixed bed reactor. *Fuel* 86, 1452–1460. doi: 10.1016/j.fuel.2006.12.017
- Park, H. J., Dong, J. I., Jeon, J. K., Yoo, K. S., Yim, J. H., Sohn, J. M., et al. (2007). Conversion of the pyrolytic vapor of radiata pine over zeolites. *J. Indus. Eng. Chem.* 13, 182–189.
- Park, H. J., Jeon, J. K., Suh, D. J., Suh, Y. W., Heo, H. S., and Park, Y. K. (2011). Catalytic vapor cracking for improvement of bio-oil quality. *Catal. Surveys Asia* 15, 161–180. doi: 10.1007/s10563-011-9119-7
- Pindoria, R. V., Megaritis, A., Herod, A. A., and Kandiyoti, R. (1998). A two-stage fixed-bed reactor for direct hydrotreatment of volatiles from the hydro-pyrolysis of biomass: effect of catalyst temperature, pressure and catalyst ageing time on product characteristics. *Fuel* 77, 1715–1726. doi: 10.1016/S0016-2361(98)00079-9
- Ragauskas, A. J., Williams, C. K., Davison, B. H., Britovsek, G., Caine, J., Eckert, C. A., et al. (2006). The path forward for biofuels and biomaterials. *Science* 311, 484–489. doi: 10.1126/science.1114736
- Rocca, P. A. D., Cerrella, E. G., Bonelli, P. R., and Cukierman, A. L. (1999). Pyrolysis of hardwoods residues: on kinetics and chars characterization. *Biomass Bioenergy* 16, 79–88. doi: 10.1016/S0961-9534(98)00067-1
- Rogatis, L. D., Montini, T., Cognigni, A., Olivi, L., and Fornasiero, P. (2009). Methane partial oxidation on ncu-based catalysts. *Catal. Today* 145, 176–185. doi: 10.1016/j.cattod.2008.04.019
- Rossetti, I., Bencini, E., Trentini, L., and Forni, L. (2005). Study of the deactivation of a commercial catalyst for ethylbenzene dehydrogenation to styrene. *Appl. Catal. A General* 292, 118–123. doi: 10.1016/j.apcata.2005.05.046
- Ryymin, E. M., Honkela, M. L., Viljava, T. R., and Krause, A. O. I. (2010). Competitive reactions and mechanisms in the simultaneous HDO of phenol and methyl heptanoate over sulphided NiMo/γ-Al₂O₃. *Appl. Catal. A General* 389, 114–121. doi: 10.1016/j.apcata.2010.09.010
- Saxena, R. C., Adhikari, D. K., and Goyal, H. B. (2009). Biomass-based energy fuel through biochemical routes: a review. *Renew. Sustain. Energy Rev.* 13, 167–178. doi: 10.1016/j.rser.2007.07.011
- Schultz, E. L., Mullen, C. A., and Boateng, A. A. (2016). Aromatic hydrocarbon production from *Eucalyptus urophylla* pyrolysis over several metal-modified ZSM-5 catalysts. *Energy Technol.* 5, 196–204. doi: 10.1002/ente.201600206
- Sharma, R. K., and Bakhshi, N. N. (1991). Catalytic upgrading of biomass-derived oils to transportation fuels and chemicals. *Can. J. Chem. Eng.* 69, 1071–1081. doi: 10.1002/cjce.5450690505
- Taarning, E., Osmundsen, C. M., Yang, X., Voss, B., Andersen, S. I., and Christensen, C. H. (2011). Zeolite-catalyzed biomass conversion to fuels and chemicals. *Energy Environ. Sci.* 4, 793–804. doi: 10.1039/C004518G
- Thangalazhy-Gopakumar, S., Adhikari, S., and Gupta, R. B. (2012). Catalytic pyrolysis of biomass over H⁺ZSM-5 under hydrogen pressure. *Energy Fuels* 26, 5300–5306. doi: 10.1021/ef3008213

- Topsøe, N. Y., Pedersen, K., and Derouane, E. G. (1981). Infrared and temperature-programmed desorption study of the acidic properties of ZSM-5-type zeolites. *J. Catal.* 70, 41–52. doi: 10.1016/0021-9517(81)90315-8
- Triantafyllidis, C. S., Vlessidis, A. G., Nalbandian, L., and Evmiridis, N. P. (2001). Effect of the degree and type of the dealumination method on the structural, compositional and acidic characteristics of H-ZSM-5 zeolites. *Microporous Mesoporous Mater.* 47, 369–388. doi: 10.1016/S1387-1811(01)00399-7
- Triantafyllidis, K. S., Iliopoulou, E. F., Antonakou, E. V., Lappas, A. A., Wang, H., and Pinnavaia, T. J. (2007). Hydrothermally stable mesoporous aluminosilicates (MSU-S) assembled from zeolite seeds as catalysts for biomass pyrolysis. *Microporous Mesoporous Mater.* 99, 132–139. doi: 10.1016/j.micromeso.2006.09.019
- Valle, B., Alonso, A., Atutxa, A., Gayubo, A. G., and Bilbao, J. (2005). Effect of nickel incorporation on the acidity and stability of HZSM-5 zeolite in the MTO process. *Catal. Today* 106, 118–122. doi: 10.1016/j.cattod.2005.07.132
- Valle, B., Gayubo, A. G., Aguayo, A. T., Olazar, M., and Bilbao, J. (2010). Selective production of aromatics by crude bio-oil valorization with a nickel-modified HZSM-5 zeolite catalyst. *Energy Fuels* 24, 2060–2070. doi: 10.1021/ef901231j
- Veses, A., Puértolas, B., López, J. M., Callén, M. S., Solsona, B., and García, T. (2016). Promoting deoxygenation of bio-oil by metal-loaded hierarchical ZSM-5 zeolites. *ACS Sustain. Chem. Eng.* 4, 1653–1660. doi: 10.1021/acssuschemeng.5b01606
- Vichaphund, S., Aht-Ong, D., Srichaenchaikul, V., and Atong, D. (2015). Production of aromatic compounds from catalytic fast pyrolysis of jatropha residues using metal/HZSM-5 prepared by ion-exchange and impregnation methods. *Renew. Energy* 79, 28–37. doi: 10.1016/j.renene.2014.10.013
- Viljava, T. R., Komulainen, R. S., and Krause, A. O. I. (2000). Effect of H₂S on the stability of CoMo/Al₂O₃ catalysts during hydrodeoxygenation. *Catal. Today* 60, 83–92. doi: 10.1016/S0920-5861(00)00320-5
- Vitolo, S., Bresci, B., Seggiani, M., and Gallo, M. G. (2001). Catalytic upgrading of pyrolytic oils over HZSM-5 zeolite: behaviour of the catalyst when used in repeated upgrading-regenerating cycles. *Fuel* 80, 17–26. doi: 10.1016/S0016-2361(00)00063-6
- Xu, J., Zhou, W., Wang, J., Li, Z., and Ma, J. (2009). Characterization and analysis of carbon deposited during the dry reforming of methane over Ni/La₂O₃/Al₂O₃ catalysts. *Chin. J. Catal.* 30, 1076–1084. doi: 10.1016/S1872-2067(08)60139-4
- Yang, Y. Q., Tye, C. T., and Smith, K. J. (2008). Influence of MoS₂ catalyst morphology on the hydrodeoxygenation of phenols. *Catal. Commun.* 9, 1364–1368. doi: 10.1016/j.catcom.2007.11.035
- Yung, M. M., Starace, A. K., Mukarakate, C., Crow, A., Leshnov, M. A., and Magrini-Bair, K. A. (2016). Biomass catalytic pyrolysis on Ni/ZSM-5: effects of nickel pretreatment and loading. *Energy Fuels* 30, 5259–5268. doi: 10.1021/acs.energyfuels.6b00239
- Zakzeski, J., Bruijninx, P. C. A., Jongerius, A. L., and Weckhuysen, B. M. (2010). The catalytic valorization of lignin for the production of renewable chemicals. *Chem. Rev.* 110, 3552–3599. doi: 10.1021/cr900354u
- Zhang, H., Cheng, Y. T., Vispute, T. P., Xiao, R., and Huber, G. W. (2011). Catalytic conversion of biomass-derived feedstocks into olefins and aromatics with ZSM-5: the hydrogen to carbon effective ratio. *Energy Environ. Sci.* 4:2297. doi: 10.1039/c1ee01230d
- Zhang, X., Wang, T., Ma, L., Zhang, Q., and Jiang, T. (2013). Hydrotreatment of bio-oil over Ni-based catalyst. *Bioresour. Technol.* 127, 306–311. doi: 10.1016/j.biortech.2012.07.119
- Zhang, Y. H. P., Himmel, M. E., and Mielenz, J. R. (2006). Outlook for cellulase improvement: screening and selection strategies. *Biotechnol. Adv.* 24, 452–481. doi: 10.1016/j.biotechadv.2006.03.003
- Zhao, C., Kasakov, S., He, J., and Lercher, J. A. (2012). Comparison of kinetics, activity and stability of Ni/HZSM-5 and Ni/Al₂O₃-HZSM-5 for phenol hydrodeoxygenation. *J. Catal.* 296, 12–23. doi: 10.1016/j.jcat.2012.08.017

Conflict of Interest: The authors declare that the research was conducted in the absence of any commercial or financial relationships that could be construed as a potential conflict of interest.

Copyright © 2020 Ding, Wang, Xiang, Yu, Li and Ke. This is an open-access article distributed under the terms of the Creative Commons Attribution License (CC BY). The use, distribution or reproduction in other forums is permitted, provided the original author(s) and the copyright owner(s) are credited and that the original publication in this journal is cited, in accordance with accepted academic practice. No use, distribution or reproduction is permitted which does not comply with these terms.



Sustainably Adjusting the Up-Conversion White-Emitting Luminescence Properties of GdAlO_3 : $\text{Er}^{3+}/\text{Yb}^{3+}/\text{Tm}^{3+}$ Phosphors

Taoli Deng, Xianbang Jiang* and Qiuyun Zhang*

School of Chemistry and Chemical Engineering, Anshun University, Anshun, China

OPEN ACCESS

Edited by:

Yaqiong Su,
Eindhoven University of
Technology, Netherlands

Reviewed by:

Wenying Zhang,
University of Warwick,
United Kingdom
Kai Wang,
Fudan University, China

*Correspondence:

Xianbang Jiang
2997055635@qq.com
Qiuyun Zhang
qyzhang.asu@gmail.com

Specialty section:

This article was submitted to
Green and Sustainable Chemistry,
a section of the journal
Frontiers in Chemistry

Received: 25 June 2020

Accepted: 28 July 2020

Published: 29 September 2020

Citation:

Deng T, Jiang X and Zhang Q (2020)
Sustainably Adjusting the
Up-Conversion White-Emitting
Luminescence Properties of GdAlO_3 :
 $\text{Er}^{3+}/\text{Yb}^{3+}/\text{Tm}^{3+}$ Phosphors.
Front. Chem. 8:788.
doi: 10.3389/fchem.2020.00788

Doping heteroatom in phosphor can effectively improve luminescent properties, which has attracted great attention recently. GdAlO_3 phosphors (GAP) doped with $\text{Er}^{3+}/\text{Yb}^{3+}/\text{Tm}^{3+}$ were prepared via the co-precipitation method. Upon 980 nm excitation, strong blue, green, and red up-conversion (UC) emissions centered at 476, 524, 546, and 659 nm were observed, which could be successfully combined to form pure white light. It was found that changing the doping concentration of Er^{3+} and Yb^{3+} ions, the calcination temperature of the precursor, the laser power of the excitation light source, and doping Li^+ could systematically adjust red/green/blue colors of $\text{GdAlO}_3:\text{Er}^{3+}/\text{Yb}^{3+}/\text{Tm}^{3+}$ phosphors to optimize the white emitting luminescence. When the Er^{3+} doping concentration of the phosphors increased, each color distribution successfully moved, making the maximum shift of the CIE coordinate. Finally, the influence of each factor on adjusting the UC white light performance and its mechanism were explored.

Keywords: sustainable chemistry, white-emitting, heteroatom-containing compounds, laser power, phosphors

INTRODUCTION

Recently, the development of green and sustainable approaches have become a particularly important theme. The use of white light-emitting diodes (WLEDs) as a promising general illumination source in lighting and display applications has attracted great attention (Du et al., 2018; Li et al., 2018; Liu et al., 2019). There are two alternative approaches to WLEDs assembly now. The first way is to mix the red, green, and blue monochromatic light sources together to modulate white light directly. Another way is to convert the ultraviolet, blue, or infrared light sources into a combination of red, green, and blue emissions by using phosphors (DiMaio et al., 2006; Liu M. et al., 2007; Liu X. M. et al., 2007). At present, the strategy widely used in producing white light is to combine a blue LED chip with a YAG: Ce yellow phosphor (Justel et al., 1998). However, the blue light LED has low luminescence efficiency, and the device color is changed by a combination of the working temperature, voltage, and the phosphor coating thickness, which makes the white light emission unstable. Meanwhile, the lack of red light components results in a white light with both a high color temperature and a poor color rendering index.

As far as we know, up-conversion photoluminescence (UCPL) can convert long wave light into short wave light and the white light obtained by UCPL can reduce the photo degradation process caused by high energy photons compared with down conversion luminescence excited by short wavelengths (Leleckaite and Kareiva, 2004; Milliez et al., 2006; Chung et al., 2012). At the same time, infrared light was used as the excitation source

which had a very low cost and was easy to obtain. It is reported that UC white light can be combined by doping rare earth ions $\text{Er}^{3+}/\text{Ho}^{3+}$ emitting red and green light and Tm^{3+} emitting blue light in fluoride under 980 nm excitation (Sivakumar et al., 2005; Wang and Liu, 2008; Chen et al., 2017). While the large-scale application and industrial production of fluoride phosphors are limited by the low stability, being unfriendly to environment, and harsh conditions in the process of synthesis, it is important to find some suitable matrix materials in the UC process to obtain white light. In recent years, lots of oxides with good chemical stability, mild synthesis conditions, that are eco-friendly, and have low phonon energy are being used as the host material to obtain UC white light which has attracted researchers' attention (Rai et al., 2013; Chen et al., 2017; Annadurai et al., 2018). The GdAlO_3 system has a orthogonal perovskite crystal structure with a Pbnm space group. The density of GdAlO_3 is $7.437\text{g}\cdot\text{cm}^{-3}$, and the phonon energy is 670 cm^{-1} , which is good for UCPL (Deng and Jiang, 2018).

In our previous research on GAP, it was found that the ratio of the red to green emissions intensity can be modified after changing the $\text{Er}^{3+}/\text{Yb}^{3+}$ doping concentration and laser power. Apart from this, the particle size and the content of impurity groups adsorbed on the surface of the GAP phosphors calcined at different temperatures will also affect the intensity and proportion of red/green emissions in UCPL (Deng et al., 2014a,b). In this paper, Yb^{3+} was used to sensitize Er^{3+} , Tm^{3+} in GdAlO_3 to obtain the UC white light, and the doping concentration of Er^{3+} and Yb^{3+} ions, the calcination temperature of the precursor, the laser power of the excitation light source, and Li^+ doping were changed to adjust the intensity and relative proportion of red, green, and blue emissions. Then the influence of each factor on UCPL performance and its mechanism were explored, which can provide guidance for the UC white light process by systematically adjusting the red /green/blue colors.

EXPERIMENTAL

The $\text{Gd}_{(1-x-y-z)}\text{Er}_x\text{Yb}_y\text{Tm}_{0.01}\text{Li}_z\text{AlO}_3$ ($x = 0.004, 0.006, 0.008$; $y = 0.10, 0.12, 0.14, 0.16$; $z = 0, 0.02$) precursors were prepared by a co-precipitation method. Firstly, stoichiometric amounts of starting rare earth (RE) oxides Gd_2O_3 (99.99%), Yb_2O_3 (99.99%), Er_2O_3 (99.99%), Tm_2O_3 (99.99%), and Li_2CO_3 (99.9%) were dissolved in HNO_3 aqueous solution with the molar ratio of RE^{3+} to NO_3^- being 1:3. Then a required amount of $\text{Al}(\text{NO}_3)_3\cdot 9\text{H}_2\text{O}$ and ethanol aqueous solution were added sequentially under vigorous stirring until the homogenous solution A was formed. The beaker containing the homogenous solution A was placed in a water bath at 45°C . The $1\text{ mol}\cdot\text{L}^{-1}$ NH_4HCO_3 aqueous solution was added into solution A at a rate of $2\text{ mL}\cdot\text{min}^{-1}$ with stirring. After completion of precipitation, the agitator was turned off and the precipitate was ripened at room temperature for 10 h. After ripening and filtration, the precipitate was washed with deionized water three times and ethanol two times, then dried at 120°C for 12 h. Finally, the precursor powders were calcined at different temperatures for 6 h. The crystalline $\text{GdAlO}_3:\text{Er}^{3+}/\text{Yb}^{3+}/\text{Tm}^{3+}$ phosphors were finally obtained.

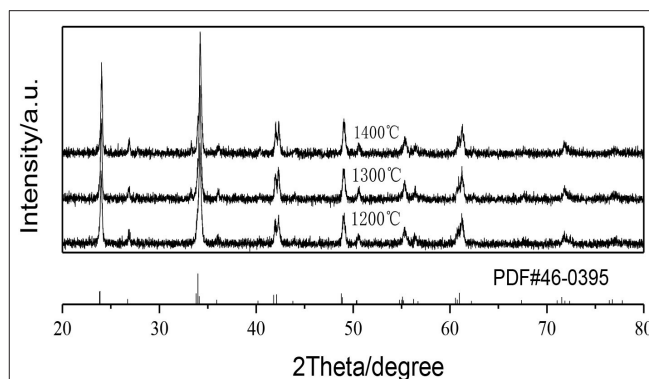


FIGURE 1 | XRD patterns of the GAP phosphors prepared by calcining the precipitate at different temperatures.

The x-ray diffraction patterns of the phosphors were tested by a Bruker D8 advance diffractometer with $\text{Cu K}\alpha$ radiation ($\lambda = 0.154056\text{ nm}$) operated at 30 mA and 40 kV. The UCPL spectra of the phosphors were recorded using an Ocean Optics PlasCalc-2000-UV-VIS-NIR plasma monitor control system and the exciting source was a MDL-H-980 980 nm infrared laser.

RESULTS AND DISCUSSION

Figure 1 shows the XRD patterns of the GAP phosphors prepared by calcining the precipitate at different temperatures. In the figure all the XRD diffraction peaks obtained at 1,200, 1,300, and 1,400°C can match the standard GdAlO_3 card (PDF#46-0395) with no impurity phase being detected (Deng and Jiang, 2018), and the GdAlO_3 host material can exist quite stably with calcination temperature from 1,200 to 1,400°C. The average sizes of the crystallites calcined at different temperatures are estimated using Scherrer's equation (Shannon, 1976):

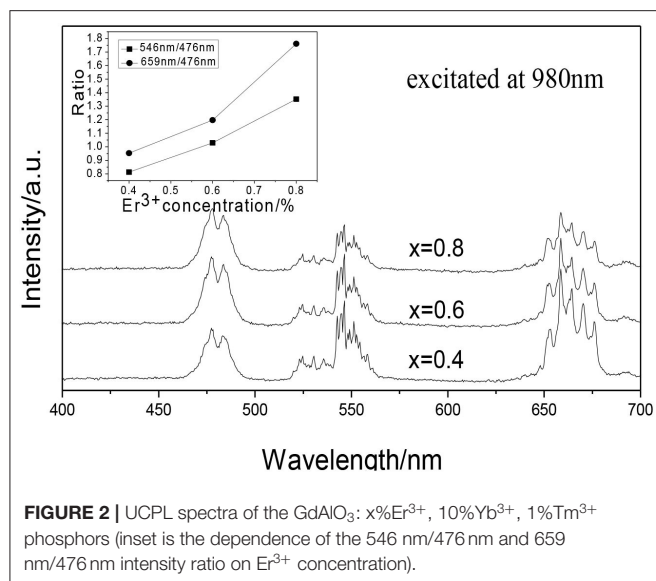
$$D = 0.89\lambda / \beta \cos \theta$$

where D is the average crystallite size, λ is the wavelength of the $\text{Cu K}\alpha$ line, β is the full-width at half maximum in radians, and θ is the Bragg angle.

The strongest peak of the phosphors by calcining the precipitate at 1,200, 1,300, and 1,400°C, respectively, are at 34.18° ($\beta = 0.00541$), 34.20° ($\beta = 0.00436$), 34.22° ($\beta = 0.00401$) and using the procedure, the prepared phosphor particles by calcining the precipitate at 1,200, 1,300, and 1,400°C had the average crystallite sizes of 30.63 nm, 38.01 nm, 41.33 nm, which showed that a higher calcination temperature resulted in larger sized phosphor particles.

The Effect of $\text{Er}^{3+}/\text{Yb}^{3+}$ Doping Concentration on the Tunable UC White Emissions

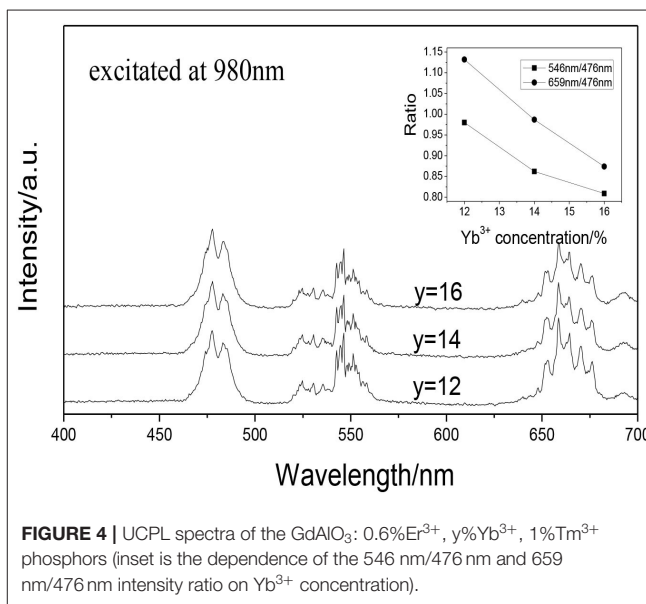
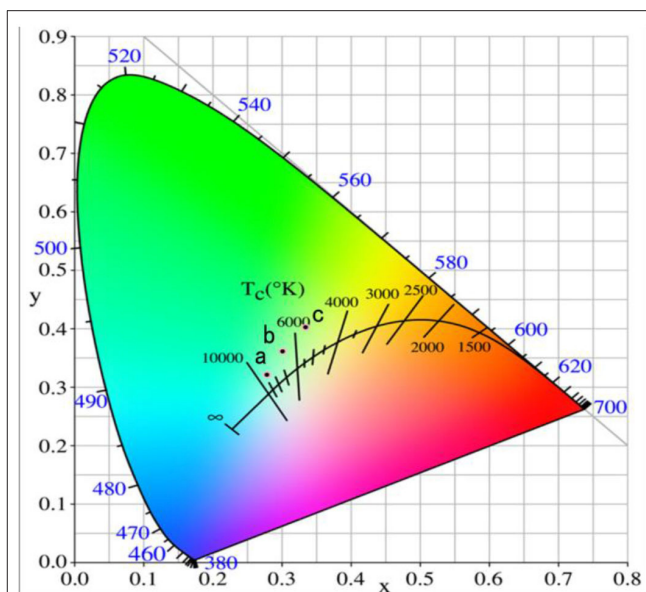
Figure 2 shows the UCPL spectra of the $\text{GdAlO}_3:x\%\text{Er}^{3+}, 10\%\text{Yb}^{3+}, 1\%\text{Tm}^{3+}$ ($x = 0.4, 0.6, 0.8$) phosphors and the dependence of the 546 nm/476 nm and 659 nm/476 nm intensity ratio on Er^{3+}



concentration. Under excitation of 980 nm, all of the GdAlO_3 : $x\%\text{Er}^{3+}$, $10\%\text{Yb}^{3+}$, $1\%\text{Tm}^{3+}$ ($x = 0.4, 0.6, 0.8$) phosphors appeared to have four main emission peaks at 476 nm (blue), 524 nm, 546 nm (green), and 659 nm (red). The blue emission peak at 476 nm belongs to the Tm^{3+} ($^1\text{G}_4 \rightarrow ^3\text{H}_6$) transition and the green emission peaks can be assigned to Er^{3+} ($^2\text{H}_{11/2} \rightarrow ^4\text{I}_{15/2}$, $^4\text{S}_{3/2} \rightarrow ^4\text{I}_{15/2}$) transitions, and the red emission peak can be ascribed to the Er^{3+} ($^4\text{F}_{9/2} \rightarrow ^4\text{I}_{15/2}$) transition (Tamrakar et al., 2016; Cao et al., 2018). It was found that different doping concentrations of Er^{3+} does not produce a change in shape or location of the emission peaks. It can be seen from the inner illustration that the ratios of red to blue emission and green to blue emission intensity are improved at different degrees with the Er^{3+} doping concentration increase, so as to change each color distribution successfully.

Figure 3 represents the chromaticity coordinate CIE diagram of the phosphors with different Er^{3+} doping concentrations. When the Er^{3+} doping concentration was 0.04, the CIE of phosphor GdAlO_3 : $4\%\text{Er}^{3+}$, $10\%\text{Yb}^{3+}$, $1\%\text{Tm}^{3+}$ is (0.2787, 0.3213) shown in point a, and the CIE changed to (0.3015, 0.3609) when the Er^{3+} doping concentration added was 0.06, shown in point b. Finally, when the Er^{3+} doping concentration was 0.08, the CIE reached (0.3349, 0.4031), shown in point c. CIE significantly moves to the red and green direction, and all the CIE of the GdAlO_3 : $x\%\text{Er}^{3+}$, $10\%\text{Yb}^{3+}$, $1\%\text{Tm}^{3+}$ ($x = 0.4, 0.6, 0.8$) phosphors fall into the nearly white light region in the CIE diagram, which makes it suitable for the fabrication of white light emitting LEDs (Shi et al., 2014; Seo et al., 2017). Therefore, the white light can be effectively adjusted by changing the Er^{3+} doping concentration.

Figure 4 shows the UCPL spectra of the GdAlO_3 : $0.6\%\text{Er}^{3+}$, $y\%\text{Yb}^{3+}$, $1\%\text{Tm}^{3+}$ ($y = 12, 14, 16$) phosphors and the dependence of the 546 nm/476 nm and 659 nm/476 nm intensity ratio on Yb^{3+} concentration. It can be seen that the relative intensity of red to blue emission and the relative intensity of green



to blue emission shows a downward trend with the increase of Yb^{3+} doping concentration.

Figure 5 represents the CIE diagram of the phosphors with different Yb^{3+} doping concentrations. The CIE are (0.2926, 0.3542), (0.2811, 0.3373), and (0.2725, 0.3272) as shown in the points a, b, and c when the Yb^{3+} doping concentration was 0.12, 0.14, and 0.16, respectively. The CIE moves to the blue light direction with the increase of the Yb^{3+} doping concentration, but the moving range was not as large as that of the Er^{3+} doping,

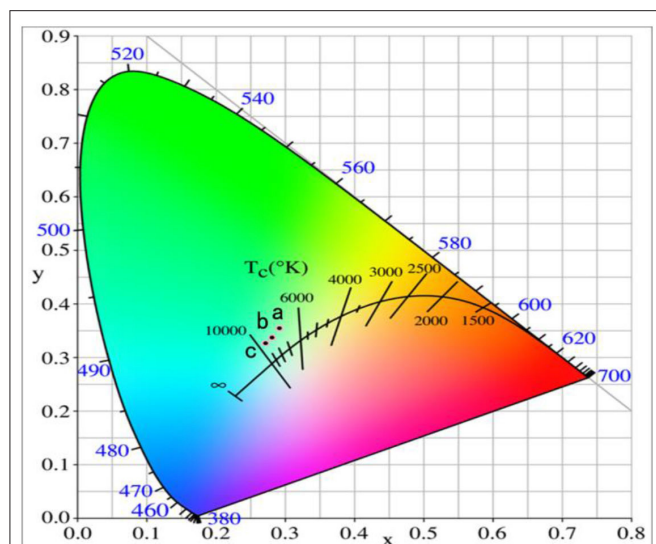


FIGURE 5 | Chromaticity coordinate of the GdAlO_3 : 0.6% Er^{3+} , $y\%$ Yb^{3+} , 1% Tm^{3+} phosphors under 980 nm excitation (a: $y = 12$, b: $y = 14$, c: $y = 16$).

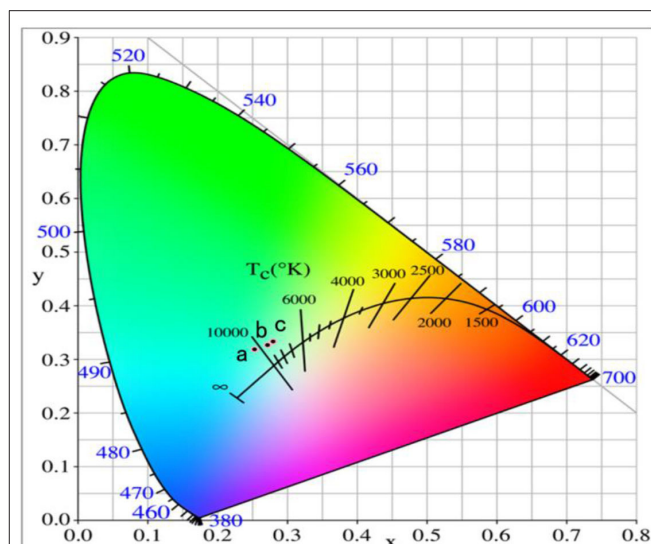


FIGURE 7 | Chromaticity coordinate of the GdAlO_3 : 0.6% Er^{3+} , 16% Yb^{3+} , 1% Tm^{3+} phosphors prepared by calcining the precipitate at different temperatures (a: 1,200°C, b: 1,300°C, c: 1,400°C).

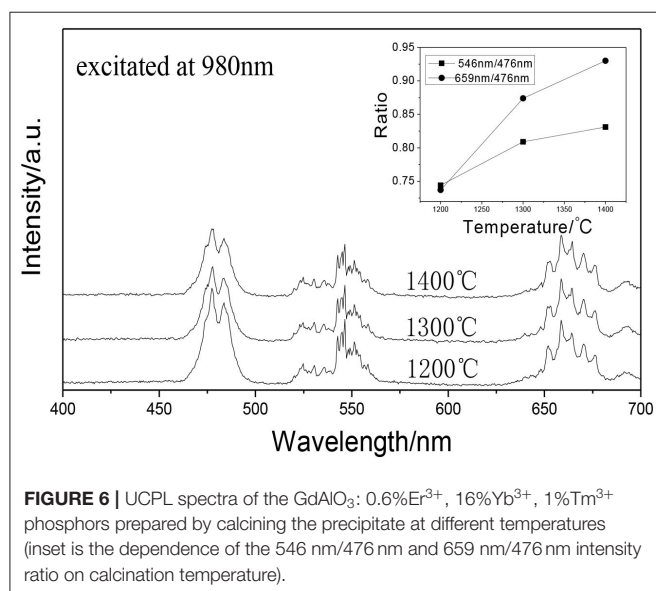


FIGURE 6 | UCPL spectra of the GdAlO_3 : 0.6% Er^{3+} , 16% Yb^{3+} , 1% Tm^{3+} phosphors prepared by calcining the precipitate at different temperatures (inset is the dependence of the 546 nm/476 nm and 659 nm/476 nm intensity ratio on calcination temperature).

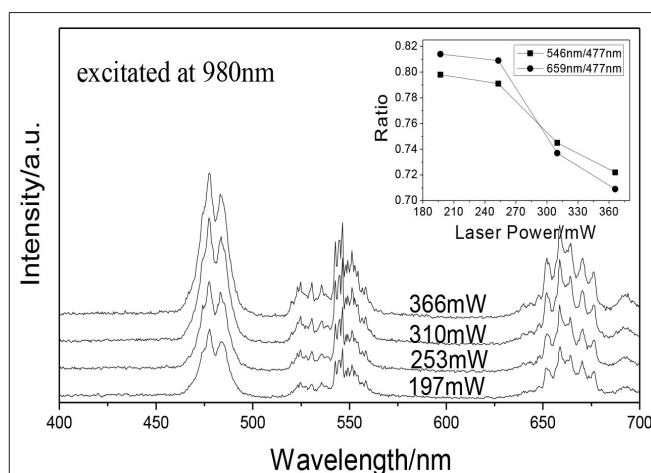


FIGURE 8 | UCPL spectra of the GdAlO_3 : 0.6% Er^{3+} , 16% Yb^{3+} , 1% Tm^{3+} phosphor under excitation at 980 nm with different laser powers (inset is the dependence of the 546 nm/476 nm and 659 nm/476 nm intensity ratio on laser power).

and the white light can be adjusted slightly by changing the Yb^{3+} doping concentration.

The Effect of the Calcining Temperatures on the Tunable UC White Emissions

It can be seen that GAP phosphor can exist stably by calcining the precipitate from 1,200 to 1,400°C in **Figure 1**. **Figure 6** shows the UCPL spectra of the GdAlO_3 : 0.6% Er^{3+} , 16% Yb^{3+} , 1% Tm^{3+} phosphors prepared by calcining the precipitate at different temperatures and the dependence of the 546 nm/476 nm and 659 nm/476 nm intensity ratios on calcination temperatures at 1,200, 1,300, and 1,400°C. It can be seen that the blue emission intensity decreases, while the ratios of red to blue emission

and green to blue emission intensity increase with the increase of the calcination temperature. The corresponding coordinates were (0.2596, 0.3189), (0.2725, 0.3272), and (0.2796, 0.3328) as shown in points a, b, and c, respectively, when the calcination temperatures were 1,200, 1,300, and 1,400°C from **Figure 7**. Moreover, all the points are located in the white light area, and the color coordinates move to the red and green emission direction. The moving range was less than that of the Er^{3+} and Yb^{3+} doping. The UC white light can be further adjusted on the basis of the Er^{3+} and Yb^{3+} doping concentration by changing the calcination temperature.

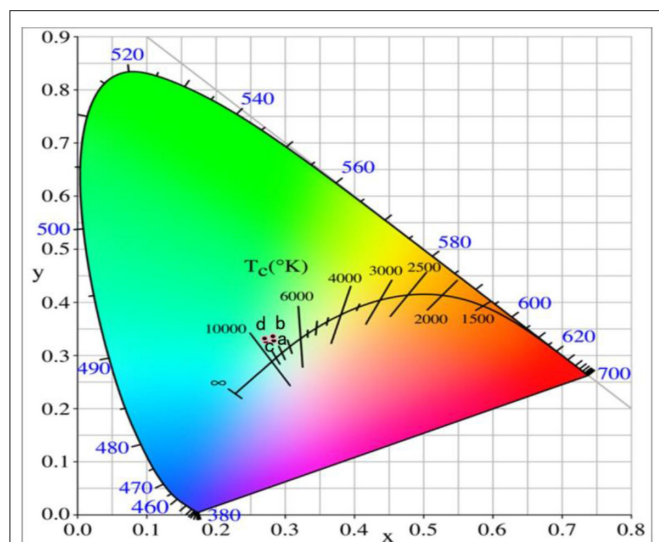


FIGURE 9 | Chromaticity coordinates of the $\text{GdAlO}_3:0.6\%\text{Er}^{3+}$, $16\%\text{Yb}^{3+}$, $1\%\text{Tm}^{3+}$ phosphor under excitation at 980 nm with different laser powers (a:197 mW, b:253 mW, c:310 mW, d:366 mW).

The Effect of the Excitation Laser Powers on the Tunable UC White Emissions

Figure 8 shows the UCPL spectra of the $\text{GdAlO}_3:0.6\%\text{Er}^{3+}$, $16\%\text{Yb}^{3+}$, $1\%\text{Tm}^{3+}$ phosphor and the dependence of the 546 nm/476 nm and 659 nm/476 nm intensity ratios under excitation at 980 nm with different laser powers. It can be seen that the intensity of each emission peak was improved with the increase of laser power, but the relative intensities of red to blue emission and green to blue emission decrease obviously. **Figure 9** presents the chromaticity coordinate of the $\text{GdAlO}_3:0.6\%\text{Er}^{3+}$, $16\%\text{Yb}^{3+}$, $1\%\text{Tm}^{3+}$ phosphor under excitation at 980 nm with different laser powers at 197 mW, 253 mW, 310 mW, and 366 mW, the CIE are (0.2846, 0.3277), (0.2825, 0.3360), (0.2725, 0.3272), and (0.2707, 0.3320) as shown in the points a, b, c, and d, respectively. Moreover, the movement of color coordinates was very small and all the points fall near the white light area.

The Effect of Doping Li^+ on the Tunable UC White Emissions

Figure 10 shows the UCPL spectra of the $\text{GdAlO}_3:0.6\%\text{Er}^{3+}$, $16\%\text{Yb}^{3+}$, $1\%\text{Tm}^{3+}$, $z\%\text{Li}^+$ phosphors and the dependence of the 546 nm/476 nm and 659 nm/476 nm intensity ratios under excitation at 980 nm. It can be seen that the blue emission intensity increases and the relative intensities of red to blue and green to blue emission decreases obviously with Li^+ doping. The CIE was (0.2626, 0.3168), when the Li^+ doping concentration was 0.02 at point b in **Figure 11**. It moves slightly to the blue direction compared with no Li^+ doping at point a (0.2725, 0.3272). Therefore, the color coordinate position of UC white light can be adjusted slightly by Li^+ doping.

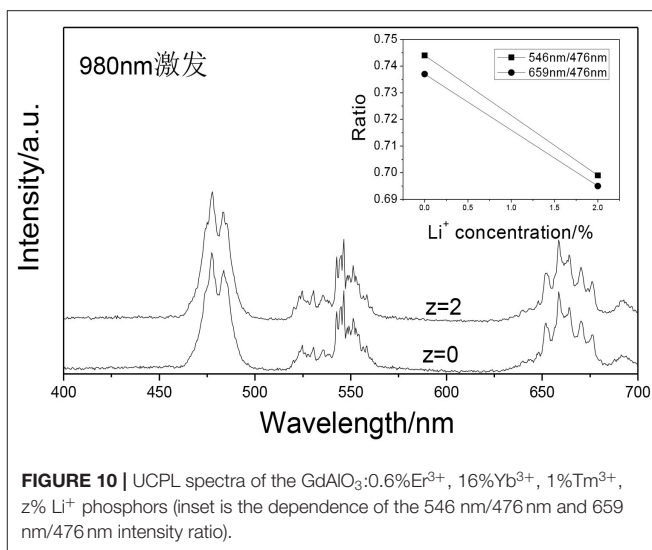


FIGURE 10 | UCPL spectra of the $\text{GdAlO}_3:0.6\%\text{Er}^{3+}$, $16\%\text{Yb}^{3+}$, $1\%\text{Tm}^{3+}$, $z\%\text{Li}^+$ phosphors (inset is the dependence of the 546 nm/476 nm and 659 nm/476 nm intensity ratio).

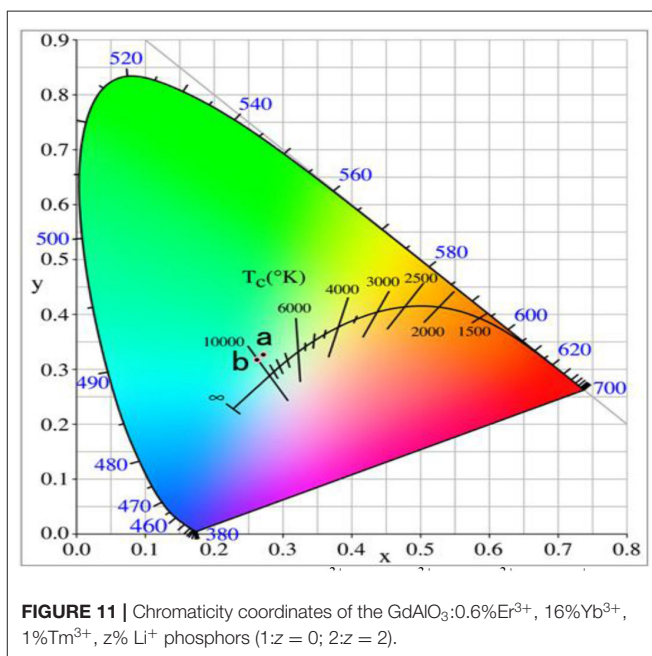
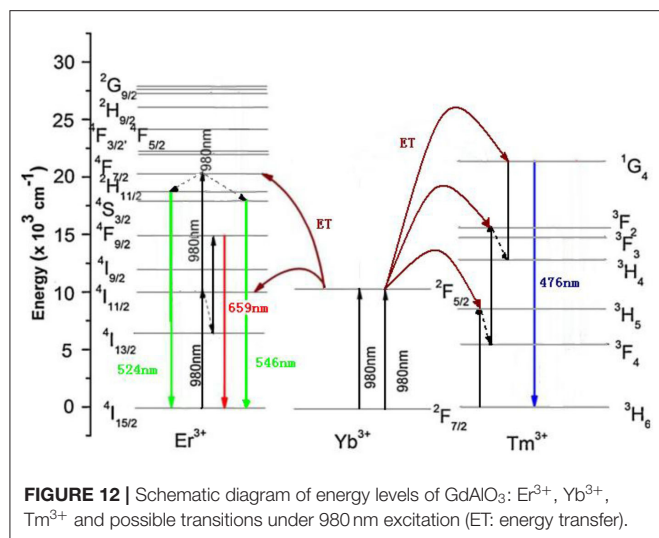


FIGURE 11 | Chromaticity coordinates of the $\text{GdAlO}_3:0.6\%\text{Er}^{3+}$, $16\%\text{Yb}^{3+}$, $1\%\text{Tm}^{3+}$, $z\%\text{Li}^+$ phosphors (1:z = 0; 2:z = 2).

UCPL Mechanism

The luminescence mechanism of $\text{GdAlO}_3:\text{Er}^{3+}$, Yb^{3+} , Tm^{3+} phosphors was analyzed to reveal the UC white light chromaticity coordinate changed with different $\text{Er}^{3+}/\text{Yb}^{3+}$ concentration doping, calcining temperatures, laser powers, and Li^+ doping. **Figure 12** shows the schematic diagram of energy levels of the Er^{3+} , Yb^{3+} , and Tm^{3+} ions and possible transitions under 980 nm excitation. Specific processes that the green emission at 524 and 546 nm are ascribed to $^2\text{H}_{11/2} \rightarrow ^4\text{I}_{15/2}$ and $^4\text{S}_{3/2} \rightarrow ^4\text{I}_{15/2}$ transitions, and the red emission at 659 nm would be observed from the $^4\text{F}_{9/2} \rightarrow ^4\text{I}_{15/2}$ transition all from Er^{3+} , which have been discussed in our previous work (Deng and Jiang, 2018). Meanwhile, both green and red emissions are the two-photon



processes. The blue emission at 476 nm would be observed from the $^1G_4 \rightarrow ^3H_6$ transition of Tm³⁺. The specific process was that Yb³⁺ ion, as a sensitizer first absorbed energy and transitioned from the $^2F_{7/2}$ level to $^2F_{5/2}$ under 980 nm irradiation, and the Tm³⁺ ion in the ground state of 3H_6 was elevated to the 3H_5 excited state via ET from an Yb³⁺ ion in the $^2F_{5/2}$ state, then Tm³⁺ in the state of 3H_5 relaxed to the 3F_4 level by non-radiative relaxations. This process was followed by a second ET from another Yb³⁺ ion also in its excited state, resulting in the population of 3F_2 of the Tm³⁺. After $^3F_2 \rightarrow ^3H_4$ fast non-radiative relaxations, the Tm³⁺ ion in the excited state of 1G_4 is pumped by the third ET from an Yb³⁺ ion. Finally, the excited Tm³⁺ ion in 1G_4 returned to the 3H_6 ground state giving the blue emission at 476 nm, which belongs to the three-photon process. Therefore, there was a relative competition between Er³⁺ and Tm³⁺ in energy transfer from Yb³⁺ ion as the same sensitizer.

Firstly, the UC white emissions of phosphors were adjusted by changing the Er³⁺ doping concentration. It was found that the red and green emission intensity of samples increased, while that of the blue emission decreased with increased Er³⁺ doping concentration. It is not difficult to explain that the luminescence mechanism that the red and green emissions belong to Er³⁺ ($^2H_{11/2}, ^4S_{3/2} \rightarrow ^4I_{15/2}$) and ($^4F_{9/2} \rightarrow ^4I_{15/2}$), while the blue emission belongs to Tm³⁺ ($^1G_4 \rightarrow ^3H_6$). Therefore, the distance between the sensitizer Yb³⁺ and luminescent Er³⁺ became closer with the increase of the Er³⁺ doping concentration, which made the energy transfer more effective, and then the luminescent intensity of green and red emissions became higher. Meanwhile, the energy transfer between Yb³⁺ and Tm³⁺ was accordingly decreased, and to some extent, the blue emission intensity was reduced. The UC white light can be further adjusted by changing the doping concentration of sensitizer Yb³⁺. It was found that the intensity ratio of red to blue and the green to blue emissions decreased, and the blue emission increased obviously with an increase in the Yb³⁺ doping concentration. This was because the blue emission belongs to the three-photon process, which requires the effective energy transfer from the sensitizer Yb³⁺ to

Tm³⁺ to reach the final blue emission level three times. While, red and green emissions belong to the two-photon process of Er³⁺, so it was more favorable to obtain the energy transfer from Yb³⁺ to Tm³⁺, which made the relative intensity of red to blue and green to blue emissions decrease.

Secondly, it can be reasonably explained that the intensity ratios of red to blue and green to blue emissions are enhanced by the increase of the calcination temperature of the precursor. As we know, the energy gap of non-radiative relaxation is very close to the vibrational frequency of the OH⁻ in the phosphor. The higher the concentration of OH⁻ impurity in the phosphor the higher the probability of $^4I_{11/2} \rightarrow ^4I_{13/2}$, $^4S_{3/2} \rightarrow ^4F_{9/2}$, $^3F_2 \rightarrow ^3H_4$, and $^3H_5 \rightarrow ^3F_4$ non-radiative transitions. The concentration of surface OH⁻ groups in the phosphor decreased gradually when the calcination temperature increased as shown in our previous work (Deng et al., 2014a). From the energy level diagram, it can be seen that the blue emission process needed three non-radiation transitions. Then, with the decrease of the OH⁻ groups on the surface of the phosphor, the probability of non-radiation transitions decreased, which mostly weakened the blue emission, resulting in the increase of relative intensity of red to blue and green to blue emissions, making the UC color coordinates move to the red and green emission direction.

Thirdly, the luminous intensity of each red, green, and blue emissions all increased with the increase of the excitation power laser. As far as we know, red and green emissions from Er³⁺ are two-photon processes, and the luminous intensity is directly proportional to the second power of the power, while the blue emission from Tm³⁺ is a three-photon process, and the luminous intensity is directly proportional to the third power of the power, so the effect of power on blue emission is more significant, resulting in the increase of blue emission intensity being larger than that of the red and green emission, then the relative intensity of red to blue emission and green to blue emission decreased, which can adjust the white light slightly again.

Finally, the UC white light was adjusted and the luminous efficiency was improved by Li⁺ doping. Li⁺ ion can work as a low melting point flux, which enhances the crystallization degree of the phosphor, meanwhile the crystal structure around the luminescent ions can be adjusted to reduce the crystal symmetry by replacing or occupying the crystal vacancy with Li⁺ doping (Zhao et al., 2013), and the color coordinate position of UC white light can be further slightly adjusted.

CONCLUSIONS

In this paper, different methods were used to adjust the UCPL performance of GdAlO₃:Er³⁺, Yb³⁺, Tm³⁺ phosphors to obtain ideal white light. The energy transfer between Er³⁺ and Yb³⁺ in the phosphors increased, then the ratios of red to blue emission and green to blue emission intensity were improved with the increase of Er³⁺ doping concentration, so as to change each color distribution successfully, and making the maximum shift of the CIE coordinate of phosphors. The UC white light could be further adjusted by changing the

doping concentration of the sensitizer Yb^{3+} , because it was good for the blue emissions of Tm^{3+} to obtain the energy transfer from Yb^{3+} than that of the red and green emissions from Er^{3+} , which made the relative intensity of red to blue and green to blue emissions decrease. The ratios of red/green to blue emissions decreased with the increased calcination temperature of the precursor, while increasing the excitation laser power was conducive to the three-photon UC emission process of Tm^{3+} , both enhanced the blue emission part of the UC white light, so as to slightly adjusted the UCPL. The crystal symmetry could be reduced by Li^+ doping, which made the color coordinate position move slightly. The four different methods on the effect of phosphors UC white luminescence were researched systematically, and the UCPL mechanism was correspondingly discussed, which played an important role in adjusting the red /green /blue colors to obtain the ideal UC white emitting luminescence.

REFERENCES

- Annadurai, G., Masilla Moses Kennedy, S., and Sivakumar, V. (2018). Synthesis of novel Dy^{3+} activated $\text{Ba}_2\text{CaZn}_2\text{Si}_6\text{O}_{17}$ phosphors for white light-emitting diodes. *Luminescence* 33, 521–527. doi: 10.1002/bio.3441
- Cao, J. F., Zhang, J., and Li, X. W. (2018). Upconversion luminescence of $\text{Ba}_3\text{La}(\text{PO}_4)_3:\text{Yb}^{3+}\text{-Er}^{3+}/\text{Tm}^{3+}$ phosphors for optimal temperature sensing. *Appl. Optics* 57, 1345–1350. doi: 10.1364/AO.57.001345
- Chen, W. P., Zhang, X. Z., and Wang, L. P. (2017). Synthesis and luminescence properties of blue-emitting phosphor $\text{Ca}_{12}\text{Al}_{14}\text{O}_{32}\text{F}_2:\text{Eu}^{2+}$ for white light-emitting diode. *Luminescence* 32, 952–956. doi: 10.1002/bio.3276
- Chung, J. H., Ryu, J. H., Mhin, S. W., Kim, K. M., and Shim, K. B. (2012). Controllable white upconversion luminescence in $\text{Ho}^{3+}/\text{Tm}^{3+}/\text{Yb}^{3+}$ co-doped CaMoO_4 . *J. Mater. Chem.* 22, 3997–4002. doi: 10.1039/c2jm15332g
- Deng, T. L., and Jiang, X. B. (2018). Comparison of the up-conversion photoluminescence for GAP, GAG and GAM phosphors. *Opt. Mater.* 78, 27–34. doi: 10.1016/j.optmat.2018.01.033
- Deng, T. L., Yan, S. R., and Hu, J. G. (2014a). Effect of calcination temperature on up-conversion photoluminescence of the $\text{GdAlO}_3:\text{Er,Yb}$ phosphor. *J. Solid State Sci. Technol.* 4, R48–R53. doi: 10.1149/2.0101503jss
- Deng, T. L., Yan, S. R., and Hu, J. G. (2014b). Preparation and up-conversion photoluminescence properties of $\text{GdAlO}_3:\text{Er}^{3+}, \text{Yb}^{3+}$ phosphors. *Acta Phys. Chim. Sin.* 30, 773–780. doi: 10.3866/PKU.WHXB201402201
- DiMaio, J. R., Kokuoz, B., and Ballato, J. (2006). White light emissions through down-conversion of rare-earth doped LaF_3 nanoparticles. *Opt. Express* 14, 11412–11417. doi: 10.1364/OE.14.011412
- Du, P., Huang, X. Y., and Yu, S. (2018). Facile synthesis of bifunctional Eu^{3+} -activated NaBiF_4 red-emitting nanoparticles for simultaneous white light-emitting diodes and field emission displays. *Chem. Eng. J.* 337, 91–100. doi: 10.1016/j.cej.2017.12.063
- Justel, T., Nikol, H., and Ronda, C. (1998). New developments in the field of luminescent materials for lighting and displays. *Angew. Chem. Int. Edn.* 110, 3250–3271. doi: 10.1002/(SICI)1521-3773(19981204)37:22<3084::AID-ANIE3084>3.0.CO;2-W
- Lelekaite, A., and Kareiva, A. (2004). Synthesis of garnet structure compounds using aqueous sol-gel processing. *Opt. Mater.* 26, 123–128. doi: 10.1016/j.optmat.2003.11.009
- Li, B., Huang, X. Y., and Lin, J. (2018). Single-phased white-emitting $\text{Ca}_3\text{Y}(\text{GaO})_3(\text{BO}_3)_4:\text{Ce}^{3+}, \text{Tb}^{3+}, \text{Sm}^{3+}$ phosphors with high-efficiency: photoluminescence, energy transfer and application in near-UV-pumped white LEDs. *J. Lumin.* 204, 410–418. doi: 10.1016/j.jlumin.2018.08.044
- Liu, M., Wang, S. W., Zhang, J., An, L. Q. L., and Chen, D. (2007). Upconversion luminescence of $\text{Y}_3\text{Al}_5\text{O}_{12}$ (YAG): $\text{Yb}^{3+}, \text{Tm}^{3+}$ nanocrystals. *Opt. Mater.* 30, 370–374. doi: 10.1016/j.optmat.2006.11.060
- Liu, X. M., Lin, C. K., and Lin, J. (2007). White light emission from Eu^{3+} in CaIn_2O_4 host lattices. *Appl. Phys. Lett.* 90:081904. doi: 10.1063/1.2539632
- Liu, Z. C., Shen, C. Y., and Yuan, L. (2019). $\text{Ca}_5\text{Ga}_6\text{O}_{14}:\text{Eu}^{3+}$: a novel phosphor with outstanding heat resistance for white light-emitting diodes. *J. Am. Ceram. Soc.* 102, 3823–3828. doi: 10.1111/jace.16352
- Milliez, J., Rapaport, A., Bass, M., Cassanho, A. H., and Jenssen, P. J. (2006). High-brightness white-light source based on up-conversion phosphors. *J. Display Technol.* 2, 307–311. doi: 10.1109/JDT.2006.879183
- Rai, V. K., Dey, R., and Kumar, K. (2013). White upconversion emission in $\text{Y}_2\text{O}_3:\text{Er}^{3+}/\text{Tm}^{3+}/\text{Yb}^{3+}$ phosphor. *Mater. Res. Bull.* 48, 2232–2236. doi: 10.1016/j.materresbull.2013.02.064
- Seo, Y. W., Choi, B. C., and Moon, B. K. (2017). Tunable up-conversion luminescence from $\text{Er}^{3+}/\text{Tm}^{3+}/\text{Yb}^{3+}$ tri-doped Sr_2CeO_4 phosphors. *J. Lumin.* 182, 240–245. doi: 10.1016/j.jlumin.2016.10.006
- Shannon, R. D. (1976). Revised effective ionic radius and systematic studies of interatomic distances in halides and chalcogenides. *Acta Crystallogr. Sect. A* 32, 751–767. doi: 10.1107/S0567739476001551
- Shi, L. S., Li, C., and F., Shen, Q.Y. (2014). White upconversion emission in $\text{Er}^{3+}/\text{Yb}^{3+}/\text{Tm}^{3+}$ codoped LiTaO_3 polycrystals. *J. Alloys Compd.* 591, 105–109. doi: 10.1016/j.jallcom.2013.12.234
- Sivakumar, S., Van Veggel, F. C., and Raudsepp, M. (2005). Bright white light through up-conversion of a single NIR source from sol-gel-derived thin film made with Ln^{3+} -doped LaF_3 nanoparticles. *J. Am. Chem. Soc.* 127, 12464–12465. doi: 10.1021/ja052583o
- Tamrakar, R. K., Upadhyay, K., and Sahu, M. (2016). Spectral characterization of $\text{Er}^{3+}, \text{Yb}^{3+}$ codoped GdAlO_3 phosphor prepared by solid state reaction method. *J. Alloy. Compd.* 689, 702–712. doi: 10.1016/j.jallcom.2016.07.327
- Wang, F., and Liu, X. G. (2008). Upconversion multicolor fine-tuning: visible to near-infrared emission from lanthanide-doped NaYF_4 nanoparticles. *J. Am. Chem. Soc.* 130, 5642–5643. doi: 10.1021/ja800868a
- Zhao, C. Z., Kong, X. G., Liu, X. M., Tu, L. P., Wu, F., Zhang, Y. L., et al. (2013). Li^+ ion doping: an approach for improving the crystallinity and upconversion emissions of $\text{NaYF}_4:\text{Yb}^{3+}, \text{Tm}^{3+}$ nanoparticles. *Nanoscale* 5, 8084–8089. doi: 10.1039/c3nr01916k

DATA AVAILABILITY STATEMENT

All datasets generated for this study are included in the article/supplementary material.

AUTHOR CONTRIBUTIONS

TD was in charge of designing the experiments and writing the manuscript. XJ performed experiments. TD and QZ were in charge of revising the manuscript. All authors contributed to the article and approved the submitted version.

FUNDING

This work was financially supported by the Youth Growth S&T Personnel Foundation of the Guizhou Education Department (KY[2017]283).

Conflict of Interest: The authors declare that the research was conducted in the absence of any commercial or financial relationships that could be construed as a potential conflict of interest.

Copyright © 2020 Deng, Jiang and Zhang. This is an open-access article distributed under the terms of the Creative Commons Attribution License (CC BY). The use, distribution or reproduction in other forums is permitted, provided the original author(s) and the copyright owner(s) are credited and that the original publication in this journal is cited, in accordance with accepted academic practice. No use, distribution or reproduction is permitted which does not comply with these terms.



Current Approaches to Alkyl Levulinates via Efficient Valorization of Biomass Derivatives

Xiaofang Liu¹, Wenjia Yang¹, Qiuyun Zhang², Can Li^{1*} and Hongguo Wu^{1,3*}

¹ Guizhou Provincial Key Laboratory for Rare Animal and Economic Insects of the Mountainous Region, College of Biology and Environmental Engineering, Guiyang University, Guiyang, China, ² School of Chemistry and Chemical Engineering, Anshun University, Anshun, China, ³ State-Local Joint Laboratory for Comprehensive Utilization of Biomass, Guizhou University, Guiyang, China

OPEN ACCESS

Edited by:

Yaqiong Su,
Eindhoven University of
Technology, Netherlands

Reviewed by:

Jian He,
Jishou University, China
Wenfeng Zhao,
Technical University of
Denmark, Denmark
Hu Pan,
Jiaxing University, China

*Correspondence:

Can Li
lican790108@163.com
Hongguo Wu
whg0408@126.com

Specialty section:

This article was submitted to
Green and Sustainable Chemistry,
a section of the journal
Frontiers in Chemistry

Received: 31 May 2020

Accepted: 29 July 2020

Published: 15 October 2020

Citation:

Liu X, Yang W, Zhang Q, Li C and
Wu H (2020) Current Approaches to
Alkyl Levulinates via Efficient
Valorization of Biomass Derivatives.
Front. Chem. 8:794.
doi: 10.3389/fchem.2020.00794

Biomass is a potential non-food, carbon-neutral, and abundant resource, which can be used as an alternative to fossil fuels during the sustainable preparation of various platform chemicals. Alkyl levulinates (ALs) have found widespread application as flavorings, plasticizing agents, and fuel additives, as well as synthetic precursors to various building blocks. Several processes have been investigated to transform biomass and its derivatives into ALs, which mainly include: (i) direct esterification of levulinic acid (LA) with alkyl alcohols and (ii) alcoholysis reactions of renewable biomass feedstocks and their derivatives, including furfuryl alcohol (FAL), chloromethyl furfural (CMF), and saccharides. This review focuses on illustrating the effects of the biomass pretreatment step, catalyst texture, possible mechanisms, acidities, and intermediates on the synthesis of ALs from sustainable resources covering a wide range of intermediates, including diethyl ether (DEE), 4,5,5-triethoxypentan-2-one (TEP), ethoxymethylfuran (EMF), ethyl-D-fructofuranoside (EDFF), and ethyl-D-glucopyranoside (EDGP).

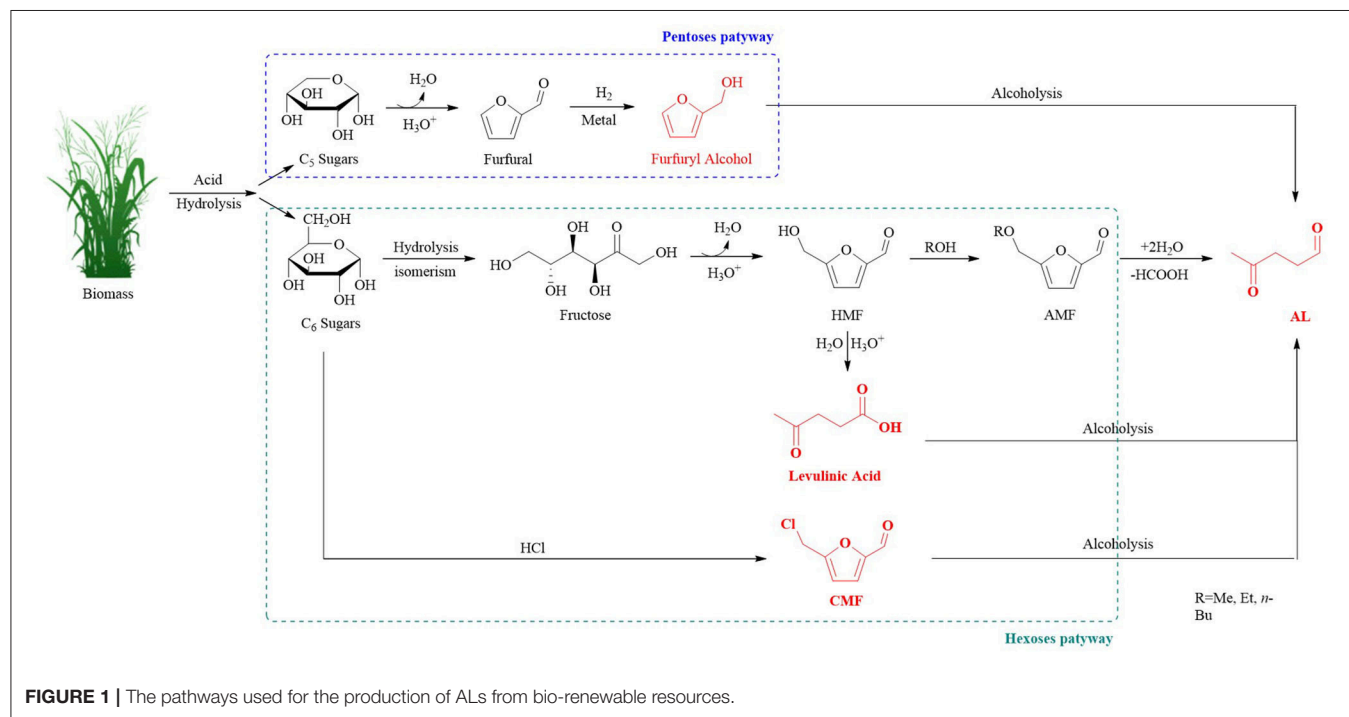
Keywords: alkyl levulinates, levulinic acid, furfuryl alcohol, chloromethyl furfural, acidic catalysts

INTRODUCTION

As the natural reserves of non-renewable resources such as petroleum, diesel, natural gases, and coal (fossil fuels) dwindle (Badgujar and Bhanage, 2015; Dhyani and Bhaskar, 2018) while causing unavoidable environmental issues, such as the emission of harmful gases and global-warming (Sun and Cheng, 2002; Wagh et al., 2016), extensive efforts must be devoted toward the search for alternative and renewable resources that are also environmentally friendly. Biomass is a carbon source used for renewable energy, which can provide multiple fuels, chemicals, and value-added platform molecules in a green and sustainable manner (Rackemann and Doherty, 2011; Tadele et al., 2017; Badgujar and Bhanage, 2018). Alkyl levulinates (ALs) derived from biomass have shown great potential for biorenewable fuels like bio-lubricants (Mukherjee et al., 2015), chemicals synthesis (Mullen et al., 2013), polymer or resin precursors (Alloaoua et al., 2014; Cousinet, 2014), green solvents (Lomba et al., 2011), plasticizers (Bloom, 2007), food-flavor agents (Yontz, 2011), and pharmaceuticals (Tsucha and Yoshida, 1994) during the effective utilization of biomass (Table 1). (Fiorentino et al., 2014). An investigation on Scopus indicated that the interest in developing ALs as a fuel has built up great momentum over the past 5 years. Research on ALs has mainly concentrated on methyl, ethyl, and butyl levulinate (Mascal and Nikitin, 2010b). Among these three levulinates, ethyl levulinate (EL) exhibits enhanced solubility with diesel (Christensen et al., 2011)

TABLE 1 | Potential alkyl levulinates applications.

Entry	Applications	Products
1	Chemical industry	Chiral reagent, polyhydroxy alkanoates, lubricants, adsorbents, formic acid, valerates
2	Fuels and fuel additives	EL, 2-methyltetrahydrofuran, γ -valerolactone, angelica lactone, methyl levulinate, and other esters
3	Pharmaceuticals	δ -aminolevulinic acid, calcium levulinate, heterocyclic derivatives of levulinic acid, angelica lactone, ketals, tetrapyrroles, succinic acid
4	Food additives	γ -valerolactone, ethyl valerate, succinic acid, valerate esters
5	Agricultural products	δ -aminolevulinic acid, formic acid, lignins, ethyl formate
6	Solvents and polymers	Diphenolic acid, succinic acid, pyridine, furans, epoxies, 1,4-butanediol, tetrahydrofuran, N-methyl-2-pyrrolidone, γ -butyrolactone



and only $\sim 4\%$ NO_x emissions upon blending in diesel (Windom et al., 2011). Therefore, research has mostly been devoted toward the effective synthesis of EL.

ALs can be produced from biomass or via the conversion of levulinic acid (LA), furfuryl alcohol (FAL) (Démolis et al., 2014; Desidery et al., 2018), or chloromethyl furfural (CMF) (Mascal and Nikitin, 2010a). All of the possible reaction pathways involved in the alcoholysis procedure performed in the presence of acid catalysts have been reported (**Figure 1**). This review comprehensively contains all of the discussed approaches used for the production of ALs and executes critical evaluation of the various types of catalysts used in the conversion reactions: i) an overall understanding of the reaction parameters, texture and chemical properties, possible mechanism, and the reaction intermediates that favor the development to achieve high yields (Chia et al., 2013; Gupta et al., 2016), ii) different catalytic routes of ALs preparation, iii) utilization of various catalysts to obtain ALs, and iv) the future challenges and opportunities for the lab scale to the industry scale development of ALs.

PREPARATION OF ALs

Numerous advantages for using solid acid catalysts have been demonstrated including their low cost, ease of recycling from the product mixture, low equipment corrosion, and high thermal stability (Su et al., 2013b), while the application of heterogeneous materials toward the production of ALs requires further detailed discussion including the reaction temperature, time, substrates, acidic density and intensity, and textural properties.

Routes to Prepare ALs From LA

Heteropolyacid (HPA) as Catalysts

The LA esterification reaction has been investigated using several solid acid catalysts toward the production of ALs in comparatively high yields (Pileidis and Titirici, 2016). Heteropolyacid (HPA) is a special species of acid composed of a combination of certain metals (tungsten, molybdenum, or vanadium) and *p*-block non-metals (silicon, phosphorus, or arsenic) with acidic hydrogen and oxygen atoms, which are

generally applied as reusable acid catalysts for the preparation of fine chemicals (Yan et al., 2013; Wu et al., 2016a,b,c; Zhou et al., 2016; Manikandan and Cheralathan, 2017; Ramli et al., 2017a; Zheng et al., 2017; Luan et al., 2018; Vilanculo et al., 2018; Lucas et al., 2019). Numerous structural combinations can be prepared upon adjusting the metal and non-metal used. Furthermore, HPAs possess very strong Brønsted acidity and can be applied as homogenous or heterogeneous catalysts and solvents (Wu et al., 2016b; Zhou et al., 2016; Ramli et al., 2017a; Zheng et al., 2017).

HPAs have several disadvantages, including high solubility in water and other polar solvents, low specific surface area and thermal stability, and difficult reusability and regeneration (Gupta and Paul, 2014; Hu et al., 2015; Yamaguchi and Shirai, 2016), which hinders their application as efficient and effective catalysts for reactions with large molecules. A variety of diverse synthetic approaches have been studied to overcome these disadvantages including their immobilization on ordered silica, zirconia, and niobium (Narkhede et al., 2015).

HPA implanted into the Wells–Dawson (WD) structure provided EL with a 76% yield upon heating at 78°C for 10 h (Pasquale et al., 2012). Luan et al. carried out the production of ethyl, methyl, and isobutyl levulinates using an organic-salt of $\text{H}_4\text{SiW}_{12}\text{O}_{40}$ as the catalyst (Luan et al., 2018). Manikandan and Cheralathan investigated heteropoly acid-supported silicalites in the synthesis of various ALs (Manikandan and Cheralathan, 2017).

Similarly, when changing WD to Keggin HPA ($\text{H}_3\text{PMo}_{12}\text{O}_{40}$), the EL yield increased to 93% under identical reaction conditions. The higher yield observed over Keggin HPA ($\text{H}_3\text{PMo}_{12}\text{O}_{40}$) was attributed to its higher acidity when compared to the WD structure. While transforming the alkylation substrates with isobutylene and methanol, WD HPA showed increased activity during the preparation of ALs when compared to Keggin HPAs, which was attributed to the higher adsorption of the reactants in the WD structure (Briand et al., 2003). Nevertheless, both WD- and Keggin-structured HPAs show comparable or higher activity than their corresponding homogeneous catalysts (Baronetti et al., 1998). However, leaching of the HPAs in polar solvents still occurs owing to the weak interactions formed between the HPAs and the support. The Keggin HPA ($\text{H}_4\text{SiW}_{12}\text{O}_{40}$) embedded in the channels of mesoporous SiO_2 gave EL a 67% yield with improved recyclability when compared to the original HPA (Yan et al., 2013). Similarly, a combination of HPAs and zeolites was reported by Nandiwale et al. Improved stability was achieved using dodecatungstophosphoric acid (DTPA) supported on desilicated HZSM-5, which gave EL a 94% yield from LA at 76°C in 240 min (Nandiwale et al., 2013). High EL yields up to 77% were achieved over four reaction cycles demonstrating the high stability of the catalyst.

Neurock, Iglesia, and co-workers carried out a series of investigations on the acidity and reactivity of Keggin HPAs, which confirmed that the deprotonation energy (DPE) of the HPA was crucial for its activity (Macht et al., 2007, 2008). The HPA DPE determines the strong acidity of the material and thereby its increased reactivity in acid-catalyzed processes. The DPE of Keggin $\text{H}_4\text{SiW}_{12}\text{O}_{40}$ was determined to be 1,105

$\text{kJ}\cdot\text{mol}^{-1}$, which was lower than Keggin $\text{H}_3\text{PMo}_{12}\text{O}_{40}$ (1,126 $\text{kJ}\cdot\text{mol}^{-1}$) (López et al., 2012). Hence, the two Keggin-structured HPAs prove the correlation between their activity and DPEs. To further enhance the acidity of Keggin HPAs, an acidic silica-like support such as ZrO_2 was applied for the preparation of a variety of hybrid Keggin HPA/ ZrO_2 composites containing both Brønsted and Lewis acid sites with increased activity toward the production of ALs when compared to HPA-silica (Su et al., 2013a). DRIFTS research on $\text{H}_3\text{PW}_{12}\text{O}_{40}/\text{ZrO}_2$ further verified the existence of Brønsted and Lewis acid sites, which was in accordance with this hypothesis (Alsalmé et al., 2010; Wu et al., 2016a). In addition, the modification of Keggin HPA-organosilica/ ZrO_2 was proposed to prepare a hybrid catalyst, whereby a maximum AL yield of up to 95% was observed (Luan et al., 2018). Subsequently, several efforts have been devoted toward designing catalysts for the transformation of LA into ALs with enhanced stability, available active sites, and recyclability.

Zeolites as Catalysts

Other factors in regard to the catalyst that influence the reactivity and selectivity during the conversion of LA into EL are its texture, porosity, specific surface area, and availability of active sites. Well-organized materials, such as zeolites, contain functionalities that can be used to control the acidity and pore size to achieve better EL yields. For example, desilicated H-ZSM-5 (DH-ZDM-5) has moderate acidity (0.73 $\text{mmol}\cdot\text{g}^{-1}$), a high surface area (427.6 $\text{m}^2\cdot\text{g}^{-1}$), and mesoporosity, which affords EL a 95% yield under autogenous pressure (Nandiwale et al., 2014). The obtained EL yield was comparable to that obtained over HPA/H-ZSM-5 at high temperature (130°C). To account for this phenomena, Janik et al. carried out DFT calculations on the mobility of the isolated protons. The results indicate the relatively low activation barrier of phosphotungstic acid ($E_a = 103.3 \text{ kJ}\cdot\text{mol}^{-1}$) (Janik et al., 2005), which was also calculated by Ryder et al. for H-ZSM-5 ($E_a = 117.2 \text{ kJ}\cdot\text{mol}^{-1}$) (Ryder et al., 2000). The activation barrier was confirmed to be significantly reduced ($E_a = 11.2 \text{ kJ}\cdot\text{mol}^{-1}$) in the presence of hydrated protons in the Keggin HPA structures (Janik et al., 2005). The acid strength was directly proportional to the protons mobility and thus, a slightly higher reaction temperature was required for the conversion of LA into EL using desilicated H-ZSM-5 (Nandiwale et al., 2014). Dharane and Bokade reported the production of butyl levulinate using dodecatungsten phosphoric acid inserted in acid-treated clay (K-10) (Dharane and Bokade, 2011). Therefore, the lower proton mobility and pore structure of zeolites lead to the higher selectivity observed toward EL during the esterification of LA, which was attributed to the highly efficient mass transfer observed within the moderate pore channels in zeolites (Yan et al., 2013). Patil et al. further demonstrated that mesoporous zeolites (micro/meso-HZ-5) with larger cavities enhanced the substrates access to the acidic sites (total acidity = 0.73 $\text{mmol}\cdot\text{g}^{-1}$) and gave a high EL yield of up to 95% when compared with a traditional microporous zeolite (H-BEA_{0.10}; total acidity = 0.69 $\text{mmol}\cdot\text{g}^{-1}$, EL yield = 39.2%) (Patil et al., 2014). The achievement was confirmed further by Nandiwale et al. on the esterification of LA with *n*-butanol

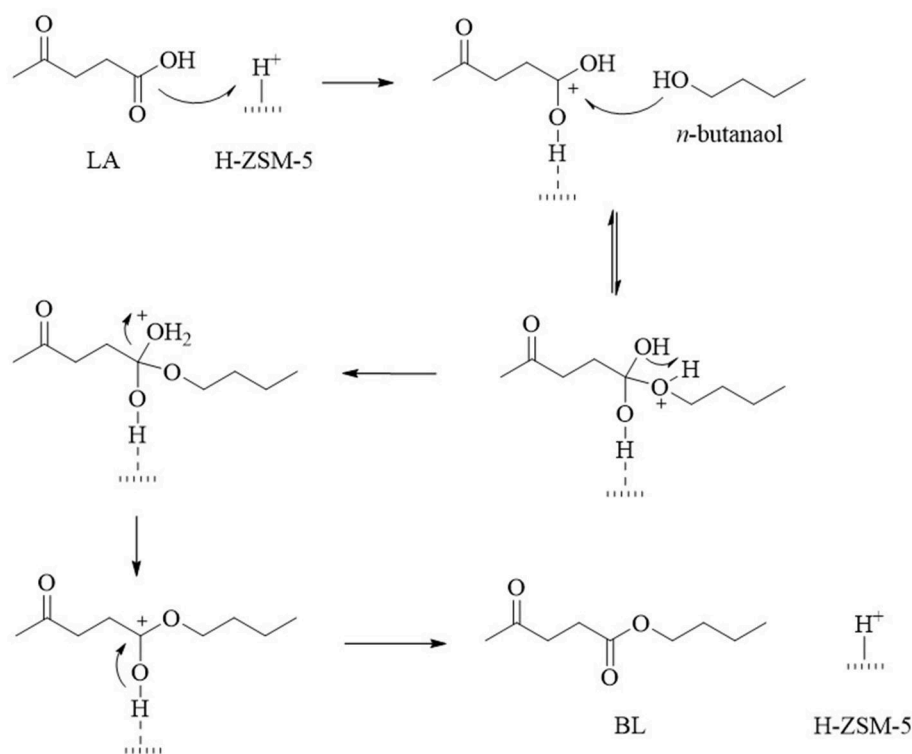


FIGURE 2 | Proposed reaction mechanism for the esterification of LA with *n*-butanol over the H-ZSM-5 catalyst.

(Nandiwale and Bokade, 2015), and the proposed mechanism is shown in **Figure 2**.

Metal Oxides as Catalysts

Mesoporous metal oxides are potential alternatives to zeolites as catalytic supports (Dave and Pant, 2011; Mondal et al., 2015). During the esterification for LA to prepare ALs, acidic catalysts are desirable. For instance, sulfated zirconia ($\text{SO}_4^{2-}/\text{ZrO}_2$) exerts a higher Hammett acid strength ($H_0 = -16.04$) than homogeneous pure sulfuric acid ($H_0 = -11.99$), which indicates it is a superacid (Yadav and Nair, 1999). Owing to their high acidity, solid superacids embedded into various metal oxides have been developed toward the transformation of LA into ALs. Sulfated tin oxide gave EL a 44% yield, which was significantly better than that observed using non-sulfated tin oxide (6% EL yield) under identical reaction conditions (Fernandes et al., 2012). For the resulting sulfated oxides, the acidity followed the order of $\text{SO}_4^{2-}/\text{ZrO}_2 > \text{SO}_4^{2-}/\text{Nb}_2\text{O}_5 > \text{SO}_4^{2-}/\text{TiO}_2 > \text{SO}_4^{2-}/\text{SnO}_2$. (Rao et al., 2006), while the EL yield trend observed with the sulfated metal oxides followed the order of $\text{SO}_4^{2-}/\text{SnO}_2 > \text{SO}_4^{2-}/\text{TiO}_2 > \text{SO}_4^{2-}/\text{ZrO}_2 > \text{SO}_4^{2-}/\text{Nb}_2\text{O}_5$ (Yadav and Nair, 1999). The acidic strength was opposite to the EL yield and could be attributed to the texture, specific surface area, and pore size of the catalyst, which in turn determines the accessibility of the active sites. Fernandes et al. carried out these investigations and the results suggested that the poor activity (14% EL yield) observed for the $\text{SO}_4^{2-}/\text{Nb}_2\text{O}_5$ catalyst can be attributed to

its lower S_{BET} ($67 \text{ m}^2\cdot\text{g}^{-1}$) when compared to $\text{SO}_4^{2-}/\text{TiO}_2$ ($107 \text{ m}^2\cdot\text{g}^{-1}$) and $\text{SO}_4^{2-}/\text{SnO}_2$ ($130 \text{ m}^2\cdot\text{g}^{-1}$) (Fernandes et al., 2012). Similarly, the low S_{BET} ($51.7 \text{ m}^2\cdot\text{g}^{-1}$) of sulfated zirconia ($\text{SO}_4^{2-}/\text{ZrO}_2$) displays an EL yield of 27.5% at 70°C , which was significantly increased up to 80% when using mingling mesoporous silica ($S_{\text{BET}} = 130 \text{ m}^2\cdot\text{g}^{-1}$) synthesized via a successive co-precipitation-impregnation method. Optimization studies confirmed that ZrO_2 with a Si content of 5.0–10 mol% Si per Zr exhibits the best catalytic performance (Kuwahara et al., 2014). However, when catalyzed using sulfated metal oxides such as $\text{SO}_4^{2-}/\text{ZrO}_2$, $\text{SO}_4^{2-}/\text{SnO}_2$, and $\text{SO}_4^{2-}/\text{Nb}_2\text{O}_5$ at elevated temperature (160°C), each catalyst showed improved EL yields ($\sim 70\%$), which was attributed to their enhanced activity (Yadav and Yadav, 2014). In addition, the higher density and availability of the active acid sites in the catalyst may enhance the EL yield (Li Z. et al., 2014). Dispersing TiO_2 onto sulfated zirconia nanoparticles increases the sulfur complex density up to 1.71 sulfate groups per nm^3 and when distributed on the surface of a $\text{ZrO}_2/\text{TiO}_2$ support results in a significant improvement when compared to their corresponding TiO_2 nanocomposites (0.35 sulfate groups per nm^3) (Li et al., 2012). Based on the above discussion, Kuwahara and co-workers reported a high EL yield of up to 80% from LA upon heating at 70°C over 1,440 min using sulfated Zr-SBA-15, which was attributed to the appropriate acid site density of sulfated ZrO_2 immobilized on the ordered and mesoporous silica template (Kuwahara et al., 2013). Therefore, the acid site density, acid strength, and predominant

morphological characteristics contribute to the higher EL yield. However, the drawback of deactivation via hydration of the sulfur complexes in sulfated metal oxide catalysts occurs in an aqueous phase or when water is produced as a product of the reaction, which impedes the development of numerous reactions.

Sulfonic Acid-Functionalized Materials as Catalysts

To overcome the limitations of sulfated metal oxides, sulfonic acid-based materials have been introduced as an alternative to performing the desired reactions. Sulfonic acid ions construct a hydrophobic microenvironment in the reaction medium, which protects the catalyst from water molecules generated during the reaction, thus guaranteeing their stability (Song et al., 2015). Therefore, sulfonic acid functionalized mesoporous materials have several advantages including high surface area, accessible active sites, appropriate pore structures, and high stability for achieving the desired ALs in good yield.

Silica has aroused great interest from researchers owing to its superior features, such as ordered porosity, low cost, adjustable surface functionalities, high surface area, and chemical and thermal stability (Melero et al., 2013; Maggi et al., 2016; Chermahini and Nazeri, 2017; Enumula et al., 2017; Ramli et al., 2018; Yang and Tang, 2019).

EL was obtained in 100% yield upon heating at 117°C for 2 h using propylsulfonic acid-functionalized mesoporous silica (Pr-SO₃H-SBA-15), which could be reused three times without needing to be regenerated (Melero et al., 2013). Similarly, Ramli et al. prepared methyl levulinate in 69% yield over sulfated silica under mild reaction conditions (Ramli et al., 2018). Meanwhile, Chermahini and Nazeri reported the use of aluminum-containing MCM-41 for the production of isobutyl and butyl levulinate, and verified that the regenerated catalyst can be recycled without any obvious loss of activity (Chermahini and Nazeri, 2017). Besides, the insertion of tungsten oxide into SBA-16 also showed enhanced acidity and catalytic performance, and gave a higher yield of the desired levulinate products. This was attributed to the uniform distribution of acidic tungsten oxide sites over the large specific surface area and ordered structure of SBA-16 (Enumula et al., 2017). These materials combined with silica-based materials are easily deactivated in polar solvents because of the H-bonding formed between the active silica-functionalized groups and polar solvent molecules.

Inspired by these outstanding results, Oliveira et al. conducted studies using carbon nanotubes (CNT) as a support with a high surface area available for sulfonation. By varying the functionalization temperature and number of acid sites, the activity of the sulfonated CNT catalyst can be easily adjusted and controlled by its acid site density. Unfortunately, the overall EL yield was relatively low (~50%) because of the selectivity and strong chemisorption of LA on the CNT surface (Oliveira and Teixeira Da Silva, 2014).

An innovative approach to prepare bifunctional acid-base catalysts using Zr-containing metal-organic frameworks (MOFs) formed using 2-aminoterephthalate ligands has been proposed by Corma and coworkers (Cirujano et al., 2015). The interactions formed between the catalyst, LA, and alcohol were activated on the catalytic centers of the metal (Zr) and amino group in the

ligand. The results demonstrate that these centers play different roles within proximity to one another and they all allowed the simultaneous activation processes to occur. The resulting NH₂-Zr-MOF catalysts afford a high EL yield (>95%) under relatively mild reaction conditions (78°C). The excellent performance was further confirmed by the turnover frequency (TOF), which was measured to be 230 h⁻¹, which was >2-fold higher than that obtained using homogeneous *p*-toluene sulfonic acid (TOF = 120 h⁻¹).

Several research groups have explored the effectiveness of various heterogeneous catalysts toward the production of EL from LA under optimal reaction conditions. Sulfonated carbon nanotubes have also been explored as a catalyst for the synthesis of ALs (Oliveira and Teixeira Da Silva, 2014). However, this type of catalyst is not recyclable when employed in the LA esterification reaction and exhibits a lower catalytic performance than that observed using the classic benchmark catalyst (Amberlyst-15).

Resins are organo-polymeric materials, which possess high surface areas, high ion-exchange capacities, and various functionalities depending on the type of resin used (Tejero et al., 2016; Marrocchi and Vaccaro, 2017; Ramli et al., 2017b; Kokare et al., 2018; Trombettoni et al., 2018). The main catalytic resins are Amberlyst-15, Amberlyst-16, Amberlyst-36, Amberlyst-70, Purolite, Dowex, and polystyrene-supported *p*-toluenesulfonic acid. The existence of sulfonic-acid groups (-SO₃H) endows the resin catalysts with acidic properties, which initiate the conversion process (Tejero et al., 2016; Ramli et al., 2017b; Kokare et al., 2018). Ramli et al. developed an ion-exchange resin (Amberlyst-15) for use as a solid acid catalyst in the production of ALs under safe media flow conditions, confirming that the process was chemically and environmentally efficient (Ramli et al., 2017b). Kokare et al. carried out response surface optimization for the preparation of *n*-butyl levulinate over Amberlyst-15 and a maximum LA conversion of 97% was achieved using a LA to *n*-butanol molar ratio of 1:4 at 124°C (Kokare et al., 2018). Meanwhile, a low divinylbenzene (DVB) content gel-type resin (Dowex 50Wx2; 2% DVB) gave good yields of the desired AL products, which was attributed to the accessibility of the reactants to the acid centers in the highly swollen and low polymer density resin (Tejero et al., 2016). The reusability of Amberlyst-15 and Amberlyst-70 is highly practical and requires a simple washing step, and are therefore less expensive when compared to other resin-based catalysts. However, the instability of Amberlyst-15 at high temperatures greatly impedes its further application. The major challenges for the employment of resins in these catalytic conversion reactions are their high cost, thermal instability, non-flexibility, H-bond formation, and destabilization of the active centers.

Routes to Prepare ALs From Biomass Feedstocks and Their Derivatives

FAL as a Feedstock

Zhang et al. have explored a wide variety of acid catalysts including zeolite, ion-exchange resins, ionic liquids (ILs), and HPA toward the synthesis of butyl levulinate (BL) (Zhang

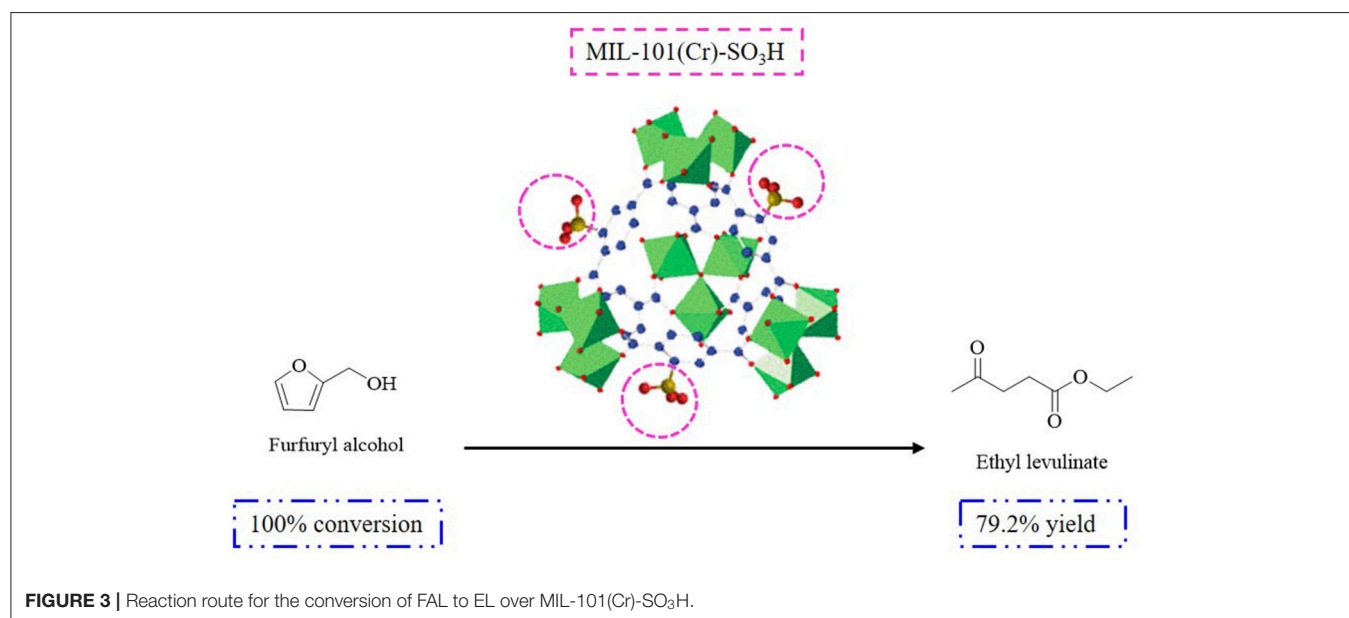
et al., 2011). The results showed that the production of 2-butoxymethylfuran (BMF) was faster than the subsequent conversion reaction to form BL. In addition, reports have speculated that BMF reacts with water, which accelerates the reaction. When one equivalent of water was added to the reaction, BL was obtained in 93% from FAL. This confirmed the higher activity observed in the presence of water when compared to the reaction performed in the absence of water (BL yield = 88%). Based on their experimental results, a proposed mechanism for the conversion of FAL into ALs indicated that the reaction may occur via the formation of an alkoxymethylfuran intermediate.

Similar conclusions have been reported by Huang et al. when studying the conversion of FAL into methyl levulinate (ML) (Huang et al., 2016). The results indicated multiple routes involving the production of methoxymethylfuran (MMF) and 4,5,5-trimethoxypentan-2-one (TMP) as intermediates occurred during the reaction. Their investigations demonstrated that TMP was formed from MMF under specific reaction conditions, which indicates that both TMP and MMF promote the synthesis of ML. When the reaction system was carried out using FAL and ethanol to prepare EL, the observation of the above-mentioned intermediates proposed in the mechanism was difficult. However, the published studies established two clear observations. The formation of the reaction intermediates (TEP and/or EMF) was slower than the reaction converting FAL into multiple intermediates. In addition, the yield of DEE formed in the reaction when compared to EL or the reaction intermediates (TEP and EMF) was low and various pathways contributed to the formation of EL.

The production of DEE during the synthesis of EL depends on the texture of the catalyst used, including the pore structure and accessibility of the active sites for ethanol dehydration derived from the ethanolysis of FAL. The results revealed the acid

catalysts used for the FAL-EL procedure, reaction temperature, time, acidic sites employed, and observed EL yields. Owing to the microporous and non-swelling structure of gel-type resins (Dowex, Amberlyst, etc.), a higher amount of DEE was formed and a lower EL yield (<60%) was obtained, which can be ascribed to the improved accessibility of the active sites to ethanol when compared to FAL (Lange et al., 2009). This was different from resin catalysts with mesoporous structures (carbon-based, silica-based, etc.), which showed better EL yields (>80%) and lower amounts of DEE depending on the superior accessibility of the acidic sites to FAL when compared to ethanol (Lange et al., 2009; González Maldonado et al., 2012). Sulfonic acid-functionalized mesoporous materials (activated carbon, silica-carbon composites, organosilica hollow nanospheres, and sulfated MOF) have been used in the production of EL utilizing the ethanolysis procedure giving EL yields in the range of 80–90% (Russo et al., 2014a,b; Zhu et al., 2014; Liu et al., 2016; Guo et al., 2020). In addition, the density of the acidic groups has been shown to affect the reaction rate. For example, adjusting the $-\text{SO}_3\text{H}$ density from 5.4 to 17% in propylsulfonic acid-functionalized ethane bridged organosilica hollow nanospheres (Pr- SO_3H -Et-HNS) gave EL yields ranging from 52.5 to 72% under the same reaction conditions. Meanwhile, with the catalyst MIL-101(Cr)- SO_3H , EL yield was enhanced up to 79.1% when FAL was used as the starting material ascribed to the MOF texture ($S_{\text{BET}} = 1,492 \text{ m}^2 \cdot \text{g}^{-1}$, titration $[\text{mmol}(\text{H}^+) \cdot \text{g}^{-1}] = 1.01$) (Figure 3).

Sulfonic acid-functionalized ILs, which have similar non-swelling properties, have also been explored by Wang et al. to obtain better EL yields (Wang et al., 2014). A comparison of sulfonic acid and non-sulfonic acid-functionalized IL catalysts bearing HSO_4^- anions was carried out. Using 3-butyl-1-methyl-1H-imidazole-3-ium [BMIm] as the cation gave a low EL yield (~34%) at 120°C , while replacing [BMIm] with BMIm-SH



produces a significantly greater yield of EL (92%) under the same reaction conditions (Wang et al., 2014). The higher yield of EL obtained using the sulfonic acid functionalized IL was ascribed to the higher acid intensity. The acid intensities of BMIm-SH and BMIm IL were 1.2 and 2.5, respectively when measured using the Hammett acidity, which was comparable to conventional acids (i.e., H_2SO_4) (Liu et al., 2008). Subsequently, the results indicated that the cationic sulfonic group facilitates proton transfer and the protonation of FAL, which then enhances the yield of the target product (Li et al., 2015a,b). Similar tendencies were verified by Hengne et al. who showed that the EL yield obtained over a non-sulfonic IL (1-methylimidazolium [MIm]) was lower (65%) than that obtained using a sulfonic acid-functionalized IL (95%) (Hengne et al., 2013).

Possessing both Brønsted and Lewis acidity, metal salts have been investigated in the acid-catalyzed transformation of biomass-derived oxygenates (Loerbroks et al., 2014). During the reaction, the Lewis acid active site coordinates with the oxygen atom in FAL, which was verified by the stability of the as-formed complex and further decreased the activation barrier (Pidko et al., 2010). To confirm the effect of the Lewis acidity, Peng et al. researched various aluminum salts (AlCl_3 , $\text{Al}_2(\text{SO}_4)_3$, $\text{Al}(\text{NO}_3)_3$, and $\text{Al}(\text{C}_6\text{H}_5\text{SO}_3)_3$) as catalysts for the FAL-EL conversion reaction. A maximum EL yield of 74% was obtained using AlCl_3 as a catalyst at 110°C for 3 h. This was attributed to the weaker Brønsted acidity of AlCl_3 ($\text{pH} = 0.89$) compared to $\text{Al}(\text{OTf})_3$, which shows greater Brønsted acidity ($\text{pH} = 0.12$) (Peng et al., 2015). The EL yield obtained using AlCl_3 was maintained over six successive runs of the reaction, demonstrating its high stability, which fulfills the requirements of its future commercialization (Peng et al., 2015). For comparison, Khusnutdinov et al. obtained a higher EL yield (95%) under milder reaction conditions (70°C) using iron(III) acetylacetonate (Khusnutdinov et al., 2007).

Heterogeneous acidic catalysts, such as zeolites, have been recently studied for the ethanolysis of FAL used to produce EL. An excellent catalytic performance has been demonstrated using hierarchical HZ-5 and HZSM-5, which give EL yields up to 73.0 and 85.8%, respectively at $100\text{--}120^\circ\text{C}$ (Zhu et al., 2014; Nandiwale et al., 2015). Nandiwale et al. were interested in the preparation of zeolite materials upon adjusting the Si/Al ratio (SAR) and further explored the effect of their Brønsted acidity on the EL yield (Nandiwale et al., 2015). A significant achievement was reported using the zeolite prepared with a SAR of 30.15 exhibiting the strongest Brønsted acidity ($\sim 0.73 \text{ mmol}\cdot\text{g}^{-1}$), which gave the maximum EL yield when compared to the other zeolites studied. Based on the published findings, the overall yield of EL obtained over the zeolite catalysts was affected by the formation of DEE, which leads to a serious loss of ethanol. These limitations can be overcome by modifying the textural properties of the zeolite materials. Antunes et al. have prepared and perfected a series of zeolite catalysts by introducing three different procedures to change the textural properties of the catalyst (Antunes et al., 2015, 2016). By introducing an organic template, Al-TUD-1 generated a smaller pore size distribution to increase the accessibility of the acidic sites to FAL, which produced a higher EL yield. Beta/TuD-1 was prepared with a reduced crystallite size and ITQ-2 was synthesized via the

delamination of MCM-22 (Lima et al., 2010a,b; Antunes et al., 2012; Neves et al., 2013). Among the three catalysts studied, Al-TUD-1 exhibited a SAR of 21 and an acidity density of $197 \mu\text{mol}\cdot\text{g}^{-1}$ and provided a significant yield of EL (80% over 24 h with negligible DEE formed) at 140°C (Neves et al., 2013). The delamination of MCM-22 was similar to Al-TUD-1, which opened the pore structure to provide increased accessibility to FAL (Corma et al., 1998). The surface area and the total acidity of the ITQ-2 catalyst were enhanced two- and 1.5-fold, respectively when compared to MCM-22. The results were in accordance with those reported by Katz et al. using layered zeolite and the delamination procedure was shown to be responsible for the enhancement in the acidity and surface area (Ogino et al., 2013). As a consequence, a significant enhancement in the EL yield (60%) was obtained using ITQ-2 when compared to MCM-22 (47%) at 140°C over 24 h (Neves et al., 2013).

Based on the above analysis, modified mesoporous aluminosilicates materials with high surface areas and appropriate pore sizes guaranteed the accessibility of the active sites for the reactants, which significantly improves the yield of EL. However, the production of undesired by-products containing aromatic compounds, cyclic hydrocarbons, and lactic acid poly-condensation compounds need to be inhibited to enhance the yield of EL (Dusselier et al., 2015).

Zhu et al. have also studied functionalized graphene oxide (GO) as an acid catalyst for the conversion of FAL into EL. The results showed that lamellar-structured nano-GO is beneficial for the accessibility of the reactants. Under the optimal reaction conditions (120°C), a high EL yield of up to 95.5% was obtained when compared to the other catalysts studied (modified zeolites, HPAs, and sulfonic acid functionalized catalysts; Zhu et al., 2014). The strong hydrogen bonding interactions formed by the synergistic effect observed between the various acid sites including sulfonic acid groups and carboxyl/hydroxyl functionalities are responsible for the excellent performance of the GO catalyst. The carboxyl/hydroxyl groups in GO have a strong affinity toward the hydroxyl group in FAL, which provides unprecedented adsorption and favors the accessibility of the active acid sites for the reactants (Zhu et al., 2015). In regard to the Brønsted acidity, the sulfonic acid density of GO is lower than H_2SO_4 and *p*-TSA, however, the higher yield of EL obtained using GO can be attributed to the crucial role played by this synergistic effect.

In addition to the catalytic performance, the recyclability of the catalyst is also a significant factor for its industrial applications. For instance, DH-ZSM-5 is reusable over five continuous runs without any significant loss in its activity. After the sixth run, the conversion of FAL decreased from 95 to 93%, demonstrating that the recycling of DH-ZSM-5 was feasible (Nandiwale et al., 2014). On the contrary, the sulfonated carbon catalyst (AC-Fe-SO₃H) reported by Zhang and Chen, for which the yield of EL decreased from 58 to 46% after three runs, showed insufficient stability for industrial application (Zhang and Chen, 2016). Similarly, the EL yield decreased from 45 to 36% over six runs using USY zeolite (Chang et al., 2015). Further exploration is needed to achieve stable, convenient, and excellent catalytic performance during the conversion of FAL into EL.

CMF as a Feedstock

Besides the existing substrates, researchers have devoted great efforts toward developing the synthesis of EL from low-cost and novel starting materials, such as CMF (Li H. et al., 2014). For example, Breeden et al. have developed the synthesis of CMF (>70% yield) from HMF, glucose, and inulin at 80°C over 15 min (Breeden et al., 2013). Mascal et al. successfully obtained high EL yields up to 84.7% from CMF at 160°C over 30 min (Mascal and Nikitin, 2010a). The investigators confirmed the feasibility of a one-pot process to produce EL directly from biomass, even seed oil, using CMF as an intermediate (Mascal and Nikitin, 2010a). At room temperature, the obtained CMF intermediate remained stable in high yield (Mascal and Nikitin, 2010a), while at elevated temperature (>100°C), the ethanolysis reaction proceeds to convert the CMF intermediate into EL via TEP during the FAL ethanolysis process.

Saccharides as a Feedstock

With respect to the starting material, EL can be directly prepared from saccharides, such as carbohydrates, sucrose, glucose, or fructose *via* a one-pot process using an acid catalyst and alcohol as the reaction media. The one-pot process generates multiple by-products, which result in a low EL yield (Liu et al., 2011; Peng et al., 2011). Fructose has been reported to display excellent activity over multiple acid catalysts when compared to other monosaccharides (glucose and mannose).

Similar to the FAL conversion reaction, sulfonic acid functionalized ILS bearing [BMIm-SO₃H] and [NEt₃B-SO₃H] cations have been developed to generate a comparable yield of EL ranging from 67 to 77% starting from fructose (Saravanamurugan et al., 2011). The difference observed in the EL yield was attributed to the acid intensity of the anions ([OMS][−], [HSO₄][−], and [NTf₂][−]). Owing to the uniform structure of SBA-15 bearing sulfonic acid functionalities, its high Brønsted acid density (731 μmol·g^{−1}) and surface area (819 m²·g^{−1}) provide EL in 70% yield under the optimum reaction conditions (140°C over 24 h) (Saravanamurugan and Riisager, 2012). Similarly, Liu et al. have introduced a sulfonic acid functionalized Amberlyst-15 catalyst for the preparation of EL in ~73% yield (Liu et al., 2013). To explore the effect of the acid density on the formation of EL, a series of sulfonated mesoporous carbon catalysts were synthesized with decreasing acid site density (5.67, 4.26, 2.89, and 1.75 mmol·g^{−1}). A declining trend in the EL yield (84, 69, 60, and 45%) was observed in the presence of the sulfonated mesoporous carbon structures (Liu et al., 2013).

The observed results indicate that the EL yield increases upon increasing the reaction time and temperature. For instance, the EL yield was improved to 37% when the reaction was conducted at a higher temperature (140°C) when compared to 130°C in the study reported by Zhu and coworkers (Wang et al., 2013). Furthermore, the utilization of a metal promoter on HPA can also afford a better EL yield. The results achieved by Zhao et al. showed that doping HPA with monovalent potassium cations (K⁺) leads to an increase in the acidity and higher EL yield (64.6%), which was further improved to 68.7% because of the use of toluene and heating at 150°C (Zhao et al., 2015).

Li et al. developed a fructose-EL conversion reaction catalyzed by HY zeolites with a SAR of 2.6 at 230°C, which achieved a 52% yield of EL (Li et al., 2016). The results were in contrast with the better EL yield (>80%) obtained at a lower temperature (<130°C) using LA and FAL as starting materials using similar zeolite-based catalysts. The reason for the lower yield can be attributed to the microporous structure of the Y-zeolite, in which the undesired 5-ethoxymethylfurfural (EMF) intermediate was formed and affected the rehydration step (Saravanamurugan and Riisager, 2012). Interestingly, H-USY zeolite has a superior BET surface area (732 m²·g^{−1}) and acid density (1383 μmol·g^{−1}), which exhibits better textural properties, to give a higher EL yield (~52%) at 160°C when compared to the weaker zeolite (699 m²·g^{−1}, 874 μmol·g^{−1}, EL yield ~40%) (Saravanamurugan and Riisager, 2012, 2013; Li et al., 2016). Thus, the structural characteristics including the pore structure, surface area, and acid site density are significant toward obtaining higher EL yields over zeolite materials, which indicates that the microporous structure of zeolite catalysts may suppress the complete conversion of fructose into the key intermediates of the reaction.

When compared with fructose, the alcoholysis of glucose to prepare ALs has been demonstrated to be difficult. The experimental results confirm that the EL yield can be significantly decreased (<13%) utilizing the same IL catalysts ([BMIm-SO₃H] and [NEt₃B-SO₃H]) when the substrate was changed from fructose to glucose under identical reaction conditions (Saravanamurugan et al., 2011). The low EL yield derived from glucose was attributed to the formation of ethyl-D-glucopyranoside (EDGP) in the presence of a Brønsted acid (Li et al., 2015c). Similar to the isomerization of glucose in fructose, EDGP isomerization to ethyl-D-fructofuranoside (EDFF) is catalyzed by a Lewis acid (Morales et al., 2014). Generally, the isomerization of EDGP into EDFF is difficult and is considered to be a rate-limiting step (Li et al., 2015c). Therefore, the combination of both Brønsted and Lewis acid sites determines the successful conversion of glucose into EL (Zhao et al., 2015). Similar to the results obtained using ILS, several other catalysts have been investigated for the glucose alcoholysis reaction, which gave low yields of the target ALs. Interestingly, HPA acts as a catalyst over a shorter reaction time (120 min) to achieve an equal yield of EL (Yang et al., 2012; Wang et al., 2013), which was attributed to the existence of both Lewis and Brønsted acid sites and the appropriate Brønsted to Lewis acid site ratio (B/L >58) (Tao et al., 2015).

Zeolites possessing both moderate Brønsted and Lewis acidity have been explored by Xu et al. in the glucose ethanolysis reaction used toward the production of EL (Xu et al., 2013). An optimum EL yield of 40% was afforded at 180°C for over 30 min using USY zeolite starting from glucose. The moderate B/L ratio (~3.7) of the USY zeolite was responsible for the good EL yield (West et al., 2010; Otomo et al., 2015). When further mineral acid (H₂SO₄) was added to the USY zeolite, a higher EL yield of 51.4% was achieved over 120 min because of the increased B/L ratio (Chang et al., 2015).

The amount of Brønsted acid in the catalyst plays an important role during the ethanolysis of glucose and fructose, giving different EL yields. This has been demonstrated during

the ethanolysis of disaccharides, such as sucrose. For instance, in the presence of sulfonic acid functionalized ILs, the EL yield achieved after 24 h via ethanolysis of sucrose was 43% at 140°C (Saravanamurugan and Riisager, 2012). This result was attributed to the molecular components in sucrose, which includes one molecule of glucose and one molecule of fructose. The EL yield (~43%) obtained from sucrose was higher than that from glucose (<13%) and lower than that from fructose (>70%). This indicates that the glucose molecule in sucrose produces EDGP, which is the rate-limiting step and difficult to isomerize, while the fructose molecule is easily converted into EDFF, which may undergo subsequent reactions to form EMF and EL. In accordance with this conclusion, Chen et al. published a similar EL synthesis (~45%) using Brønsted acidic IL-based HPAs [3.2H]₃(PW₁₂O₄₀)₂ (IL POM) to convert sucrose into EL (Chen et al., 2014). Generally, in the presence of only a Brønsted acid, the fructose molecule in sucrose can be converted into EL without the transformation of glucose. For example, sulfonated SBA-15 has been applied as a catalyst and the yield of EL from sucrose decreased (~35%) when compared to that obtained from fructose (Saravanamurugan and Riisager, 2012). However, in the presence of both Brønsted and Lewis acid sites, two molecules of sucrose can simultaneously undergo ethanolysis to form EL (Li et al., 2016). Different from sucrose, maltose contains two units of glucose, whose properties are similar to glucose. Therefore, the reactivity of maltose is similar to glucose, providing a better yield of EL when using the catalyst with an optimum ratio of Brønsted and Lewis acidity. The experimental exploration concluded by Hu et al. using maltose confirmed the above-mentioned hypothesis that a lower yield of EL (20%) is obtained in the presence of Amberlyst-70 when compared with the EL yield (47%) observed using H-USY (Hu et al., 2013; Saravanamurugan and Riisager, 2013).

Saravanamurugan et al. have studied polysaccharides constructed from fructose monomers, such as inulin, which provide excellent EL yields. The production of EL was found to conform to the same tendency as the Brønsted acidity of the catalyst used. For instance, high EL yields of up to 39.0, 52.3, and 67.0% have been obtained over H-USY zeolite, HPA, and IL functionalized polyoxometalate salts (IL-POM), respectively (Saravanamurugan and Riisager, 2013; Chen et al., 2014; Zhao et al., 2015). The Brønsted acidity followed the order of H-USY < HPA < IL-POM. Considering that cellulose is a glucose-based polysaccharide, the ethanolysis reaction was different under mild conditions for the production of EDGP and EL. Thus, the ethanolysis of cellulose conducted at temperatures >170°C can offer an appreciable EL yield. Deng et al. reported an EL yield of 27% via the ethanolysis of cellulose using HPA (H₄SiW₁₂O₄₀) at 205°C over 30 min (Deng et al., 2011). However, multiple undesired by-products which formed via polymerization may affect the overall EL selectivity, which was responsible for the low EL yield gained during cellulose ethanolysis using metal-doped HPA as a catalyst at an elevated temperature of 220°C (Zhao et al., 2015). Consequently, Amarasekara et al. introduced ethanol and water as the solvent medium for the

ethanolysis of cellulose using an IL (1-(1-propylsulfonic)-3-methylimidazolium chloride) as a catalyst. The existence of water favored the isomerization of glucose into fructose and avoided the formation of EDGP, resulting in a high yield of EL (38.5%) (Amarasekara and Wiredu, 2014).

Le Van Mao et al. have developed two different approaches for the one-pot conversion of lignocellulosic biomass into EL catalyzed by an acid catalyst (Le Van Mao et al., 2011). The first method showed that biomass can be directly converted into EL in ethanol under acidic catalysis, while the second method proposed that biomass was first hydrolyzed to produce a complex mixture, which then undergoes the ethanolysis reaction. Both approaches used woody biomass or grass and were conducted in a high-pressure batch reactor in the presence of sulfuric acid at 190°C for 2 h. The best yield was 16.6 wt.%.

Chang et al. have investigated the direct conversion of wheat straw in one-pot to produce EL using H₂SO₄ as a catalyst (Chang et al., 2012). Under the optimal reaction conditions, a maximum EL yield of 17.9 wt.% was observed from wheat straw. No significant increase in the EL yield was obtained upon increasing the sulfuric acid loading (Chang et al., 2015).

CONCLUSIONS AND PERSPECTIVES

This review summarizes the trends observed for the yields obtained for ALs from various starting materials including LA, FAL, CMF, monosaccharides, disaccharides, polysaccharides, and biomass residues using acid catalysts in the alcoholysis reaction. The esterification reaction used to produce EL mainly depends on the acid intensity, acid site density, and accessibility of the acid sites. The conversion of FAL depends on the intermediates obtained during the reaction. Glucose is difficult to react when compared to fructose, which avoids the isomerization step. An appropriate combination of Lewis and Brønsted acidity is needed for the transformation of glucose-based saccharides.

We can conclude that efficient catalytic procedures for the one-pot conversion of biomass directly into ALs and the separation and purification of ALs are urgently needed. Due to the complex structure of biomass and multifunctional active sites in the catalyst, green and sustainable process are highly desirable. As an alternative reaction approach, microwave irradiation has exhibited significant potential for reaction time reduction with fewer undesired products. The extensive exploration of microwave reactions for the transformation from lab scale to the industry scale to the synthesis of ALs needs to be studied further.

AUTHOR CONTRIBUTIONS

XL performed critical reviews and wrote the manuscript. CL and HW designed the structure of the manuscript and is responsible for the work. WY and QZ assisted XL in preparing and completing the review. All authors discussed the results, wrote, and commented on the manuscript.

FUNDING

This work was financially supported by the National Natural Science Foundation of China (22065004), Basic Research Program of Guizhou Province [(2019)1009], the Guizhou Provincial Key Laboratory for Rare Animal and Economic Insects of the Mountainous Region

REFERENCES

- Alloaoua, I., Goi, B. E., Obadia, M. M., Debuigne, A., and Detrembleur, C. (2014). (Co) Polymerization of vinyl levulinate by cobalt-mediated radical polymerization and functionalization by ketoxime click chemistry. *Polym. Chem.* 5, 2923–2929. doi: 10.1039/c3py01505j
- Alsalmé, A. M., Wiper, P. V., Khimyak, Y. Z., Kozhevnikova, E. F., and Kozhevnikov, I. V. (2010). Solid acid catalysts based on $H_3PW_{12}O_{40}$ heteropoly acid: acid and catalytic properties at a gas-solid interface. *J. Catal.* 276, 181–189. doi: 10.1016/j.jcat.2010.09.014
- Amarasekara, A. S., and Wierdu, B. (2014). Acidic ionic liquid catalyzed one-pot conversion of cellulose to ethyl levulinate and levulinic acid in ethanol-water solvent system. *BioEnergy Res.* 7, 1237–1243. doi: 10.1007/s12155-014-9459-z
- Antunes, M. M., Lima, S., Fernandes, A., Pillinger, M., Ribeiro, M. F., and Valente, A. A. (2012). Aqueous-phase dehydration of xylose to furfural in the presence of MCM-22 and ITQ-2 solid acid catalysts. *Appl. Catal. A* 417–418, 243–252. doi: 10.1016/j.apcata.2011.12.046
- Antunes, M. M., Lima, S., Neves, P., Magalhães, A. L., Fazio, E., Fernandes, A., et al. (2015). One-pot conversion of furfural to useful bio-products in the presence of a Sn,Al-containing zeolite beta catalyst prepared via post-synthesis routes. *J. Catal.* 329, 522–537. doi: 10.1016/j.jcat.2015.05.022
- Antunes, M. M., Lima, S., Neves, P., Magalhães, A. L., Fazio, E., Neri, F., et al. (2016). Integrated reduction and acid-catalysed conversion of furfural in alcohol medium using Zr, Al-containing ordered micro/mesoporous silicates. *Appl. Catal. B* 182, 485–503. doi: 10.1016/j.apcatb.2015.09.053
- Badgujar, K. C., and Bhanage, B. M. (2015). Factors governing dissolution process of lignocellulosic biomass in ionic liquid: current status, overview and challenges. *Bioresour. Technol.* 178, 2–18. doi: 10.1016/j.biortech.2014.09.138
- Badgujar, K. C., and Bhanage, B. M. (2018). *Dedicated and Waste Feedstocks for Biorefinery: An Approach to Develop a Sustainable Society in Waste Biorefinery Potential and Perspective* (India: Waste Biorefinery). ISBN: 978-0-444-63992-9.
- Baronetti, G., Briand, L., Sedran, U., and Thomas, H. (1998). Heteropolyacid-based catalysis. Dawson acid for MTBE synthesis in gas phase. *Appl. Catal.* 172, 265–272. doi: 10.1016/S0926-860X(98)00134-3
- Bloom, P. (2007). Levulinic acid ester derivatives as reactive plasticizers and coalescent solvents. *Patent WO2007094922A2*.
- Breiden, S. W., Clark, J. H., Farmer, T. J., Macquarrie, D. J., Meimoun, J. S., Nonne, Y., et al. (2013). Microwave heating for rapid conversion of sugars and polysaccharides to 5-chloromethyl furfural. *Green Chem.* 15, 72–75. doi: 10.1039/C2GC36290B
- Briand, L. E., Baronetti, G. T., and Thomas, H. J. (2003). The state of the art on Wells-Dawson heteropoly-compounds A review of their properties and applications. *Appl. Catal., A* 256, 37–50. doi: 10.1016/S0926-860X(03)00387-9
- Chang, C., Xu, G., and Jiang, X. (2012). Production of ethyl levulinate by direct conversion of wheat straw in ethanol media. *Bioresour. Technol.* 121, 93–99. doi: 10.1016/j.biortech.2012.06.105
- Chang, C., Xu, G., Zhu, W., Bai, J., and Fang, S. (2015). One-pot production of a liquid biofuel candidate—ethyl levulinate from glucose and furfural residues using a combination of extremely low sulfuric acid and zeolite USY. *Fuel* 140, 365–370. doi: 10.1016/j.fuel.2014.09.102
- Chen, J., Zhao, G., and Chen, L. (2014). Efficient production of 5-hydroxymethylfurfural and alkyl levulinate from biomass carbohydrate using ionic liquid-based polyoxometalate salts. *RSC Adv.* 4, 4194–4202. doi: 10.1039/C3RA45632C
- Chermahini, A. N., and Nazeri, M. (2017). Esterification of the levulinic acid with *n*-butyl and isobutyl alcohols over aluminum-containing [(2018)5102], the Scientific Research Platform For Qian Ke He [(2017)5725], the Joint Science and Technology Funds of the Youth Growth S&T Personnel Foundation of Guizhou Education Department [No. KY (2018)292], and the Discipline and Master's Site Construction Project of Guiyang University by Guiyang City Financial Support Guiyang University (SH-2020).
- MCM-41. *Fuel Process. Technol.* 167, 442–450. doi: 10.1016/j.fuproc.2017.07.034
- Chia, M., Haider, M. A., Pollock, G., Kraus, G. A., Neurock, M., and Dumesic, J. A. (2013). Mechanistic insights into ring-opening and decarboxylation of 2-pyrones in liquid water and tetrahydrofuran. *J. Am. Chem. Soc.* 135, 5699–5708. doi: 10.1021/ja312075r
- Christensen, E., Williams, A., Paul, S., Burton, S., and McCormick, R. L. (2011). Properties and performance of levulinate esters as diesel blend components. *Energ. Fuels* 25, 5422–5428. doi: 10.1021/ef201229j
- Cirujano, F. G., Corma, A., and Llabrés i Xamena, F. X. (2015). Conversion of levulinic acid into chemicals: Synthesis of biomass derived levulinate esters over Zr-containing MOFs. *Chem. Eng. Sci.* 124, 52–60. doi: 10.1016/j.ces.2014.09.047
- Corma, A., Fornes, V., Pergher, S. B., Maesen, T. L. M., and Buglass, J. G. (1998). Delaminated zeolite precursors as selective acidic catalysts. *Nature* 396, 353–356. doi: 10.1038/24592
- Cousinet, S. (2014). Biobased vinyl levulinate as styrene replacement for unsaturated polyester resin. *Polym. Chem.* 52, 3356–3364. doi: 10.1002/pola.27397
- Dave, C. D., and Pant, K. K. (2011). Glycerol conversion in the experimental study of catalytic hydrolysis of triglycerides for fatty acids production using Ni or Pd on Al_2O_3 or SiO_2 . *Renew. Energ.* 36, 3195–3202. doi: 10.1016/j.renene.2013.11.006
- Démolis, A., Essayem, N., and Rataboul, F. (2014). Synthesis and applications of alkyl levulinates. *ACS Sustain. Chem. Eng.* 2, 1338–1352. doi: 10.1021/sc500082n
- Deng, W., Liu, M., Zhang, Q., and Wang, Y. (2011). Direct transformation of cellulose into methyl and ethyl glucosides in methanol and ethanol media catalyzed by heteropolyacids. *Catal. Today* 164, 461–466. doi: 10.1016/j.cattod.2010.10.055
- Desideri, L., Yusubov, M. S., Zhuikov, S., and Verpoort, F. (2018). Fully-sulfonated hydrated UiO66 as efficient catalyst for ethyl levulinate production by esterification. *Catal. Commun.* 117, 33–37. doi: 10.1016/j.catcom.2018.08.020
- Dharne, S., and Bokade, V. V. (2011). Esterification of levulinic acid to *n*-butyl levulinate over heteropolyacid supported on acid-treated clay. *J. Nat. Gas Chem.* 20, 18–24. doi: 10.1016/S1003-9953(10)60147-8
- Dhyani, V., and Bhaskar, T. (2018). A comprehensive review on the pyrolysis of lignocellulosic biomass. *Renew. Energy* 129, 695–716. doi: 10.1016/j.renene.2017.04.035
- Dusselier, M., Van Wouwe, P., and Dewaele, A. (2015). Shape-selective zeolite catalysis for bioplastics production. *Science* 349, 78–80. doi: 10.1126/science.aaa7169
- Enumula, S. S., Gurram, V. R. B., Chada, R. R., Burri, D. R., and Kamaraju, S. R. R. (2017). Clean synthesis of alkyl levulinates from levulinic acid over one pot Synthesized WO_3 -SBA-16 catalyst. *J. Mol. Catal. A Chem.* 426, 30–38. doi: 10.1016/j.molcata.2016.10.032
- Fernandes, D. R., Rocha, A. S., Mai, E. F., Mota, C. J. A., and Teixeira Da Silva, V. (2012). Levulinic acid esterification with ethanol to ethyl levulinate production over solid acid catalysts. *Appl. Catal. A* 425–426, 199–204. doi: 10.1016/j.apcata.2012.03.020
- Fiorentino, G., Ripa, M., Mellino, S., Fahd, S., and Ulgiati, S. (2014). Life cycle assessment of *Brassica carinata* biomass conversion to bioenergy and platform chemicals. *J. Cleaner Prod.* 66, 174–187. doi: 10.1016/j.jclepro.2013.11.043
- González Maldonado, G. M., Assary, R. S., Dumesic, J. A., and Curtiss, L. A. (2012). Acid-catalyzed conversion of furfuryl alcohol to ethyl levulinate in liquid ethanol. *Energ. Environ. Sci.* 5, 8990–8997. doi: 10.1039/c2ee22486k

- Guo, H. X., Hirrosaki, Y., Qi, X. H., and Smith, R. L. (2020). Synthesis of ethyl levulinate over amino-sulfonated functional carbon materials. *Renew. Energ.* 157, 951–958. doi: 10.1016/j.renene.2020.05.103
- Gupta, P., and Paul, S. (2014). Solid acids: green alternatives for acid catalysis. *Catal. Today* 236, 153–170. doi: 10.1016/j.cattod.2014.04.010
- Gupta, S., Arora, R., Sinha, N., Alam, M. I., and Haider, M. A. (2016). Mechanistic insights into the ring-opening of biomass derived lactones. *RSC Adv.* 6, 12932–12942. doi: 10.1039/C5RA22832H
- Hengne, A. M., Kamble, S. B., and Rode, C. V. (2013). Single pot conversion of furfuryl alcohol to levulinic esters and γ -valerolactone in the presence of sulfonic acid functionalized ILs and metal catalysts. *Green Chem.* 15, 2540–2547. doi: 10.1039/c3gc41098f
- Hu, L., Lin, L., Wu, Z., Zhou, S. Y., and Liu, S. J. (2015). Chemocatalytic hydrolysis of cellulose into glucose over solid acid catalysts. *Appl. Catal. B Environ.* 174–175, 225–243. doi: 10.1016/j.apcatb.2015.03.003
- Hu, X., Wu, L., Wang, Y., Song, Y., Mourant, D., Gunawan, R., et al. (2013). Acid-catalyzed conversion of mono- and poly-sugars into platform chemicals: effects of molecular structure of sugar substrate. *Bioresour. Technol.* 133, 469–474. doi: 10.1016/j.biortech.2013.01.080
- Huang, Y., Yang, T., Zhou, M., and Fu, Y. (2016). Microwave-assisted alcoholysis of furfural alcohol into alkyl levulinates catalyzed by metal salts. *Green Chem.* 18, 1516–1523. doi: 10.1039/C5GC01581B
- Janik, M. J., Davis, R. J., and Neurock, M. (2005). Anhydrous and water-assisted proton mobility in phosphotungstic acid. *J. Am. Chem. Soc.* 127, 5238–5245. doi: 10.1021/ja042742o
- Khusnutdinov, R. I., Baiguzina, A. R., Smirnov, A. A., Mukminov, R. R., and Dzhemilev, U. M. (2007). Furfuryl alcohol in synthesis of levulinic acid esters and difurylmethane with Fe and Rh complexes. *Russ. J. Appl. Chem.* 80, 1687–1690. doi: 10.1134/S1070427207100163
- Kokare, M. B., Rajani, V., and Mathpati, C. S. (2018). Response surface optimization, kinetic study and process design of n-butyl levulinate synthesis. *Chem. Eng. Res. Des.* 137, 577–588.
- Kuwahara, Y., Fujitani, T., and Yamashita, H. (2013). Esterification of levulinic acid with ethanol over sulfated mesoporous zirconosilicates: influences of the preparation conditions on the structural properties and catalytic performances. *Catal. Today* 237, 18–28. doi: 10.1016/j.cattod.2013.11.008
- Kuwahara, Y., Kaburagi, W., Nemoto, K., and Fujitani, T. (2014). Esterification of levulinic acid with ethanol over sulfated Si-doped ZrO₂ solid acid catalyst: study of the structure-activity relationships. *Appl. Catal. A* 476, 186–196. doi: 10.1016/j.apcata.2014.02.032
- Lange, J., Van De Graaf, W. D., and Haan, R. J. (2009). Conversion of furfuryl alcohol into ethyl levulinate using solid acid catalysts. *ChemSusChem* 2, 437–441. doi: 10.1002/cssc.200800216
- Le Van Mao, R., Zhao, Q., Dima, G., and Petraccone, D. (2011). New process for the acid-catalyzed conversion of cellulosic biomass (AC₃B) into alkyl levulinates and other esters using a unique one-pot system of reaction and product extraction. *Catal. Lett.* 141, 271–276. doi: 10.1007/s10562-010-0493-y
- Li, H., Bhadury, P. S., Riisager, A., and Yang, S. (2014). One-pot transformation of polysaccharides via multi-catalytic processes. *Catal. Sci. Technol.* 4, 4138–4168. doi: 10.1039/C4CY00711E
- Li, H., Fang, Z., and Yang, S. (2016). Direct conversion of sugars and ethyl levulinate into γ -valerolactone with superparamagnetic acid-base bifunctional ZrFeO_x nanocatalysts. *ACS Sustainable Chem. Eng.* 4, 236–246. doi: 10.1021/acssuschemeng.5b01480
- Li, H., Saravanamurugan, S., Yang, S., and Riisager, A. (2015a). Direct transformation of carbohydrates to the biofuel 5-ethoxymethylfurfural by solid acid catalysts. *Green Chem.* 18, 726–734. doi: 10.1039/C5GC01043H
- Li, J., Li, J., Zhang, D., and Liu, C. (2015b). Theoretical Elucidation of Glucose Dehydration to 5-Hydroxymethylfurfural Catalyzed by a SO₃H-Functionalized Ionic Liquid. *J. Phys. Chem. B* 119, 13398–13406. doi: 10.1021/acs.jpcc.5b07773
- Li, J., Li, J., Zhang, D., and Liu, C. (2015c). Theoretical explanation for how SO₃H-functionalized ionic liquids promote the conversion of cellulose to glucose. *ChemPhysChem* 16, 3044–3048. doi: 10.1002/cphc.201500424
- Li, Z., Liu, Y., Kwapinski, W., and Leahy, J. J. (2014). ZrO₂-modified TiO₂ nanorod composite: hydrothermal synthesis, characterization and application in esterification of organic acid. *Mater. Chem. Phys.* 145, 82–89. doi: 10.1016/j.matchemphys.2014.01.037
- Li, Z., Wnetrzak, R., Kwapinski, W., and Leahy, J. J. (2012). Synthesis and characterization of sulfated TiO₂ nanorods and ZrO₂/TiO₂ nanocomposites for the esterification of biobased organic acid. *ACS Appl. Mater. Interfaces* 4, 4499–4505. doi: 10.1021/am300510u
- Lima, S., Antunes, M. M., Fernandes, A., Pillinger, M., Ribeiro, M. F., and Valente, A. A. (2010a). Catalytic cyclodehydration of xylose to furfural in the presence of zeolite H-Beta and a micro/mesoporous Beta/TUD-1 composite material. *Appl. Catal. A* 388, 141–148. doi: 10.1016/j.apcata.2010.08.040
- Lima, S., Antunes, M. M., Fernandes, A., Pillinger, M., Ribeiro, M. F., and Valente, A. A. (2010b). Acid-Catalysed Conversion of Saccharides into Furanic Aldehydes in the Presence of Three-Dimensional Mesoporous Al-TUD-1. *Molecules* 15, 3863–3877. doi: 10.3390/molecules15063863
- Liu, G., Wu, J., Zhang, I. Y., Chen, Z., Li, Y., and Xu, X. (2011). Theoretical studies on thermochemistry for conversion of 5-chloromethylfurfural into valuable. *J. Phys. Chem. A* 115, 13628–13641. doi: 10.1021/jp207641g
- Liu, R., Chen, J., Huang, X., Chen, L., Ma, L., and Li, X. (2013). Conversion of fructose into 5-hydroxymethylfurfural and alkyl levulinates catalyzed by sulfonic acid-functionalized carbon materials. *Green Chem.* 15, 2895–2903. doi: 10.1039/c3gc41139g
- Liu, X., Zhou, J., Guo, X., Liu, M., Ma, X., Song, C., et al. (2008). SO₃H-functionalized ionic liquids for selective alkylation of *p*-cresol with tert-butanol. *Ind. Eng. Chem.* 47, 5298–5303. doi: 10.1021/ie070647t
- Liu, X. F., Li, H., Zhang, H., Eng., Pan, H., Huang, S., Yang, K. L., et al. (2016). Efficient conversion of furfuryl alcohol to ethyl levulinate with sulfonic acid-functionalized MIL-101(Cr). *RSC Adv.* 6, 90232–90238. doi: 10.1039/C6RA19116A
- Loerbroeks, C., van Rijn, J., Ruby, M. P., Tong, Q., Schuth, F., and Thiel, W. (2014). Reactivity of metal catalysts in glucose-fructose conversion. *Chemistry* 20, 12298–12309. doi: 10.1002/chem.201402437
- Lomba, L., Giner, B., Bandres, I., Lafuente, C., and Pino, M. R. (2011). Physicochemical properties of green solvents derived from biomass. *Green Chem.* 13, 2062–2070. doi: 10.1039/c0gc00853b
- López, X., Carbó, J. J., Bo, C., and Poblet, J. M. (2012). Structure, properties and reactivity of polyoxometalates: a theoretical perspective. *Chem. Soc. Rev.* 41, 7537–7571. doi: 10.1039/c2cs35168d
- Luan, Q. J., Liu, L. J., Gong, S. W., Lu, J., Wang, X., and Lv, D. M. (2018). Clean efficient conversion of renewable levulinic acid to levulinic esters catalyzed by an organic-salt of H₄SiW₁₂O₄₀. *Process Saf. Environ. Prot.* 117, 341–349. doi: 10.1016/j.psep.2018.05.015
- Lucas, N., Gurrall, L., and Athawale, A. (2019). Heteropolyacids supported on mesoporous AISBA-15 as efficient catalysts for esterification of levulinic acid. *J. Porous Mater.* 26, 1335–1343. doi: 10.1007/s10934-019-00734-w
- Macht, J., Janik, M. J., Neurock, M., and Iglesia, E. (2007). Catalytic consequences of composition in polyoxometalate clusters with Keggin structure. *Angew. Chem. Int. Ed.* 46, 7864–7868. doi: 10.1002/anie.200701292
- Macht, J., Janik, M. J., Neurock, M., and Iglesia, E. (2008). Mechanistic consequences of composition in acid catalysis by polyoxometalate Keggin clusters. *J. Am. Chem. Soc.* 130, 10369–10379. doi: 10.1021/ja803114r
- Maggi, R., Shiju, N. R., Santacroce, V., Maestri, G., Bigi, F., and Rothenberg, G. (2016). Silicasupported sulfonic acids as recyclable catalyst for esterification of levulinic acid with stoichiometric amounts of alcohols. *Beilstein J. Org. Chem.* 12, 2173–2180. doi: 10.3762/bjoc.12.207
- Manikandan, K., and Cheralathan, K. K. (2017). Heteropoly acid supported on silicalite-1 possessing intracrystalline nanovoids prepared using biomass—an efficient and recyclable catalyst for esterification of levulinic acid. *Appl. Catal. A Gen.* 547, 237–247. doi: 10.1016/j.apcata.2017.09.007
- Marrocchi, A., and Vaccaro, L. (2017). Efficient catalytic upgrading of levulinic acid into alkyl levulinates by resin-supported acids and flow reactors. *Catalysts* 7, 235–248. doi: 10.3390/catal7080235
- Mascal, M., and Nikitin, E. B. (2010a). Co-processing of carbohydrates and lipids in oil crops to produce a hybrid biodiesel. *Energy Fuels* 24, 2170–2171. doi: 10.1021/ef9013373
- Mascal, M., and Nikitin, E. B. (2010b). High-yield conversion of plant biomass into the key value-added feedstocks 5-(hydroxymethyl)furfural, levulinic acid, and levulinic esters via 5-(chloromethyl)furfural. *Green Chem.* 12, 370–373. doi: 10.1039/B918922J

- Melero, J. A., Morales, G., Iglesias, J., Paniagua, M., Hernández, B., and Penedo, S. (2013). Efficient conversion of levulinic acid into alkyl levulinates catalyzed by sulfonic mesostructured silicas. *Appl. Catal. A* 466, 116–122. doi: 10.1016/j.apcata.2013.06.035
- Mondal, T., Pant, K. K., and Dalai, A. K. (2015). Catalytic oxidative steam reforming of bio-ethanol for hydrogen production over Rh promoted Ni/CeO₂-ZrO₂ catalyst. *Int. J. Hydro. Energy* 40, 2529–2544. doi: 10.1016/j.ijhydene.2014.12.070
- Morales, G., Osatiashtiani, A., Herna, B., Iglesias, J., Melero, J. A., Paniagua, M., et al. (2014). Conformal sulfated zirconia monolayer catalysts for the one-pot synthesis of ethyl levulinate from glucose. *Chem. Commun.* 50, 11742–11745. doi: 10.1039/C4CC04594G
- Mukherjee, A., Dumont, M. J., and Raghavan, V. (2015). Review: sustainable production of hydroxymethylfurfural and levulinic acid: challenges and opportunities. *Biomass Bioenerg.* 72, 143–183. doi: 10.1016/j.biombioe.2014.11.007
- Mullen, B. D., Badarinarayana, V., Hall, E. S., Tjossas, M. J., and Leibig, C. M. (2013). Stabilized levulinic ester ketals. *Patent WO2013055781A1*.
- Nandiwale, K. Y., and Bokade, V. V. (2015). Esterification of renewable levulinic acid to *n*-butyl levulinate over modified H-ZSM-5. *Chem. Eng. Technol.* 38, 246–252. doi: 10.1002/ceat.201400326
- Nandiwale, K. Y., Niphadkar, P. S., Deshpande, S. S., and Bokade, V. V. (2014). Esterification of renewable levulinic acid to ethyl levulinate biodiesel catalyzed by highly active and reusable desilicated H-ZSM-5. *J. Chem. Technol. Biotechnol.* 89, 1507–1515. doi: 10.1002/jctb.4228
- Nandiwale, K. Y., Pande, A. M., and Bokade, V. V. (2015). One step synthesis of ethyl levulinate biofuel by ethanolysis of renewable furfuryl alcohol over hierarchical zeolite catalyst. *RSC Adv.* 5, 79224–79231. doi: 10.1039/C5RA13520F
- Nandiwale, K. Y., Sonar, S. K., Niphadkar, P. S., Joshi, P. N., Deshpande, S. S., Patil, V. S., et al. (2013). *Appl. Catal. A* 460–461, 90–98. doi: 10.1016/j.apcata.2013.04.024
- Narkhede, N., Singh, S., and Patel, A. (2015). Recent progress on supported polyoxometalates for biodiesel synthesis via esterification and transesterification. *Green Chem.* 17, 89–107. doi: 10.1039/C4GC01743A
- Neves, P., Lima, S., Pillinger, M., Rocha, S. M., Rocha, J., and Valente, A. A. (2013). Conversion of furfuryl alcohol to ethyl levulinate using porous aluminosilicate acid catalysts. *Catal. Today* 218–219, 76–84. doi: 10.1016/j.cattod.2013.04.035
- Ogino, I., Eilertsen, E. A., Hwang, S. J., Rea, T., Xie, D., Ouyang, X., et al. (2013). Heteroatom-tolerant delamination of layered zeolite precursor materials. *Chem. Mater.* 25, 1502–1509. doi: 10.1021/cm3032785
- Oliveira, B. L., and Teixeira Da Silva, V. (2014). Synthesis of ethyl levulinate, a perspective biocomponent of motor fuels. *Sci. Net. Catal. Today* 234, 257–263. doi: 10.1016/j.cattod.2013.11.028
- Otomo, R., Yokoi, T., and Tatsumi, T. (2015). OSDA-free zeolite beta with high aluminum content efficiently catalyzes a tandem reaction for conversion of glucose to 5-hydroxymethylfurfural. *ChemCatChem* 7, 4180–4187. doi: 10.1002/cctc.201500837
- Pasquale, G., Vázquez, P., Romanelli, G., and Baronetti, G. (2012). Catalytic upgrading of levulinic acid to ethyl levulinate using reusable silica-included Wells-Dawson heteropolyacid as catalyst. *Catal. Commun.* 18, 115–120. doi: 10.1016/j.catcom.2011.12.004
- Patil, C. R., Niphadkar, P. S., Bokade, V. V., and Joshi, P. N. (2014). Esterification of levulinic acid to ethyl levulinate over bimodal micro-mesoporous H/BEA zeolite derivatives. *Catal. Commun.* 43, 188–191. doi: 10.1016/j.catcom.2013.10.006
- Peng, L., Gao, X., and Chen, K. (2015). Catalytic upgrading of renewable furfuryl alcohol to alkyl levulinates using AlCl₃ as a facile, efficient, and reusable catalyst. *Fuel* 160, 123–131. doi: 10.1016/j.fuel.2015.07.086
- Peng, L., Lin, L., Zhang, J., Shi, J., and Liu, S. (2011). Solid acid catalyzed glucose conversion to ethyl levulinate. *Appl. Catal. A* 397, 259–265. doi: 10.1016/j.apcata.2011.03.008
- Pidko, E. A., Degirmenci, V., Van Santen, R. A., and Hensen, E. J. M. (2010). Glucose activation by transient Cr²⁺ dimers. *Angew. Chem. Int. Ed.* 49, 2530–2534. doi: 10.1002/anie.201000250
- Pileidis, F. D., and Titirici, M. M. (2016). Levulinic acid biorefineries: new challenges for efficient utilization of biomass. *ChemSusChem* 9, 562–582. doi: 10.1002/cssc.201501405
- Rackemann, D. W., Doherty, W. O. S. (2011). The conversion of lignocellulosics to levulinic acid. *Biofuels Bioprod Bioref* 5, 198–214. doi: 10.1002/bbb.267
- Ramli, N. A. S., Amin, N. A. S., and Sivasubramaniam, D. (2017a). Esterification of levulinic acid using ZrO₂-supported phosphotungstic acid catalyst for ethyl levulinate production. *Bioenerg. Res.* 10, 1–12. doi: 10.1007/s12155-017-9872-1
- Ramli, N. A. S., Hisham, N. I., and Amin, A. S. (2018). Esterification of levulinic acid to levulinate esters in the presence of sulfated silica catalyst. *Sains Malays.* 47, 1131–1138. doi: 10.17576/jsm-2018-4706-08
- Ramli, N. A. S., Zaharuddin, N. H., and Amin, N. A. S. (2017b). Esterification of renewable levulinic acid to levulinate ester using Amberlyst 15 as a solid acid catalyst. *J. Teknologi.* 79, 137–142. doi: 10.11113/jt.v79.8095
- Rao, Y., Trudeau, M., and Antonelli, D. (2006). Sulfated and phosphated mesoporous Nb oxide in the benzylation of anisole and toluene by benzyl alcohol. *J. Am. Chem. Soc.* 128, 13996–13997. doi: 10.1021/ja0647147
- Russo, P. A., Antunes, M. M., Neves, P., Wiper, P. V., Fazio, E., Neri, F., et al. (2014a). Mesoporous carbon-silica solid acid catalysts for producing useful bio-products within the sugar-platform of biorefineries. *Green Chem.* 16, 4292–4305. doi: 10.1039/C4GC01037J
- Russo, P. A., Antunes, M. M., Neves, P., Wiper, P. V., Fazio, E., Neri, F., et al. (2014b). Solid acids with SO₃H groups and tunable surface properties: versatile catalysts for biomass conversion. *J. Mater. Chem. A* 2, 11813–11824. doi: 10.1039/C4TA02320J
- Ryder, J. A., Chakraborty, A. K., and Bell, A. T. (2000). Density functional theory study of proton mobility in zeolites: proton migration and hydrogen exchange in ZSM-5. *J. Phys. Chem. B* 104, 6998–7011. doi: 10.1021/jp9943427
- Saravanamurugan, S., and Riisager, A. (2012). Solid acid catalyzed formation of ethyl levulinate and ethyl glucopyranoside from mono- and disaccharides. *Catal. Commun.* 17, 71–75. doi: 10.1016/j.catcom.2011.10.001
- Saravanamurugan, S., and Riisager, A. (2013). Zeolite catalyzed transformation of carbohydrates to alkyl levulinates. *ChemCatChem* 5, 1754–1757. doi: 10.1002/cctc.201300006
- Saravanamurugan, S., Van Buu, O. N., and Riisager, A. (2011). Conversion of mono- and disaccharides to ethyl levulinate and ethyl pyranoside with sulfonic acid-functionalized ionic liquids. *ChemSusChem* 4, 723–726. doi: 10.1002/cssc.201100137
- Song, D., An, S., Lu, B., Guo, Y., and Leng, J. (2015). Arylsulfonic acid functionalized hollow mesoporous carbon spheres for efficient conversion of levulinic acid or furfuryl alcohol to ethyl levulinate. *Appl. Catal., B* 179, 445–457. doi: 10.1016/j.apcatb.2015.05.047
- Su, F., Ma, L., Song, D., Zhang, X., and Guo, Y. (2013a). Design of a highly ordered mesoporous H₃PW₁₂O₄₀/ZrO₂²⁻ Si(Ph)Si hybrid catalyst for methyl levulinate synthesis. *Green Chem.* 15, 885–890. doi: 10.1039/c3gc36912a
- Su, F., Wu, Q., Song, D., Zhang, X., Wang, M., and Guo, Y. (2013b). Pore morphology-controlled preparation of ZrO₂-based hybrid catalysts functionalized by both organosilica moieties and Keggin-type heteropoly acid for the synthesis of levulinate esters. *J. Mater. Chem. A* 1, 13209–13221. doi: 10.1039/c3ta12412f
- Sun, Y., and Cheng, J. (2002). Hydrolysis of lignocellulosic materials for ethanol production: a review. *Bioresour. Technol.* 83, 1–11. doi: 10.1016/S0960-8524(01)00212-7
- Tadele, K., Verma, S., Gonzalez, M. A., and Varma, R. S. (2017). A sustainable approach to empower the bio-based future: upgrading of biomass via process intensification. *Green Chem.* 19, 1624–1627. doi: 10.1039/C6GC03568J
- Tao, M., Xue, L., Sun, Z., Wang, S., Wang, X., and Shi, J. (2015). Tailoring the synergistic bronsted-lewis acidic effects in heteropolyacid catalysts: applied in esterification and transesterification reactions. *Sci. Rep.* 5:13764. doi: 10.1038/srep13764
- Tejero, M. A., Ramírez, E., Fité, C., Tejero, J., and Cunill, F. (2016). Esterification of levulinic acid with butanol over ion exchange resins. *Appl. Catal. A Gen.* 517, 56–66. doi: 10.1016/j.apcata.2016.02.032
- Trombettoni, V., Bianchi, L., Zupanic, A., Porciello, A., Cuomo, M., Piermatti, O., et al. (2018). Response surface optimization, kinetic study and process design of *n*-butyl levulinate synthesis. *Chem. Eng. Res. Des.* 137, 577–588. doi: 10.1016/j.cherd.2018.07.036
- Tsucha, J., and Yoshida, K. (1994). Skin cosmetics containing levulinates, glycyrrizates, and resorcinol or isopropylmethylphenol. *Japanese patent 05320023 to Kanebo*.

- Vilanculo, C. B., Leles, L. C. A., and Silva, M. J. (2018). $\text{H}_4\text{SiW}_{12}\text{O}_{40}$ -catalyzed levulinic acid esterification at room temperature for production of fuel bioadditives. *Waste Biomass Valori.* 11, 1895–1904. doi: 10.1007/s12649-018-00549-x
- Wagh, K. V., Badgujar, K. C., Patil, N. M., and Bhanage, B. M. (2016). Recent trends of ionic liquids for the synthesis of 5-hydroxymethylfurfural. *Curr. Org. Chem.* 20, 736–751. doi: 10.2174/1385272819666150716173605
- Wang, G., Zhang, Z., and Song, L. (2014). Efficient and selective alcoholysis of furfuryl alcohol to alkyl levulinates catalyzed by double SO_3H -functionalized ionic liquids. *Green Chem.* 16, 1436–1443. doi: 10.1039/C3GC41693C
- Wang, H., Deng, T., Wang, Y., Qi, Y., Hou, X., and Zhu, Y. (2013). Efficient catalytic system for the conversion of fructose into 5-ethoxymethylfurfural. *Bioresour. Technol.* 136, 394–400. doi: 10.1016/j.biortech.2013.02.110
- West, R. M., Holm, M. S., Saravanamurugan, S., Xiong, J., Beversdorf, Z., Taarning, E., et al. (2010). Zeolite H-USY for the production of lactic acid and methyl lactate from C3-sugars. *J. Catal.* 269, 122–130. doi: 10.1016/j.jcat.2009.10.023
- Windom, B. C., Lovestead, T. M., Mascall, M., Nikitin, E. B., and Bruno, T. J. (2011). Advanced distillation curve analysis on ethyl levulinate as a diesel fuel oxygenate and a hybrid biodiesel fuel. *Energ Fuels* 25, 1878–1890. doi: 10.1021/ef200239x
- Wu, M., Zhang, X., Su, X., Li, X., Zheng, X., Guan, X., et al. (2016b). 3D graphene aerogel anchored tungstophosphoric acid catalysts: characterization and catalytic performance for levulinic acid esterification with ethanol. *Catal. Commun.* 85, 66–69. doi: 10.1016/j.catcom.2016.07.023
- Wu, M., Zhao, Q.-Q., Li, J., Su, X.-L., Wu, H.-Y., Guan, X.-X., et al. (2016a). Tungstophosphoric acid-based mesoporous materials anchored to MCM-41: characterization and catalytic performance in esterification of levulinic acid with ethanol. *J. Porous. Mater.* 23, 1329–1338. doi: 10.1007/s10934-016-0192-1
- Wu, M., Zhao, Q. Q., Li, J., Wu, H. Y., Zheng, X. C., Guan, X. X., et al. (2016c). Esterification of levulinic acid into hexyl levulinate over dodecatungstophosphoric acid anchored to Al-MCM-41. *J. Exp. Nanosci.* 11, 1331–1347. doi: 10.1080/17458080.2016.1214985
- Xu, G., Chang, C., Zhu, W., Li, B., and Du, F. (2013). A comparative study on direct production of ethyl levulinate from glucose in ethanol media catalysed by different acid catalysts. *Chem. Pap.* 67, 1355–1363. doi: 10.2478/s11696-013-0410-0
- Yadav, G. D., and Nair, J. J. (1999). Sulfated zirconia and its modified versions as promising catalysts for industrial processes. *Micro. Meso. Mater.* 33, 1–48. doi: 10.1016/S1387-1811(99)00147-X
- Yadav, G. D., and Yadav, A. R. (2014). Synthesis of ethyl levulinate as fuel additives using heterogeneous solid superacidic catalysts: efficacy and kinetic modeling. *Chem. Eng. J.* 243, 556–563. doi: 10.1016/j.cej.2014.01.013
- Yamaguchi, A., and Shirai, M. (2016). Catalytic production of sugar alcohols from lignocellulosic biomass. *Catal. Today* 265, 199–202. doi: 10.1016/j.cattod.2015.08.026
- Yan, K., Wu, G., Wen, J., and Chen, A. (2013). One-step synthesis of mesoporous $\text{H}_4\text{SiW}_{12}\text{O}_{40}$ catalysts for the production of methyl and ethyl levulinate biodiesel. *Catal. Commun.* 34, 58–63. doi: 10.1016/j.catcom.2013.01.010
- Yang, F., and Tang, J. (2019). Catalytic upgrading of renewable levulinic acid to levulinate esters using perchloric acid decorated nanoporous silica gels. *Chem. Select* 1403–1409. doi: 10.1002/slct.201803608
- Yang, Y., Abu-Omar, M. M., and Hu, C. (2012). Heteropolyacid catalyzed conversion of fructose, sucrose, and inulin to 5-ethoxymethylfurfural, a liquid biofuel candidate. *Appl. Energ.* 99, 80–84. doi: 10.1016/j.apenergy.2012.04.049
- Yontz, D. J. (2011). Fabricating fragrant formulations from essential oils and solvents as olfactory flavorants for food, fragrances for candles, cosmetics, soaps or other uses. *U.S. Patent US20110274643A1*.
- Zhang, J., and Chen, J. (2016). Modified solid acids derived from biomass based cellulose for one-step conversion of carbohydrates into ethyl levulinate. *J. Energy Chem.* 25, 747–753. doi: 10.1016/j.jechem.2016.06.005
- Zhang, Z., Dong, K., and Zhao, Z. (2011). Efficient conversion of furfuryl alcohol into alkyl levulinates catalyzed by an organic-inorganic hybrid solid acid catalyst. *ChemSusChem* 4, 112–118. doi: 10.1002/cssc.201000231
- Zhao, S., Xu, G., Chang, C., Fang, S., Liu, Z., and Du, F. (2015). Direct conversion of carbohydrates into ethyl levulinate with potassium phosphotungstate as an efficient catalyst. *Catalysts* 5, 1897–1910. doi: 10.3390/catal5041897
- Zheng, X. C., Guan, X., Li, N., Zhang, X. L., and Wu, M. (2017). Synthesis of biofuel via levulinic acid esterification over porous solid acid consisting of tungstophosphoric acid and reduced graphene oxide. *Res. Chem. Intermed.* 43, 6651–6664. doi: 10.1007/s11164-017-3012-6
- Zhou, X., Li, Z. X., Zhang, C., Gao, X. P., Dai, Y. Z., and Wang, G. Y. (2016). Efficient conversion of renewable levulinic acid to n-butyl levulinate catalyzed by ammonium and silver co-doped phosphotungstic acid. *J. Mol. Catal. A Chem.* 417, 71–75. doi: 10.1016/j.molcata.2016.03.006
- Zhu, S., Chen, C., Xue, Y., Wu, J., Wang, J., and Fan, W. (2014). Graphene oxide: an efficient acid catalyst for alcoholysis and esterification reactions. *ChemCatChem* 6, 3080–3083. doi: 10.1002/cctc.201402574
- Zhu, S., Wang, J., and Fan, W. (2015). Graphene-based catalysis for biomass conversion. *Catal. Sci. Technol.* 5, 3845–3858. doi: 10.1039/C5CY00339C

Conflict of Interest: The authors declare that the research was conducted in the absence of any commercial or financial relationships that could be construed as a potential conflict of interest.

Copyright © 2020 Liu, Yang, Zhang, Li and Wu. This is an open-access article distributed under the terms of the Creative Commons Attribution License (CC BY). The use, distribution or reproduction in other forums is permitted, provided the original author(s) and the copyright owner(s) are credited and that the original publication in this journal is cited, in accordance with accepted academic practice. No use, distribution or reproduction is permitted which does not comply with these terms.

Advantages of publishing in Frontiers



OPEN ACCESS

Articles are free to read
for greatest visibility
and readership



FAST PUBLICATION

Around 90 days
from submission
to decision



HIGH QUALITY PEER-REVIEW

Rigorous, collaborative,
and constructive
peer-review



TRANSPARENT PEER-REVIEW

Editors and reviewers
acknowledged by name
on published articles

Frontiers

Avenue du Tribunal-Fédéral 34
1005 Lausanne | Switzerland

Visit us: www.frontiersin.org

Contact us: frontiersin.org/about/contact



REPRODUCIBILITY OF RESEARCH

Support open data
and methods to enhance
research reproducibility



DIGITAL PUBLISHING

Articles designed
for optimal readership
across devices



FOLLOW US

@frontiersin



IMPACT METRICS

Advanced article metrics
track visibility across
digital media



EXTENSIVE PROMOTION

Marketing
and promotion
of impactful research



LOOP RESEARCH NETWORK

Our network
increases your
article's readership